CONTRACTOR REPORT

SAND84-8192
UC-62d
Unlimited Release

Experimental Study of Free and Fixed Convective Flow of Air in a Heated Cavity

Mechanical Engineering Department
University of California, Berkeley
Berkeley, California

Prepared by Sandia National Laboratories, Albuquerque, New Mexico 87185 and Livermore, California 94550 for the United States Department of Energy under Contract DE-AC04-76DP00789.

Printed April 1985

The research and development described in this report was conducted within the U. S. Department of Energy's (DOE) Solar Thermal Technology Program. The Solar Thermal Technology Program directs efforts to advance solar thermal technologies through research and development of solar thermal materials, components, and subsystems, and through testing and evaluation of solar thermal systems. These efforts are carried out through DOE and its network of national laboratories who work with private industry. Together they have established a goal-directed program for providing technically proven and economically competitive options for incorporation into the Nation's energy supply.

There are two primary solar thermal technologies: central receivers and distributed receivers. These two technologies use various point and line-focus optics to concentrate sunlight onto receivers where the solar energy is absorbed as heat and converted to electricity or used as process heat. In central receiver systems, which this report considers, fields of heliostats (two-axis tracking mirrors) focus sunlight onto a single receiver mounted on a tower. The radiant energy is absorbed by a working fluid circulating within the receiver and is transformed into high temperature thermal energy. Temperatures in central receivers may exceed 1500°C.

Printed in the United States of America
Available from
National Technical Information Service
5285 Port Royal Road
Springfield, VA 22161

NTIS price codes
Printed copy: A14
Microfiche copy: A01

SAND84-8192
Unlimited Release
Printed April 1985

EXPERIMENTAL STUDY OF FREE AND MIXED CONVECTIVE FLOW OF AIR IN A HEATED CAVITY*

UC-62d

by

Joseph A.C. Humphrey (Principal Investigator)
Frederick S. Sherman (Co-Principal Investigator)
Kang S. Chen (Research Assistant)

Mechanical Engineering Department
University of California, Berkeley
Berkeley, California 94720

Report No. 83-1

December 1983

* Final Report Submitted to Sandia National Laboratories Relating to the Experimental Work Performed for Contract No. 20-1012 Entitled - "Investigation of Free-Forced Convection Flows in Cavity-Type Receivers" October 1, 1979 to March 31, 1984

Final Report Relating to Numerical Modeling Submitted Separately

ABSTRACT

Free and mixed convection in a strongly-heated rectangular open cavity have been investigated experimentally, to observe the effects of cavity shape and inclination, and of ambient wind, on the velocity and temperature distribution.

The long edges (c = 0.533 m) of the cavity were horizontal, and parallel to an axis around which the cavity could be rotated. The aperture plane was either vertical ($\alpha = 0°$), or inclined downward at $\alpha = 20°$ or $\alpha = 45°$. The height of the aperture, b, was always 0.0947 m, while the depth of the cavity, a, was set so that a/b = 0.5, 1.0, or 1.46. The bottom and back walls were electrically heated - the top wall was indirectly heated by conduction, radiation and convection. The average wall temperature, T_c, and the ambient temperature T_∞ were used to defined the dimensionless overheat and Grashof numbers, typical values of which were $(T_c - T_\infty)/T_\infty = 1.21$, $Gr = g(T_c - T_\infty)b^3/\nu_\infty{}^2 T_\infty = 4.2 \times 10^7$. The Prandtl number was that of air, $Pr \approx 0.7$.

In the studies of mixed convection, the axis of rotation was horizontal and normal to the ambient wind. When the aperture faced directly upstream, $\alpha = 0°$. The Reynolds number, $Re = bU_\infty/\nu_\infty$, was varied from Re = 120 - 1100, in which range free convection was dominant, to Re = 2000 - 8740, in which range forced convection was dominant.

For both free and mixed convection, wall and gas temperature were measured with thermocouples, and shadowgraph pictures were taken. For pure free convection, three time-averaged velocity components, the corresponding normal Reynolds stress components, and one off-diagonal Reynolds stress component were measured with a two-color laser-Doppler velocimeter. The LDV operated in the backscatter, counter mode, and was mounted on a motorized tra-

versing table. A PDP-11/34 minicomputer controlled the sequence of automatic data acquisition, the statistical data reduction and its storage. Statistical results are presented numerically and graphically for two averaging procedures. Physical interpretations and computed rates of heat transfer are based on the procedure which seems to us most likely to remove "velocity bias" from the averages.

The principal quantitative result for free convection is that the rate of convective heat loss across the cavity aperture plane is reduced both by increasing a/b and by increasing α. When $\alpha = 0°$, the Nusselt number, $Nu = \dot{Q}_b/(k_\infty c(T_c - T_\infty))$, is reduced from 54 to 27 as a/b is increased from 0.5 to 1.0. If, with a/b = 1.0, α is increased to 45°, the Nusselt number drops again, to 17.

A wealth of qualitative observations is recorded and discussed. The most striking observation was the appearance of a periodic oscillation of frequency 2-5.5 Hz, which appeared when $Gr/Re^2 > 200$, $\alpha = 0$-$20°$, a/b = 0.5 and 1.0. Other observations document some of the complexities that must be accounted for in any attempt to construct a successful theoretical model of the time-averaged flow.

CONTENTS

ACKNOWLEDGEMENTS

Thanks are due to the technical staff of the Mechanical Engineering Department of the University of California, Berkeley, for their helpful cooperation during the performance of this investigation. Funding for the work was provided by Sandia National Laboratories through Contract Number 20-1012. We welcome the opportunity to express our appreciation for this support. Special thanks go to Mrs. Judy Reed for the typing of this manuscript.

FOREWORD

Problem Motivation and Research Goals

The study of convective heat losses from central solar energy receivers was instituted by the Department of Energy when it was concluded (1) that there was no practical way to eliminate these losses (for example, by admitting the sunlight to the energy absorbing surface through a totally transparent window enclosing an evacuated space), and (2) that the losses could be economically significant.

A survey of the technical literature and of expert opinion revealed that very little was known about free convection from such large and very hot bodies. Prototype Grashof numbers, based on ambient temperature properties, would far exceed values readily obtainable in model studies which employ air, and the dimensionless surface overheat, $\Delta T/T_\infty$, would greatly exceed the values typical of most previous controlled experiments. The modification of strong free convection by ambient winds, and by the configuration of the solar receiver, are likewise subjects on which little past experience can be brought to bear.

Research sponsored under the Convective Loss Program, and related research concerned with natural and man-made fires, is beginning to elucidate these unfamiliar phenomena and to develop tools for experimental observation and theoretical description. However, as was clearly revealed at the July 1982 Natural Convection Workshop sponsored by NSF, the body of relevant knowledge is still small and the knowledgeable workers are few. To some extent, particularly in programs of experimental observation, recent work has identified difficulties without as yet showing how to circumvent them. Nevertheless, considerable relevant progress has been made, and this report provides an extensive description and evaluation of our contribution to this progress.

Our overall goals have been to develop computational methods appropriate for laminar and turbulent buoyant flow, in situations to which neither the boundary-layer approximation nor the Boussinesq approximation apply, and to perform small-scale laboratory experiments involving a simple heated cavity configuration in both free and mixed convection. The computational study is being documented in detail in a separate report. The experimental aspects of the research program are presented here.

The direct objectives of the experimental work were two:

1) to begin to develop a useful taxonomy of buoyant cavity flows, identifying characteristic phenomena which may be expected to appear in recognizable form whenever certain ranges of dimensionless parameters and geometrical configurations are encountered,
2) to provide data adequate for testing computational methods under varied and relevant circumstances.

The experimental work has had the necessary concomitant objective of advancing the art of measurement of flows that are:

1) easily disturbed by intrusive techniques.
2) highly unsteady, turbulent and non-uniform.
3) thermodynamically complex and, to a degree, hostile.

Measurement Techniques and Errors

Our selection of quantities to be measured, and of techniques of measurement, represents a compromise between the desire to establish a data base which would be maximally helpful to our efforts in theoretical modeling of buoyant turbulent flows, or which would be most revealing for taxonomical purposes, and the costs and development time of promising techniques for which we were not already equipped and experienced.

Wishing to establish a correspondence between quantitative local measurements and the corresponding synoptic picture, we have made extensive use of shadowgraph photography, obtaining high-speed (10^{-3} sec) snapshots, movies and, for periodically oscillating flows, stroboscopically "frozen" time exposures.

For local velocity measurements, we rely on laser Doppler velocimetry (LDV), operating in the "single-particle" or "counter" mode. This work constitutes an application of LDV to a task of unprecedented complexity, because four difficulties must be simultaneously confronted. These are:

1) A very low data rate (10 - 100 Hz), arising from the difficulty of introducing a high density of uniformly sized scattering particles without disturbing the flow. This results in very sparse sampling of the history of velocity in the measuring volume, and raises difficult questions concerning how well the mean and other low moments of the sample represent the corresponding properties of the complete history. Studies of the "velocity bias" which may originate in this sparse sampling are proceeding in several laboratories, but no definitively optimal "correction" for the bias has been found, or is likely to be found until the statistics of the flow, which the measurements are supposed to reveal, become known.
2) Proportionally very large velocity fluctuations, with frequent reversals of the measured component of velocity. This difficulty is largely circumvented by shifting the frequency of one of the laser beams.
3) Difficulty in achieving uniform seeding of all air within the cavity, where the seeding source must of necessity be kept far from the cavity and we must trust to luck that particles so introduced are

uniformly distributed. If the seeding is non-uniform, the LDV can record an unintended "conditional average" at a point visited intermittently by seeded and unseeded flow.

4) Relatively large variations of index of refraction in the non-uniformly heated air. These can cause both uncertainty in the exact mean location of the measuring volume, and a spurious indication of local velocity fluctuations due to "dancing" and the consequent phase shift between a pair of laser beams.

Because of their possible detrimental impact on the quality of the LDV measurements obtained in this study, the above and related sources of error are discussed, and when possible estimated, in the report.

For local temperature measurements, we use an intrusive technique, introducing relatively fine (75 μm dia) chromel-alumel thermocouple wires in the flow. Actually, the disturbance of the flow by these wires, which typically have a Reynolds number less than 1, is certain to be negligible, but the information that can be gained from the thermocouple signals is limited by the relatively low rates of convective heat transfer between the wire and the air. In addition, positioning error, conduction end losses and radiation heat transfer all affect the quality of the measurements. These error sources and estimates of their respective magnitudes are evaluated in the report.

Impact of this Study

While this investigation has proceded in parallel with several other recent studies on buoyancy-affected cavity flows (appropriately referenced in the report), it differs markedly from all of them in various respects.

From the start, emphasis was placed on understanding the effects which changes in cavity cross-section and orientation would produce in free or mixed convection flows. In this respect, the flow visualization observations and

corresponding temperature measurements, have proved invaluable. Earlier attempts by others to use the LDV technique for measuring air flows in heated cavities were limited to low temperature differences and laminar flow regime, and were poorly documented. This study demonstrates and carefully documents the applicability of the technique to high temperature differences in the turbulent flow regime. The quality of the measurements obtained for mean velocity and turbulent stress components makes the data base very useful for advancing and testing new concepts in turbulence modeling.

The need to accomplish the objectives of this investigation in a reasonable amount of time and at affordable cost dictated the construction of a cavity test section which would fit in the plenum chamber of the subsonic wind tunnel of the Department of Mechanical Engineering, University of California, Berkeley. The test section was designed to emphasize the mean two-dimensional features of the flow. Because the Grashof number in the experiment reported here is only $Gr \sim 10^7$, compared to $Gr \sim 10^{14}$ in projected solar receiver applications, emphasis must be placed on qualitative uses of the present results when seeking analogies between configurations. In the two cavity studies known to us where relatively large Grashof numbers have been attained, no information was obtained concerning the influence of cavity aspect ratio or turbulence on the flow. In neither of these studies were detailed LDV measurements obtained nor was the mixed convection regime investigated. To a large extent then, the Grashof number limitation in the present work is offset by the more detailed nature of the information obtained, which is lacking in the other investigations.

NOTATION

A	area; generally of the cavity aperture plane
a	cavity depth (y-direction in Fig. 1)
b	cavity height (x-direction in Fig. 1)
C_t	terminal velocity of a spherical particle falling in a fluid at rest
c	cavity width (z-direction in Fig. 1)
c_p	specific heat at constant pressure
c_v	specific heat at constant volume
f	pulsation frequency of air in the cavity
f_d	Doppler-shifted frequency of a moving particle
g	magnitude of gravity vector
Gr	$\left(\equiv \frac{g(T_c - T_\infty)\, b^3}{\nu_\infty^2\, T_\infty}\right)$ cavity Grashof number for the configuration of Fig. 1; alternative definitions given in text
h	$\left(\equiv \frac{\dot{Q}_b/c}{b\,(T_c - T_\infty)}\right)$ cavity aperture plane heat transfer coefficient; also denotes enthalpy
k	thermal conductivity; k_∞ at ambient conditions
L	characteristic length; in the cavity L = b (Fig. 1)
M	Mach number
$\dot{m}_b$	mass flow of air
N	number of measurements in a population sample
N_f	number of interference fringes crossed by a particle
Nu	$\left(\equiv \frac{hb}{k_\infty} = \frac{\dot{Q}_b/c}{k_\infty (T_c - T_\infty)}\right)$ aperture plane Nusselt number
p	pressure
Pr	$(\equiv \frac{\mu\, c_p}{k})$ Prandtl number
$\dot{Q}_b$	aperture plane heat flow due to convection
$\dot{Q}_w$	heat flow from walls to air within cavity

$\underset{\sim}{q}$ conductive heat flux vector

R wind tunnel contraction ratio; also perfect gas constant

Ra ($\equiv$ Gr Pr) Rayleigh number

Re $\left(\equiv \frac{b\ U_\infty}{\nu_\infty}\right)$ cavity Reynolds number

r particle radius

St particle Stokes number; also Strouhal number; both defined in text

T temperature; generally an average value; T_∞ at ambient conditions

T_{bac} average temperature of cavity back wall

T_{bot} average temperature of cavity bottom wall

T_c characteristic cavity wall temperature (defined in text)

T_{top} average temperature of cavity top wall

T_w wall temperature

ΔT ($\equiv T_c - T_\infty$) difference between cavity and ambient temperatures

t time

U x-direction velocity component in Fig. 1; mean value defined in text

U_∞ mean velocity of wind approaching cavity

U_i ith realization of U in a measurement sample

$\underset{\sim}{u}$ velocity vector

u characteristic velocity; also denotes instantaneous value of velocity

$u_f(t)$ fluid velocity at time t

$u_p(t)$ particle velocity at time t

$\overline{uv}$ x-y shear stress component; notation $\overline{u'v'}$ also used in some figures

$\overline{u^2}$ x-direction normal stress; notation $\overline{u'^2}$ also used in some figures; u' denotes fluctuation

V y-direction velocity component in Fig. 1; mean value defined in text

V_f speed of frequency-shifted probe volume fringes

V_i ith realization of V in a measurement sample

$\overline{v^2}$ y-direction normal stress; notation $\overline{v'^2}$ also used in some figures; v' denotes fluctuation

W z-direction velocity component in Fig. 1; mean value defined in text

W_i ith realization of W in a measurement sample

$\overline{w^2}$ z-direction normal stress; notation $\overline{w'^2}$ also used in some figures; w' denotes fluctuation

x x-coordinate direction in Fig. 1; also referred to as "longitudinal" or "streamwise" direction

y y-coordinate in Fig. 1; also referred to as "transverse" direction

z z-coordinate direction in Fig. 1; also referred to as "spanwise" direction

Greek Letters

α cavity inclination angle with respect to vertical (gravity) direction in Fig. 1

β ($\equiv \frac{1}{T}$) coefficient of volume expansion, in this study taken as $(1/T_\infty)$; also denotes wind orientation angle with respect to cavity in Fig. 1

γ ($\equiv c_p/c_v$) specific heat ratio

$\gamma/2$ half angle between a pair of intersecting laser beams

Δt_i particle residence time in optical probe volume

δ characteristic length for conduction and viscous dissipation

δ_f fringe spacing in optical probe volume

η index of refraction of air

θ ($\equiv \frac{T-T_\infty}{T_c-T_\infty}$) dimensionless temperature

λ laser beam radiation wavelength

μ viscosity

ν kinematic viscosity; ν_∞ at ambient conditions

ρ density; ρ_∞ at ambient conditions

ρ_p density of seeding agent particles

σ standard deviation

τ characteristic time; also time constant of thermocouple wire

Φ viscous dissipation function

ω frequency

ω_i velocity weighting factor

Subscripts

c cavity or cavity value

i ith realization of a statistical event

in moving into the cavity

o reference value

out moving out of the cavity

p particle phase

w generally denotes wall value

x x-coordinate direction

y y-coordinate direction

∞ refers to ambient conditions

Superscripts

' denotes fluctuating component (used mostly in figures)

— mean value or time average

Symbols

Δ difference or increment

$|\ |$ absolute value

$\sim$ vector quantity

1. INTRODUCTION

1.1 Problem Background and Research Objectives

Natural or free convection flows are induced by the action of gravity on fluids of horizontally varying density. Most commonly, the density variations are associated with heat transfer.

When the temperature variations that initiate and sustain the flow are small enough, the temperature dependence of transport properties and the divergence of the velocity field are negligible. Then the dimensionless parameters that determine dynamic similarity are only two: the Grashof number and the Prandtl number. In particular, the transition between laminar and turbulent flow is associated, for each boundary geometry and Prandtl number, with a critical range of the Grashof number.

In the experiments reported here, the dimensionless overheat ratio, $\Delta T/T_\infty$, is large enough so that the above-mentioned phenomena could be significant. They are not expected to give rise to qualitative modifications of the flow or heat transfer, but may produce quantitatively important changes in critical Grashof numbers, or in the values of Nusselt number to be expected for given Grashof and Prandtl numbers.

The fluid mechanics of buoyancy-affected flows has long been a subject of interest to scientists and engineers; see Turner [1973]. In particular, the enhancement and suppression of flow instabilities by buoyant forces have interested meteorologists for decades, and environmental engineers more recently. In various fields of engineering there have been sustained efforts to measure, understand and make predictable the behavior of flows with buoyant effects. This is because many transport processes of engineering interest are influenced by buoyant forces, and frequently it is of special concern to control the rates of thermal energy transport arising in them. Examples are:

air conditioning of buildings; fire spread in rooms and corridors; cooling of electronic components or of turbine blades in combustors.

Solar central receivers have been proposed as potential energy conversion devices for large amounts of process heat, or for electric power generation; see Siebers et al [1979]. The concept underlying a solar receiver is the redirection of solar insolation to an absorbing heat transfer surface by means of a heliostat field. A working fluid is pumped through this surface to a desired location for further useful energy conversion.

Central receivers can be broadly divided into two categories: the cavity-type receiver (internal receiver), and the external receiver. The external receiver collects radiation on surfaces directly exposed to the surroundings. By contrast, radiation to a cavity-type receiver is directed onto interior surfaces through an opening or aperture. In either case, the thermal efficiency of a receiver will depend strongly on the receiver heat losses due to conduction along the receiver walls, free-forced convection to the ambient air, and reflection and re-radiation to the surroundings. Among these three modes of heat loss, conduction, reflection and radiation can (in principle) be adequately analyzed by current state-of-the-art knowledge. However, convection losses, especially in cavity flows, are very poorly documented; see the review by Humphrey, et al [1980].

In particular, little is known about the effects of relatively complex boundary geometries, large overheat ratios, extremely high Grashof numbers, and the interactions between the buoyancy-driven flow and naturally occuring winds.

The great cost and difficulty of field experiments, in which all complicating factors could be simultaneously present, motivates an effort to improve

our understanding of basic transport mechanisms in somewhat simplified circumstances. Thus, in this study, the shape and orientation of the heated cavity are designed to encourage a flow that is two-dimensional in a time-averaged sense, and to provide surroundings that are either quiescent or in steady uniform motion, while the dimensionless overheat ratio is allowed to be large enough to be independently important.

The specific objectives of the work are two: (1) to explore and document phenomena related to the cavity geometry and to a limited class of interactions between free- and forced flows; and, (2) to establish a data base of velocity and temperature measurements, which could serve simultaneously to guide and to test the development of improved numerical models of this class of flows.

1.2 Literature Review

There is an abundance of literature on the topics of free and mixed convection. A substantial portion of this information deals with the flat plate configuration (vertical, horizontal or inclined) and the enclosure configuration for different orientation angles. A recent review of the literature corresponding to these two shapes has been tabulated by Humphrey et al [1980]. Their main observations are summarized below.

The bulk of the studies are for two-dimensional (2-D) laminar and/or turbulent flows, but 3-D flows and transition to turbulence have also been documented. In various studies due consideration has been given to the relative influence on flow stability of the heated surface orientation with respect to gravity.

With few exceptions, the analytical, numerical and experimental investigations deal with circumstances well described by the Boussinesq approxima-

tion. (See, for example, Gray and Giorgini [1976] for a detailed discussion of this approximation.)

Since the pioneering analysis of laminar free convection past a vertical plate, (Ostrach [1953]), considerable progress has been made in the numerical description of laminar flows past plates and within enclosures. Progress has been made, too, in the computational modeling and empirical representation of buoyant turbulent flows. (See, for example, George and Capp [1979].)

1.2.1 Forced convection in the cavity configuration

High Reynolds number flows in the cavity configuration, induced by the shear of an externally applied flow field over the cavity opening, have been of considerable interest for some time, particularly in aeronautical engineering applications. Many of the studies address high Mach number conditions ($M > 1.5$), in which pressure fluctuations and cavity resonance effects were the issues of main concern. In this regard, the following are noteworthy contributions: Larson [1959], Charwat et al [1961-a,b], Nicoll [1964], Rossiter [1964], Hahn [1969], McGregor and White [1970], White [1971]. At low Mach numbers ($M \leq 0.3$) there have been a corresponding number of contributions. These include the notable flow visualization study by Maull and East [1963], the experimental and analytical studies by Haugen and Dhanak [1966, 1967] on cavity size effects on heat transfer and fluid flow, the heat transfer and air flow transverse rectangular notch study by Fox [1965], the turbulent flow and heat transfer predictions by Chin et al [1972], and the laminar flow heat transfer predictions of Humphrey and Jacobs [1981] for inclined channels with cavities of different orientation.

A review of separated and reattaching flows with heat transfer has been made by Chilcott [1966]. More recent topics on heat transfer in recirculating

flows are contained in Launder and Humphrey [1980]. The problem of obtaining numerical solutions of laminar separated flows has been addressed by Roache and Muller [1970], while the more general problem of assessing numerical schemes for predicting recirculating flows in cavities has been reviewed by Olson and Tuann [1978].

1.2.2 Free and mixed convection in the cavity configuration

In contrast to the above, free and mixed convection flows in the cavity configuration have received sparse attention. Laminar flow free convection in very deep cavities ($a/b \gg 1$ in Fig. 1) has been studied by, for example, Bejan and Kimura [1981], and Bejan and Tien [1978]. However, these flows are dominated by the very large aspect ratios of the cavity and as a consequence are of limited interest to the present problem. Recent studies of free convection in the shallow cavity configuration ($a/b < 3$, approximately) have been motivated by: interest in the fire and smoke spread problem (Ku et al [1976], Mao et al [1982] and Markatos et al [1982]); the convective cooling of electronic components (Humphrey and Jacobs [1981]); and the need to evaluate convection losses from central solar receivers (discussed below). The only study identified by the present authors in the mixed convection regime is that by Orlandi et al [1978] concerning buoyancy-affected atmospheric flows in valleys.

Among the early contributions to the problem of evaluating free convection heat transfer from relatively shallow cavities are the numerical studies by Eyler [1980], Le Quere et al [1981] and Penot [1982]. These authors have made 2-D predictions of the flow and thermal fields in rectangular cavities for various combinations of Grashof number and cavity orientation. The procedure of Le Quere et al [1981], unlike the other two, was not subject to the Boussinesq approximation.

Experimental contributions to the problem of free convection in shallow cavities have also emerged recently. Chen et al [1983] report the low frequency pulsating nature of buoyancy-driven 2-D cavity flows for $\Delta T/T_\infty \simeq 0.44$ using the experimental system described in this work. Humphrey et al [1981] provide flow visualization and temperature measurements for the same configuration at $\Delta T/T_\infty = 1.37$. Sernas and Kyriakides [1982] investigated the 2-D flow of air in a cavity with a/b = 1 and $Gr = 10^7$. They made limited laser-Doppler velocimeter (LDV) measurements of velocity and determined the heat transfer rates at the back and top walls (the bottom wall was maintained at ambient temperature). Hess and Henze [1981] performed several interesting experiments using flow visualization and the LDV technique in a 3-D cavity. The use of water as a fluid medium allowed them to attain Rayleigh numbers ranging from 2×10^{10} to 2×10^{11}, and permitted the study of transition to turbulence at relatively low values of $\Delta T/T_\infty$. In their study, only the back wall of the cube was heated. As in the work by Sernas and Kyriakides [1982], fairly thin, streamlined, boundary layer flows were observed at the walls, but at $Ra = 7 \times 10^{10} - 9 \times 10^{10}$ the flow became turbulent. In their experiment, Hess and Henze [1981] investigated the effects on fluid motion and heat transfer of constricting the flow entering and leaving through the cavity aperture plane.

In consecutive investigations using the same apparatus, Penot [1981] and Mirenayat [1981] have studied the free convection of air in a cubical cavity, all five solid walls of which were heated to the same temperature. Flow visualization and limited measurements using the LDV technique were performed. However, very extensive measurements of heat transfer were made as a function of Grashof number and cavity orientation. Mirenayat [1981] defined an overall

heat transfer coefficient as $h_c = \dot{Q}/5L^2\Delta T$, where $5L^2$ is the total heated area with heat flow $\dot{Q}$ induced by the temperature different $\Delta T = T_c - T_\infty$. The Nusselt number was then defined as $Nu = h_c L/k_\infty$, and a correlation was reported in the form

$$Nu = a\ Gr^b \tag{1-1}$$

with the Grashof number given by

$$Gr = \frac{g\,\beta(T_c - T_\infty)L^3}{\nu_\infty^2} \tag{1-2}$$

Here, a and b denote parameters depending on the cavity inclination angle α, L is the cube side and $\beta = 1/T_\infty$. Typically, $0.03 \leq a \leq 0.12$ and $0.30 \leq b \leq 0.37$, strongly supporting the 1/3 power dependence of Gr proposed by Mirenayat [1981] over the Gr range investigated ($10^7 < Gr < 10^{10}$).

Kraabel [1983] has also investigated the free convection of air in a cubical cavity. The large characteristic dimension of the cavity (2.2 m) permitted obtaining values of Grashof as large as 1.2×10^{12} for overheat ratios ranging between $\Delta T/T_\infty = 0.39$ and 2.55 approximately. All five solid walls were heated. Measurements in the aperture plane were used to determine the air temperature, velocity, enthalpy flux and radiative heat flux distributions. From these data convective (and radiative) heat losses from the cavity were found. The sum of these agreed well with the measured electric power used to heat the cavity, when small corrections to the latter were made to account for heat leaks to the insulation backing up the solid walls.

Kraabel [1983] defined Nusselt and Grashof numbers by the same formulas as did Mirenayat [1981], and found the correlation

$$Nu = 0.088\ Gr^{1/3} \left(\frac{T_c}{T_\infty}\right)^{0.18} \qquad (1\text{-}3)$$

over the range $10^7 \lesssim Gr \lesssim 1.2 \times 10^{12}$. This is for the inclination angle $\alpha = 0°$, the only case Kraabel could test, and the correlation agrees well with that of Mirenayat [1981], who found a = 0.093 and b = 0.33 for $\alpha = 0°$. Both sets of data imply, because $Gr^{1/3}$ is linearly proportional to L, that the average heat transfer coefficient is independent of cavity size.

The above investigations have all been performed for purely free convection flows. No relevant work was found in the literature pertaining to the mixed convection regime.

1.2.3 Studies of related interest

Because the elemental component of the heated cavity configuration is the flat plate, it seems reasonable to expect that some of the features of heated cavity flows will be similar (or due) to some of those associated with the flat plate configuration. The same logic leads us to expect similarities between the flows in cavities and the flows in enclosures (sealed cavities). For these reasons, it seems appropriate to review some specific investigations dealing with the flat plate and enclosure configurations which may be especially meaningful to this work.

Flat Plates

Rotem and Claassen [1969] performed theoretical analysis and flow visualization of the free-convection flow of air over horizontal flat plates with the heated surfaces facing up. In each case the experimental flow was symmetrical and consisted of two boundary layers starting at the opposing edges of a plate. The boundary layers met at the plate center from where the fluid rose in a thermal plume. At a certain distance, x, from the plate edge,

correlated by $Gr_x^{1/3} \approx 80$ to 100, the gravitationally unstable boundary layers broke down, and intermittently rising buoyant plumes broke away- to merge into the general central plume mentioned above. The technique of flow visualization did not reveal whether this phenomenon was two-dimensional, but that seems unlikely. By comparing with the work of Tritton [1963], the authors concluded that the point of instability moves away from the lower edge when the plate is inclined to the horizontal.

Pera and Gebhart [1973] observed the flow above nearly-horizontal heated plates which formed a symmetric low-pitched roof resting on a horizontal plane at ambient temperature. The buoyancy-induced flow approached the heated plates horizontally, with no threat of separation at the leading edge of the plates, whereas the flows of Rotem and Claassen [1969] swept up past the leading edges, from below.

Pera and Gebhart used glass side walls to promote two-dimensional base flows, and introduced two-dimensional disturbances with a vibrating ribbon. Nevertheless, they observed a highly three-dimensional evolution of these disturbances in a region where the buoyant fluid erupted away from the plate. In many respects their findings corresponded to those of Rotem and Claassen [1969], and these two investigations have greatly influenced our interpretation of the flows we see near the bottom wall of the open cavity.

Several authors, including Pera and Gebhart [1973], have investigated the instability of buoyant laminar flows along inclined plates. The theoretical work (e.g. Pera and Gebhart [1973], Chen and Tszoo [1982]) has focussed on disturbances that are either two-dimensional in space and oscillatory in time, or three-dimensional in space and steady in time. The latter class has high amplification rates when the plate is nearly horizontal, the former when the

plate is nearly vertical. Over a wide range of angles, the two classes coexist, and presumably interact when they reach finite amplitudes. Many interesting studies, both theoretical and experimental, have contributed to our understanding of these flows. These include, for example, the work of Gebhart [1969] and Gill and Davey [1969] using linear stability, Lloyd and Sparrow [1970] and Lloyd et al [1972] employing an electrochemical technique, and Jaluria and Gebhart [1974] employing hot wire anemometers. The flow past heated inclined flat plates has also been investigated by Rich [1953], Kierkus [1968], Vliet [1969], Lloyd et al [1972] and Vliet and Ross [1975].

There are many studies on the free convection flow past vertical flat plates. Among the early experimental works are the contributions by Goldstein and Eckert [1960], Warner and Arpaci [1968], and Lock and Trotter [1968]. More recent experimental turbulent flow studies using the LDV technique have been conducted by Cheesewright and Ierokipiotis [1981] for a $\Delta T/T_\infty$ of about 0.20, and by Cairnie and Harrison [1982] for $0.26 < \Delta T/T_\infty < 1.28$. Cheesewright and Doan [1978] have performed a fairly detailed study of space-time correlations using the hot wire technique.

In a rather unique investigation, Siebers et al [1983] have measured the free-convection heat transfer coefficient and temperature profiles for the flat plate configuration for $1.7 \times 10^{11} < Gr < 1.86\ 10^{12}$ with $0.14 < \Delta T/T_\infty < 1.73$. They found

$$Nu_x = 0.098\ Gr_x^{1/3} \left(\frac{T_w}{T_\infty}\right)^{-0.14} \qquad (1\text{-}4)$$

where: x is distance from the bottom of the plate, $Nu_x = hx/k_\infty$ and $Gr_x = g\,\beta\,(T_w - T_\infty)x^3/\nu_\infty^2$. Equation (1-4) shows that the local heat transfer

coefficient is independent of position, so that the average h is independent of plate size. The residual dependence on T_w/T_∞ differs from that found by Kraabel, for as yet unknown reasons.

Theoretical analyses of vertical flat plate flows have been performed by, for example, Ostrach [1953] and Hasan and Eichhorn [1979] for the laminar regime, and by Eckert and Jackson [1951], Bayley [1955], Oosthuizen [1967] and Kato et al [1968] for the turbulent regime. The calculations by Hasan and Eichhorn [1979] show that while there is an appreciable effect of plate inclination on the velocity field, the corresponding influence on the temperature field is weak. Numerical predictions using eddy viscosity models of turbulence have been made by Mason and Seban [1974], Cebeci and Khattab [1975], and Siebers [1979]. Predictions based on the low Reynolds number $k-\epsilon$ turbulence model of Jones and Launder [1972] have been made by Plumb and Kennedy [1977] and Lin and Churchill [1978]. In general, both the theoretical analyses and the numerical procedures show good agreement with experiment.

Enclosures

Thermally driven flows in enclosures have been investigated extensively; experimentally, analytically and numerically. Among the classical contributions to the problem are the laminar and turbulent investigations by Elder [1965-a,b] revealing multi-cellular motions. Stability considerations nave been addressed by, for example, Vest and Arpaci [1969], Gill [1970] and Korpela et al [1973]. Recently, LDV measurements in turbulent regime have been made by Schmidt and Wang [1982]. Inclined enclosures have been investigated experimentally by Arnold et al [1976] and Randall et al [1979]. The effect of varying enclosure aspect ratio has been evaluated by MacGregor and Emery [1969] and more recently by Duxbury [1979], who also provides detailed

visualization of the air flow. The effects of including partitions in an enclosure flow have been investigated by Bauman et al [1980] and by Nansteel and Greif [1981] using flow visualization and heat transfer measurement techniques.

Numerical predictions in the laminar flow regime have been made by Pepper and Harris [1978], Jones [1979], Mallinson and de Vahl Davis [1977], Kublbeck et al [1980], and by Forester and Emery [1972] without invoking the Boussinesq approximation. Numerical predictions in turbulent flow regime have been performed by Fraikin et al [1980], Salcudean and Abdelrehin [1980], Hjertager and Magnussen [1976]. In these studies two types of k-ϵ models were used corresponding to high and low Reynolds number formulations respectively. Within the context of the Boussinesq approximation, Fraikin et al [1980] included buoyancy effects in the modeled equations for kinetic energy of turbulence and its rate of dissipation. Predictions to date appear to be restricted to values of $Gr < 10^9$ approximately, and low $\Delta T/T_\infty$ ratio (Boussinesq approximation).

1.3 Analytical Approximations Applicable to this Work

Although this is a report of laboratory measurements, the interpretation of some of the data requires justification of underlying theoretical approximations. This has been given elsewhere (Le Quere, et al [1981]) but is included here for ready reference.

The main point to be established is that, under the conditions of our experiment, we can neglect the terms on the right hand side of the energy equation

$$\nabla \cdot (\rho h \underset{\sim}{u} + \underset{\sim}{q}) = -\frac{\partial}{\partial t}(\rho h) + \frac{Dp}{Dt} + \Phi \qquad (1\text{-}5)$$

Our arguments will rely on the perfect-gas relationship $\rho h = \gamma p/(\gamma - 1)$, where the ratio of specific heats, γ, is assumed constant. Then equation (1-5), which is exact, can be reformulated as

$$\frac{\gamma}{\gamma - 1}\, p(\nabla \cdot \underset{\sim}{u}) + (\nabla \cdot \underset{\sim}{q}) = - \frac{1}{\gamma - 1}\, \frac{Dp}{Dt} + \Phi \quad , \tag{1-6}$$

which is exact for a perfect gas. Our aim is to show that (1-6) is accurately approximated by

$$\frac{\gamma}{\gamma - 1}\, p_\infty (\nabla \cdot \underset{\sim}{u}) + (\nabla \cdot \underset{\sim}{q}) = 0 \quad . \tag{1-7}$$

The first step is to show that p, as a coefficient of $\nabla \cdot \underset{\sim}{u}$, can be approximated by the constant atmospheric pressure, p_∞. For this, we assume that any deviation from p_∞ is no bigger than ρu^2, where ρ and u are typical density and speed values. We take:

$\rho = 0.6$ kg/m^3 (half of standard atmospheric density);

$u = 0.8$ m/s (the highest speed observed in any of the present tests);

$p_\infty = 10^5$ N/m^2.

We then calculate $\rho u^2/p_\infty \approx 4 \times 10^{-6}$, clearly negligible in this context. A similar ratio arises if we ask whether p_∞ varies significantly with elevation over the small height of the test cavity.

The second step compares Φ to $\nabla \cdot \underset{\sim}{q}$. We estimate $\nabla \cdot \underset{\sim}{q} \approx k\, \Delta T/\delta^2$ and $\Phi \approx \mu u^2/\delta^2$, assuming that the characteristic length, δ, is the same for both conduction and viscous dissipation. This is certainly true in laminar flow, because the Prandtl number is nearly unity - and it seems likely to be true also in turbulent flow, because heat conduction is intimately connected with

the baroclinic generation of vorticity, and the scale of the vortices is the smallest scale on which dissipation is likely to be strong. Thus we accept

$$\Phi/(\nabla\cdot\underset{\sim}{q}) \approx \mu u^2/k\,\Delta T \ .$$

We use $\mu \approx 3 \times 10^{-5}$ kg/m·s, $k \approx 0.05$ Watt/m K, $\Delta T \approx 380$ K and $u \approx 0.8$ m/s, getting $\Phi/\nabla\cdot\underset{\sim}{q} \approx 10^{-6}$, again quite small.

Finally, we estimate Dp/Dt very generously, supposing that the largest expected Δp disappears entirely in a millisecond.

$$Dp/Dt \approx \rho u^2/\tau \ .$$

Using $\rho = 0.6$ kg/m^3, $u = 0.8$ m/s, $\tau = 10^{-3}$ sec, we find $Dp/Dt \approx 4 \times 10^2$ Watts/m^3. On the other hand, we make a stingy estimate of $(\nabla\cdot\underset{\sim}{q})$, using $\delta \approx 0.01$ m (nearly the largest observed thickness of the heated layers in our tests). This gives $\nabla\cdot\underset{\sim}{q} \approx 2 \times 10^5$ Watts/m^3. Thus $\frac{1}{\gamma - 1}\, Dp/Dt \div (\nabla\cdot\underset{\sim}{q})$ seems sure to be less than 5×10^{-3}, once more safely small, and the accuracy of equation (1-7) is established.

The qualitative implication of equation (1-7) is that we should not expect to see new flow features, such as shock waves or acoustic resonances, simply because $\Delta T/T_\infty \gtrsim 1$. Where the conductive heat flux converges, thermal expansion causes simultaneous divergence of the velocity field. Elsewhere the velocity field is solenoidal.

A quantitative application of (1-7) suggests that the net heat loss from the cavity can be experimentally estimated by measuring the average normal velocity component in the aperture plane. We integrate (1-7) over the volume enclosed by the cavity walls and the aperture plane and denote by $\dot{Q}_w$ the heat flux into that volume from the solid walls. The result is

$$\dot{Q}_w = \iint_{A_o} \left(\frac{\gamma}{\gamma - 1} p_\infty V - k \frac{\partial T}{\partial y} \right) dA \qquad (1\text{-}8)$$

where A_o is the aperture plane surface, normal to the y-axis.

To reduce this to a formula involving V alone, we need to show that the net heat conduction across A_o is negligible. Because of the geometrical complexity of the velocity and temperature fields, no simple order-of-magnitude estimate is likely to be accurate. We use, instead, finite-difference calculations - made for laminar and turbulent flows at $Gr \simeq 4 \times 10^7$ by W.-M. To [1984], using the scheme of Le Quere et al [1981]. These show, for the geometries of present interest, that no more than 2% of the total heat transfer is due to molecular conduction across the aperture plane. We assume that this fraction is a decreasing function of Grashof number.

Our working approximation is thus $\dot{Q}_w \simeq \dot{Q}_b$, the convective heat flow, given by

$$\dot{Q}_b = \frac{\gamma}{\gamma - 1} p_\infty \iint_{A_o} V \, dA \, . \qquad (1\text{-}9)$$

With a dubious assumption of strictly two-dimensional flow, we have reduced (1-9) to

$$\dot{Q}_b = \frac{\gamma}{\gamma - 1} p_\infty \, c \int_0^b V \, dx \qquad (1\text{-}10)$$

and use this to compute the heat transfer results that are discussed in Section 3. An interesting special feature of equation (1-10) is the linear dependence of $\dot{Q}_b$ on V. This implies that the time-averaged value of $\dot{Q}_b$ in turbulent flow is given by (1-10), with V replaced by its mean value.

Our data have been reduced to a Nusselt number, using the aperture plane area, bc, in the definition of the heat transfer coefficient; and the aperture height, b, as the reference length in the connection between heat transfer coefficient and Nusselt number. Thus, we write

$$Nu = hb/k_\infty \tag{1-11}$$

with

$$h = \frac{\dot{Q}_b}{bc(T_c - T_\infty)} \tag{1-12}$$

1.4 Some Experimental Considerations and the Scope of this Investigation

The literature review shows that in spite of the fact that the heated cavity problem is one of considerable interest, there is little in the way of detailed flow visualization and velocity measurements. Attention has been focused mostly on determining the heat transfer characteristics of fairly complex three dimensional (3-D) configurations; Penot [1981], Mirenayat [1981], and Kraabel [1982]. Exceptions are the studies of Hess and Henze [1981] and Sernas and Kyriakides [1982]. However, due to the boundary conditions in the latter two flows, neither of these investigations revealed significant turbulent motions in the bulk flow.

To reduce the amount of measurement needed for an adequate description of time-average velocity and temperature fields, while still retaining enough geometrical complexity to engender a phenomenologically rich flow, we chose to make our cavity relatively long in the horizontal dimension, c, of the aperture plane. It was hoped that a ratio $c/b > 5$ would suffice to make the time-averaged flow nearly independent of z, so that it could be adequately

characterized by measurements taken at midspan. This would also ease the interpretation of shadowgraph pictures. While a two-dimensional mean flow does not present all the challenges to a numerical simulation scheme, which could appear in a real cavity-type solar receiver, it was expected to produce plenty for an initial investigation. To be sure of this, we arranged to vary the relative depth, a/b, and inclination, α, of the cavity.

The practical problem that motivated this study encouraged us to concentrate our observations on flows in strongly-heated cavities ($T_c \approx 400°C$), so that the related numerical simulation must deal with velocity divergence, temperature-dependent transport properties, and turbulence. A compromise between the desire for high Grashof numbers, and the cost and inconvenience of work with a very large cavity, determined a cavity size for which the maximum Grashof number, $Gr = g\beta_\infty (T_c - T_\infty) b^3/\nu_\infty^2$, was about 4.2×10^7. The Prandtl number was that of air, $Pr \approx 0.7$.

Mixed convection experiments were planned for execution in a subsonic wind tunnel which constrained $|\beta| = 90° - |\alpha|$ in Fig. 1. The wind tunnel speed was variable, allowing a range of Reynolds number to be explored. Whereas the wind tunnel experiment would be well protected from variations in conditions of temperature and air drafts, precautions would be necessary to ensure that the free-convection experiments would also be uninfluenced by variations in ambient conditions.

Flow visualization, measurements of mean temperature and, for free convection regime, detailed measurements of velocity and of the flow turbulence characteristics would be required. Because of its simplicity, and because of the qualitative nature of the visualized results, the shadowgraph technique was chosen for flow visualization. The technique is described in Holman

[1978]. Measurements of temperature would be obtained with a thermocouple rake containing twelve, unevenly spaced, Chromel-Alumel thermocouples, aligned along the aperture plane of the cavity. Measurements of mean velocity and of the flow turbulence characteristics were planned using the laser-Doppler velocimetry (LDV) technique. The technique is non-intrusive, and seemed, after a preliminary consideration of the possibilities of hot-wire anemometry, to be almost the only technique suitable to this application. Various difficulties due to refraction of the laser beams, inhomogeneous seeding of the light-scattering particles, and sparse sampling of the velocity history, were anticipated but expected to be tolerable. Each of these difficulties had been noted and discussed in the literature, as will be detailed here, in Section 4.

As discussed in Section 1.3, integration of velocity component measurements normal to the cavity aperture plane in free convection regime will give an approximation to the convective heat loss from the cavity. The precision of this approximation will be determined by that of the LDV data. The accuracy will depend on that of the LDV data, and on the accuracy of the assumption of statistically stationary, two-dimensional flow. A careful error analysis, will obviously be required.

Data acquisition for an experiment as complex as this, even though it was planned to be as simple as possible, would have to be automated. To this end, a PDP 11/34 minicomputer was used, both to acquire and subsequently reduce the data by statistical methods.

1.5 Report Outline

The remainder of this report is divided into five sections. Section 2 deals with the experiment. It provides a description of the test section, the measurement instrumentation, and the experimental procedures. Section 3 con-

tains the results and discussion of this study, pertaining to the free and mixed convection experiments. Section 4 contains error analyses of the velocity and temperature measurement techniques. Conclusions and recommendations are presented in Section 5. The Appendices provided in this report contain the original and statistically processed experimental data for future reference, as well as computer listings of the software used to control the data acquisition and its statistical reduction.

2. THE EXPERIMENT

2.1 Description of the Apparatus

2.1.1 Test section and temperature control

Detailed descriptions of the experimental apparatus and method for temperature control have already been given by Humphrey et al [1980]. An extended summary of the descriptions is provided here.

Schematic views of the test section are shown in Fig. 1. Photographs of the test section and its steel support structure are shown in Figs. 2. Detailed side and front views of the test section, with linear dimensions given in inches, are shown in Figs. 3.

Three copper slabs and two borosilicate glass end-plates delimit the flow region referred to as the "cavity" in this work. Two of the slabs, the bottom and back walls in Fig. 1-b, consisted of pairs of copper plates having a total thickness of 1 1/8 in. (2.86 cm.) between which Incoloy strip heaters were sandwiched for electrical heating (see Fig. 3-a). The third slab, the top wall in Fig. 1-b, consisted of a single plate 1/4 in. thick (0.64 cm.) which was not heated electrically. The glass end plates were 1/8 in. thick (0.32 cm.) and allowed visualization of the flow along the spanwise coordinate of the cavity (z-direction in Fig. 1-a).

The copper slabs were supported in an aluminum frame by means of 1/4 in. (0.64 cm.) steel bolts. Fiberfrax Duraboard insulation was placed between the copper slabs and the aluminum frame to diminish heat losses through conduction (see Fig. 3-a). Conduction losses through the steel bolts to the aluminum frame were inevitable but were offset by increasing the power level to the heaters.

A total of 42 Chromel-Alumel (K-type) thermocouples (0.006 in. diameter, 152 μm) were placed in the cavity to monitor the copper slab temperature distributions. The thermocouples were arranged in cruciform arrays, 14 per slab, as shown in Fig. 4. Each thermocouple was inserted through the back of its respective copper slab, to within 1/32 in. (0.80 mm.) of the surface in contact with the air in the cavity. Each thermocouple wire pair was embedded in MgO packing contained in a stainless steel cladding. Each thermocouple pair was wired to a Type-K terminal block connector. Chromel-Alumel extension wires were used to connect the terminal blocks with Multiplexer boards in an Auto Data Nine data recorder.

Each Multiplexer board contains ten ports, to which the thermocouple wires were connected. The Auto Data Nine has a built-in microprocessor with compensation circuits to display the voltage from the thermocouple wires directly in millivolts or in pre-chosen units of temperature on a video-screen. Temperature readings can also be printed by a strip-paper recorder. In the present work three multiplexers were used for a maximum of 30 thermocouple wires at a time. Readings were taken sequentially at the rate of one thermocouple channel per second. The readings were made in degrees centigrade and were rounded off to the nearest integer value.

Five control units were used to power the strip heaters embedded in the cavity back and bottom copper walls, as shown in Fig. 5-a. Four units controlled two heaters each, and the fifth unit controlled one heater. Each control unit (see Fig. 5-b) consists of an RFL model 76 K-1 temperature controller, an RFL temperature indicator and a thermocouple wire. The temperature controller is a time proportional controller on the zero-crossing firing of a triac. Electrical power was fed to the heaters (rated at 1000

Watts/heater at 240 V) until pre-selected temperature levels were attained at five monitoring stations, distributed on the three copper walls. The temperature settings were controlled to within ± 0.1°C.

Measurements from the 42 wall-embedded thermocouples showed very even distributions of temperature on each copper wall. The maximum spanwise temperature gradient observed in the course of experimentation was less than 10°C/0.5 m for a typical wall temperature of 400°C. Variations transverse to the walls, along the y coordinate in Fig. 1-b, were always less than 5°C/0.1 m at a wall temperature of about 400°C. Thus, very uniform temperature distributions could be set at the bottom and back walls in the cavity, ranging from ambient condition to about 400°C, the maximum value imposed in practice.

The top wall in the cavity was heated by conduction, along the line of contact with the back wall, by radiation exchanges with the bottom and back walls, and by convection from the heated air moving in the cavity. Experiments were performed only when all three walls had attained a steady state condition, as indicated by time-recordings of temperature from the thermocouples embedded in the walls. The maximum temperature ever attained by the top wall during the course of experimentation was $T_{top} \simeq 340°C$, corresponding to back and bottom wall temperatures of $T_{bac} \simeq 420°C$, and $T_{bot} \simeq 400°C$, respectively.

A characteristic cavity wall temperature was defined by:

$$T_c = \frac{1}{3}(T_{bot} + T_{bac} + T_{top}) \qquad (2\text{-}1)$$

Printed time records were made of the temperature distribution of each wall from which the individual wall averages (T_{bot}, T_{bac}, T_{top}) and T_c were

obtained. The relatively fast response of the control units to changes in temperature at the monitoring locations constrained time variations about an average wall temperature to less than about ± 0.33°C/min. No problems were experienced with the long-term temperature stability of the test section.

The cavity aspect ratio, a/b, was continuously variable between 0 (flat wall condition) and 1.56 (the deepest cavity condition). The aspect ratio was changed by displacing the back wall copper slab. This slab was connected to a chain and sprocket assembly by means of two 1/2 in. (1.27 cm.) steel bolts; see Fig. 3-a.

The entire test section was supported from a Unistrut frame, as shown in Figs. 2. The inclination angle of the test section, and hence the orientation of the cavity with respect to gravity, was continuously variable between - 60° and 60° (see Fig. 1-b). Inclination of the cavity was achieved by means of a winch and pulley arrangement. This mechanism guided a steel cable connected to a steel harness. The harness pivoted on brackets mounted on the end walls of the aluminum frame (see Figs. 2). The Unistrut frame was placed on four casters to facilitate the displacement of the entire apparatus in the laboratory.

2.1.2 Air temperature measurements in the cavity aperture plane

Twelve Chromel-Alumel thermocouple wires of diameter 0.003 in. (76 μm) were used to measure the mean temperature of the air in the cavity aperture plane. The thermocouple wires were tautly strung on a steel harness (shown in Figs. 6) which, when mounted onto the test section aluminum frame, positioned the thermocouple beads to within ± 5 mm of the test section symmetry plane, and to within ± 1 mm of the aperture plane of the cavity. The wires were kept in place by fitting them into cut-out slots on cylindrical Teflon

bars located at either end of the harness. There were 50 cut-out slots on each bar which permitted unequal spacing of the thermocouples in the aperture plane. The slots were spaced at intervals of 0.1 in. (2.54 mm.). Bent paper clips provided the necessary tension to keep the wires from sagging due to expansion at high temperatures. The accuracy of location is discussed further in Section 4.

Chromel-Alumel extension wires were connected between the terminal blocks mounted on the side of the harness and the Auto Data Nine used for analog to digital recording of temperature. For each experiment, between 50 to 100 individual measurements of temperature were made per wire location. From these samples, statistical means and standard deviations were determined. Errors associated with these procedures are discussed in Section 4.

2.1.3 Wind tunnel facility and wind speed measurement

The subsonic wind tunnel facility located in Hesse Hall, University of California at Berkeley, was used for investigating the mixed convection flow regime in the cavity. Flow visualization and temperature measurements for pure free convection were also performed in the tunnel. The tunnel is an open-loop with a 10×10 ft^2 (3.05×3.05 m^2) cross-section in the stagnation chamber and a 32×32 in^2 (0.81×0.81 m^2) cross-section in the downstream section. The contraction ratio is 14:1. The facility and its performance characteristics have been reported by Laitone and Laitone [1983].

The flow of air in the wind tunnel is driven by a "squirrel-cage" blower. Speed control is obtained by varying the blower speed, and by dumping various proportions of the blower discharge before it enters the wind tunnel. The mean airspeed in the stagnation chamber is deduced from the pressure drop between stagnation and test chambers, with application of Bernoulli's equation

and a one-dimensional continuity equation. The pressure difference is sensed with an AVA Betz water manometer. The formula is

$$U_\infty = 0.289 \sqrt{\Delta h} \quad [m/sec] \tag{2-2}$$

with Δh expressed in mm of water. The effective least count of the manometer is 0.02 mm, so the least speed that can be measured with ± 10% precision is 0.09 m/sec. The maximum air speed employed was 1.4 m/s.

The cavity and its support structure were placed inside the stagnation chamber. For this, the tunnel was modified by cutting out a space and placing a door in order to allow access to the stagnation chamber when required. Figure 7 shows a schematic view of the test section located in the stagnation chamber. The drawing is roughly to scale. When placed horizontally ($\alpha = 0°$), the test section obstructed an area of 25 3/4 × 15 47/64 in^2 (0.65 × 0.4 m^2). This reduction in flow cross-section represents 2.8% of the stagnation chamber cross-section and produced negligible effects on the distribution of air velocity approaching the test section. Indeed, a person could stand in the stagnation chamber a few feet from the cavity with no observable effect on the flow near the cavity.

2.1.4 Flow visualization

Borosilicate glass end plates contained the flow of air in the cavity while allowing optical visualization in the spanwise direction (z-direction in Fig. 1). The shadowgraph technique (illustrated schematically in Fig. 8) was the principal method used for flow visualization. Smoke generated from the tips of $TiCl_4$ sticks (due to the formation of microscopic water droplets, induced by the hygroscopic action of the HCl produced through a decomposition reaction) was also used. In several experiments where shadowgraph visualiza-

tion showed strong periodic pulsations in the cavity flow, a General Radio 1531-A Stroboscopic light was used to determine the pulsation frequencies. This was done by continuously adjusting the light source pulsing frequency until the structures in the flow had been "frozen" in place.

The flow-visualization studies were exploratory and largely qualitative. They allowed quick identification and approximate location of various flow features. Because of this modest aim, comparatively simple light sources were used and no great effort was made to obtain an exactly parallel beam of illumination. As a result, the shadowgraph image, formed on a sheet of vellum which covered one window of the wind tunnel or was held in a frame when the cavity was in the room, was somewhat fuzzy. The image was also quite sensitive to the exact placement of the light source (either a 1000-Watt Argon-Xenon lamp with collimating lens, or a 300-Watt Kodak slide-projector lamp). The lamp was always placed so that the optical axis coincided roughly with the z-axis of our coordinate system.

Stills and movie films were made of free and mixed convection flows for a variety of experimental conditions. The stills were taken with an Autoreflex A Konica camera and the movies were made with an electrically driven Paillard Bolex H 16 camera. In all cases, Tri-X 400 ASA Kodak film was used. The results are presented and discussed in Section 3.

2.1.5 Laser-Doppler velocimeter (LDV) and related instrumentation

In free-convection flow, simultaneous two-component measurements of mean velocity and turbulent stresses were made using the laser-Doppler velocimeter technique in backscatter mode; see Drain [1980] and Durst et al [1976]. For measurements inside the cavity, where data rates were low, the one-component mode was used.

The velocimeter and some of its associated instrumentation are shown in Figs. 9. The velocimeter comprised a 2 Watt Lexel Argon-Ion water-cooled laser, a mirror stage for reflecting the laser beam 180° into the velocimeter optics, and the optics. The optics were of the DISA 55X Modular Series and consisted of: two separately adjustable 1/4-wavelength retardation plates; a 50:50 neutral beam splitter; a 55N10 Bragg cell section (with corresponding electronic downmixers); a color beam splitter; a backscatter unit (containing a mirror inclined 45° with respect to the velocimeter optical axis, and serving to support at right angles to the optical axis the photomultiplier optics consisting of: a color separator; two interference filters; and two RCA-4526 photomultiplier tubes); a pinhole section, a beam translator; a beam expander; and a 505 mm achromatic focusing lens.

The velocimeter optical probe volume was formed by the intersection of two pairs of beams at right angles, one beam being common to each pair and containing both radiation wavelengths: 514.5 nm (green), and 488 nm (blue). In this way two sets of fringes were formed at right angles. Table 2.1 provides a listing of the relevant optical parameters for each wavelength as used in the experiment.

The laser and velocimeter optics were mounted to the top of a thick aluminum table, which was itself firmly bolted to an x, y, z traversing mechanism. The traversing mechanism could displace the table top ± 7.5 cm. in 5 μm increments along any of the coordinate axes by means of three linearly encoded stepping motors interfaced with a PDP 11/34 minicomputer. The minicomputer functioned as the central data acquisition and reduction controller. In addition to directing the spatial sequence of an experimental run, the computer was programmed to conduct the acquisition, statistical processing and storage

of Doppler data validated and measured by two DISA 55L96 Doppler signal processors.

The minicomputer has a 256 K 16 bit random access memory and is equipped with dual hard RL01 magnetic disc drives (5 Mbytes each). Various input and output devices are interfaced with the minicomputer through UNIBUS lines. The minicomputer interacts with these devices by means of system or user-written control programs. Commands from a console terminal or other input devices go through the UNIBUS lines directly to the minicomputer to perform the sequence of table movements, data acquisition, data statistical processing, data storage, and data printing, etc. Further discussion on the use of the computerized data acquisition and processing system is given in Section 2.2.2 below.

2.2 Experimental Conditions and Procedure

This section describes the conditions and methodology followed for conducting mixed and free convection experiments.

Most of the flow visualization and temperature measurements were performed inside the subsonic wind tunnel in Hesse Hall. Practical considerations precluded moving the rather bulky and very sensitive LDV/minicomputer system from its permanent location to Hesse Hall, in order to conduct velocimetry experiments in the wind tunnel. Instead, the more portable test section and its support structure were moved to the 5th floor of Etcheverry Hall, the location of the computerized LDV data acquisition system. Unfortunately, this limited LDV measurements to the free convection regime.

It should be remarked that, in principle, there is no reason why LDV experiments should not be possible in the wind tunnel. However, there are specific reasons why these would be difficult to perform. The long path

lengths required of the laser beams to access the interior of the wind tunnel, index of refraction variations due to large temperature changes, and low data rates due to the difficulty of seeding large volumes of air, contribute to the difficulties of performing accurate LDV measurements in a reasonable amount of time.

2.2.1 General considerations for mixed and free convection experiments

When the cavity was in the wind tunnel, its axis of rotation was horizontal and perpendicular to the direction of the air flow. It was placed slightly to one side of the tunnel centerplane, about 0.5 meters downstream of the last wind tunnel screen. Although thermal radiation from the cavity undoubtedly transferred heat to the screens, this resulted in no measurable preheating of the air approaching the cavity.

The flow in the test section of the wind tunnel, when the stagnation chamber is unobstructed, is very uniform and quiescent, with an approximate turbulence level, $(\overline{u^2})^{1/2}/U_\infty \approx 2 \times 10^{-4}$. One can argue that the contraction ratio, R = 14, reduces the turbulence level by a factor $\approx R^2$, so in the stagnation chamber we can expect $(\overline{u^2})^{1/2}/U_\infty \approx 0.04$.

The bulk of the mixed and free convection experiments were performed for average wall temperature conditions differing only slightly from the following values:

$$\begin{aligned} T_{bot} &\approx 673 \text{ K } (400°C) \\ T_{bac} &\approx 673 \text{ K } (400°C) \\ T_{top} &\approx 611 \text{ K } (338°C) \\ T_\infty &\approx 295 \text{ K } (22°C) \end{aligned} \qquad (2\text{-}3)$$

For these values:

$$T_c \simeq 652 \text{ K } (379°C)$$
$$\Delta T/T_\infty = (T_c - T_\infty)/T_\infty \simeq 1.21 \qquad (2\text{-}4)$$
$$Gr = (g\Delta T\, b^3)/(T_\infty\, \nu_\infty{}^2) \simeq 4.2 \times 10^7$$

The actual experimental conditions for specific combinations of cavity aspect ratio and inclination angle are shown in figures and data listings provided in this work, and in Table 3.1. Typically, variations in corresponding average wall temperatures between runs were less than about 4%, leading to similar values in the variations of $\Delta T/T_\infty$ and Gr between runs. Table 3.1 shows that Gr/Re^2 was varied between 0.55 and a number which ranged from 110.4 to 718.9 for experiments in the mixed convection regime. The Reynolds number, $Re = b\, U_\infty/\nu_\infty$ was varied between 0 (pure free convection) and 8740, corresponding to the highest velocity investigated in the mixed convection regime.

Whereas the free convection experiments conducted in the wind tunnel were protected from variations in ambient conditions, particularly air drafts, special care was taken to minimize the influence of disturbances in the LDV experiments performed outside of the wind tunnel in free convection regime. To achieve this, a heavy semi-permeable canvas cloth was draped around a boxlike frame surrounding the test section and its support structure. The frame had a base of cross-section 1.5×1.5 m^2. A 0.3 m gap between the floor and the bottom edge of the cloth allowed the entry and flow of air vertically upwards, past the test section. Two small holes in the sides of the canvas permitted optical access for LDV measurements and shadowgraphs at the level of the cavity. In addition to this precaution, the ventilation in the room where the test section was located was shut off prior to and during the LDV experiments. Similarly, doors and windows in the room were kept closed, and move-

ments of the experimenters in the immediate vicinity of the cavity were kept to a minimum during measurement. The room was large enough so that stratification of air in the surroundings was negligible during the course of an experimental run. Subsequently, measurements and flow visualization showed that the large buoyant forces set up in the cavity rendered the flow fairly insensitive to residual perturbations in the surroundings and the possible influence of the canvas cloth.

Before an experimental run, the cavity inclination angle and aspect ratio were set to the desired values. The cavity was brushed clean of copper oxide scale formed from previous runs. Power was then applied to the strip heaters until steady state conditions had been achieved, as indicated by the measurements of temperature at the cavity walls. This warm-up period lasted about 2 1/2 to 3 hours.

For the studies in the wind tunnel, changes in wind speed had little effect on the surface temperatures of the cavity, the gas temperatures responded swiftly to changes in wind speed, and the photographs and temperature data could be taken as soon as the new wind speed was stabilized and measured. Each of the twelve aperture plane thermocouples was read 100 times at one-second intervals, so the time for each run was approximately 25 minutes. Runs in which LDV data were gathered were much more time-consuming, typically lasting five hours. The long-term stability of the temperature control system, and - to a lesser degree - the constancy of ambient conditions, were obviously important. These long tests were ordinarily run at night.

In mixed convection, an experimental run consisted in making measurements of temperature and photographing the flow for a range of Gr/Re^2, using the

techniques of Section 2.1. In free convection, a run consisted in making detailed measurements of the mean velocity and turbulent stress components of the flow at various locations, including the cavity aperture plane. Special considerations relating to the LDV technique are described in the next section.

2.2.2 Special considerations for LDV measurements in free convection

Alignment

Prior to its use, the LDV optical system was aligned internally to permit simultaneous measurement of two velocity components in the back-scatter mode. The alignment instructions provided by the LDV manufacturer (DISA), and those recently documented by Turi [1981] for the present system, served for this purpose.

The optical system was then aligned relative to the cavity test section. The optical probe volume formed by the intersection of the converging laser beams was centered on the top (or bottom) corner of the cavity aperture, on the cavity symmetry plane. For heated wall conditions, the control volume could be placed to within ± 0.3 mm in the x and y directions, and within ± 2 mm in the z direction.

After successful tests of symmetry, measurements in the x-y plane were restricted to the symmetry plane, z = 0 in Fig. 1. To avoid having to pass one laser beam through the cavity window during measurements in the aperture plane, the optical axis was slightly tilted, as shown in Fig. 10. This tilt was ignored in the data reduction, causing a systematic error less than 0.06 percent.

The above procedure permitted measurements of U, V, $\overline{u^2}$, $\overline{v^2}$ and $\overline{uv}$. To measure W and $\overline{w^2}$ (and also to check the values found for U and $\overline{u^2}$) the cavity

was turned 90 degrees by rotating the test section stand about its vertical axis. In this way the optical axis of the velocimeter was aligned normal to the projected cavity aperture plane to within ± 0.01°.

With the LDV system aligned relative to the test section, pre-chosen measurement locations were read to the computer software controlling the motorized traversing mechanism and automatic data acquisition. As a precaution and check, at the end of a profile scan the optical volume was restored to its starting point by a reversed sequence of commands.

For performing x-y plane measurements in inclined cavities ($\alpha > 0°$), it was necessary to rotate the velocimeter optical system by the amount of the cavity inclination angle in order to preserve the original relative orientation of the light beams with respect to the cavity. Because the internal alignment of the velocimeter optical system is independent of rotation about its optical axis, the optical probe volume dimensions, the probe volume location, and the quality of the interference fringes remained essentially unaltered.

Data Validation and Storage

Figure 11 schematically describes the velocimeter-control, signal-processing, and data-reduction hardware. Doppler signals, initiated by the passage of vegetable oil droplets through the optical control volume, are detected by the photomultiplier tubes and sent to separate, calibrated DISA 55N14 electronic downmixers. In this way the 40 MHz optical shift imparted by the 55N10 Bragg cell to the Doppler signals was reduced electronically to a net shift of 0.5017 MHz per channel. Each electronic downmixer was connected to a DISA 55L96 signal processor or "counter" for signal validation and frequency determination. Prior to determining the final signal frequency, each

counter imposed a 5/8 validation criterion on its respective Doppler signal, subject to a pre-selected comparator accuracy (6% in the present work). Signal amplification and threshold settings on the counters were fixed to maximize the data rate; due to the low air speed and oil droplet density the data rate displayed by the counters was probably never higher than 100 Hz on either channel. The optimized settings led to between 20 and 50% data validation on the counters.

For two-component measurements, signals validated on the counters were checked by a coincidence logic circuit (see Fig. 11) to ensure that the signal in each counter had originated from the same particle. To achieve this, a 25 μs coincidence window was allowed between validated signals from the two counters. Thus, validated signals separated by more than 25 μs were rejected. In the case of one-component measurements performed inside the cavity, the amplification gain on the unwanted counter (the undesired velocity component) was set high so as to obtain the highest data rate possible on that channel. In this way, the validated signal rate from the desired channel was not restricted by the coincidence window check.

The coincidence circuit was wired on a logic conversion circuit (LCC) board which in turn was wired between the counter output ports and the DR11-L interface board (a product of Digital Equipment Corporation). The first signal validated by either counter was sent to the LCC where it awaited a second signal from the other counter. The counter issuing the first validated signal was inhibited by the logic circuit in the LCC. If the second signal came within 25 μs, the logic conversion circuit sent triggering pulses to activate both counters and restart the measurement sequence. The DR11-L interface board consists of two ports to handle two separate devices. Signals

in binary form are transmitted in parallel. Each port has two 16-bit words, one for the Control Status Register (CSR), and one for the Data Buffer Register (DBR). These two registers are viewed as two memory locations by the PDP-11 Central Processor. When validated signals from both counters satisfied the coincidence check, Data Ready and Request bits on the CSR were set, and the counter data was sent to the DBR.

A handshake module loop was programmed in software to continuously check the Request bit setting. If the Request bit was set, data located in the DBR was fetched by the computer and stored in a temporary array. Then arming pulses were issued to the counters through the logic conversion circuit to activate them and restart a new sequence of measurements at the same location until a predetermined sample size was obtained. A conservative estimate of the time interval between a successful data acquisition and counter activation was about 0.6 ms, whereas the mean interval between successful acquisitions exceeded 10 ms.

In the present work, sample sizes of 1000 separate realizations were used for two-component measurements while samples of 500 realizations were used for one-component measurements. Upon completion of data acquisition at a measurement location, the data collected was processed statistically and stored in a permanent file. The software package then directed the stepping motors to the next measurement location where a new sequence of signal detection, validation, coincidence check, handshaking, data processing and storage, occurred.

The low data rates encountered in the experiments dictated the samples of 1000 or 500 Doppler signal realizations per measurement location. This choice of sample sizes was determined by the practical consideration of having to complete the experiments in a reasonable amount of time but with acceptable

precision. Measurements consisting of samples of 1000 data points were taken in the cavity aperture plane and outside of the cavity, where the data rate was higher. At these locations two-component velocity determinations were made and the coincidence check was imposed. The measurements consisting of samples of 500 data points were taken inside the cavity where the data rate was lower. To raise the data rate inside the cavity, measurements were restricted to a single velocity component in order to bypass the coincidence check. While this practice yielded less velocity component information per measurement location, it raised the data rate within the cavity to a level comparable to that in the aperture plane and outside; effectively, 10 to 50 Hz. Subsequent checks (discussed further on) showed that the sample sizes chosen were sufficiently large to obtain values of mean velocity and turbulent stresses with sufficient precision for the requirements of this study.

Seeding Considerations

Vegetable oil droplets were generated by a pressure-regulated blast atomizer of the type described by Drain [1980] to provide a seeding level adequate for practical measurement purposes; see Fig. 12. The droplets ranged in size from 0.2 to 2 μm, as measured optically by means of a microscope. The flow from the blast atomizer was injected into a plenum chamber which was connected to an airline to allow redistribution of the seeding agent. The seeded flow was connected to both ends of a metal tube 1.27 cm in diameter from which it issued through a narrow slot, 17.8 x 0.64 cm^2. In this way, the droplets were gently blown upwards into the buoyancy-induced draft, which entrained them into the heated cavity. Care was taken to ensure that the jet issuing from the slot did not perturb the buoyant flow in and around the cavity. This was guaranteed by positioning the slot below the cavity at a distance of 1 m.

Unfortunately, many particles never reached the measurement locations. Instead, they were carried off to the sides, or behind the cavity, by the buoyancy-induced draft of air. To reduce particle loss, a plywood board was placed beneath the cavity test section as shown in Fig. 12. It was verified by flow visualization that the presence of this board did not alter the fluid mechanic characteristics of the flow occurring in the cavity or its vicinity. The tent-like enclosure surrounding the test section also served to confine the particles to the vicinity of the test area.

In spite of these efforts, the number of oil droplets per unit volume was probably not perfectly uniform throughout the region in which LDV measurements were made. The possibility of a resulting systematic error is analyzed in Section 4. Errors due to a possible slip velocity between the air and oil droplets or due to the difference in density between these two fluids were shown to be negligible. This was done by substituting physical properties for the two phases into the integrated form of the equation of motion for a particle in a moving fluid given by Tchen [1947]. For the case of interest here the equation reduces to

$$u_p(t) = u_f(t) - C_t \tag{2-5}$$

where $u_p(t)$ is the velocity of the particle at time t, $u_f(t)$ is the velocity of the fluid and

$$C_t = \frac{2}{9} \frac{g\, r^2}{\nu} \frac{\rho_p - \rho}{\rho} \tag{2-6}$$

is the terminal velocity of a spherical particle falling in a fluid at rest, when the velocity of fall is slow. In eqn. (2-6) r is the particle radius, g the gravitational constant, ν the kinematic viscosity of air, ρ_p the density

of the oil and ρ the density of air. For the present case $C_t \simeq 10^{-7}$ m/s and it follows that, except for exceedingly low speed flows, the particle and fluid velocities are essentially the same. Since the smallest measured fluid velocity was greater than 10^{-3} m/s, particle free fall effects had no influence on the measurements obtained.

The response of particles to turbulent fluctuations in the flow was also considered. Using results from the study by Dring [1982] it is possible to show that particles with a Stokes number:

$$St = \frac{\rho_p \omega 4r^2}{18 \nu \rho} \tag{2-7}$$

less than 0.14 will follow oscillations of frequency ω with better than 99% speed accuracy and with less than 8° in phase lag. For oil droplets of maximum size 2 μm the corresponding frequency is ω_{max} = 12,500 Hz, approximately. Since this frequency is at least two orders of magnitude greater than the highest frequency expected in the present flow it is concluded that the particles responded faithfully to the fastest turbulent fluctuations.

Statistical Data Reduction

Mean velocities and turbulent stresses were determined from the formulae listed below:

$$U = \frac{\sum_{i=1}^{N} U_i \omega_i}{\sum_{i=1}^{N} \omega_i} \tag{2-8}$$

$$V = \frac{\sum_{i=1}^{N} V_i \omega_i}{\sum_{i=1}^{N} \omega_i} \tag{2-9}$$

$$W = \frac{\sum_{i=1}^{N} W_i \omega_i}{\sum_{i=1}^{N} \omega_i} \tag{2-10}$$

$$\overline{u^2} = \frac{\sum_{i=1}^{N} (U_i - U)^2 \omega_i}{\sum_{i=1}^{N} \omega_i} \tag{2-11}$$

$$\overline{v^2} = \frac{\sum_{i=1}^{N} (V_i - V)^2 \omega_i}{\sum_{i=1}^{N} \omega_i} \tag{2-12}$$

$$\overline{w^2} = \frac{\sum_{i=1}^{N} (W_i - W)^2 \omega_i}{\sum_{i=1}^{N} \omega_i} \tag{2-13}$$

$$\overline{uv} = \frac{\sum_{i=1}^{N} (U_i - U)(V_i - V) \omega_i}{\sum_{i=1}^{N} \omega_i} \tag{2-14}$$

In the above formulae N is the sample size. It consists of the total number of instantaneous realizations, i. The quantity ω_i is the weight factor for the i'th realization. If $\omega_i = 1$ the simple arithmetic mean is obtained; equal weight being given to each measurement.

Many authors, following McLaughlin and Tiederman [1973] have observed that equal weighting is inappropriate in principle, even for a uniformly-seeded fluid, because fast-moving particles will traverse the optical probe volume more frequently than slow ones. Buchave et al. [1979] conclude from this that the proper weight factor is the duration of the signal returned from the ith scattering particle, Δt_i. Thus the time-averaging integral operation

$$U = \frac{1}{t}\int_{t_o}^{t_o+t} u(t')dt' \qquad (2\text{-}15)$$

is to approximated by

$$U = \sum_{i=1}^{N} U_i \Delta t_i \Big/ \sum_{i=1}^{N} \Delta t_i \ . \qquad (2\text{-}16)$$

The signals returned from fast particles are given smaller weights in the sum, in a way which exactly compensates for their abnormally frequent appearance.

Before trying to use equation (2-16), we need assurance that nothing in the signal-processing chain discriminates against particular signals, because of the speed of the light-scattering particle. This could happen, for example, if the computer were not ready to examine a new signal whenever it arrived, thus discriminating against the more closely-spaced signals from fast-moving particles. In our work, the mean time between signals exceeds the computer processing time by a factor of at least 30, and this particular worry can be dismissed.

One might also worry that particles passing through the optical probe volume on trajectories nearly parallel to the fringes would escape detection, by failing to cross the requisite number of fringes. However, in our tests the fringes themselves sweep across the probe volume with a speed approximately equal to 3.5 m/s. This exceeds the highest measured particle speed by a factor of at least three, and insures that a particle will cross eight fringes while the particle is actually moving only about 1.5×10^{-5} m. This distance is only about 10^{-4} times the probe volume diameter, so the particle is extremely unlikely to escape detection by running away from the fringes.

Unfortunately, our data acquisition computer was not programmed to record the duration of each burst, and we could only estimate Δt_i from the measured values of U_i and V_i, the two velocity components normal to the axis of the optical probe volume. Because the probe volume is very slender, the axial component of particle speed has very little effect on the duration of the burst. Thus, when the two-component system was in use, equation (2-16) could well be replaced by

$$U = \sum_{i=1}^{N} U_i (U_i^2 + V_i^2)^{-1/2} / \sum_{i=1}^{N} (U_i^2 + V_i^2)^{-1/2} \qquad (2\text{-}17)$$

When the one-component system was in use, the only data from which Δt_i could be estimated were: U_i; the speed of the fringes, V_f; the number of fringes crossed during the burst, N_f; and the distance between fringes, δ_f. Then

$$\Delta t_i = N_f \delta_f / (V_f + U_i) \qquad (2\text{-}18)$$

This would be an excellent estimate, except that the counter logic imposes a maximum value on N_f, equal to 255, and there is no provision for the recording of N_f.

Lacking any definitive estimates of particle residence time, we used two simple data-reduction schemes for the one-component measurements. The first was the simple equal-weight scheme for all signals, $\omega_i = 1$. The second assigned equal weight to all signals for which the measured velocity was less than 0.05 m/s, and a weight equal to $0.05/|u_i|$ for faster particles. Complete listings of both weighted and unweighted data are given in Appendix A.

Software for Data Acquisition and Reduction

Software was developed and programmed to perform the computerized data acquisition and statistical reduction discussed in this section. The details of the subroutines written to conduct these tasks are not important here. However, because much time and effort was put into developing a successful data acquisition and reduction package, listings of the subroutines are provided in Appendix C. In addition, a flow chart is provided for the interrelated subroutines. This information should be of value to researchers with requirements similar to those addressed in the present work.

3. RESULTS AND DISCUSSION

This section presents the results obtained from the experiment conducted in the heated cavity configuration for free and mixed convection regime. The results are discussed and interpretations of the phenomena observed are offered.

Table 3.1 shows the conditions investigated and the variables determined in the study. Conditions were limited to three aspect ratios (a/b = 0.5, 1.0 and 1.46) and three inclination angles (α = 0°, 20° and 45°). The table shows that in studies of mixed convection the parameter Gr/Re^2 was varied between 0.55 and 720 approximately. Except for a few experiments aimed at exploring small $\Delta T/T_\infty$ conditions, the bulk of the measurements were made for $\Delta T/T_\infty \simeq 1.21$ and $Gr \simeq 4.2 \times 10^7$. The precise experimental conditions are given in the tables and figures discussed in this section. Listings of the data are provided in Appendices A and B.

3.1 Free Convection

3.1.1 Flow visualization

Several movie films and many 35 mm stills were made of the heated cavity flow using the shadowgraph technique discussed in Section 2.1.4. Fig. 13 is a composite of typical free convection flows corresponding to the conditions listed in the caption. It is important to note that the cavity aperture plane dimension (b) was the same for all experiments. Unequal photographic reductions give the false impression that b varied.

The earlier free convection flow visualization experiment reported by Humphrey et al [1981] showed that residual fluctuations in the surroundings could affect the far field flow in the experiment. In the present work these

were virtually eliminated by conducting the experiment inside the wind tunnel plenum chamber, allowing air to be entrained through the trap doors; see Fig. 7.

Characteristic visible features of the flow included the following:

a) a strongly pre-heated boundary layer along the outer edge of the bottom heated plate.

b) separation of that boundary layer at the sharp entry corner, when $\alpha = 0°$ and 20°, with a highly unsteady reattachment about halfway along the bottom wall when $a/b = 1.46$ and 1.0, and reattachment on the back wall, at $x/b \simeq 0.25$, when $a/b = 0.5$. The size of the recirculation zone decreases as α is increased, and the zone is barely visible when $\alpha = 45°$.

c) irregular detachment of plumes from the thermally unstable bottom boundary layer, starting at values of y/b which increased with increasing α. It is believed, from the experiments of Rotem and Claassen [1969], Lloyd and Sparrow [1970], and Pera and Gebhart [1973], and from the theoretical calculations of Chen and Tszoo [1982], that these plumes manifest the instability of bottom-heated boundary layers on nearly horizontal plates, to longitudinal vortex instabilities. No clear evidence of Tollmien-Schlichting (transverse wave) type instabilities was seen, nor was it to be expected, according to Chen and Tszoo [1982].

The theory of Chen and Tszoo predicts critical values of y, at which this instability is first possible for a given overall Grashof number. For our standard condition, $Gr = 4.2 \times 10^7$, the critical values of y/b are shown in the first column of Table 3.2. The fourth column shows our fairly crude estimates of the position, y/b, at which the plumes seemed clearly visible. Our values are, of course, much larger than those predicted to mark the onset of

instability, since the disturbances grow fairly slowly. They show the same qualitative trends with α, as predicted by the theory.

For $\alpha = 0°$, we can make a comparison with the experimental result of Rotem and Claassen [1969]. Their result, $(Gr_y)^{1/3} = 80$ to 100, translates into $- y/b = 0.23$ to 0.28, in close agreement with our observed values. Similar agreement is found with the observations of Pera and Gebhart [1973]. To adapt the results of authors who assumed $\Delta T/T_\infty << 1$ for theoretical purposes, or who did experiments with small overheat, we have based our Grashof number on ambient-temperature properties. Had we used properties evaluated at a mean temperature, the corresponding values of $- y/b$ would be increased by about a factor of 2.

We believe that this instability plays a key role in initiating the unsteadiness and eventually the turbulence seen in our cavity, even at relatively low Grashof numbers. At first, it was suspected that the inflexional instability of the separated flow near the bottom lip of the cavity might be the trigger for unsteadiness, and a temporary turning vane was installed - to show what would happen when the separated zone was nearly eliminated. The flow became a bit more steady as a result, but the thermally-driven instabilities grew as before and the flow could still not be made steady.

d) a thin hot boundary layer on the back wall, into which the bottom boundary layer and some of the plumes emerging from the latter are entrained.

e) a fairly sharp, stably stratified, roughly horizontal thermocline, which marks the bottom of a comparatively quiescent pool of hot air. This pool receives the back-wall boundary layer and the plumes which have escaped entrainment. When $\alpha = 45°$, and to a lesser extent when $\alpha = 20°$, the discharge of the back-wall boundary layer into this pool is very reminiscent of the bottom of a waterfall, upside-down.

f) a fairly sharply-defined outflow from the hot pool, which separates from the upper edge of the aperture, reattaching soon thereafter, particularly when $\alpha > 0°$.

The flow visualization also gave a clear impression of the effects of a/b and α, on the degree of unsteadiness of the flow. Our observations generally support the notion that the unsteadiness originates in the instability of the bottom boundary layer, to wit:

1) Increase of α, at fixed a/b, generally reduced the degree of unsteadiness. As α increases, the onset of plume formation is moved toward the back wall, so that a smaller fraction of the cavity volume is involved with plume motion. Plumes formed near the rear of the cavity, at $\alpha = 20°$ and especially at $\alpha = 45°$, rise only a short distance before merging with the backwall boundary layer or penetrating the thermocline. This restricts the size and vigor of unsteady motions associated with the plumes.

2) Increase of a/b, at fixed α, generally increases the degree of unsteadiness, especially at the lower values of α. It increases the fraction of cavity volume that can be involved with plumes, at least until the bottom of the back wall retreats beyond the line where the thermocline intersects the bottom wall. (This happens at $\alpha = 45°$, once a/b exceeds about 0.8.)

3) Unsteadiness can be almost completely suppressed by increasing α and decreasing a/b. Thus for $\alpha = 45°$ and a/b = 0.5, the flow is almost perfectly steady.

In most cases, the hot air above the thermocline appeared to act as a sort of shock absorber, quickly reducing the vertical velocity of warm air parcels which are positively buoyant below the thermocline, and negatively buoyant above it. At $\alpha = 45°$ there was a prominent, nearly steady penetrating

and rebounding current where the backwall boundary layer enters this top layer. A stationary wave on the thermocline accompanies this structure, and is clearly seen in the lower right frame of Fig. 13. The current was made more clearly visible with smoke from $TiCl_4$ sticks.

3.1.2 Measurements of temperature

Normalized mean temperature profiles across the aperture plane of the cavity are given in Figs. 14 to 22 for both free and mixed convection flows. The profiles corresponding to $Gr/Re^2 = \infty$ (or $Re = 0$) are the ones of interest here. They display the following general characteristics.

a) For all aspect ratios and inclination angles, steep temperature gradients and high levels of fluctuation are observed near the top and bottom of the aperture plane. The hot layer near the bottom edge, which is associated with the separation of flow from that edge, is essentially independent of a/b, and becomes thinner as α is increased. The hot layer in the top third of the aperture plane is thickest when a/b and α are both largest. Its profile changes more with α, at fixed a/b, than vice-versa. At $\alpha = 45°$, the entire temperature distribution is essentially independent of a/b.

b) The fluctuation levels, represented in the figures by bars of length 2σ, are substantial in the region of high gradient, for all α and a/b. However, they decrease as α increases, especially in the lower layer. The fluctuations also diminish, particularly in the upper layer, when a/b is increased at constant α. This may be due to the increasing volume of the "shock-absorbing" hot pool but, with the data available, it is risky to propose an explanation of these trends. We should be reminded, too, of the limited frequency resolution of these measure-

ments.

c) Especially when $\alpha = 45°$, $\partial T/\partial x$ is very nearly constant across the upper heated flow, having a value of about 8850°K/m. If we assumed that the isotherms are nearly horizontal in this region, the vertical temperature gradient would be about $\sqrt{2}$ times as large. Taking the mean temperature to be about 475°K, we can estimate a Brunt-Vaisala frequency for the hot layer, of magnitude

$$N = \left(\frac{g}{T}\sqrt{2}\,\frac{\partial T}{\partial x}\right)^{1/2} \approx 16 \text{ Hz} .$$

This estimate is intended to give an upper limit to the frequency of internal waves that might propagate in this stably-stratified region. It cannot be taken too seriously, since the region is also sheared, bounded by a nearly isothermal region on the bottom, and by a strongly-sloping roof above. Of special interest is the possibility of resonant standing-wave modes with horizontal wavelength equal to twice the length of the thermocline. A highly simplified linearized analysis in Appendix D suggests that these would have frequencies of order N/3 or N/4. These preliminary ideas are relevant to a discussion of periodic, finite-amplitude oscillations observed in the mixed-convection regime.

3.1.3 Measurements of velocity and turbulent stress components

The bulk of the velocity and turbulent stress data were measured on the cavity symmetry plane, $z/(c/2) = 0$ in Fig. 1. Figure 23 shows the actual locations scanned in the symmetry plane. A limited number of measurements were also performed to check the degree of spanwise uniformity in the flow.

The results are shown in Fig. 24a and 24b, and they strongly support the notion of a flow which is essentially two-dimensional in the mean. Earlier measurements of temperature by Humphrey et al [1981] also revealed spanwise uniformity. Further checks on flow symmetry were considered unnecessary and were not performed. The measurements obtained on the cavity symmetry plane locations indicated in Fig. 23 are plotted in Figs. 25 to 30 and are discussed below.

Flow Through and In Front of the Aperture Plane

Three configurations were selected for exploration by Laser-Doppler velocimetry. The results are plotted in Fig. 25 a,b,c for $a/b = 0.5$, $\alpha = 0°$; in Fig. 26 a,b,c for $a/b = 1.0$, $\alpha = 0°$; and in Fig. 27 a,b,c for $a/b = 1.0$, $\alpha = 45°$. For additional clarification and comparison, Fig. 31 a,b,c,d shows the aperture-plane profiles of V and T, superposed, with bars to indicate the fluctuation levels on the same scales. The length of each bar is twice the standard deviation of the fluctuating values of the corresponding quantity. Fig. 31 emphasizes the fact that these are highly fluctuating velocity fields, and confirms the impression gained from flow visualization and temperature measurements: that the fluctuations are most vigorous in the shallow cavity at $\alpha = 0°$ and least vigorous in the deep cavity at $\alpha = 45°$. Figure 31d directly compares the three V(x) profiles, without the indications of fluctuation level. Note that the strength of inflow and outflow increase as a/b increases from 0.5 to 1.0, and then as α increases from 0° to 45°, but that the profiles become more nearly symmetric about $x/b = 0.5$ as this happens. Numerical integration shows that the net volume flow rate out of the cavity shows just the opposite trend.

Figure 32 compares the time-averaged streamline fields in the region just in front of the cavity (the region bounded by planes a-b-c-d in Fig. 23). Numerical values of the stream function around most of the boundary could be computed from the measured velocity and temperature data, or with an assumption that $T = T_\infty$ on portions of the boundary when the shadowgraph pictures show no temperature disturbance. Flow directions were measured all around the boundary. Streamlines were then sketched by eye, at equal increments of stream function. Figures 32 a,b confirm what has been said before (Section 3.1.1) about the separation bubble near the bottom edge of the aperture plane, and adds the somewhat surprising information that the time-averaged streamline actually springs outward from that corner, before turning sharply back inward. This feature has disappeared when the cavity is inclined to $\alpha = 45°$.

A few measurements were made farther in front of the cavity, which showed that the velocity is less than 0.01 m/sec if $x/b > 1$. Although the flow in the far field is induced mostly by the buoyant plume rising from the cavity itself, it was noted that the outer test section surfaces became as warm as 40 - 70°C, depending on location, so that some of the induced far-field flow - and in particular, some of the fluctuations in the flow approaching the cavity from below, may be due to these more widely distributed sources of buoyancy.

Several features of the measured turbulent stress components deserve comment:

1) The flow entering from below across the outward extension of the bottom wall ($x/b = 0$, $y > 0$) was virtually devoid of the turbulent shear stress $\overline{u'v'}$, although it was highly sheared out to about $y/a = 1/8$. By contrast, $\overline{u'v'}$ reached substantial values on the corresponding extension of the top wall. (See Figs. 25c, 26c and 27c).

2) The turbulent kinetic energy is by no means isotropically distributed anywhere in the flow. There are striking increases in the horizontal components, $\overline{v'^2}$ and $\overline{w'^2}$, but usually a slight decrease in the vertical component, $\overline{u'^2}$, in the stably-stratified region, $x/b > 2/3$. (See Figs. 25b and 26b). Even at $\alpha = 45°$, where u' and v' are equally inclined to the vertical, $\overline{u'^2}$ is systematically quite a bit smaller than either $\overline{v'^2}$ or $\overline{w'^2}$. Of course, all these observations must be accepted with caution, because of the "false turbulence" engendered by index-of-refraction fluctuations. The characteristically lower values of $\overline{u'^2}$ are seen, however, even well in front of the cavity, where the laser beams should be traversing mostly isothermal air.

3) To the extent that we can estimate $E_{xy} = \partial V/\partial x + \partial U/\partial y$ along the aperture plane and along the outward extensions of the top and bottom walls, we infer the following relationship between $\overline{u'v'}$ and E_{xy}.

   a) Along $x/b = 0$, $y/b \gtrsim 0.02$: $E_{xy} < 0$, while $\overline{u'v'} \approx 0$.

   b) Along $x/b = 1$, $y/b \gtrsim 0.04$: $E_{xy} < 0$ while $\overline{u'v'} > 0$.

   c) In the upper half of the aperture plane: $E_{xy} > 0$ while $\overline{u'v'} > 0$.

   d) In the lower half of the aperture plane, where $0.05 \lesssim x/b \lesssim 0.5$, $E_{xy} > 0$ while $\overline{u'v'} < 0$.

   e) Very close to the bottom wall, but on the upper side of the separation bubble, $E_{xy} < 0$ while $\overline{u'v'} > 0$.

Qualitatively, these relationships imply a positive eddy viscosity in the regions of unstable or ineffectual density stratification, but a <u>negative</u> eddy viscosity in regions of strong <u>stable</u> stratification. In the latter regions the product $-\overline{u'v'}\,E_{xy}$, which ordinarily is positive and represents a transfer

of kinetic energy from the mean-flow account to the eddy account, is locally negative and thus represents a reverse transfer. Such a transfer has been shown to take place in stably stratified shear layers, in the vicinity of the critical layer, at which the flow speed and the wave speed coincide. The linearized model of internal waves, shown in Appendix D, yields wave speeds in the range 0.1 to 0.3 m/sec. Since these lie in the range of our measured values of V, it is possible that we are seeing something like the absorption of internal waves at a critical layer; see Booker and Bretherton [1967].

Inner Flow

Limited, single component measurements of the flow inside a cavity with aspect ratio a/b = 1 were obtained for conditions of α = 0° and α = 45° respectively. As shown in Figs. 28 to 30, the measurements were taken along the planes x/b = 0.5 (U-component) and y/a = - 0.5 (V-component). For the case α = 0°, only unweighted data are available. Interception of the laser beams by the top wall in the cavity impeded near-wall measurements in this region of the flow. Likewise, beam deflection due to refractive index gradients precluded making measurements very near the back and bottom walls. The plotted results are in accordance with the observations made earlier. For both inclination angles the V-component profiles in Figs. 28a, 29a and 30a display the flow reversals corresponding to the separated recirculating flow region on the bottom wall. The profiles show clearly that inclining the cavity decreases the size of the recirculation zone.

To illustrate graphically the degree to which velocity bias can affect the measurements if it is not corrected, unweighted (simple arithmetic average) velocity and normal stress profiles were obtained from the data for a/b = 1.0 and α = 45°. The results are plotted in Figs. 30 and should be com-

pared with the corresponding profiles in Figs. 29. Since weighting decreases the relative contributions of large velocities to the average result (recall the discussion in Section 2.2.2) a small recirculation zone is shown in the weighted V-component profile plotted in Fig. 29-b. For the same reason, larger than normal scatter in the normal stress measurements is reduced when weighting is applied. These considerations should be borne in mind when interpreting the unweighted measurements for a/b = 1 and α = 0° plotted in Figs. 28, particularly the normal stresses.

3.1.4 Mass flux and convective heat transfer

Volume and mass fluxes can be computed from the velocity and temperature data presented in Figs. 14 through 31. The quadratures employed the trapezoidal rule. The uncertainties assigned to the integrals were computed on the assumption that each velocity measurement had an uncertainty of ± 0.005 m/s.

Table 3.3 shows the convective heat fluxes, calculated by application of equations like (1.10) to the surfaces a,b,c and d shown in Fig. 23. Since these surfaces entirely surround a region within which there are no heat sources, the sum $\sum \dot{Q}_i$ should equal zero. Positive entries in the table denote heat flux out of the enclosed volume.

The predicted statistical uncertainty in $\sum \dot{Q}_i$ suggests that the residuals are statistically significant and hence indicative of some systematic error in the velocity data or its interpretation. This will be discussed further in Section 4.

Table 3.4 presents more detailed results for surface (b), the aperture plane. The integral is separated into two parts, one covering that part of the aperture where there is outflow; the other covering the inflow. The predicted standard deviation of the net outflow again is based on a ± 0.005 m/s

uncertainty in each measured value of V. We see clearly that the trend in the net outflow, versus a/b and α, is opposite to the trend in $\dot{Q}$ (in) or $\dot{Q}$ (out). We also can see how sensitive $\dot{Q}$ (net) is to any small systematic uncertainty in the measurement of V.

For the aperture plane, where temperature was also measured, we can estimate mass flow rates by use of the quadrature

$$\dot{m}_b/c = \int_0^b \overline{\rho}\, V\, dx = \frac{p_\infty}{R} \int_0^b (V/T)\, dx \ . \qquad (3\text{-}1)$$

Table 3.5 shows the results of this calculation, again broken down into inflow, outflow and residual. It also shows the average densities of the inflow and the outflow, calculated from

$$\overline{\rho}_{in}/\rho_\infty = (\dot{m}_b(in)/\dot{Q}_b(in)) \frac{\gamma}{\gamma - 1} R\, T_\infty \qquad (3\text{-}2)$$

and a similar formula for $\overline{\rho}_{out}$.

The average densities seem remarkably independent of a/b and α, as though they depended only upon Gr and $\Delta T/T_\infty$. The fact that $\overline{\rho}_{in}/\rho_\infty < 1$ is due mostly to preheating of the air by the outer surfaces below the cavity.

Of course, for turbulent flow we do not expect the quadrature (3-1) to give an accurate mean value of the mass flux, because density and velocity fluctuations may be correlated. This is discussed in greater detail in Section 4.

Table 3.6 displays our final heat transfer results, reduced to heat transfer coefficients and Nusselt numbers according to equations (1-11) and (1-12). The uncertainties noted here are directly proportional to the values of σ(net) shown in Table 3.4. They are based on the observed scatter of

measured velocities and include no allowance for possible systematic errors. The latter are discussed in Section 4.

There is, at present, no secure standard against which to test the accuracy of these results. There is the experiment of Mirenayat [1981], in which a cubical cavity heated on all sides was employed. This situation is very different from ours, but Mirenayat observed about the same fractional reduction of heat loss as we did, when α is increased from 0° to 45°.

We note that Mirenayat and other authors have based their overall heat transfer coefficients on the total area of the heated walls, rather than the area of the aperture plane. If our data is reduced on this basis, the heat transfer coefficient for a/b = 0.5 is reduced to 7.5 ($W/m^2°K$), while those for a/b = 1 are reduced by a factor of three, to 2.5 and 1.5 ($W/m^2°K$). This enhances the contrast between the results for a/b = 0.5 and a/b = 1.0.

3.2 Mixed Convection

Before discussing the experimental results for mixed convection, we consider some very rough models of the purely forced flow.

Figure 33 shows the distribution of velocity over the upstream face of an inclined flat plate, in two-dimensional potential flow. That flow surrounds both the plate and a dead-air wake, in which the pressure is the pressure of the unperturbed stream. The location of the stagnation point, relative to the shaded section of the plate - which represents the position of our cavity opening - is the principal feature of interest.

A comparable theoretical calculation for a plate indented by an upstream-facing cavity would be quite difficult, but it seems intuitively clear that the presence of the cavity would displace the stagnation point slightly away from the cavity.

The influence of the finite length of the cavity along its axis of rotation is potentially quite important. While b/c is quite small, the aspect ratio of the cavity plus its upward and downward extensions, $(b_1 + b + b_2)/c$, is not small, and the forced flow is bound to be significantly three-dimensional. Near the aperture plane, the resulting z-component of velocity will be, very approximately, $W \approx U(z/c) \cos \alpha$ for $2\ z/c \lesssim 0.7$, increasing more steeply thereafter, to $W \approx \pm U \cos \alpha$ at $z = \pm c/2$. This lateral flow divergence would presumably increase V somewhat in the region just in front of the cavity. More importantly, in the mixed flow, this divergence will stretch the vortex lines associated with the buoyancy-driven convection.

3.2.1 The experimental results

The tests performed with the procedures and instrumentation which have been described in Section 2 resulted in the photographs of Figs. 34-40 and the temperature profiles of Figs. 14-22. There were three general results of phenomenological interest, to wit:

a) a general stabilizing effect of weak winds;

b) periodic, two-dimensional oscillation of the cavity flow, in the presence of weak winds;

c) migration of the stagnation points of the time-averaged flow, from the competition between free- and forced-convection when $\alpha = 20°$ and 45°.

3.2.2 Qualitative effects of very weak winds

The most surprising and thought-provoking result of the mixed-convection experiments occurred with very weak winds, $U_\infty \approx 4$ to 6 cm/sec. These winds strongly inhibited the chaotic and three-dimensional fluctuations that characterized most of the free-convection flows, leading to flows that were either almost perfectly steady, or periodically oscillating. The effect was first

noticed when the forced flow was dying away after power to the blower was cut off. One could monitor the deceleration by noting the orientation of a small plume of hot air, which was originally swept downstream by the forced flow. When the plume was inclined about 10°-30° downstream, the flow in the cavity would be dramatically stabilized. Just after the plume became vertical, the cavity flow would burst into irregular fluctuations, which persisted until the blower was started again.

The wind tunnel speed was then held steady in the range 4 to 6 cm/sec, and quantitative evidence of the reduction of fluctuations was obtained. This appears in the contrast between the bottom two temperature profiles in each of Figs. 14-22. The bottom profile is for free convection; the next profile shows the effect of the weak wind. The cavity flow was not made perfectly steady, but fluctuations became either very periodic, or very few and far between. Because the temperatures were sampled periodically, at a frequency nearly equal to an integral fraction of the oscillation frequency, a striking reduction of the variance of the temperature samples does not necessarily discriminate between the steady flows and the periodic ones.

It seems likely that weak horizontal winds stabilize the cavity flow by two separate but cooperating mechanisms.

1) They carry away those wisps of vorticity that would otherwise separate from the bottom edge of the aperture-plane extension and be carried into the cavity by the buoyancy-induced flow. These might not be vigorous enough to be noticed by themselves, but might serve to trigger instabilities in the boundary layer on the heated bottom wall.
2) By stretching the vortex lines of the two-dimensional buoyancy-induced flow, they may inhibit the onset of the three-dimensional

instabilities, to which the bottom boundary layer is first subject (c.f. Chen & Tszoo [1982]). At the same time, they could enhance local concentration of span-wise (z-component) vorticity, which is essential to the onset of the oscillating two-dimensional instability, allowing it to reach finite amplitude first, even on nearly horizontal surfaces (c.f. Pera and Gebhart [1973]).

It is impossible to put these suggestions on a firm base of experimental facts, with the few and mostly qualitative observations we have, or to see theoretically just how the vortex stretching would work inside the cavity, where it must be inhibited by the glass windows. We simply record them here - hoping to return to the problem when competing research priorities are less pressing.

3.2.3 Periodic oscillations

The periodic oscillations shown in Figs. 39 and 40 seemed to be the natural outcome when α was between 0° and 20°, and a/b was 0.5 or 1.0. The oscillation frequencies were measured either by displaying a prominently fluctuating wire temperature on a chart recorder, or by "freezing" the shadowgraph image with stroboscopic illumination. The frequencies fell in the range 2.2 - 5 Hz, and the oscillating flows seemed quite two-dimensional[1]. The amplitude of oscillatory motion was highest near the top of the aperture plane, where well-formed blobs of hot air were periodically expelled from the cavity. A synchronous flapping of the backwall boundary layer and of the rearward part of the bottom boundary layer, was usually noticeable. Temperature fluctuations in the heated portion of the inflow, near the bottom of the aperture plane, were dramatically reduced.

****

[1]With only shadowgraph images, we could not definitely distinguish between two dimensional flows and flows that might have a periodic waviness in z.

Unfortunately, time and research priorities did not permit a comprehensive delineation of the parameter space in which oscillatory behavior occurs, but Table 3.7 summarizes such data as we gathered.

The reason for such prominent oscillatory behavior has not been conclusively demonstrated, but some possibilities have been identified and others have been tentatively eliminated. The scenario which we believe to be most likely involves a resonant sloshing motion of the upper, stably-stratified layer, in response to periodic impulses delivered to that layer at the rear of the cavity. These impulses would arrive as a consequence of an oscillatory instability of the bottom boundary layer, being transmitted mainly via a modulated momentum flux in the back-wall boundary layer. Since the distances between these layers are not large compared to the observed wavelength of the sloshing motion, an effective feedback loop via the pressure field may be a component of the observed process.

To sustain this hypothesis, we first rule out some less interesting possibilities, such as forcing at a frequency set by the speed of rotation and number of blades of the wind tunnel blower. This was done by achieving the same flow speed, and the same oscillations, at various different blower speeds, by varying the impedance of the wind tunnel circuit.

A second "external" cause, eddy-shedding from the sharp edges of the cavity extensions, is also easily ruled out. If we accept $St \equiv fL/U_\infty \approx 1/4$ as a basis for an estimate, and take $U_\infty = 0.05$ m/s and $L = 0.5$ m we get $f \approx 0.02 - 0.03$ Hz, which is far below the observed frequencies.

Highly simplified analyses of the possibility of a resonantly-forced sloshing mode of the stably stratified upper layer (see Appendix D), also yield eigenfrequencies close to those observed.

The possible role of barotropic instabilities of the separating flow at the entry lip of the cavity is very hard to assess. When the turning vane was used, this kind of instability would be suppressed, and indeed it then seemed harder, but not impossible, to find the oscillations. A theoretical estimate of frequencies to be expected was attempted, but was inconclusive because essentially nothing was known about the unperturbed base flow. It was easy to predict oscillations of the observed frequency by assigning a plausible mean speed of translation of the vortices into which the shear layer coalesces, but this procedure is arbitrary and unconvincing. On the positive side, we found clearly measurable temperature fluctuations in this layer when the cavity was oscillating, indicating either a locally generated instability, or feedback from oscillations generated by baroclinic mechanisms farther downstream.

Our best clue to the possibility of a driving baroclinic instability is the work of Pera and Gebhart [1973]. That work was limited to small values of $\Delta T/T_\infty$ and α, so that some guesswork is needed to apply it to our circumstances. If we calculate our Grashof numbers from $Gr_y = g \frac{\Delta T}{T_\infty} \frac{y^3}{\nu_\infty^2}$ and assume that $\Delta T/T_\infty$ has no independent effect on the quantities predicted or measured by Pera and Gebhart [1973], we conclude that two-dimensional oscillatory disturbances, with frequencies equal to those we observe, are unstable at $|y/b| > 0.35$ when $\alpha = 0°$, but that they are probably stable for $\alpha = 20°$ for $|y/b| < 1$. Even when unstable, they are slowly growing, so that amplification into something clearly visible is unlikely, unless the disturbance is strongly forced. If we were to evaluate the β/ν^2 in Gr_y at T_c or some simple average of T_c and T_∞, we should conclude that Pera and Gebharts' oscillatory disturbances would not be seen at all in our apparatus.

Pera and Gebhart found experimentally, that their observed oscillations, though forced in a two-dimensional way, developed in a highly three-dimensional way. This was expected because, for small α, a steady instability with longitudinal vortices is the first to become unstable [Chen and Tszoo, 1982]. They remarked, however, that this three-dimensional behavior was not suggested by the appearance of their interferograms, but was detected only when smoke filaments were introduced. Since our shadowgraph, like the interferometer, can't really discriminate between a two-dimensional disturbance and one that is periodic in the spanwise (z) coordinate, we cannot really rule against the baroclinic instability on the grounds that what we see is two-dimensional.

In summary, we find that either of two distinct mechanisms -

(1) barotropic instability of the separated shear layer at the lower lip of the cavity, and

(2) baroclinic instability of the bottom boundary layer -

could conceivably trigger the observed oscillations, but we cannot conclude that one alone is responsible. Further experimentation, to delineate the exact range of parameters in which the oscillations appear, and to determine whether they are two-dimensional or three dimensional, would probably settle the issue.

3.2.4 Movement of the stagnation lines; escape of the heated air

A broad and relevant question about our mixed convection flows is - by what path does heated air escape from the cavity? If we believe the flow to be essentially two-dimensional, we are led to pay special attention to the occurrence and migration of stagnation lines of the time-averaged velocity

field, and to the stream surfaces that arrive at or depart from these stagnation lines.

In this section, we pursue this point of view until some of its inevitable conclusions are seen to conflict seriously with our measured temperature profiles, and with the implications of some of the shadowgraph pictures. We then retrace parts of the argument, with the assumption that convection along the z-axis plays an essential role.

Figures 41 display sketches, intended to show the time-average streamlines and the regions occupied by heated air, in the three qualitatively distinct regimes of mixed flow which arise when $\alpha > 0°$. The sketches were guided by the assumption that the shadowgraph images result from gas conditions that are at least statistically independent of z. For example, we infer from Figure 34, that there is heated fluid at any x in the aperture plane, for $Gr/Re^2 < 16.2$, because we see evidence of light refraction on both sides of the aperture plane. The sketches make no attempt to indicate the effects of cavity depth, which seems to have little influence on the migration of the stagnation lines.

The two-dimensional interpretation.

Figure 41a shows the cavity at $\alpha = 20°$, in pure free convection. The flow entering the cavity is drawn up mostly from below, to replace the hot air that is propelled upward by a hydrostatic pressure gradient which exceeds the local specific weight. This flow is quite two-dimensional.

Figure 41b shows the first effects of a very weak wind. Two new stagnation points appear, one (0) where the oncoming wind divides, to go upward or downward, outside of the rising buoyant flow. The other (0') appears on the wall below the cavity, at a point below which the flow is nowhere buoyant.

The upward drift along the lower wall is entirely overwhelmed by the local forced flow, which accelerates as the bottom edge of the aperture-plane extension is approached. The process by which this happens when the forced flow is started may be imagined as a sequence of events, to wit

1) a velocity field approximately identical to a potential flow over the unheated apparatus is suddenly superposed on the weak updraft of the free convection flow.

2) This produces an illegal downward slip-velocity at the wall, which is countered by the introduction there of a compensating vortex sheet.

3) This new vorticity diffuses out to form the new boundary layer, cancelling the pre-existing vorticity of opposite sign, which was in the boundary layer of the induced flow.

Because the upward velocity of the induced flow decreases, while the downward velocity of the forced flow increases, as distance down from the cavity increases, the weakest steady wind obtainable with the wind tunnel suffices to make O' appear somewhat on the wall, as shown. The supply of fluid to the cavity then comes through a narrow stream channel, just below the stagnation streamline that leads to point O.

The effects of the forced flow between O and the upper lip of the cavity are too weak (the forced flow is locally much slower, and the pressure gradient weaker, than at O') to block the upward escape of the hot air. This flow can be quite steady, or oscillating but still quite laminar.

The situation depicted in Figure 41b persists as Re^2/Gr is increased until, quite suddenly, the mean situation changes to that shown in Figure 41c. Stagnation point O has moved to the wall, the upward escape of hot air is cut off by the new stagnation (or separation) line O", and a trapped vortex

appears in the cavity. Hot air still escapes from the cavity, but it must now be transferred across the mean flow streamlines by vigorous turbulent eddying, and it now escapes downward.

To imagine how 0" would appear in a transient process, in which an adequately strong wind is suddenly started, we can add one more effect to the scenario described above for the lower wall. This is a reduction of the x-direction "buoyancy force" from $(\rho_\infty - \rho)g\cos\alpha$ to $(\rho_\infty - \rho)g\cos\alpha + \rho_\infty UdU/dx$, where U is the forced flow velocity just outside of the thermal boundary layer. Between 0 and the upper lip of the cavity $UdU/dx < 0$.

It is hard to predict the point at which the upward motion of the hot air will be reversed, but it is relatively easy to see why the new stagnation point, 0", suddenly appears near the upper lip of the cavity, instead of moving slowly down from the vicinity of 0 as the wind speed is increased. Both U, which determines the amount of vorticity introduced at the wall, and UdU/dx, which reduces and eventually reverses the baroclinic generation of vorticity in the heated air, increase in absolute value from 0 to the lip. Thus the local obstacles to upward progress of the hot air are, for a given wind speed, highest at the lip. If the hot air has sufficient inertia and residual buoyancy to pass the point where 0" is sketched, it may then continue up to 0, past which point the forced flow helps it along. This is not to deny that a gradual movement of 0" might appear in a set of careful experiments designed to reveal it, but to explain why we saw so little movement either as a function of U_∞, or as the result of temporary additions to the aperture plane extensions.

A rough upper estimate of the value of U_∞ above which 0" appears can be made by setting $(\rho_\infty - \rho)g\cos\alpha + \rho_\infty UdU/dx = 0$, and relating UdU/dx to U_∞^2/b

and x/b by use of the potential-flow calculations shown in Appendix D. This gives $U_\infty \approx 4.4$ m/s for $\alpha = 20°$, $U_\infty \approx 2.4$ m/s for $\alpha = 45°$, if we set $\rho = 0.5\,\rho_\infty$. These values are about 8 times the corresponding observed values.

Discrepancies in the two-dimensional interpretation.

A clear implication of this interpretation of the photos is that we should find elevated mean temperatures and large temperature fluctuations in the lower part of the aperture plane, under conditions corresponding to Figs. 41b and c. This expectation is not borne out by our temperature data, as is shown dramatically for $\alpha = 20°$ in the upper few curves of Figs. 15, 18 and 21. These show that at $z = 0$, $T \approx T_\infty$ over much of the aperture plane, and that the extent of the ambient-temperature region increases rather rapidly with increasing U_∞, (and somewhat with increasing a/b) once $Gr/Re^2 < 5.8$. Compare the impression given by the corresponding shadowgraphs in Figs. 35, 36 and 37.

A second embarrassment is implied by details shown particularly vividly in Figs. 36 and 37. Note that the curves of light and dark, which we identify roughly with material surfaces, appear to spiral inward toward a vortex center.

If these snapshots indicate a quasi-steady state of affairs, material surfaces would coincide approximately with stream surfaces, and fluid, both hot and cold, would appear to be moving in toward the vortex center. This would violate the continuity equation in a strictly two-dimensional flow, but not in one featuring a finite value of $\partial W/\partial z$.

A three-dimensional interpretation.

Figure 42 presents a fairly speculative idea of what may actually be happening in the flows shown in the bottom row of shadowgraphs, in Figure 37.

Ambient air enters the cavity at points such as A and A', and passes under and behind the main vortex. If it enters close to the bottom wall it becomes heated by conduction. Throughout most of the span of the cavity, the pressure is low in the vortex core and the particle spirals slowly inward while drifting toward the nearer side window. The spanwise flow in the vortex core is arrested by the window, and something akin to a vortex breakdown or explosion may occur close to the windows[2]. This weakens or even reverses the radial pressure gradient, so that the particle suddenly spirals out again. The outer edges of the exploded vortex are responsible for the light refraction seen in those regions where the centrally located thermocouples register only ambient temperatures.

In the shallow cavity and at lower wind speeds, the central body of the vortex may extend out to the aperture plane, leaving a corresponding signature on the mean temperature distribution. This is seen prominently in Figs. 15 and 16, in which a local minimum in $T(x)$ appears around $x/b = 0.8$ (at $Gr/Re^2 = 2.35$ and 1.18 when $\alpha = 45°$, $Gr/Re^2 = 16.19$ and 5.65 when $\alpha = 20°$). One can speculate that this marks the average location of the main tongue of ambient-temperature fluid, which wraps completely around the vortex core before being warmed by conduction.

At higher wind speeds and in deeper cavities, the main vortex is pushed back away from the aperture plane and leaves no identifying thermal signature there.

****

[2]The theoretical possibilities of such a situation has been analyzed by Serrin [1972]. What we suggest here is akin to Serrin's "second kind of motion" (see his page 326).

The implication of the above interpretation, should it prove correct, is that results obtained by simulating the mean flow with a computational scheme that accommodates only two-dimensional motion are bound to differ from the real three-dimensional flow.

4. ANALYSIS OF EXPERIMENTAL ERROR

This section presents an evaluation and discussion of the major error sources possibly affecting the precision and accuracy of the measurements. The errors arise in connection with positioning of the measurement probe (mechanical or optical), radiation and conduction heat transfer to thermocouple wires, bias in velocity measurements due to the dependence on particles to track the flow and compounded by refractive index effects, and the finite sample size of the measurements. Wherever possible the magnitudes of the errors have been quantified and tabulated, either by reference to analytical considerations or experimental calibration. Because of the qualitative nature of results obtained via the shadowgraph technique, errors associated with flow visualization have not been considered.

Further discussion and tabulations of measurement errors, especially relatively minor ones associated with the LDV technique, not discussed here, are given in Chen [1983].

4.1 Temperature Measurements

4.1.1 Positioning error

It was pointed out in Section 2.1.2 that the thermocouples mounted on the harness, for determining aperture plane temperatures, could be positioned to within ± 5 mm of the cavity symmetry plane. This corresponds to a ± 1% uncertainty based on the spanwise dimension of the cavity.

The locations of the thermocouple junctions, in the x- and y-directions were assigned uncertainties of ± 0.25 mm, by direct measurement when the cavity was cold. Thermal expansion of the heated cavity added some systematic uncertainty in the position of the junctions relative to the cavity. The

height of the cavity opening, b, was observed to increase by about 1 mm as the cavity came to its usual test temperature. The yoke holding the wires did not get very warm, so we assume that the wires did not move. To make a conservative (pessimistic) estimate of the resulting uncertainty, we assumed that the distance of each junction from the lower lip of the cavity was not changed by heating, and then plotted T versus x/b with two different values of b (93.66 mm, cold; versus 94.66 mm, hot). The maximum difference in T for a given x/b occurred in the high-gradient region near the top, and amounted to about 10°C.

4.1.2 Systematic differences between thermocouple temperature and air temperature

The convective heat exchange which drives the thermocouple temperature toward the local, instantaneous air temperature has to compete with radiant heat exchange, metallic conduction along the thermocouple leads, and the heat capacity of the wire. These familiar error sources were all analyzed in a conventional way (see Scadron and Warshawsky [1952], Hinze [1975]). The full details of this analysis are given in Chen [1983], a summary is provided here.

The convective heat transfer coefficient for the 76 micron diameter wire was estimated to range from 160 to 400 $W/m^2°K$. The corresponding time constant ranged from 0.2 to 0.5 seconds.

The radiant emissivity of the wire was estimated to be about 0.48, from observations of the thermocouple temperature in regions where the air was at ambient temperature. The measured temperature profile for one or two runs was corrected for radiation effects, as is shown in Figure 43. The temperature data is reported without corrections, because the error is relatively small and no highly quantitative deductions were drawn from this data. The correc-

tions had no important influence on the mass-flow quadratures exhibited in Table 3.5.

On the assumption that the convective heat transfer coefficient is uniform along the wire that spans the cavity, metallic conduction effects were found to be negligible. On the other hand, they were large enough to have masked any short-wavelength variations of gas temperature in the z-direction, had we tried to measure these by traversing wires.

The finite time constant of the thermocouple attenuates a harmonic air-temperature oscillation of frequency f, by a factor $(1 + (2\pi f\tau)^2)^{-1}$. Thus, oscillations for which $f \geq 2$ Hz are only weakly represented in the thermocouple signal. Since the signal was sampled periodically, at one second intervals, exactly periodic fluctuations of air temperature will not show up in the sample if their frequencies are exact integral multiples of the sampling frequency. In this pathological case, even the mean air temperature may be misrepresented.

All these considerations lead us to place little faith in the quantitative observations of air temperature fluctuations. Since no quantitative use is made of them, this is not too serious. Table 4.1 presents a summary of estimated uncertainties for the mean temperature measurements.

4.2 Velocity Measurements

The LDV technique is simple in principle, because of the linear relation between the Doppler shift of the frequency of laser light, Mie-scattered from a small particle, and the velocity of the particle. For an LDV system based on the differential Doppler technique, Drain [1980], the relation is:

$$U = \frac{\lambda}{\sin \gamma/2} f_d \qquad (4\text{-}1)$$

In this relation λ is the radiation wavelength, $\gamma/2$ is the half angle between the pair of beams creating the optical fringe pattern, f_d is the Doppler-shift in the radiation scattered by the particle and U is the component of particle velocity, normal to the fringes. The practical complications with which we must be concerned in this study fall into two classes:

1) Those that affect the accuracy and precision with which individual values of U can be determined from individual bursts of scattered light.
2) Those that limit what we can deduce, from a sequence of U-values, about the statistical properties of an unsteady fluid velocity.

Both classes of complications have been extensively discussed in the literature; for example by Durst et al [1976], Buchave et al [1979], Drain [1980]. They are discussed here in the next two sections.

4.2.1 Uncertainty of individual measurements

As each oil droplet traverses the optical probe volume, the photomultiplier tube produces an oscillating voltage. Because the flow is non-uniform and unsteady, and the probe volume is finite, the frequency of oscillation may vary somewhat during the lifetime of the signal (the "burst"). The computer verifies that the frequency is substantially constant over an interval of about 15 to 20 microseconds (the time to cross 8 fringes), and calculates the corresponding value of U. The burst may continue for a considerably longer time - perhaps lasting from fifty to several hundred microseconds, but no further information is obtained from it because the recovery time of the computer is about 600 μ sec.

Minor effects

It is clear that the exact position of the particle at the time of measurement is slightly uncertain, so that the statistical processing of the 500 or 1000 measurements made at each "point", involves a bit of volume averaging as well as ensemble or time averaging. On the scale to which our results are presented graphically, the averaging volume is quite invisible.

The value of U itself is uncertain to a degree determined in part by clock errors in the counter, shift errors in the electronic downmixers, and Bragg-cell bias. In view of the manufacturer's guarantees or calibration procedures carried out during the tests, we believe these uncertainties to be negligible.

Additional uncertainties in U arise if the particle does not faithfully follow the unsteady motions of the fluid, or if the optical fringe field is displaced or dances about as a result of variation of index of refraction along the path of the incident laser beams. We have already been assured that the first point is not troublesome in our case, but we find substantial reason to worry about the latter.

Refractive Index Effects

Uncertainties due to variable index of refraction have been analyzed and discussed by Buchhave et al [1979, Section 4] and some useful illustrative calculations of beam deflections in regions with specified variations of index have been given by Schmidt and Wang [1982]. It is clear from the strong shadowgraph images we have obtained, that significant bending of light beams occurred in the present tests. The following calculations and test were made, to evaluate this source of error in our results.

To estimate the mean deflection of the laser beam that traverses the greatest length of heated air, we employed the approximation

$$x_1 - x_0 \approx \frac{\partial n}{\partial x} \frac{(z_1 - z_0)^2}{2} \qquad (4\text{-}2)$$

The coordinates x and z are defined as in Fig. 1, the beam deflection is illustrated in Fig. 44. This approximation is adequate if the index of refraction, n, is very nearly equal to 1, and if $\partial n/\partial x$ is constant along the path of the beam. For air, we used the formula given by Buchhave et al [1979, eqn. 4.1.1]

$$n = 1 + 7.92 \times 10^{-7}\ p\ (\text{pascal})/T(\text{Kelvin}) \qquad (4\text{-}3)$$

and set $p = 1.01 \times 10^5$ pascal (atmospheric pressure). Inserting $z_1 - z_0 = 267$ mm (the half-span of the aperture plane), and selecting representative values of $T^{-2}\,\partial T/\partial x$ from Figs. 31 a,b and c, we estimate the following maximum beam deflections

a/b	α	x_0 (mm)	$x_1 - x_0$ (mm)
0.5	0	2.65	.36
0.5	0	92.37	-.22
1.0	0	2.65	.34
1.0	0	92.37	-.20
1.0	45°	2.65	.60
1.0	45°	92.37	-.11

These deflections are small enough to justify the assumption of constant mean

$\partial n/\partial x$. Because they are largest where V is also largest, they may have a significant effect on the computed net heat transfer. This effect is estimated by displacing all the nominal points of measurement by amounts computed as above, and recalculating the integral $\int_0^b V\,dx$. This shows that in the case of lowest heat transfer, a/b = 1 and $\alpha = 45°$, a correction of about - 10% should be made to $\dot{Q}_b$ on this score. For the other cases, the corresponding corrections would be less than - 2%.

The laser beams may also be deflected in the y direction, so that velocity data nominally acquired at y = 0 really came from points slightly outside the aperture plane. The effect of this on local values of V can be roughly estimated from the formula

$$\Delta V \approx - (y - y_o)\, \partial U/\partial x \ ,$$

and $\partial U/\partial x$ can be estimated from our data.

It appears that this error source leads to systematic underestimates of $\dot{Q}_b$, so that the errors due to horizontal displacements tend to reduce those due to vertical displacements. In summary, it appears that this source of uncertainty is a minor one.

Besides the mean deflection of the laser beams, refraction variations will induce a spurious level of fluctuations, discussed in some detail by Buchhave et al [1979]. We made two tests to estimate the severity of these problems in the present study.

In the first test, a laser beam which had traversed the entire span of the cavity, through a region of vigorously fluctuating temperature, was intercepted by a translucent screen. The center of the illuminated spot wandered over a circle of diameter no greater than the diameter of the spot itself.

This implies a corresponding increase in the inherent uncertainty of the location of a light-scattering particle at the time a burst is recorded.

To obtain a measure of the "false turbulence" due to dancing of the fringe pattern, the optical probe volume was focussed on the top outer corner of the cavity, on the symmetry plane. The solid corner served as a stationary scattering center. From a blank run with an unheated cavity, it was confirmed that the means obtained from several samples of 1000 burst frequencies each very nearly corresponded, for each counter, to the frequency set on its electronic downmixer, and that the standard deviation of this sample of frequencies was nil. Then the cavity was heated to its standard operating temperature, and the apparent motion of the stationary corner was observed. No particle seeding was done in either test.

The individual values of V and U scattered widely when the cavity was hot, and the variances of V and U in this test were about half as large as the corresponding quantities inferred from signals returned from oil droplets at a point 1.8 mm below the top wall corner. The table below summarizes these results, which apply to the geometry $a/b = 0.5$, $\alpha = 0°$.

Test	V	U	$\overline{v^2}$	$\overline{u^2}$
	m/s	m/s	m^2/s^2	m^2/s^2
A	0.000	0.000	0.0011	0.0006
B	0.013	0.007	0.0557	0.0067
C	0.345	0.351	0.0912	0.0158

Test code: A: unheated cavity, beams focussed on corner.

B: heated cavity, beams focussed on corner.

C: heated cavity, light scattered from oil droplets at a point 1.8 mm below top wall corner.

It is not obvious why the fluctuations in V were so much larger than those in U, or why the mean offsets in V and U should be positive. One of the beams used to measure V traverses a mostly isothermal region (the one shown at γ degrees with respect to the aperture plane in Fig. 10-b), whereas both of the beams used to measure U are in the heated region of the aperture plane for most of their length at the x positions chosen for illustration. This could lead us to expect a difference, but what difference it is hard to say. For the moment, we simply notice that these false mean velocities amount to about 3 or 4 percent of the measured gas velocities near the corner - introducing an uncertainty which is small in itself, but which could contribute very significantly to uncertainty in $\int_0^b V\,dx$. "False turbulence" due to variation in the refraction of the beams seems, from this limited test, to be a comparatively serious problem. If the experiments were to be repeated, it would probably be wise to employ some sort of comparator technique, in which each data sample from the moving droplets is matched with a sample gathered from light scat-

tered from a nearby stationary fine wire. The data rate for the comparison test (involving the wire) might so greatly exceed that of the fluid-motion test, that it would be unnecessary to make the comparison tests in unseeded air. As a first approximation, the true variance of the fluid-velocity sample could be found by subtracting the variance of the wire-scattered signals from that of the droplet-scattered samples. This assumes that the apparent velocity fluctuations, which result from cumulative effects of refraction along the entire paths of the beams, are statistically independent of the actual fluctuations, which are more locally determined.

4.2.2 Uncertainties of statistical interpretation

Velocity bias

This has been discussed in Section 2.2.2, and we restate here only the conclusion that our statistical procedures should eliminate this bias in the two-component data. For the one-component data, there may be residual uncertainties, which we have no immediate way of quantifying.

The differences between our weighted and unweighted averages (see Appendix A) are large, particularly for $\overline{uv}$, and it is important to remember that our discussion of results is based on the weighted averages. Quite a different picture of the flow would be deduced from the unweighted averages.

Effects of non-uniform seeding

In our preliminary discussion of the interpretation of LDV data, and most explicitly in our interpretations of various surface integrals - as being approximately equivalent to convective heat fluxes or mass fluxes - we have treated the mean velocity (U, V, W) as a time-average of instantaneous velocities. Actually, since the probability of observing a particular value of instantaneous velocity is proportional to the density of scattering centers in

the observation volume when the air there has that velocity, the LDV system gives a density-weighted average.

The relevant density is the number density of the scattering centers (here droplets), but we expect this to be proportional to the density of the air, providing that:

1) the particles become uniformly dispersed throughout the air, before the latter is non-uniformly heated; and

2) the particles do not subsequently diffuse through the air, but move with it.

When these circumstances prevail, our application of equation (2-16) leads us to density-weighted (Favre) averages of the fluctuating velocity. Since the ideal circumstances are unlikely to prevail, and since we have no simultaneous local measurements of density, the identity of the average we have formed is somewhat ambiguous.

The quantitative implications of this ambiguity may be roughly estimated by the following model, in which the number density of particles is taken to be proportional to the gas density. We attempt to estimate the difference between the two averages

$$V = \sum_{i}^{N} V_i \, \Delta t_i \Big/ \sum_{i}^{N} \Delta t_i \qquad (2\text{-}16)$$

and

$$V_F = \sum_{i}^{N} \rho_i V_i \, \Delta t_i \Big/ \sum_{i}^{N} \rho_i \, \Delta t_i \qquad (4\text{-}4)$$

Having no reason to suspect a correlation between ρ_i and Δt_i, we simply set

$$\sum_i^N \rho_i \, \Delta t_i = \bar{\rho} \sum \Delta t_i \quad , \text{ so then}$$

$$V_F = \sum_i^N \left(\frac{\rho_i}{\bar{\rho}}\right) V_i \, \Delta t_i / \sum \Delta t_i$$

$$= V + \sum_i^N \Delta\rho_i \, \Delta V_i \, \Delta t_i / \bar{\rho} \sum \Delta t_i \qquad (4\text{-}5)$$

where $\Delta\rho_i = \rho_i - \bar{\rho}$, and $\Delta V_i = V_i - V$. To represent this more compactly, we introduce a correlation coefficient r, such that

$$\sum_i^N \Delta\rho_i \, \Delta V_i \, \Delta t_i / \sum_i^N \Delta t_i = r \, \sigma_\rho \, \sigma_v \qquad (4\text{-}6)$$

where σ_ρ and σ_v are standard deviations of the experimental samples of ρ and V. Thus we get

$$V_F = V + r \, \sigma_\rho \, \sigma_v / \bar{\rho} \qquad (4\text{-}7)$$

This, of course, proves nothing, but simply expresses the proposition in terms of quantities for which we have experimental estimates ($\sigma_\rho / \bar{\rho}$ and σ_v), or which we can plausibly guess (r).

We now consider the specific situation in the aperture plane. We have an estimate of σ_v, calculated from equation (2-12), with $\sigma_v = (\overline{v^2})^{1/2}$. We also have a fairly suspect estimate of $\sigma_\rho / \bar{\rho}$, from the thermocouple data, presented in Appendix B. (We assume, for this purpose, that $\sigma_\rho / \bar{\rho} = \sigma_T / \bar{T}$.) Because of the sluggish response of the thermocouples, and visual evidence that the frequency spectrum of density fluctuations would probably exhibit significant amplitudes at frequencies at least up to 10 Hz, we suspect that true values of σ_ρ would be at least twice the values tabulated.

Finally, in the aperture plane, it seems certain that r will be negative, since air entering the cavity ($v' < 0$) is likely to be cold and relatively dense ($\rho' > 0$), while air leaving the cavity is likely to be hot and relatively expanded.

For sample estimates, we have assumed $r = -0.5$, and have doubled the values of $\sigma_T/\overline{T}$, which were calculated from the thermocouple data. Calculations were done for all three cases for which we had LDV data.

The calculations show that V, which we intended to measure, is everywhere more positive (outward from the cavity) than V_F, which we actually did measure if the droplets are distributed in the way supposed in the model. The difference, $V - V_F$, was greatest (2 cm/sec) near the top of the shallow cavity, almost as great (1.5 cm/sec) very near the bottom of the deeper, horizontal cavity, and very much smaller (< 0.2 cm/sec) in the much quieter flow of the deeper, inclined cavity. The differences never exceeded about 7 percent of V_F, but a major cumulative effect appears in the integral across the aperture, to wit

$$\int_0^b (V - V_F)dx \Big/ \int_0^b V_F\, dx = \begin{array}{ll} 0.23 & (a/b = 0.5,\ \alpha = 0°) \\ 0.50 & (a/b = 1.0,\ \alpha = 0°) \\ 0.16 & (a/b = 1.0,\ \alpha = 45°) \end{array} .$$

Before these differences are interpreted as uncertainties in the computed convective heat transfer, we need to reexamine the assumptions that allowed us to write equation (1-10) and the comment below it.

If our measurements have more nearly defined V_F, rather than V, we need to reconsider the application of (1-10) to a highly fluctuating flow. Formerly we wrote

$$\overline{\rho v T} = \overline{\rho T}\ V + \overline{(\rho T)'v'}\ , = \frac{p_\infty}{R} V + \overline{(\rho T)'v'} \qquad (4\text{-}8)$$

and asserted that $(\rho T)'$ was ≈ 0 because $\rho T = p_\infty/R$ is an accurate approximation to the equation of state. Now we must consider ρv as a single variable, and write

$$\overline{\rho v T} = \overline{\rho v}\ \overline{T} + \overline{(\rho v)'T'} = \overline{\rho}\ V_F\ \overline{T} + \overline{(\rho v)'T'}$$

$$= \frac{p_\infty}{R} V_F + \overline{(\rho v)'T'} \ . \qquad (4\text{-}9)$$

If what we previously thought to be σ_v is in reality $\sigma_{\rho v}/\overline{\rho}$ we have an experimental measure of it, and know that it is large. We also have our suspect measure of σ_T, and we still have intuitive grounds for associating positive values of $(\rho v)'$ with outflow, and hence with positive values of T'.[3] In fact, we recognize that $\overline{(\rho v)'T'}$ is probably nearly equal to $\overline{\rho}\ \overline{T}(V - V_F)$. From either interpretation, it is clear that V, rather than V_F, belongs in equation (1-10). Since $V > V_F$ everywhere in the aperture plane, we shall underestimate $\dot{Q}_b$ if the quantities we insert into (1-10) are closer to V_F than to V.

To complicate matters further, it is by no means certain that the droplets were uniformly dispersed throughout the air before the air was heated. It is even possible that our technique of seeding may accidentally have offset some of the tendency toward Favre averaging, by introducing a somewhat greater concentration of particles into that portion of the air that will subsequently become hottest. On the other hand, there is a known tendency for small particles to migrate away from hot regions in a gas (thermophoresis), and this has been a limiting factor in some previous LDV work.

****

[3]Note that $(\rho v)' \neq \rho' v'$. In particular, $(\rho v)'$ has the same sign as v'.

The conclusion of this point of discussion is that unintended bias of our average velocities, caused by non-uniform concentration of scattering particles, is a major source of experimental uncertainty. It probably introduces only a few percent uncertainty into the individual velocity values, but may introduce major systematic errors into our estimates of convective heat transfer. The component of this error due to temperature fluctuations in the gas may be as large as 15 to 50 percent if the correlation coefficient for v' and T' fluctuations is as large as 0.5.

Further insight into this question is sought in the next section, by examining the residual heat and mass fluxes which are presented in Tables 3.3 and 3.5.

Fluctuations and finite sample size

The above subsections question whether the technique of sampling the velocity biases the statistical population from which the sample is drawn. Our final concern is that we draw large enough samples to obtain adequately precise measures of the means, variances, and cross-correlations characteristic of the sample populations. See Bowker and Lieberman [1972].

Either 1000 or 500 measurements were processed for each statistical calculation. The resulting uncertanties in V range from about ± 0.005 m/s to ± 0.015 m/s. The propagation of these uncertaintities through the calculation of $\dot{Q}_b$ results in the uncertainty estimates listed in Table 3.4

4.2.3 Conservation tests - assuming two-dimensional flow

The calculations of heat flux through the surfaces (a), (b), (c) and (d) of Figure 23, (see Table 3.3) and of the mass flux through the aperture plane (Table 3.5) were made in the hope that they would establish limits on systematic error in our data gathering or interpretation. Ideally, $\sum \dot{Q}_i$ in Table 3.3,

and $\dot{m}_b$ (net) in Table 3.5, should equal zero, because there are no heat or mass sources within either control volume. The non-zero residuals are shown in Tables 3.3 and 3.5 to be statistically significant, so we seek possible explanations of systematic effects.

The assumption of two-dimensional flow

The conservation statements apply in principle to enclosed control volumes, which we visualize as thin pancakes, bisected by the symmetry plane, $z = 0$. By asserting that there should be no net flow through the narrow edges of the pancake, we assume that there is none through the broad faces. In the limit of an infinitely thin control volume, still bisected by a symmetry plane, $z = 0$, the exact conservation statement, say

$$\int\int_A \underset{\sim}{V} \cdot \underset{\sim}{n}\, dA = 0 \tag{4-10}$$

becomes

$$\oint_c [V\, dx + U\, dy] + 2A_z \left.\overline{\frac{\partial W}{\partial z}}\right|_{z=0^+} = 0 \tag{4-11}$$

Here c is the curve along which U and V were measured, A_z is the area enclosed by that curve, and $\left.\overline{(\partial W/\partial z)}\right|_{z=0^+}$ is an average over A_z. When we assume strictly two-dimensional flow, we drop the last term in (4-11). We now ask whether $\overline{\partial W/\partial z}$ could possibly be large enough to explain the residuals shown in Tables 3.3 and 3.5.

A simple calculation shows that the values of $\overline{\partial W/\partial z}$ necessary to account for the residual, $\sum \dot{Q}_i$, in Table 3.3 are

$$\overline{\partial W/\partial z} = \begin{cases} 0.073 \text{ sec}^{-1} & a/b = 0.5,\ \alpha = 0° \\ 0.028 \text{ sec}^{-1} & a/b = 1.0,\ \alpha = 0° \\ 0.107 \text{ sec}^{-1} & a/b = 1.0,\ \alpha = 45° \end{cases} \quad \text{for}$$

We measured W(z) in the aperture plane, for four values of x/b (a/b = 1.0, α = 0°). However, when we try to evaluate $\partial W/\partial z$ by a least-squares fit to these data, we encounter a statistical uncertainty considerably larger than the value itself. Thus we can neither confirm nor rule out the possibility that leakage through A_z explains the residuals in Table 3.3.

The same conclusion unfortunately applies to the values of net heat loss from the cavity, listed in Table 3.4. The values of $\partial W/\partial z$ required to throw our heat loss calculations completely into doubt are only slightly larger than those shown above, and this fact cannot be ruled out.

From these calculations, it seems clear that a more valuable test of two-dimensionality would have involved repeating the profiling of U and V at two extra values of z, perhaps at $z \pm c/4$.

Long-term temporal stability

Since it took a few hours to complete each profiling operation, it is clearly possible that the residuals may have resulted from drifting conditions. If, for example, the cavity were to warm up slightly while an aperture-plane profile was being measured from bottom to top, $\dot{Q}_b$ (out) would presumably be greater, and $\dot{Q}_b$ (in) smaller, that the values found, had the cavity remained exactly at the mean of its initial and final temperatures. The change in $\dot{Q}_b$ net could then be considerable.

For a quantitative estimate, we can assume that ΔT increases from 348 to 353°C during a run. This is about a 1.5 percent change and we assume it induces a 0.75 percent change in V. If we increase $\dot{Q}_b$ (out) by 0.75 percent and

hold $\dot{Q}_b$ (in) unchanged, we get changes in $\dot{Q}_b$ (net), equal to 2%, 5% and 11% for a/b = 0.5, α = 0°; a/b = 1.0, α = 0°; and a/b = 1.0, α = 45°. We conclude that the residuals shown in Tables 3.3 and 3.5 are probably not due to long-term temperature drift.

The cumulative effects of non-uniform seeding

The discussion of non-uniform seeding leads to a somewhat paradoxical conclusion, concerning the $\oint$ (U dy + V dx) around the exterior control circuit shown in Figure 23. If the seeding were miraculously uniform, so that we truly measure V, $\sum \dot{Q}_i$ should vanish because there are no heat sources within the control volume. If the droplet concentration is, on the other hand, exactly proportional to the air density, so that we measure V_F rather than V, the integral $\oint$ (U_F dy + V_F dx) should vanish because there are no mass sources, within the control volume.

Thus the presence of residuals in Table 3.3 tells us little or nothing about the uniformity of seeding.

A similar consideration of $\dot{Q}_b$ and $\dot{m}_b$ - flows through the aperture plane - leads to somewhat different conclusions. If we measure V, then we are correct in treating $\dot{m}_b$ (net) in Table 3.5 as an evidence of experimental error. If, however, we have measured V_F, then it is $\dot{Q}_b$ (net) in Tables 3.3 and 3.4 that should have vanished and the values that we have reported as heat transfer coefficients and Nusselt numbers are only an evidence of error.

We are forced to two unhappy conclusions about the integral conservation tests; to wit:

1) They do not provide adequate documentation of two-dimensional flow, so that the accounting for inflows and outflows is decisively incomplete.

2) By a curious juxtaposition of physical circumstances, they fail to shed light on one of the principal suspected sources of systematic error - the non-uniform distribution of light-scattering droplets.

4.3 Reproducibility and Control of Experimental Conditions

When geometrical and cavity-temperature conditions were reproduced at various times, the visual appearance of the flow was always the same. That is, visually prominent features always appeared in the same place, and the degree and character of transient fluctuations appeared to be unchanged.

For more quantitative tests, some velocity and temperature measurements were repeated on different days, for nominally identical conditions.

Table 4.2 exhibits some typical results. The numbers shown for velocities are sample arithmetic averages of the columns of values listed on page A31, for $a/b = 0.5$ and $\alpha = 0°$, compared with corresponding averages of the values obtained at the same measurement stations on another day. Thus they refer to x-profiles in the middle of the aperture plane ($y = z = 0$).

4.4 Summary Evaluation of Experimental Accuracy

In the light of all this discussion we must ask: what faith, if any, can we place in the data reported in Tables 3.3 to 3.6?

To be fair to our hopes for the data, we note that no systematic error has been detected, but that the scope and precision of our data do not allow us to rule out significant errors that may plausibly be suspected.

The principal grounds for suspicion are the residues in the integral balances on the external control volume. These would not be alarming in themselves, except that they are almost as large as the flux through the aperture plane, which is the quantity of primary interest. There are good physical grounds to expect residues of the sign we found, because the heated plume from the cavity entrains air from the sides as well as from the front. One can also believe that this effect is much attenuated inside the cavity, where the side windows obstruct spanwise flow. Thus it may be unduly pessimistic to

suspect that the flux through the aperture plane is significantly influenced by spanwise flow convergence (or divergence), just because we have a hint of such convergence in the flow outside the cavity.

The ambiguity of our averaging procedures, due to non-uniform droplet concentration, has been at least partially estimated with the conclusion that, whether we are measuring V or V_F, the dependence of the heat transfer on cavity geometry is qualitatively the same. It seems safe to trust these trends.

The uncertainties in the velocities are by themselves small enough so that mean profiles plotted to the scale of Figure 31d would suffer an almost invisible change as a result of any likely systematic error. However, the data for velocity fluctuations are quantitatively suspect, both because of non-uniform seeding and because of beam dancing.

5. SUMMARY, CONCLUSIONS AND RECOMMENDATIONS

5.1 Summary

Free and mixed convection were observed in airflow, in and around a strongly heated open cavity of rectangular cross section. The open face of the cavity is a rectangle with edge dimensions b = 0.0946 m, c = 0.5334 m. The horizontal dimension, c, is made relatively long to encourage two-dimensional flow.

The depth of the cavity, a, was set so that a/b = 0.5, 1.0, or 1.46. The aperture plane was either vertical ($\alpha = 0°$) or inclined downward at $\alpha = 20°$ or 45°.

Almost all tests were made at a dimensionless overheat, $\Delta T/T_\infty \approx 1.2$, and at a Grashof number = 4.2×10^7, β and ν being evaluated at room temperature.

Mixed convection studies employed a uniform wind-tunnel flow of speed U_∞, which could be varied from about 0.04 m/sec to 1.40 m/sec, to reveal the principal qualitative transition between purely-free and strongly-forced convection.

Air temperatures were measured at mid-span of the aperture plane, and shadowgraph pictures were taken, for all combinations of the experimental parameters. For free convection only, extensive flow surveys were made with a two-component Laser Doppler Velocimeter. The velocity and temperature profiles are presented as targets for numerical simulation schemes.

The velocity data for free convection was processed to provide estimates of the convective heat loss from the cavity.

A careful analysis of random errors and possible systematic errors is presented for all the quantitative data. Some rudimentary theoretical models are presented, as an aid to description of the mixed-convection flows.

5.2 Conclusions

1. In pure free convection, the time-averaged flow is, as hoped, very nearly two-dimensional. Specifically, no systematic variation of W or U as functions of z was found in the aperture plane, for $- c/6 \leq z \leq + c/6$; and in this same region no statistically significant non-zero value of W was found. The instantaneous flow is unsteady and three dimensional, the velocity fluctuations being large compared to the mean velocities in many parts of the flow.

2. Downward inclination of the cavity reduced the relative level of fluctuations, primarily by reducing both the severity of flow separation from the lower lip of the cavity, and the baroclinic instability of the boundary layer on the bottom wall. Many of the observed trends seemed consistent with those found by Rotem and Claassen [1969] and by Pera and Gebhart [1973] in studies of flow above a horizontal or slightly inclined flat plate.

3. Mean velocity and temperature profiles are determined with sufficient accuracy to establish significant targets for a demonstration of the effectiveness of computational simulations, but with too little accuracy to permit reliable estimation of the net convective heat transfer. The dominant sources of uncertainty are associated with the possibilities of non-uniform seeding, fluctuations in index of refraction and weak flows in the spanwise direction.

4. The uncertainty of the heat transfer, due to the possibility of non-uniform seeding, can be roughly estimated, and this inspires confidence in the trends of Nu versus geometry, shown in Table 3.6. These show a substantial reduction of Nu at $\alpha = 0°$, when a/b is increased from 0.5 to 1.0; and a further substantial decrease at $a/b = 1.0$, when α is increased from 0° to 45°. The effect of inclination is roughly the same as found by Mirenayat [1981], for a cubical cavity.

5. When the cavity is faced into a very gentle wind ($U_\infty \approx 4$ to 6 cm/sec), the irregular unsteadiness of the flow is greatly reduced. The result may be either a very nearly steady flow, or a flow that oscillates very periodically, with a frequency ranging from 2 to 5 Hz. The oscillations may be mostly two-dimensional, but our observations do not rule out a spanwise modulation of phase, which might be expected in the light of the work of Pera and Gebhart [1973] and the stability theory of Chen and Tszoo [1982].

When $\alpha = 20°$ and 45°, these weak winds cut off the induced flow from below, which is the main supply of ambient air which enters the cavity in pure free convection. The new supply comes from a layer just below the dividing streamsurface of the forced flow. The hot air escapes upward from the cavity, as in free convection.

6. Stronger winds cause major discrepancies between our temperature data and any interpretation of the shadowgraph pictures that assumes two-dimensional flow. The upward escape of hot air is blocked by the locally downward forced flow, and any direct escape downward seems kinematically unlikely and has escaped experimental detection. It seems likely that ambient air rushes directly into the lower part of the aperture plane, rises behind a major coherent vortex, is wrapped around and entrained into the vortex, together with heated, vorticity-bearing fluid from the outer regions of the boundary layers. The air drifts towards the nearer side window while spiraling around the vortex until, near the window, the vortex "explodes" in a manner akin to the "second kind of flows" discussed by Serrin [1972]. The air then escapes from the cavity near the side windows, being cast out like sparks from a pinwheel.

5.3 Recommendations

The work has revealed many problems which deserve more detailed investigation.

Several of these have to do with the use of LDV in strong free convection flows. The use of fibre optics to minimize displacement and false-turbulence effects due to beam dancing looks promising. Should it fail, work could be done on a comparator technique, in which a fine wire stretched tautly along the nominal path of a velocity survey could serve as a local stationary scattering target.

Panoramic observations of the scattering-particle density field, by use of a thin sheet of laser light, would help to set to rest, or to emphasize, worries about non-uniform seeding.

Simultaneous density and velocity measurements, using Rayleigh scattering as a measure of air density, are being attempted in a number of laboratories. When developed, these would seem to offer essential advantages for LDV work in flows such as ours.

It would certainly be interesting to return to the wind tunnel for a more comprehensive mapping of the conditions that lead to periodic oscillations, and for flow visualization studies that reveal spanwise variations. It would be easy, and potentially very interesting, to investigate the effect of spanwise solid extensions of the aperture plane, to make the forced flow more nearly two dimensional.

REFERENCES

Arnold, J.N., Catton, I. and Edwards, K.D. 1976 Experimental investigation of natural convection in inclined rectangular regions of differing aspect ratios. J. Heat Transfer 98, 67-71.

Bauman, F., Gadgil, A., Kammerud, R. and Greif, R. 1980 Buoyancy driven convection in rectangular enclosures: Experimental results and numerical calculations. Paper ASME 80-HT-66, presented at the joint ASME/AIChE National Heat Trasnfer Conf., Orlando, Florida.

Bayley, F.J. 1955 An analysis of turbulent, free-convection heat transfer. Proc. Inst. Mech. Eng. 169, 361-370.

Bejan, A. and Kimura, S. 1981 Penetration of free convection into a lateral cavity. J. Fluid Mech. 103, 465-478.

Bejan, A. and Tien, C.L. 1978 Laminar free convection heat transfer through horizontal duct connecting two fluid reservoirs at different temperatures. J. Heat Transfer 100, 725-727.

Booker, J.R. and Bretherton, F.P. 1967 The critical layer for internal gravity waves in a shear flow. J. Fluid Mech. 27, 513-519.

Bowker, A.H. and Lieberman, G.J. 1972 Engineering statistics, Prentice Hall, Englewood Cliffs, New Jersey.

Buchhave, P., George, W.K., Jr. and Lumley, J.L. 1979 The measurement of turbulence with the laser-Doppler anemometer. Ann. Rev. Fluid Mech. 11, 443-503.

Cairnie, L.R. and Harrison, A.J. 1982 Natural convection adjacent to a vertical isothermal hot plate with a high surface-to-ambient temperature difference. Int. J. Heat Mass Transfer 25, 925-934.

Cebeci, T. and Khattab, A. 1975 Prediction of turbulent-free-convective-heat transfer from a vertical flat plate. J. Heat Transfer 97C, 469-471.

Charwat, A.F., Roos, J.N., Dewey, F.C., Jr. and Hitz, J.A. 1961a An investigation of separated flows - Part I: The pressure field. J. Aerospace Sciences 28, 457-470.

Charwat, A.F., Roos, J.N., Dewey, F.C., Jr. and Hitz, J.A. 1961b An investigation of separated flows - Part II: Flow in cavity and heat transfer. J. Aerospace Sciences 28, 513-527.

Cheesewright, R. and Doan, K.S. 1978 Space-time correlation measurements in a turbulent natural convection boundary layer. Int. J. Heat Mass Transfer 21, 911-921.

Cheesewright, R. and Ierokipiotis 1981 Velocity measurements in a natural convection boundary layer, Q.M.C. Faculty of Engineering Research Report EP 5022, University of London.

Chen, K.S. 1983 Experimental investigation of strongly heated open cavity flow. Ph.D. Thesis, University of California, Berkeley.

Chen, K.S., Humphrey, J.A.C. and Miller, L. 1983 Note on the pulsating nature of thermally driven open cavity flow. Int. J. Heat Mass Transfer 26, 1090-1093.

Chen, T.S. and Tszoo, K.L. 1982 Vortex instability of free convection flow over horizontal and inclined surfaces. J. Heat Transfer, 104, 637.

Chilcott, R.E. 1966 A review of separated and reattaching flows with heat transfer. Int. J. Heat Mass Transfer 10, 783-797.

Chin, E., Rafiinejad, D. and Seban, R.A. 1972 Prediction of the flow and heat transfer in a rectangular cavity with turbulent flow. J. Appl. Mech. 39, 351-358.

Drain, L.E. 1980 The laser doppler technique, John Wiley and Sons, New York.

Dring, R.P. 1982 Sizing criteria for laser anemometry particles. J. Fluids Engr. 104, 15-17.

Durst, F., Melling, A. and Whitelaw, J.H. 1976 Principles and practice of laser-doppler anemometry, Academic Press, New York.

Duxbury, D. 1979 An interferometer study of natural convection in enclosed plane air layers with complete and partial central vertical divisions. Ph.D. thesis, University of Salford.

Eckert, E.R.G. and Jackson, T.W. 1951 Analysis of turbulent free convection boundary layer on flat plate, NACA TR 1015, Washington D.C.

Elder, J.W. 1965a Laminar free convection in a vertical slot. J. Fluid Mech. 23, 77-98.

Elder, J.W. 1965b Turbulent free convection in a vertical slot. J. Fluid Mech. 23, 99-111.

Eyler, L.L. 1980 Predictions of convective losses from a solar cavity receiver, Paper No. 80-C2/SQ1-8, presented at the Century 2 Solar Energy Conference, San Francisco, California.

Forester, C.K. and Emery, A.F. 1972 A computational method for low Mach number unsteady compressible free convection flows. J. Comp. Phys. 10, 487-502.

Fox, J. 1965 Flow regimes in transverse rectangular cavities. Proceedings of the 1965 Heat Transfer and Fluid Mechanics Institute, Stanford University Press, 230-247.

Fraikin, M.P., Portier, J.J. and Fraikin, C.J. 1980 Application of k-ε turbulence model to an enclosed buoyancy driven recirculating flow. Paper ASME 80-HT-83, presented at the joint ASME/AIChE National Heat Transfer Conf., Orlando, Florida.

Gebhart, B. 1969 Natural convection flow, instability and transition. J. Heat Transfer 91, 293-308.

George, W.K., Jr. and Capp. S. 1979 A theory for natural convection turbulent boundary layers next to heated vertical surfaces. Int. J. Heat Mass Transfer 22, 813-826.

Gill, A.E. 1970 A note on the stability of convection in a vertical slot. J. Fluid Mech. 42, 125-127.

Gill, A.E. and Davey, A. 1969 Instabilities of a buoyancy-driven system. J. Fluid Mech. 35, 775-798.

Goldstein, R.J. and Eckert, E.R.G. 1960 The steady and transition free convection boundary layer on a uniformly heated vertical plate. Int. J. Heat Mass Transfer 1, 208-218.

Gray, D.D. and Giorgini, A. 1976 The validity of the Boussinesq approximation for liquids and gases, Int. J. Heat and Mass Transfer 19, 545-551.

Hahn, M. 1969 Experimental investigation of separated flow over a cavity at hypersonic speed. AIAA J. 7, 1082-1088.

Hasan, M.M. and Eichhorn, R. 1979 Local non-similarity solution of free convection flow and heat transfer from an inclined isothermal plate. J. Heat Transfer 101, 642-647.

Haugen, R.L. and Dhanak, A.M. 1966 Momentum transfer in turbulent separated flow past a rectangular cavity. J. Appl. Mech. 23, 641-646.

Haugen, R.L. and Dhanak, A.M. 1967 Heat transfer in turbulent boundary-layer separation over a surface cavity. J. Heat Transfer 89, 335-340.

Hess, C. and Henze, R. 1981 Experimental investigation of natural convection losses from open cavities. Final report for Department of Energy, Contract No. DE-AC01-79ET21105.

Hinze, J.O. 1975 Turbulence, McGraw-Hill, N.Y., 2nd ed.

Hjertager, B.H. and Magnussen, B.F. 1976 Numerical prediction of three-dimensional turbulent buoyant flow in a ventilated room. In Heat Transfer and Buoyant Convection, Studies and Applications for Natural Environments, Buildings and Engineering Systems, (D.B. Spalding and N. Afgan, eds.) Hemisphere Publishing Corp., Washington.

Holman, J.P. 1978 Experimental methods for engineers, McGraw-Hill, New York, 3rd ed.

Humphrey, J.A.C. and Jacobs, E.W. 1981 Free-forced flow convective heat transfer from a rectangular cavity in a channel with variable inclination. Int. J. Heat Mass Transfer 24, 1589-1597.

Humphrey, J.A.C., Miller, L. and Chen, K.S. 1981 Experimental investigation of thermally driven flow in open cavities of rectangular cross-section. In

Convective Losses from Solar Central Receivers (ed. P.K. Falcone), Proceedings of a DOE/SERI/SNLL Workshop, Sandia National Labs., Report No. SAND81-8014.

Humphrey, J.A.C., Sherman, F.S., Le Quere, P.L. and Chen, K.S. 1980 Investigation of free-forced convection flow in cavity-type receivers. Mid-Term Report to Sandia National Laboratories. Also available as Report No. FM-80-6, Department of Mechanical Engineering, University of California, Berkeley.

Jaluria, Y. and Gebhart, B. 1974 On transition mechanisms in vertical natural convection flow. J. Fluid Mech. 66, 307.

Jones, I.P. 1979 A numerical study of natural convection in an air fitted cavity: comparison with experiment. Num. Heat Transfer 2, 193-213.

Jones, W.P. and Launder, B.E. 1972 The prediction of laminarization with a two-equation model of turbulence. Int. J. Heat Mass Transfer 15, 301.

Kato, H., Nishiwaki, N. and Hirata, M. 1968 On the turbulent heat transfer by free convection from a vertical plate. Int. J. Heat Mass Transfer 11, 1117-1125.

Kierkus, W.T. 1968 An analysis of laminar free convection flow and heat transfer about an inclined isothermal plate. Int. J. Heat Mass Transfer 11, 241-253.

Korpela, S.A., Gozum, D. and Baxi, C.B. 1973 On the stability of the conduction regime of natural convection in a vertical slot. Int. J. Heat Mass Transfer 16, 1683-1690.

Kraabel, J.S. 1983 An experimental investigation of the natural convection from a side-facing cubical cavity. Proceedings of the ASME-JSME Thermal Engineering Joint Conference, Vol. 1, pp. 299-306, Honolulu, Hawaii.

Ku, A.C., Doria, M.L. and Lloyd, J.R. 1976 Numerical methods of unsteady buoyant flows generated by fire in a corridor, 16th Symp. Int. Combustion Proc. 10, 1373-1384.

Kublbeck, K., Merker, G.P. and Straub, J. 1980 Advanced numerical computation of two-dimensional time-dependent free convection in cavities. Int. J. Heat Mass Transfer 23, 203-217.

Laitone, E.V. and Laitone, J.A. 1983 Aerodynamic lift at Reynolds number under 70,000 (submitted to J. Fluid Mech.).

Larson, H.K. 1959 Heat transfer in separated flows. J. Aerospace Sciences 26, 731-738.

Launder, B.E. and Humphrey, J.A.C. (eds) 1980 Momentum and heat transfer processes in recirculating flows, HTD-Vol. 13, presented at the 1980 Winter Annual Meeting of the American Society of Mechanical Engineers, Chicago, Illinois.

Le Quere, P.L., Humphrey, J.A.C. and Sherman, F.S. 1981 Numerical calculation of thermally-driven two-dimensional unsteady laminar flow in cavities of rectangular cross-section. Num. Heat Transfer 4, 249-283.

Lin, S.J. and Churchill, S.W. 1978 Turbulent free convection from a vertical, isothermal plate. Num. Heat Transfer 1, 129-145.

Lloyd, J.R. and Sparrow, E.M. 1970 On the instability of natural convection flow on inclined plates. J. Fluid Mech. 42, 465.

Lloyd, J.R., Sparrow, E.M. and Eckert, E.R.G. 1972 Laminar, transition and turbulent natural convection adjacent to inclined and vertical surfaces. Int. J. Heat Mass Transfer 15, 457-473.

Lock, G.S.H. and Trotter, F.J. deB 1968 Observations on the structure of a turbulent free convection boundary layer. Int. J. Heat Mass Transfer 11, 1225.

MacGregor, R.K. and Emery, A.F. 1969 Free convection through vertical plane layers - Moderate and high Prandtl number fluids. J. Heat Transfer 91, 391-403.

Mallinson, G.D. and de Vahl Davis, G. 1977 3-dimensional natural convection in a box: a numerical study. J. Fluid Mech. 83, 1-31.

Mao, C.P., Fernandez-Pello, A.C. and Humphrey, J.A.C. 1982 An investigation of steady wall-ceiling and partial enclosure fires. J. Heat Transfer, 106, 221-228.

Markatos, N.C., Malin, M.R. and Cox, G. 1982 Mathematical modelling of buoyancy-induced smoke flow in enclosures. Int. J. Heat Mass Transfer 25, 63-75.

Mason, H.B. and Seban, R.A. 1974 Numerical predictions for turbulent free convection from vertical surfaces. Int. J. Heat Mass Transfer 17, 1329-1336.

Maull, D.J. and East, L.F. 1963 Three-dimensional flow in cavities, J. Fluid Mech. 16, 620-632.

McGregor, O.W. and White, R.A. 1970 Drag of rectangular cavities in supersonic and transonic flow including the effects of cavity resonance. AIAA J. 8, 1959-1964.

McLaughlin, D.K. and Tiederman, W.G. 1973 Biasing correction for individual realization of laser anemometer measurements in turbulent flows. Phys. of Fluids 16, 1082-1088.

Mirenayat, H. 1981 Etude experimentale de transfert de chaleur par convection naturelle dans une cavite isotherme ouverte. Ph.D. thesis, University of Poitiers, France.

Nansteel, M.W. and Greif, R. 1981 Natural convection in individual and partially divided rectangular enclosures. J. Heat Transfer 103, 623-629.

Nicoll, K.M. 1964 A study of laminar hypersonic cavity flows. AIAA J. 2, 1535-1541.

Olson, M.D. and Tuann, S.Y. 1978 Computing methods for recirculating flow in a cavity. Numerical Methods in Laminar and Turbulent Flow, Proc. of 1st Inst. Conf., University of College, Swansea.

Oosthuizen, P.H. 1967 Heat transfer by turbulent free-convection from a vertical plate. S. Afr. Mech. Eng. 16, 260-264.

Orlandi, P., Onofri, M. and Subetta, F. 1978 Interaction between natural and forced convection in a complex geometry, Proceedings of the 1978 Heat Transfer and Fluid Mechanics Institute, Stanford University Press.

Ostrach, S. 1953 An analysis of laminar free-convection flow and heat transfer about a flat plate parallel to the direction of the generating body force. NACA Tech. Report No. 1111.

Penot, F. 1981 Contribution a l'Etude de la convection naturelle dans less espaces semi-confines. Ph.D. thesis, University of Poitiers, France.

Penot, F. 1982 Natural convection in isothermal open cavities. Num. Heat Transfer 5, 421-437.

Pepper, D.W. and Harris, S.D. 1978 Numerical solution of three dimensional natural convection by the strongly implicit procedure. Paper No. 78-WA/HT-10, presented at the ASME Winter Annual Meeting, San Francisco, California.

Pera, L. and Gebhart, B. 1973 On the stability of natural convection boundary layer flow over horizontal and slightly inclined surfaces. Int. J. Heat Mass Transfer 16, 1147-1163.

Phillips, O.M. 1966 The dynamics of the upper ocean, Cambridge University Press.

Plumb, O.A. and Kennedy, L.A. 1977 Application of a k-ϵ turbulence model to natural convection from a vertical isothermal surface. J. Heat Transfer 99, 79-85.

Randall, K.R., Mitchell, J.W. and El-Wake, M.M. 1979 Natural convection heat transfer characteristics of flat plate enclosures. J. Heat Transfer 101, 120-125.

Rich, B.R. 1953 An investigation of heat transfer from an inclined flat plate in free convection. TRAS. ASME, 75, 489.

Roache, P.J. and Muller, T.J. 1970 Numerical solutions of laminar separated flows. AIAA J. 8, 530-538.

Rossiter, J.E. 1964 Wind-tunnel experiments on the flow over rectangular cavities at subsonic and transonic speeds. Aeronautical Research Council. Reports and Memoranda No. 3438.

Rotem, Z. and Claassen, L. 1969 Natural convection above unconfined horizontal surfaces. J. Fluid Mech. 39, 173-192.

Salcudean, M. and Abdelrehim, I. 1980 Heat transfer in turbulent recirculatory flows affected by buoyancy forces in rectangular cavities. Chem. Eng. Commun. 4, 249-268.

Scadron, M.D. and Warshawsky, I. 1952 Experimental determination of time constants and Nusselt number for bare-wire thermocouples in high-velocity air

streams and analytical approximation of conduction and radiation errors, NACA TN 2599.

Schmidt, F.W. and Wang, D.F. 1982 Experimental study of turbulent natural convection in an enclosure. Paper No. 82-WA/HT-72, presented at the ASME Winter Annual Meeting, Nov. 14-19, Phoenix, Arizona.

Sernas, V. and Kyriakides, I. 1982 Natural convection in an open cavity, Proceedings of the Seventh International Heat Transfer Conference, Munich, Fed. Rep. of Germany 2, 275-280.

Serrin, J. 1972 The Swirling Vortex. Phil. Trans. Roy. Soc. A 271 325-360.

Siebers, D. 1979 Natural convective heat transfer from an external receiver, Report SAND78-8276, Sandia National Laboratories, Livermore.

Siebers, D.L., Abrams, M. and Gallagher, R.J. 1979 Solar thermal central receiver systems, paper 79-WA/HT-38, presented at the ASME Winter Annual Meeting, New York, N.Y.

Siebers, D.L., Moffat, R.J. and Schwind, R.G. 1983 Experimental variable properties natural convection from a large, vertical, flat surface. Proceedings of the ASME-JSME Thermal Engineering Joint Conference, Vol. 3, 269-278, Honolulu, Hawaii.

Tchen, C.M. 1947 Mean value and correlation problems connected with the motion of small particles suspended in a turbulent fluid. Ph.D. Thesis, Delft.

To, W.M. 1984 Numerical investigation of strongly heated open cavity flow, Ph.D. Thesis, University of California.

Tritton, D.J. 1963 Transition to turbulence in the free convection boundary layers on an inclined heated plate. J. Fluid Mech. 16, 417-435.

Turi, P. 1981 A laser-Doppler velocimetry system designed for two-phase flow. Master Report, Department of Mechanical Engineering, University of California, Berkeley.

Turner, J.S. 1973 Buoyancy effects in fluids, Cambridge, University Press.

Vest, C.M. and Arpaci, V.S. 1969 Stability of natural convection in a vertical slot. J. Fluid Mech. 36, 1-15.

Vliet, G.C. 1969 Natural convection local heat transfer on constant-heat-flux inclined surfaces. J. Heat Transfer 91, 511-516.

Vliet, G.C. and Ross, D.C. 1975 Turbulent natural convection on upward and downward facing inclined constant heat flux surfaces. J. Heat Transfer 97, 549-555.

Warner, C.Y. and Arpaci, V.S. 1968 An experimental investigation of turbulent natural convection in air at low pressure along a vertical heated flat plate. Int. J. Heat Mass Transfer 11, 397.

White, R.A. 1971 Some results on the heat transfer within resonant cavities at subsonic and supersonic Mach numbers. J. Basic Engr. 93, 537-542.

	Laser Beam	
Parameters	Green	Blue
Wavelength of Laser Beam (nm)	514.5	488.0
Focal Length (mm)	505	505
Expansion Ratio	1.9375	1.9375
Beam Separation (mm)	35.65	35.65
Beam Intersection Angle γ, (deg.)	4.04	4.04
Beam Half-Angle, $\gamma/2$ (deg.)	2.02	2.02
Probe Volume Diameter (mm)	0.1365	0.1365
Probe Volume Length (mm)	3.87	3.67
Fringe Spacing (μm)	7.29	6.91
Number of Fringes in Probe Volume	18	18
Calibration Factor (m s^{-1}/MHz)	7.29	6.91

Table 2.1 LDV optical system parameters

			VARIABLE DETERMINED		
a/b	α		U, V, W $\overline{u^2}$, $\overline{v^2}$, $\overline{w^2}$, $\overline{uv}$	T	Photographs
0.5	0°	$\Delta T/T_\infty$ Gr_∞ Gr/Re^2	1.2 4.2×10^7 ∞	1.18 4.01×10^7 459.8 - 0.56 and ∞	1.18 4.01×10^7 439.7 - 5.38 and ∞
	20°	$\Delta T/T_\infty$ Gr_∞ Gr/Re^2	——	1.18 4×10^7 110.4 - 0.56 and ∞	1.18 4×10^7 683.6 - 0.55 and ∞
	45°	$\Delta T/T_\infty$ Gr_∞ Gr/Re^2	——	1.2 4.06×10^7 274 - 1.16 and ∞	——
1.0	0°	$\Delta T/T_\infty$ Gr_∞ Gr/Re^2	1.19 4.14×10^7 ∞	1.19 4.03×10^7 225.3 - 0.55 and ∞	1.19 4.03×10^7 306.9 - 0.55 and ∞
	20°	$\Delta T/T_\infty$ Gr_∞ Gr/Re^2	——	1.26 4.28×10^7 231.9 - 0.58 and ∞	1.26 4.28×10^7 324.7 - 0.58 and ∞
	45°	$\Delta T/T_\infty$ Gr_∞ Gr/Re^2	1.19 4.2×10^7 ∞	1.26 4.27×10^7 233.7 - 0.57 and ∞	1.26 4.27×10^7 324.7 - 0.58 and ∞
1.46	0°	$\Delta T/T_\infty$ Gr_∞ Gr/Re^2	——	1.24 4.2×10^7 117.4 - 0.57 and ∞	1.24 4.2×10^7 718.9 - 0.57 and ∞
	20°	$\Delta T/T_\infty$ Gr_∞ Gr/Re^2	——	1.21 4.09×10^7 701.6 - 0.58 and ∞	1.21 4.09×10^7 667.7 - 0.56 and ∞
	45°	$\Delta T/T_\infty$ Gr_∞ Gr/Re^2	——	1.2 4.07×10^7 695.8 - 0.58 and ∞	1.2 4.07×10^7 662.2 - 0.56 and ∞

Table 3.1 Test matrix of experimental conditions

α	$-y/b = -(Gr_y/Gr_b)^{1/3}$			
	Theoretical critical value (Chen & Tszoo) 1982	Value inferred from expt. (Rotem & Claassen) 1969	Value inferred from expt. (Pera & Gebhart) 1973	Value for first visible plumes (this study)
0°	0.020	0.23 - 0.28	0.35	0.23 - 0.48
20°	0.037	—	probably > 1.0 (extrapolation)	0.39 - 0.54
45°	0.083	—	—	0.82

Table 3.2 Instability and plume formation on bottom wall (Other authors present values of Gr_y. Our value of $Gr_b = 4.2 \times 10^7$)

	$\dot{Q}_a/c$ (W/m)	$\dot{Q}_b/c$ (W/m)	$\dot{Q}_c/c$ (W/m)	$\dot{Q}_d/c$ (W/m)	$\Sigma\dot{Q}_i/c$ (W/m)	σ_Σ (W/m)
a/b = 0.5 α = 0°	3750	- 500	- 3510	490	230	± 70
a/b = 1.0 α = 0°	4150	- 250	- 2850	- 960	90	± 50
a/b = 1.0 α = 45°	2490	- 150	- 2190	20	170	± 40

Table 3.3 Heat convection across control surfaces a,b,c and d shown in Fig. 23.

	$\dot{Q}_b/c$ (out)	$\dot{Q}_b/c$ (in)	$\dot{Q}_b/c$ (net out)	σ (net)
$a/b = 0.5$ $\alpha = 0°$	1280	780	500	± 35
$a/b = 1.0$ $\alpha = 0°$	1690	1440	250	± 29
$a/b = 1.0$ $\alpha = 45°$	2150	2000	150	± 29

Table 3.4 Heat convection, in and out, across the aperture plane. (Watts/m)

	$\dot{m}_b/c$ (out) $\times 10^3$ (kg/m·s)	$\dot{m}_b/c$ (in) $\times 10^3$ (kg/m·s)	$\dot{m}_b/c$ (net) $\times 10^3$ (kg/m·s)	σ (net) $\times 10^3$ (kg/m·s)	$\frac{\bar{\rho}_{out}}{\rho_\infty}$	$\frac{\bar{\rho}_{in}}{\rho_\infty}$
a/b = 0.5 α = 0°	3.16	2.45	0.71	± 0.13	0.730	0.952
a/b = 1.0 α = 0°	4.14	4.60	- 0.46	± 0.10	0.730	0.909
a/b = 1.0 α = 45°	5.27	6.10	- 0.83	± 0.10	0.736	0.936

Table 3.5 Mass flux and mean densities;

$$\dot{m}_b/c = \frac{p_\infty}{R} \int_0^b (V/T)\, dx \quad \text{in the aperture plane}$$

	h ($W/m^2 °K$)	Nu	Gr	$\Delta T/T_\infty$
a/b = 0.5 α = 0°	14.9 ± 1.0	54.1 ± 3.8	4.2×10^7	1.20
a/b = 1.0 α = 0°	7.5 ± 0.9	27.2 ± 3.2	4.1×10^7	1.19
a/b = 1.0 α = 45°	4.6 ± 0.9	16.6 ± 3.2	4.2×10^7	1.19

Table 3.6 Aperture-plane heat transfer coefficients and nusselt numbers. (The reference area for h is that of the aperture plane. The reference length in Nu is b, the height of the aperture plane.)

		$\alpha = 0°$	$\alpha = 20°$	
a/b = 0.5	$T_{bac}(K)$	678	678	
	$\Delta T/T_\infty$	1.19	1.18	
	Gr	4.03×10^7	$4. \times 10^7$	
	Re	190.64	362.68	
	Gr/Re^2	459.78	304.1	
	f(Hz)	3^{++}	5.5^{+}	
	Photos	---	Figs. 39 (A-D)	
a/b = 1.0	$T_{bac}(K)$	678	690	476
	$\Delta T/T_\infty$	1.19	1.26	0.46
	Gr	4.03×10^7	4.27×10^7	1.56×10^7
	Re	422.94	246.83	*
	Gr/Re^2	225.29	700.85	*
	f(Hz)	5^{++}	$4\text{-}5^{+++}$	$2\text{-}3^{+++}$
	Photos	---	Fig. 40a	Fig. 40b

\+ stroboscopic lamp
++ temperature time trace at x/b = 0.87
+++ counting with stop watch
* wind is about to stop

Table 3.7 Experimental conditions for periodic oscillation

Error Source	Error Type	
	SYSTEMATIC given as percent deviation from local mean value	RANDOM given as percent r.m.s. variation about local mean value
Thermocouple positioning *	< 10°C	< 3°C
Radiation effects	< 10°C	nil
Conduction losses	nil	nil
Statistical uncertainty due to finite sample size. Estimated for samples of 100 measurements	nil, except **	± 1 to 5°C

* Error limited to fairly small regions of the flow.
** Indeterminate if flow fluctuates periodically, at an integer multiple of sampling frequency - a rare occurrence.

Table 4.1 Sources and magnitudes of maximum estimates errors affecting temperature measurements

	Run		
Variable	Run 1 (ϕ_1)	Run 2 (ϕ_2)	$\frac{\lvert\phi_1 - \phi_2\rvert}{\lvert\phi_1 + \phi_2\rvert/2} \times 100\%$
U (m/s)	0.169	0.166	1.8%
$\lvert V\rvert$ (m/s)	0.091	0.099	8.4%
W (m/s)	-	-	-
$\overline{u^2}$ (m^2/s^2)	0.0085	0.0095	11.2%
$\overline{v^2}$ (m^2/s^2)	0.0373	0.0329	12.5%
$\overline{w^2}$ (m^2/s^2)	-	-	-
$\overline{uv}$ (m^2/s^2)	0.0017	0.0015	16.8%
T (K)	365.1	362.2	0.4%

Table 4.2 Experimental reproducibility shown as percent deviation between variables measured on separate occasions for nominally identical conditions: velocity and turbulent stresses were for the case of $a/b = 0.5$, $\alpha = 0°$, $\Delta T/T_\infty \simeq 1.2$, $Gr = 4.2 \times 10^7$; temperature was for the case of $a/b = 0.5$, $\alpha = 20°$, $\Delta T/T_\infty = 1.18$, $Gr = 4.0 \times 10^7$.

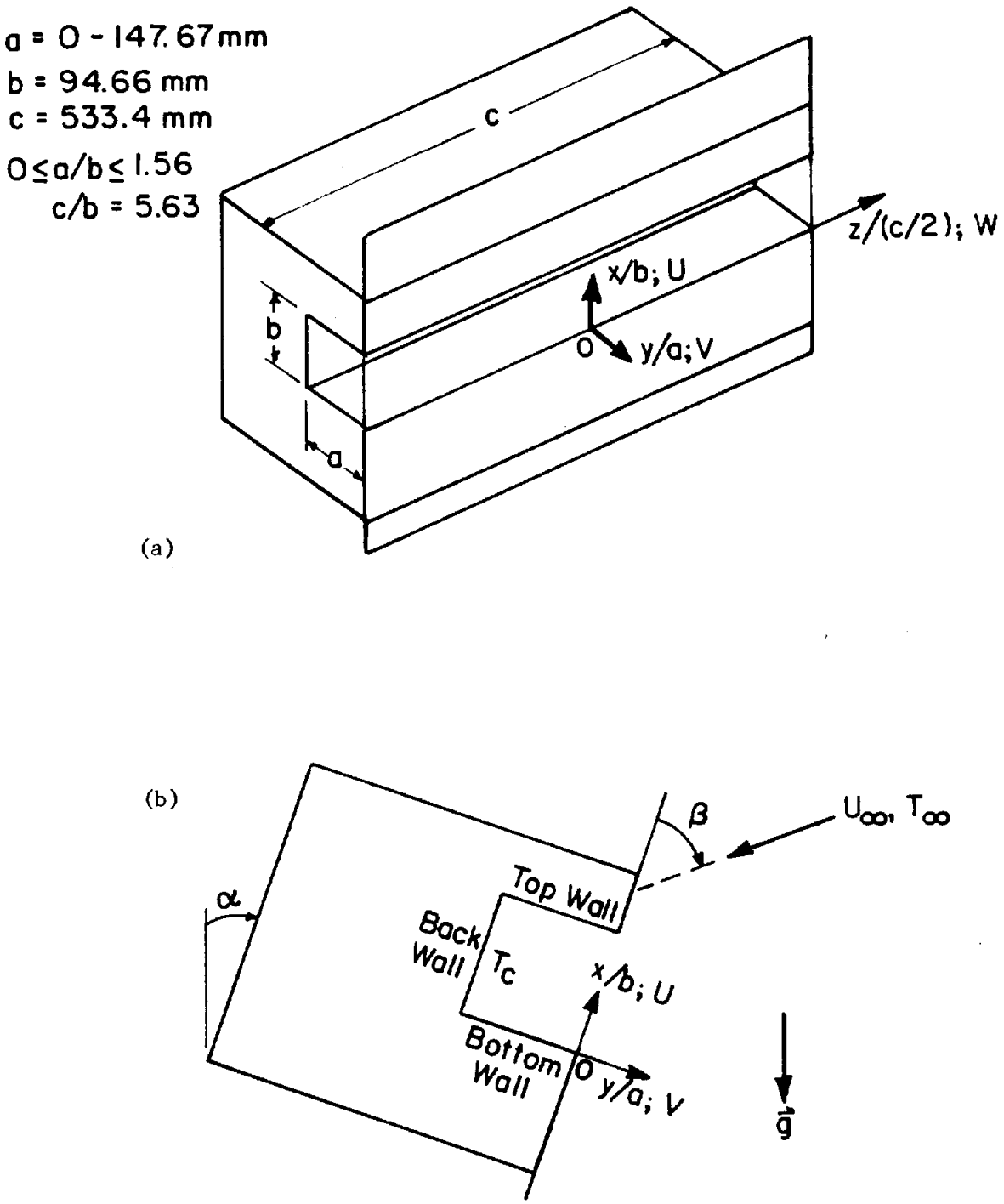

Figure 1 Perspective (a) and side (b) views of the cavity test section. Coordinates and characteristic dimensions indicated.

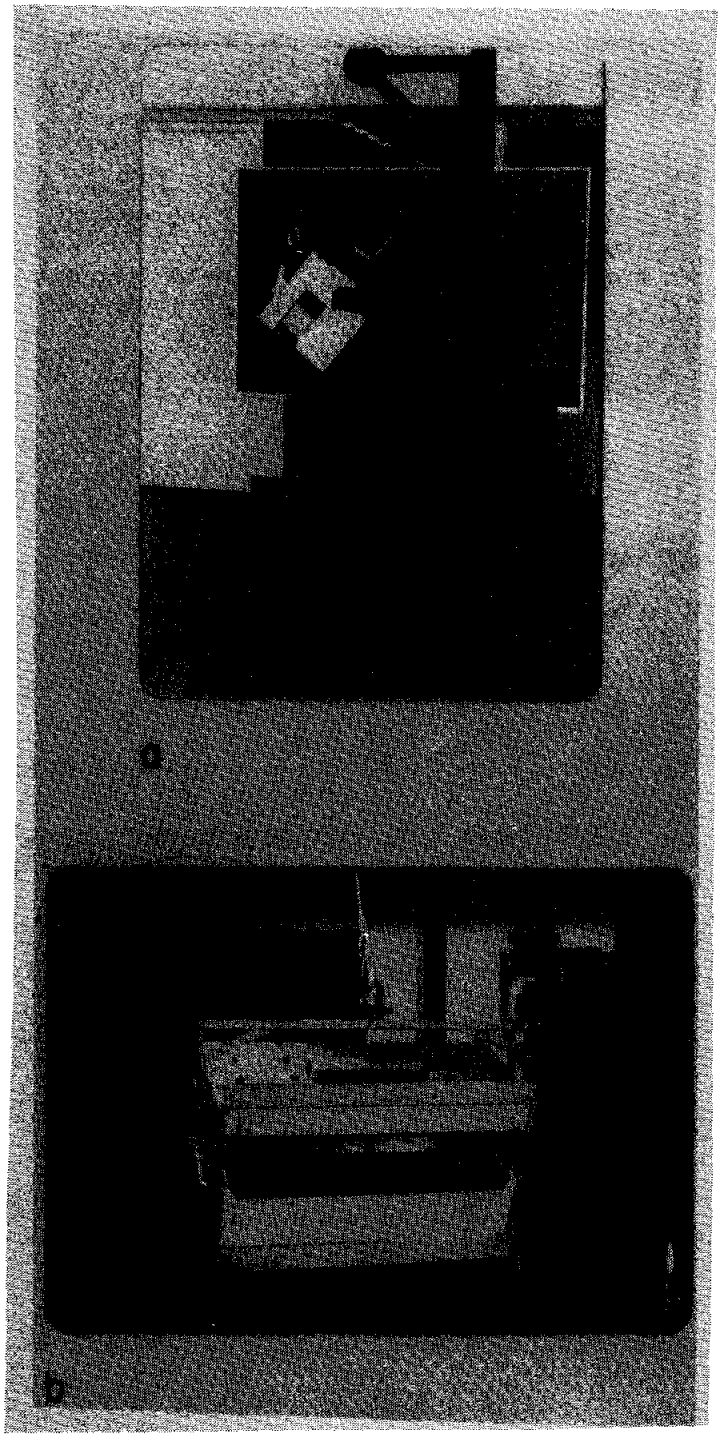

Figure 2 Different views of cavity test section and its supporting frame.

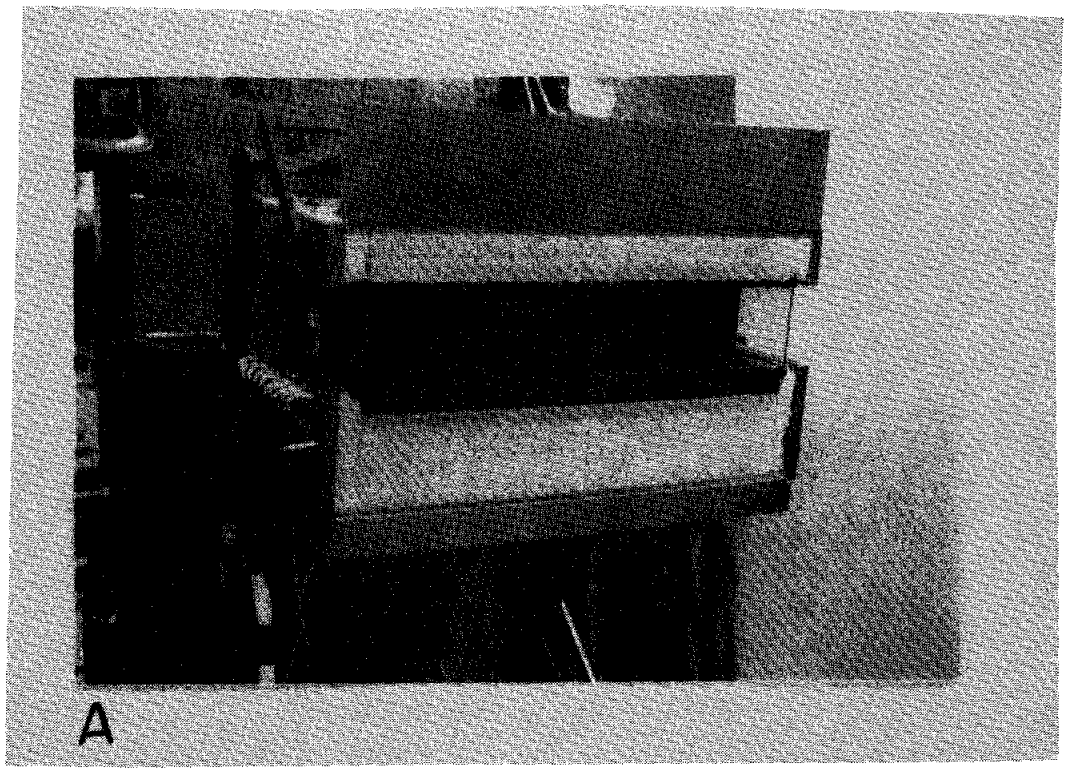

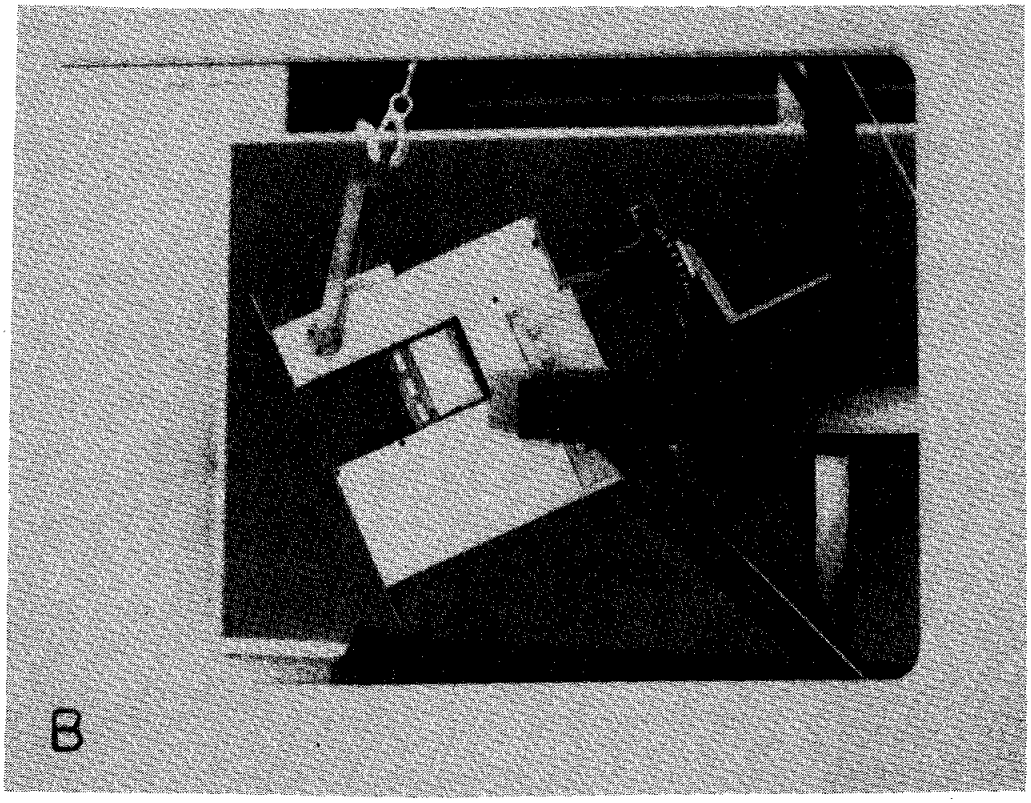

Figure 2 Different views of cavity test section and its supporting frame.

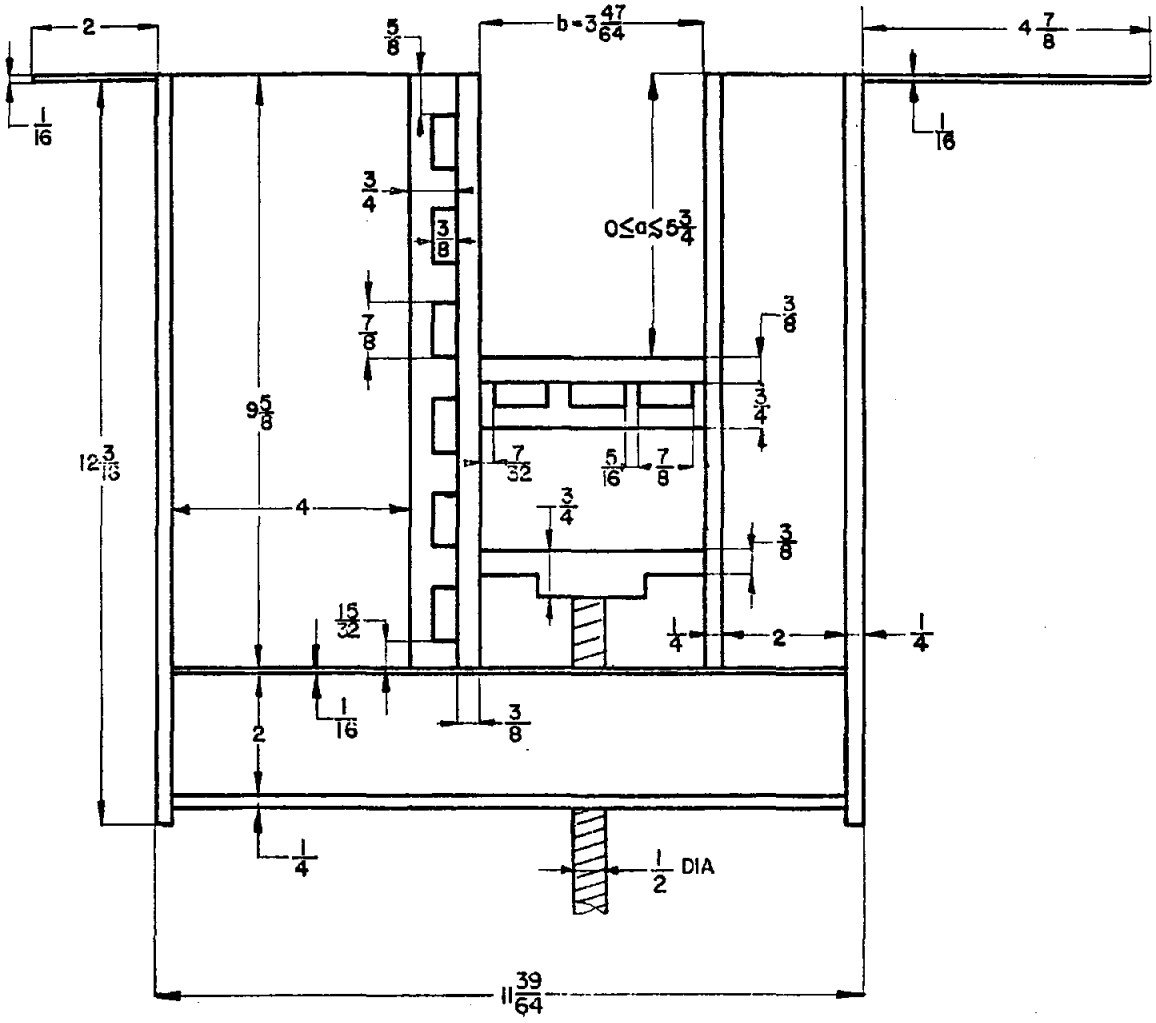

(a)

Figure 3 Test section dimensions: a) side view; b) front view.

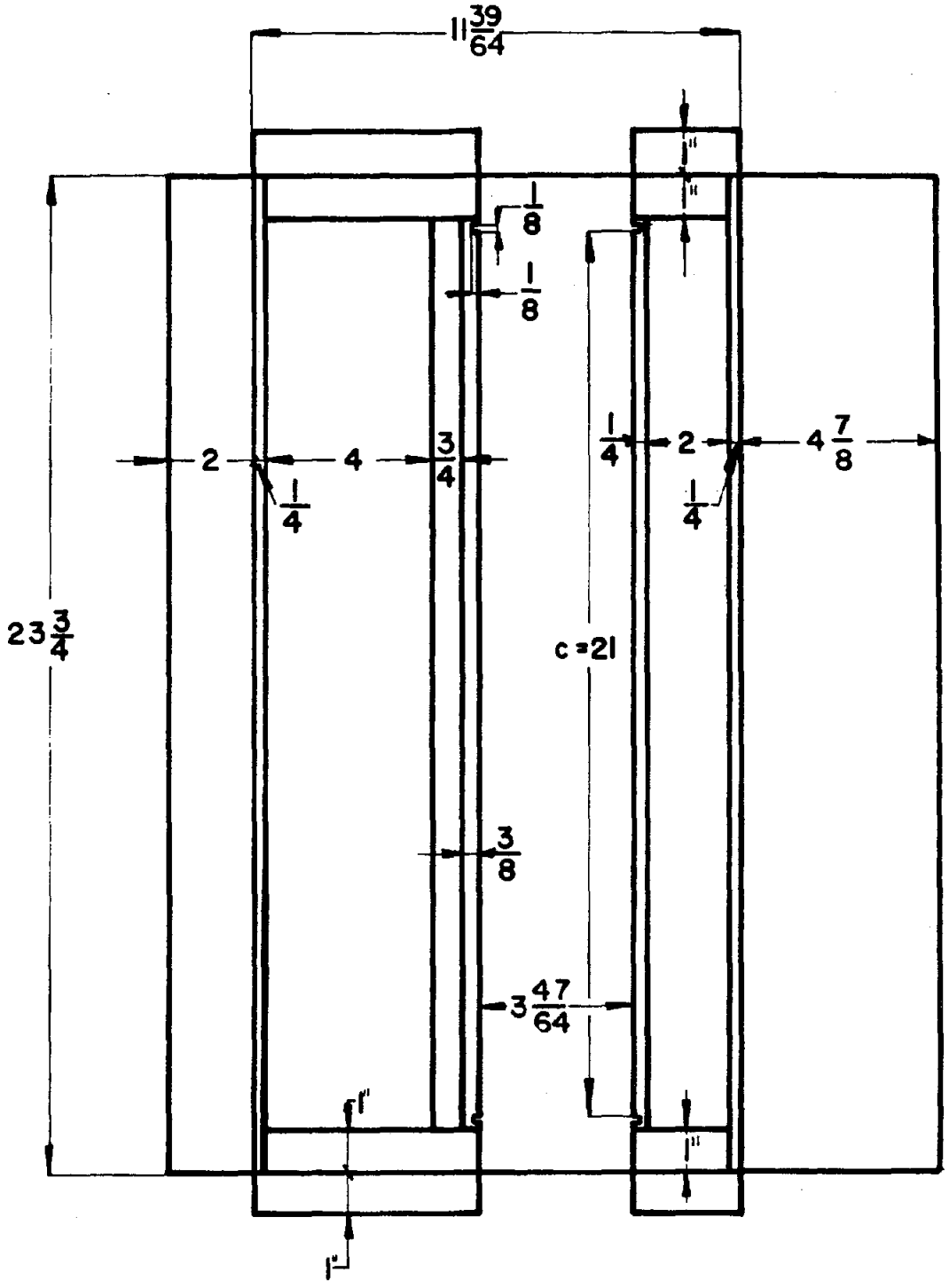

(b)

Figure 3 Test section dimensions: a) side view; b) front view.

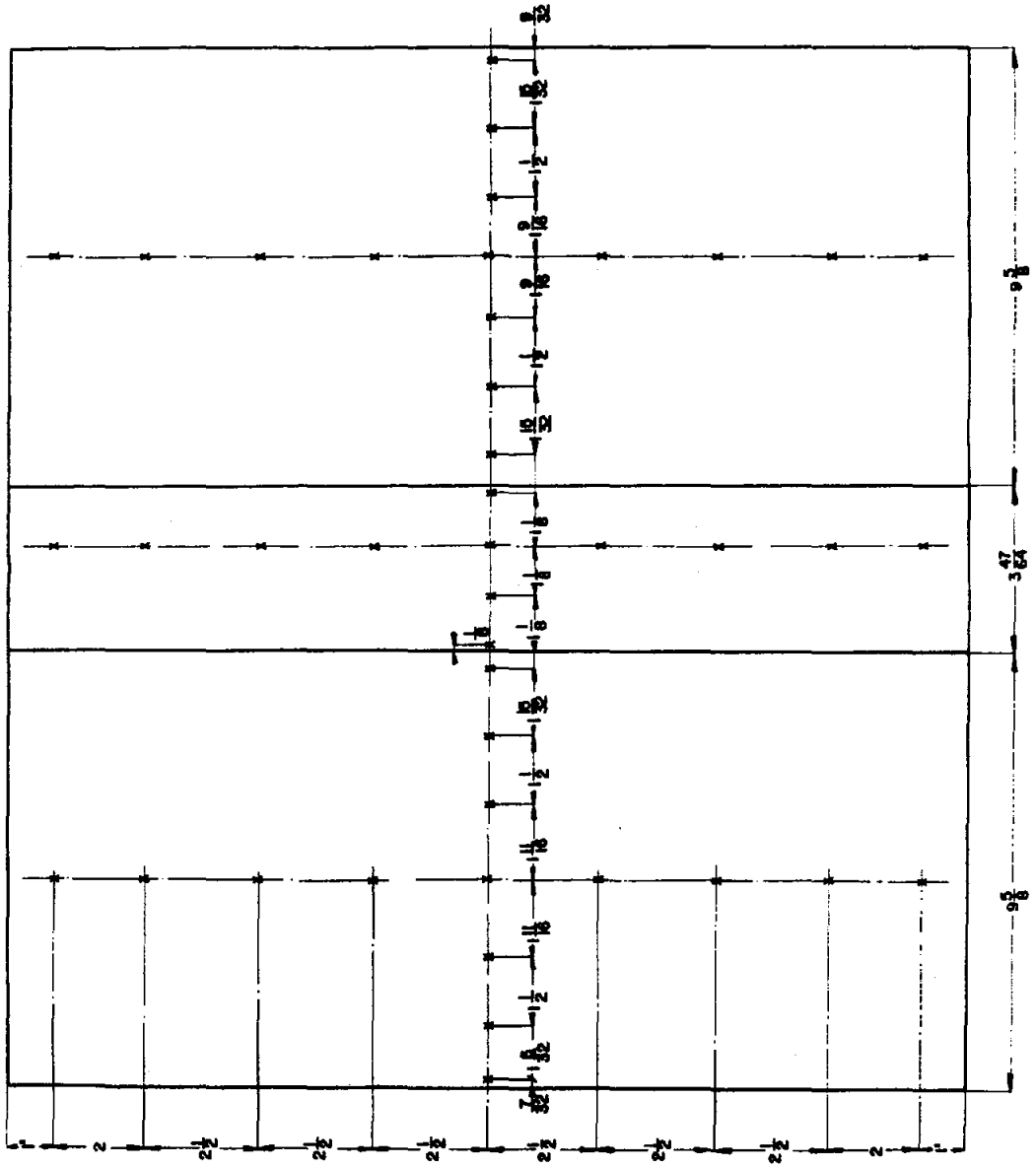

Figure 4 Unfolded view of thermocouple locations on cavity copper walls, spacings given in inches.

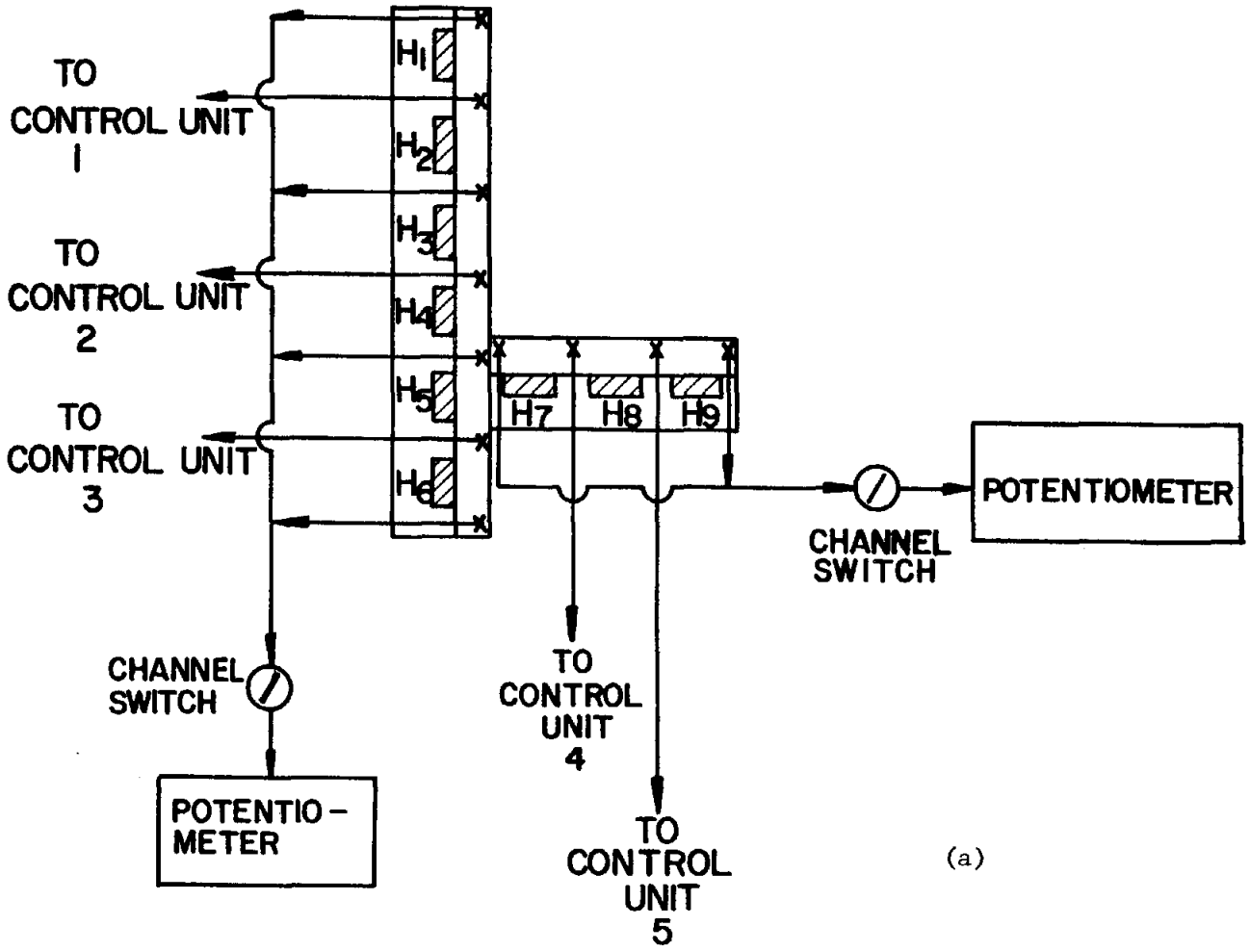

Figure 5 Block diagrams of: a) temperature control unit wiring to heaters; and, b) connections between a control unit and its heaters.

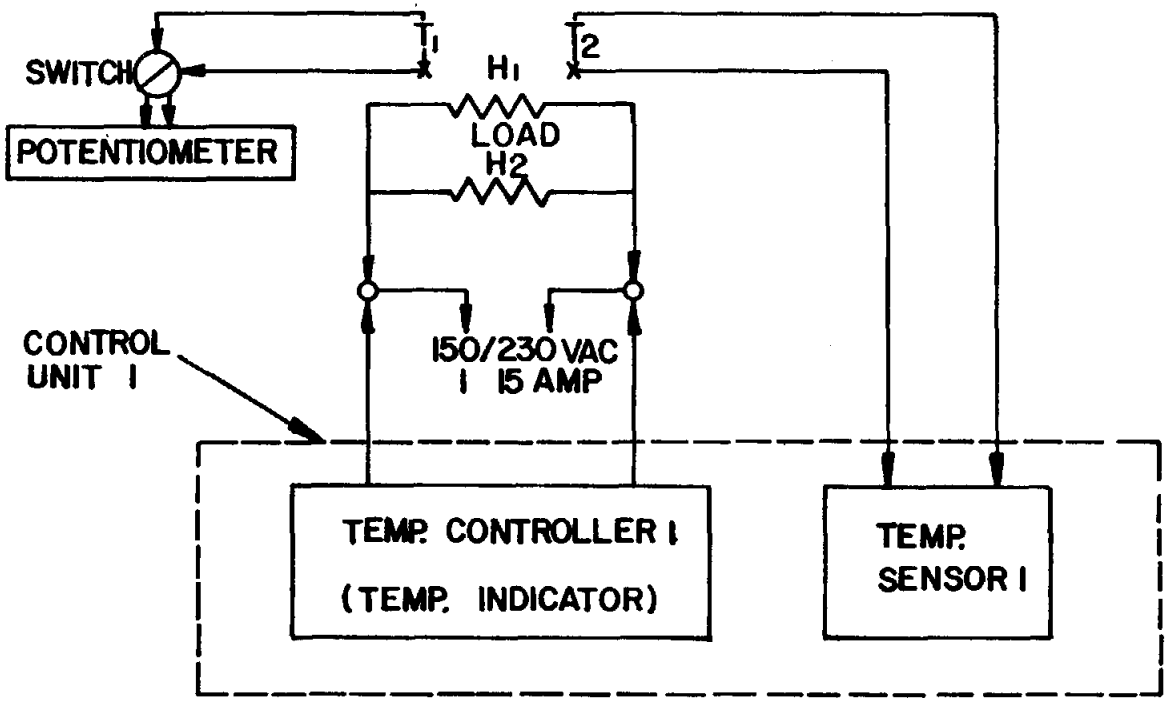

(b)

Figure 5 Block diagrams of: a) temperature control unit wiring to heaters; and, b) connections between a control unit and its heaters.

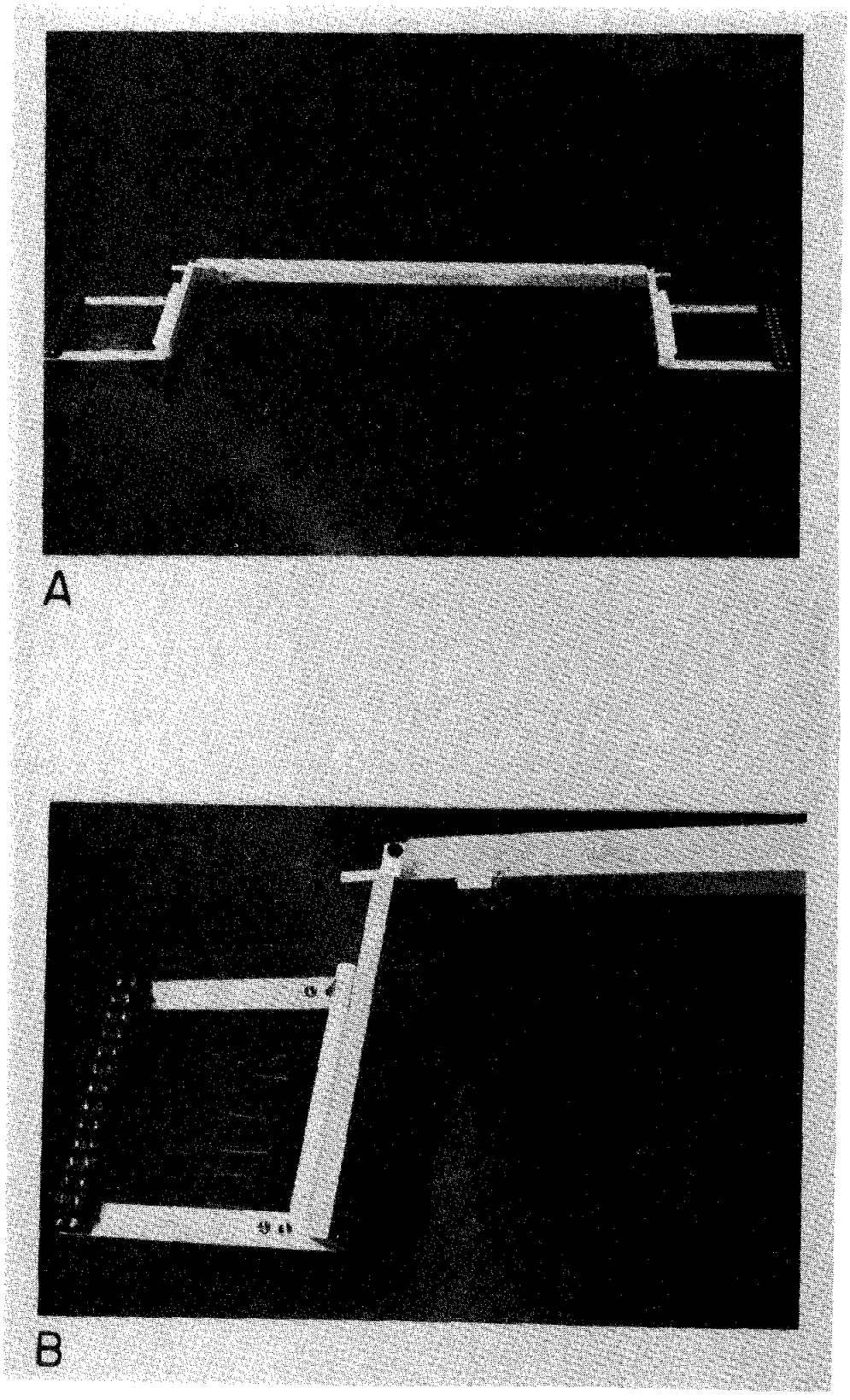

Figure 6 Photographs of aperture plane thermocouple harness: A) full view; B) detail of paper-clip spring mounts and teflon spacing bar.

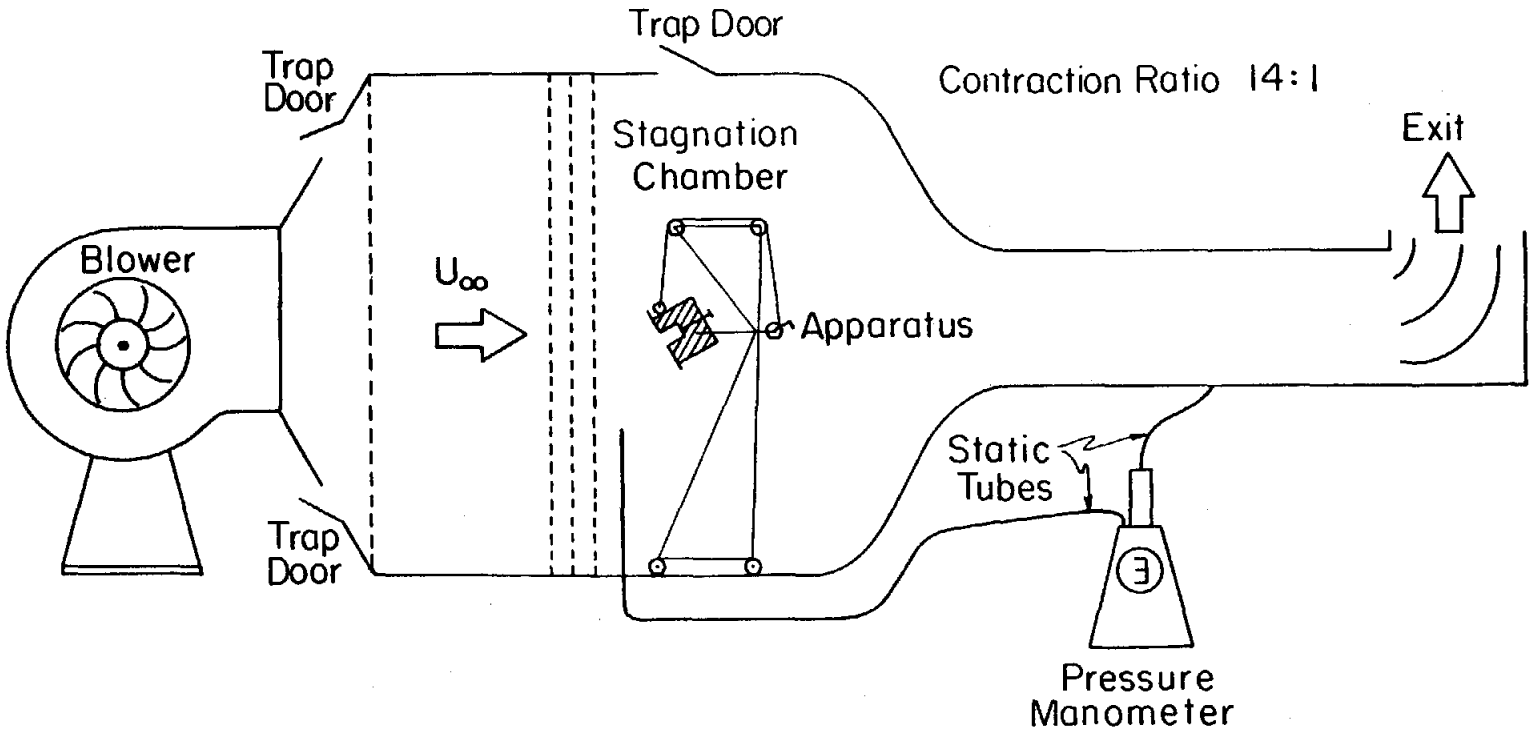

Figure 7 Schematic of subsonic wind-tunnel with apparatus placed in the stagnation chamber (roughly to scale).

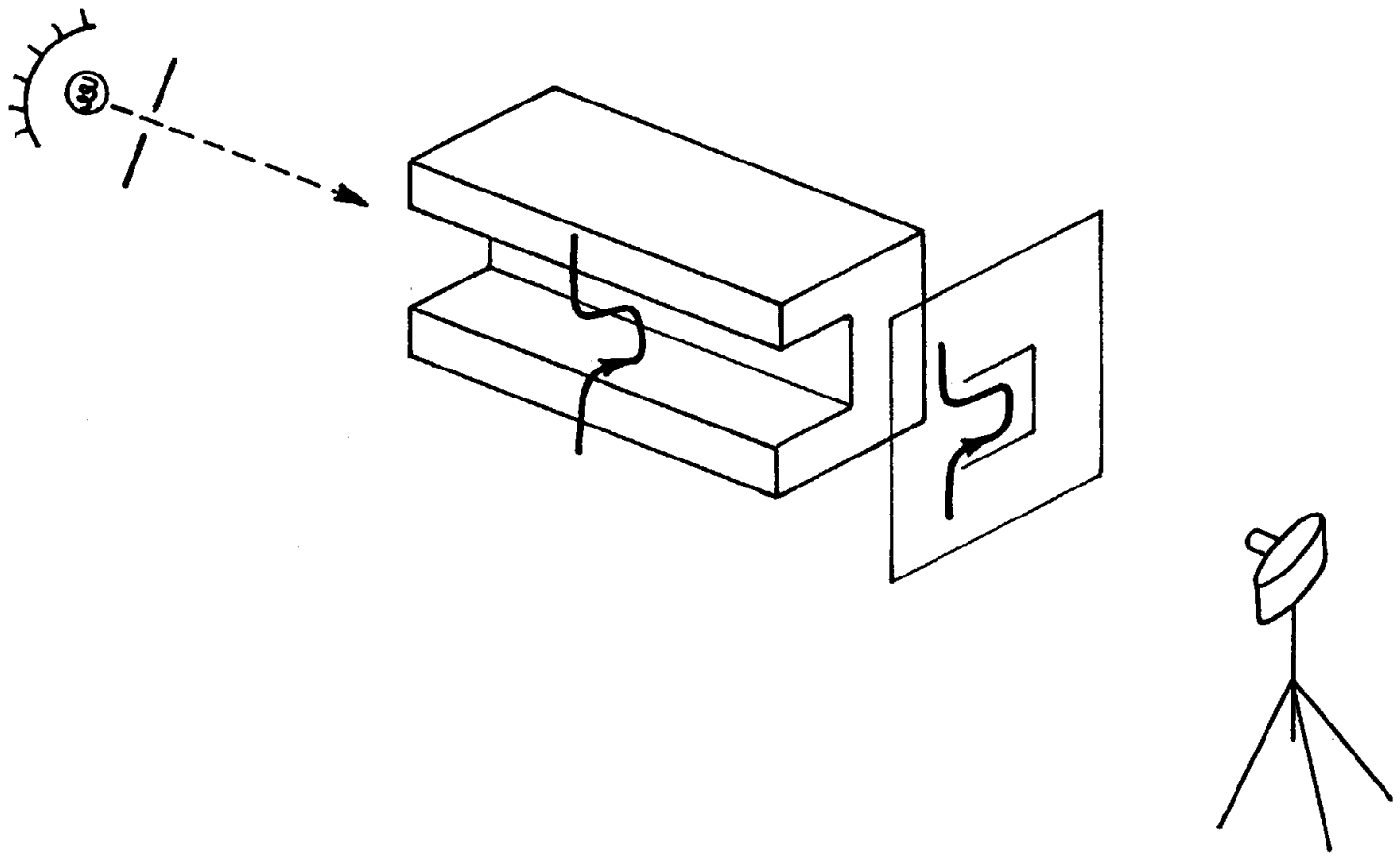

Figure 8 Schematic of shadowgraph optical arrangement.

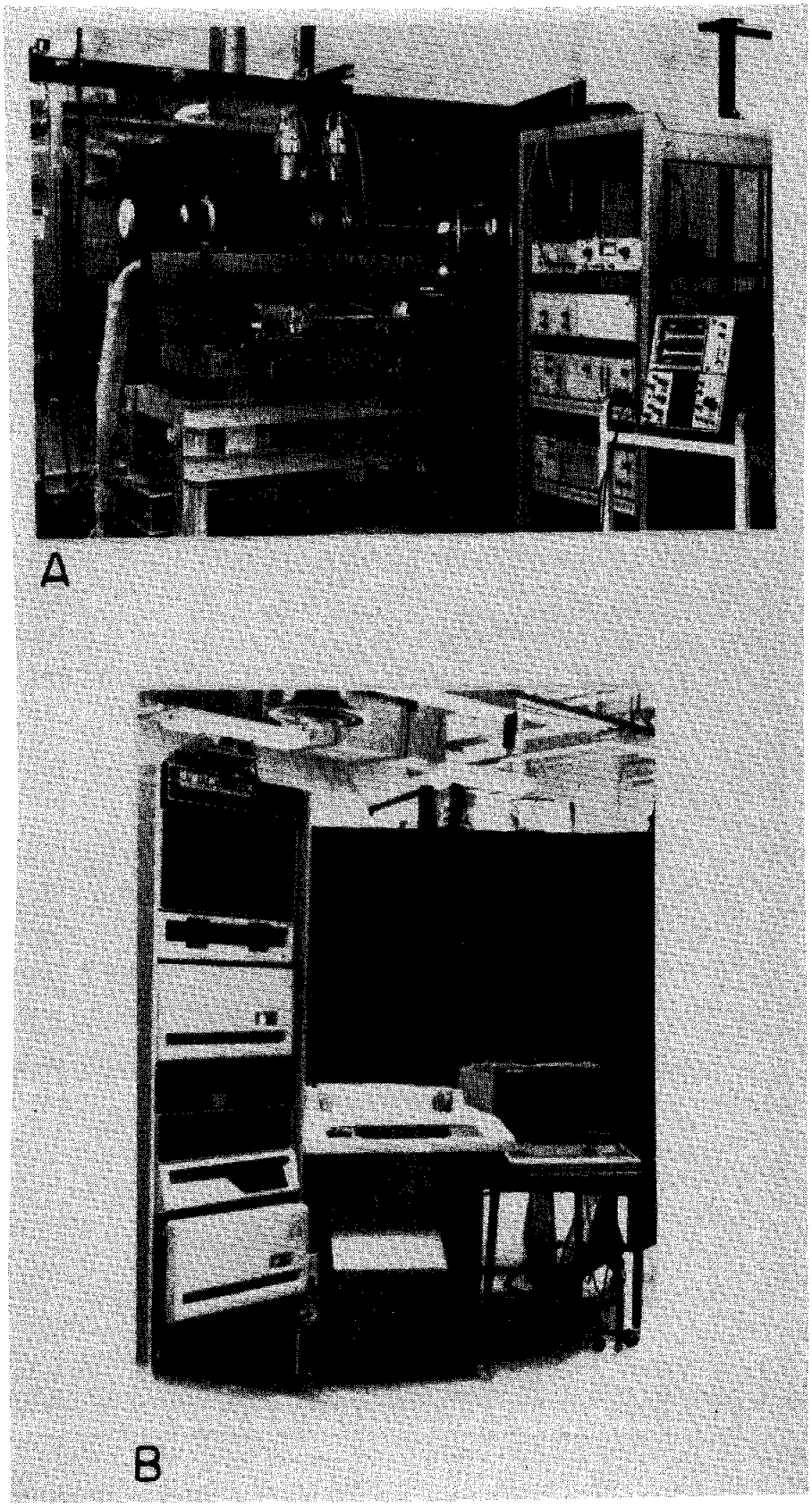

Figure 9 Photographs of laser-Doppler velocimeter and associated instrumentation: A) velocimeter; B) minicomputer.

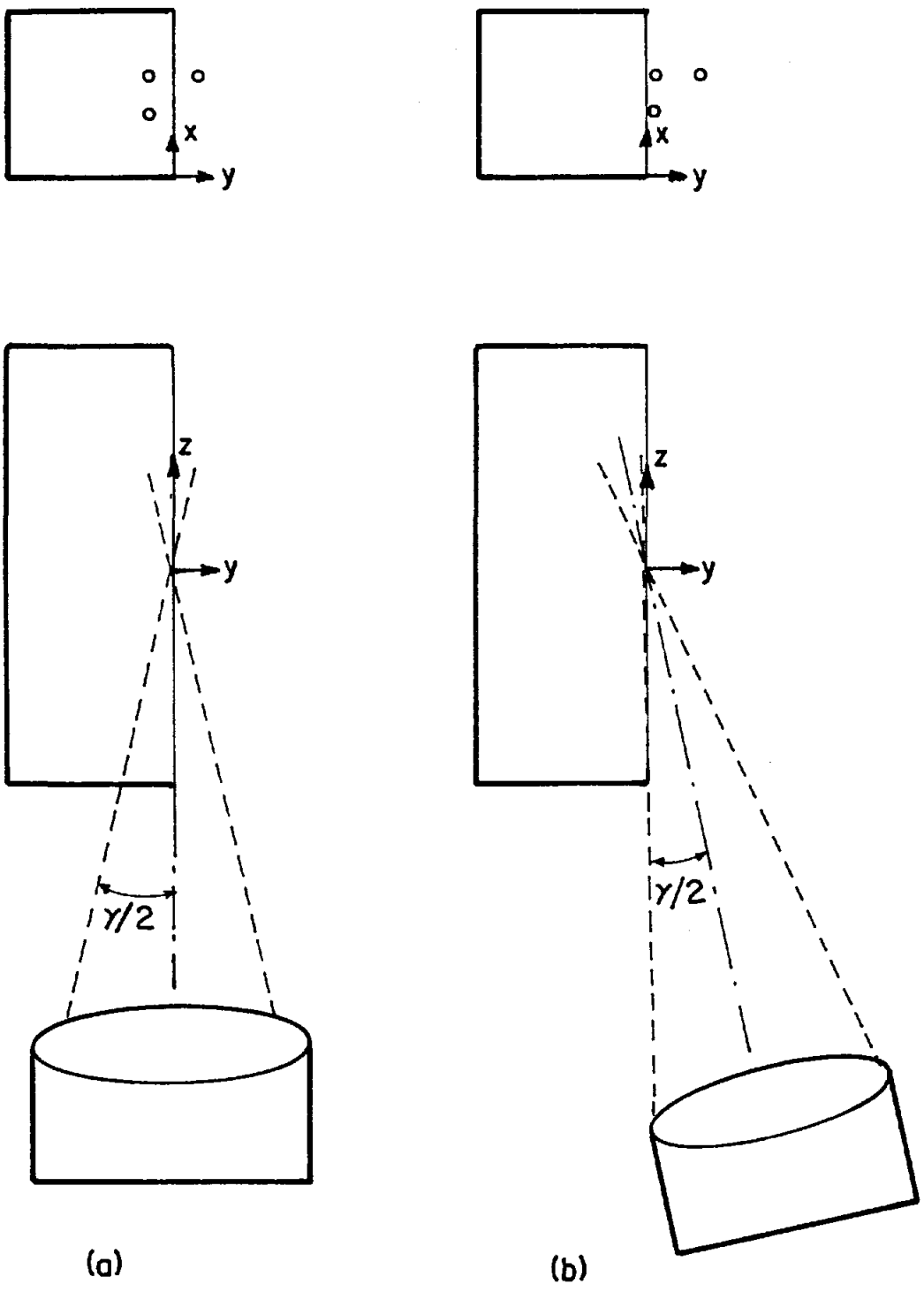

Figure 10 Optical alignment unequal path length problem (a), and solution (b).

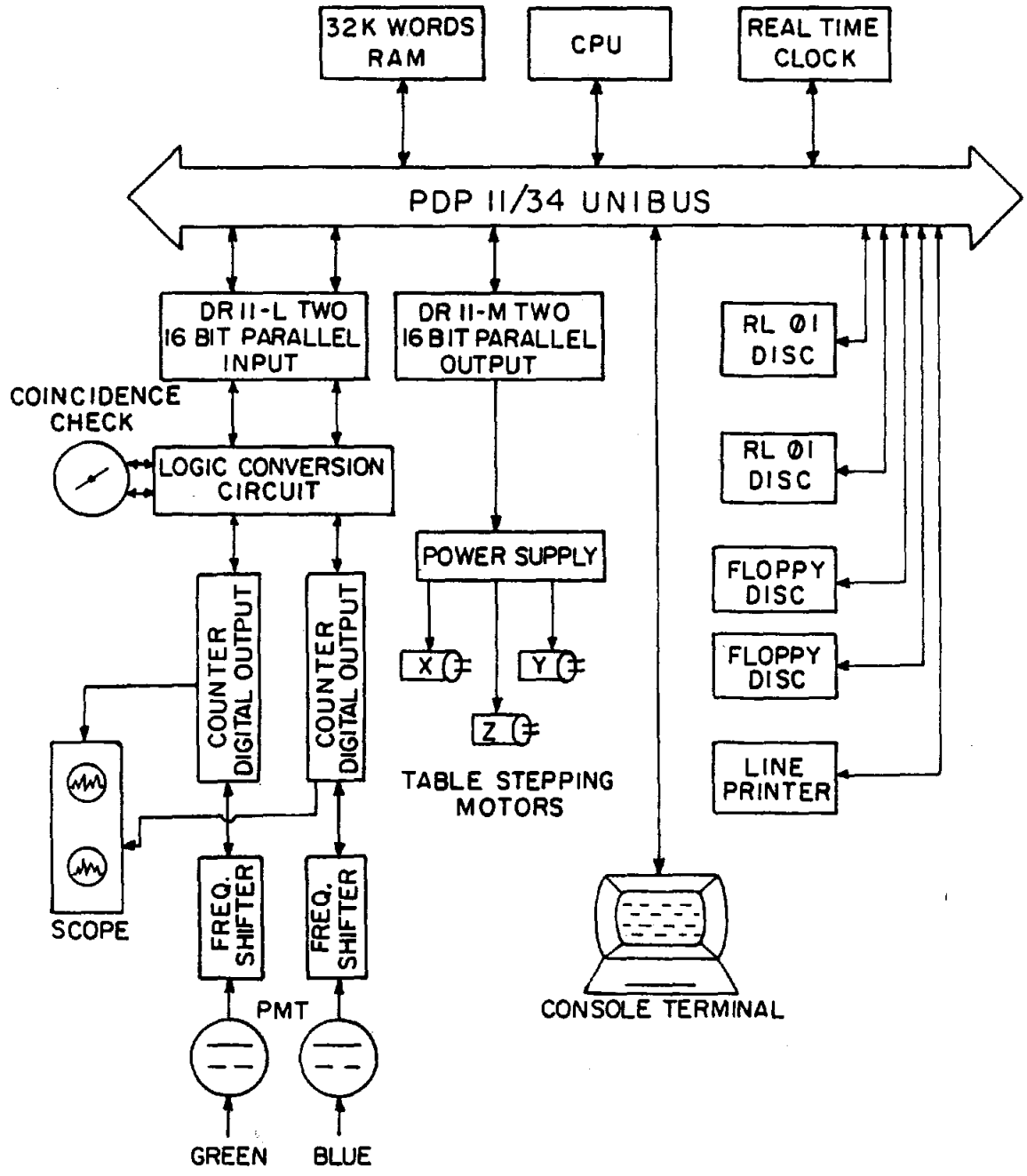

Figure 11 Schematic showing interconnected velocimeter electronic components and coincidence check hardware.

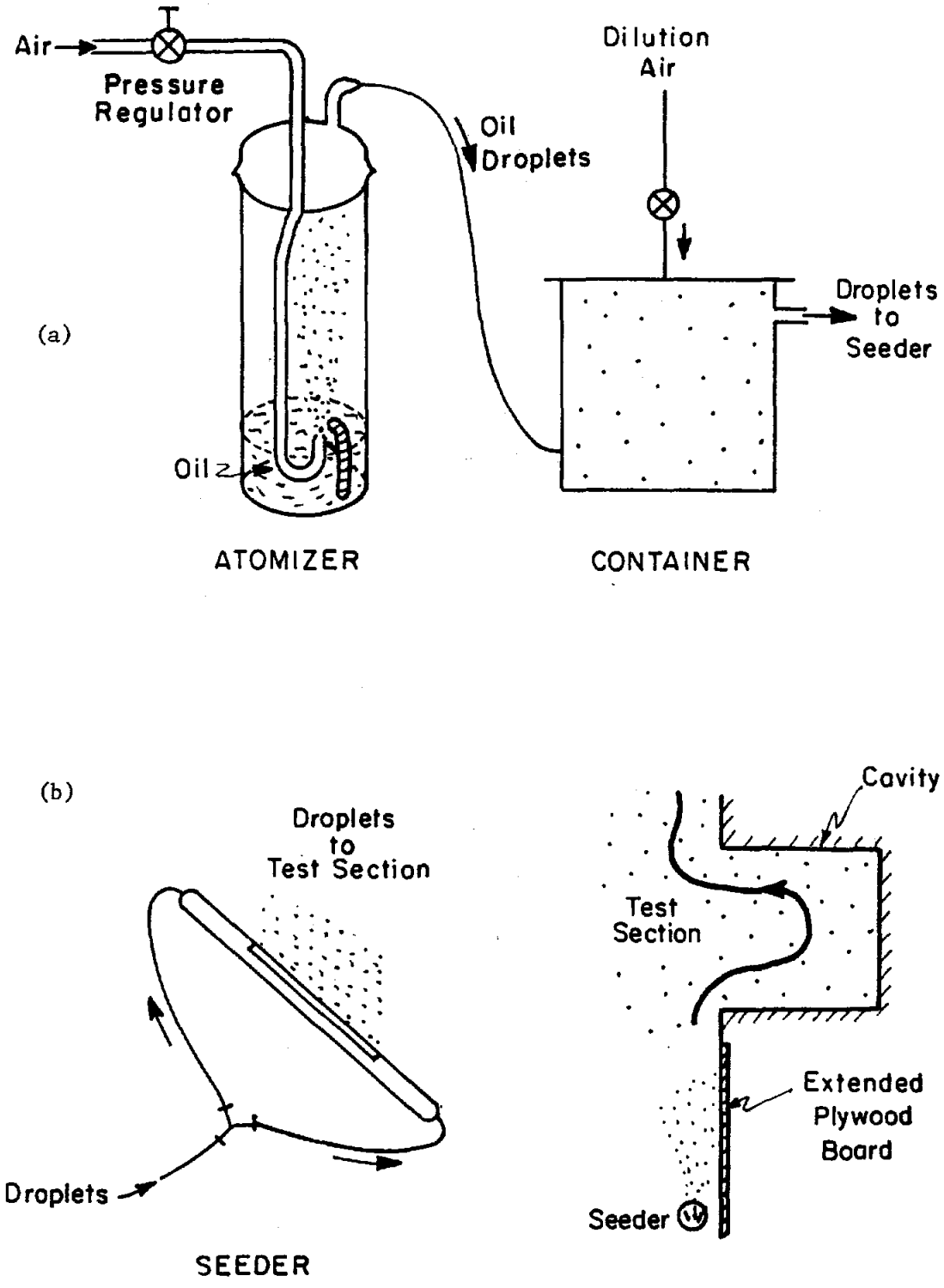

Figure 12 Schematics of: (a) blast atomizer; and (b) seed distributor relative to test section.

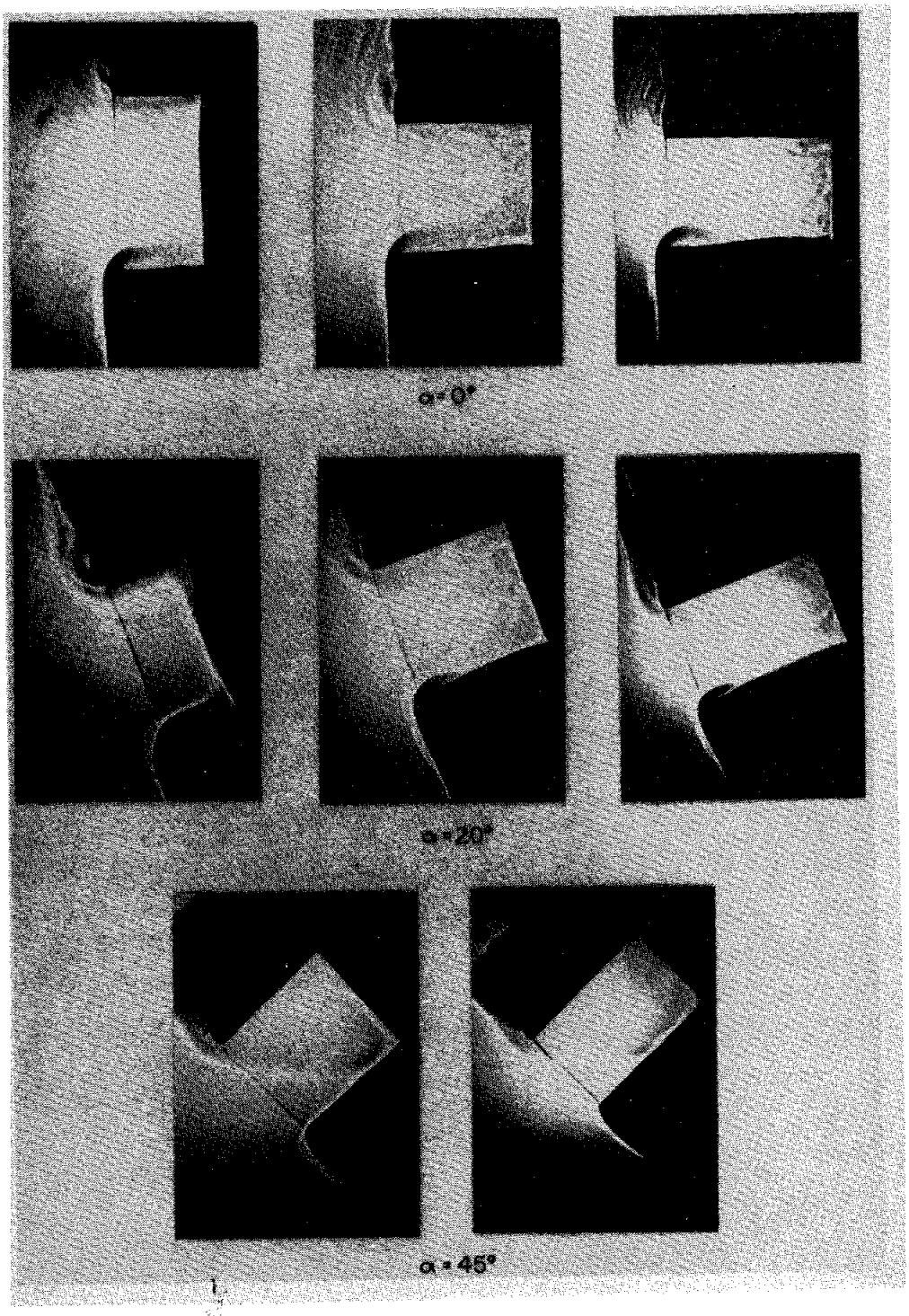

Figure 13 Shadowgraphs of the free convection flow of air in rectangular cavities with a/b = 0.5, 1.0 and 1.46 (left to right) for three inclination angles α = 0°, 20° and 45°. Flow conditions: $\Delta T/T_\infty \simeq 1.2$, $Gr \simeq 4.2 \times 10^7$, $Pr \simeq 0.7$. In all experiments the cavity aperture dimension (b) was the same. Unequal photographic reductions give false impression that b varied.

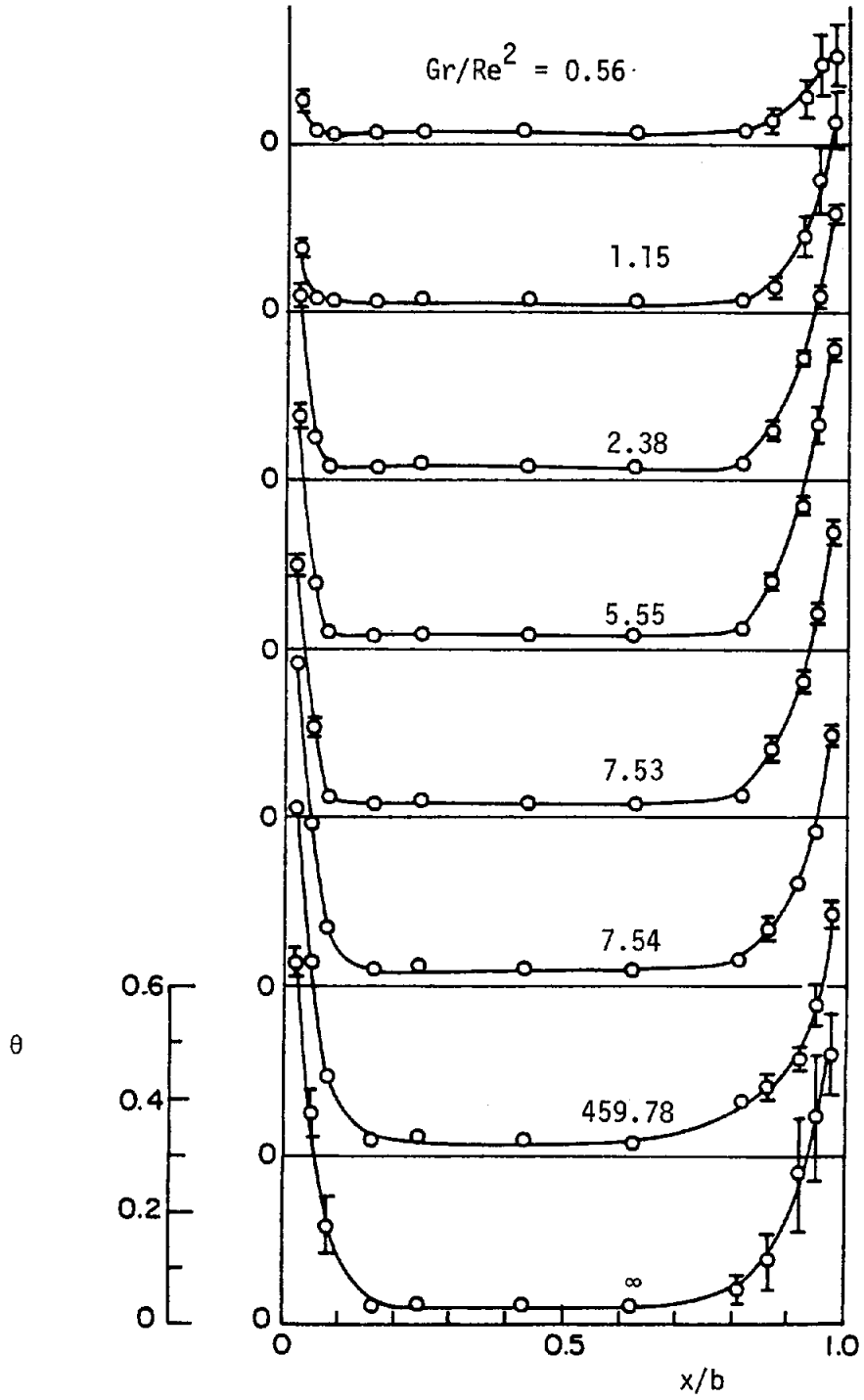

Figure 14 Cavity aperture plane temperature distributions in mixed convection regime for: $a/b = 0.5$, $\alpha = 0°$, $\Delta T/T_\infty = 1.19$, $Gr = 4.02 \times 10^7$, $T_\infty = 298.2°K$.

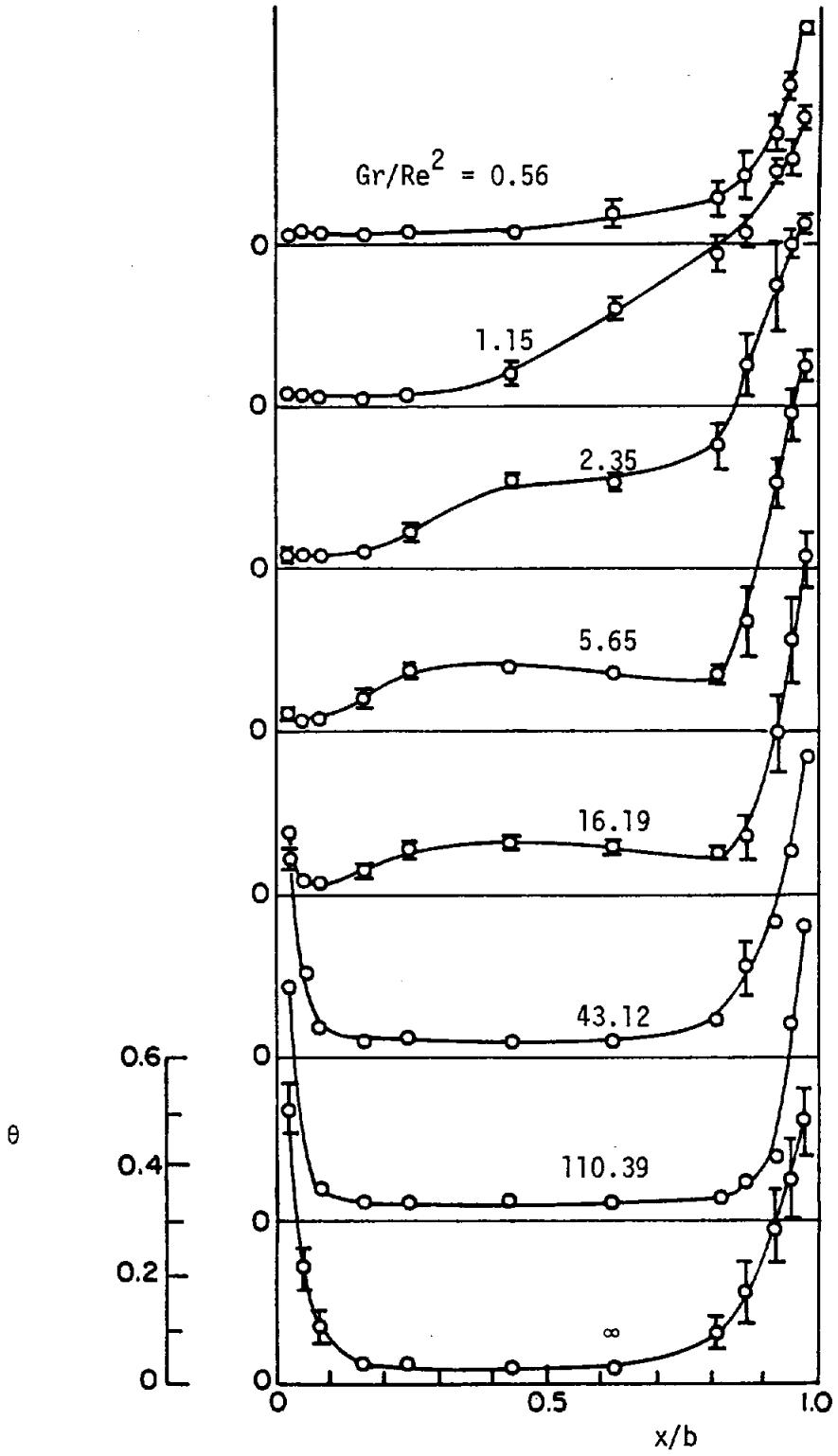

Figure 15 Cavity aperture plane temperature distributions in mixed convection regime for: a/b = 0.5, α = 20°, $\Delta T/T_\infty$ = 1.18, Gr = 4.0×10^7, T_∞ = 295.8°K.

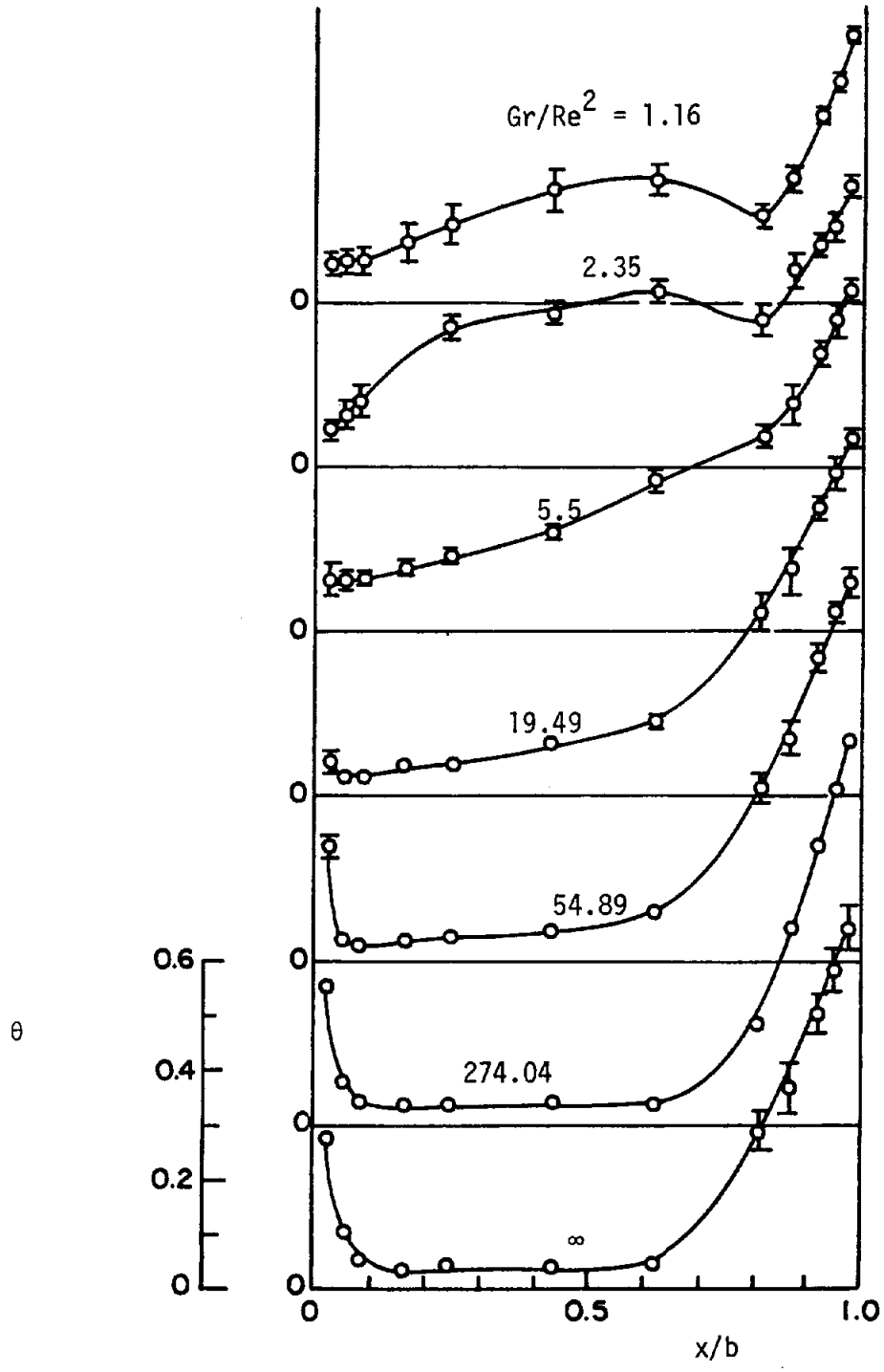

Figure 16 Cavity aperture plane temperature distributions in mixed convection regime for: a/b = 0.5, α = 45°, $\Delta T/T_\infty$ = 1.20, Gr = 4.06 × 10^7, T_∞ = 294.1°K.

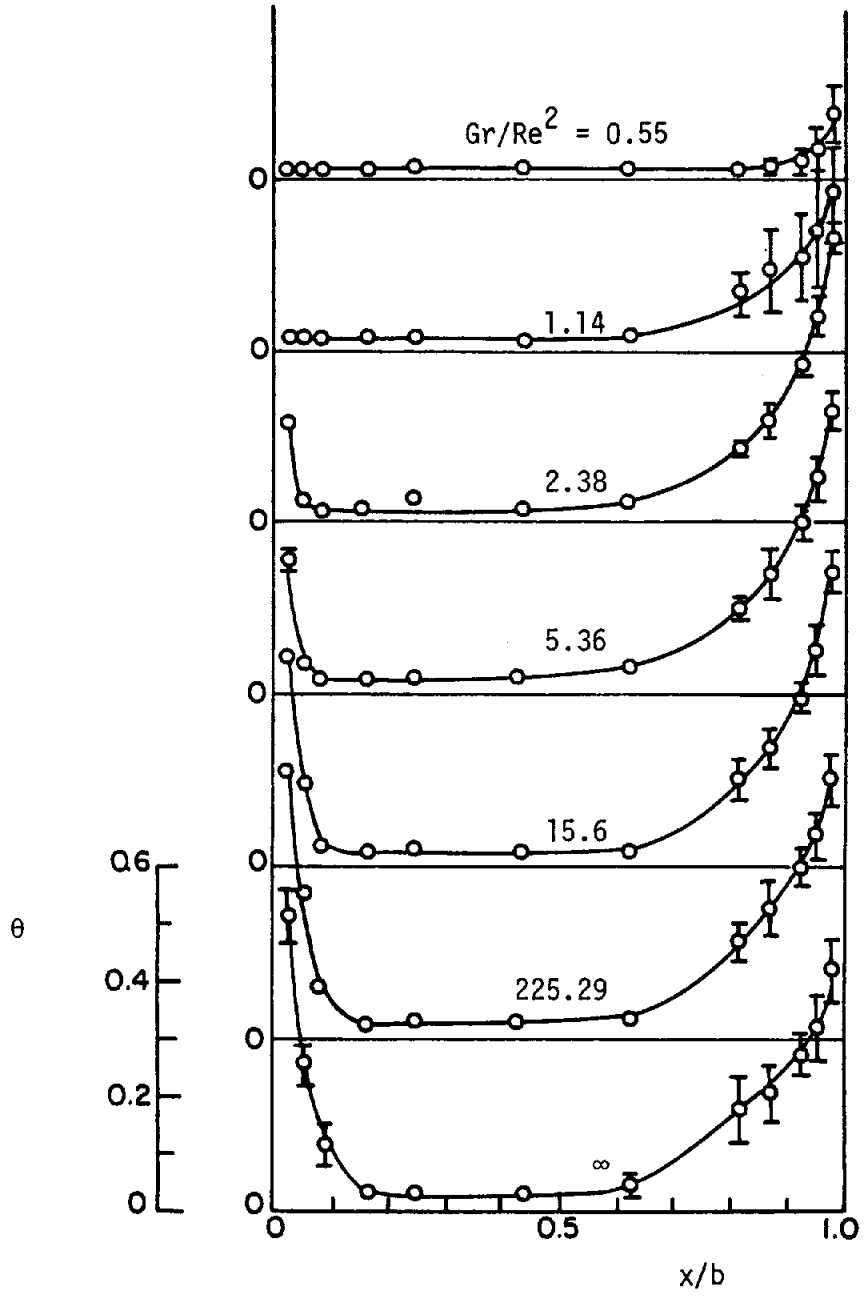

Figure 17 Cavity aperture plane temperature distributions in mixed convection regime for: a/b = 1.0, α = 0°, $\Delta T/T_\infty$ = 1.19, Gr = 4.03×10^7, T_∞ = 297.8°K.

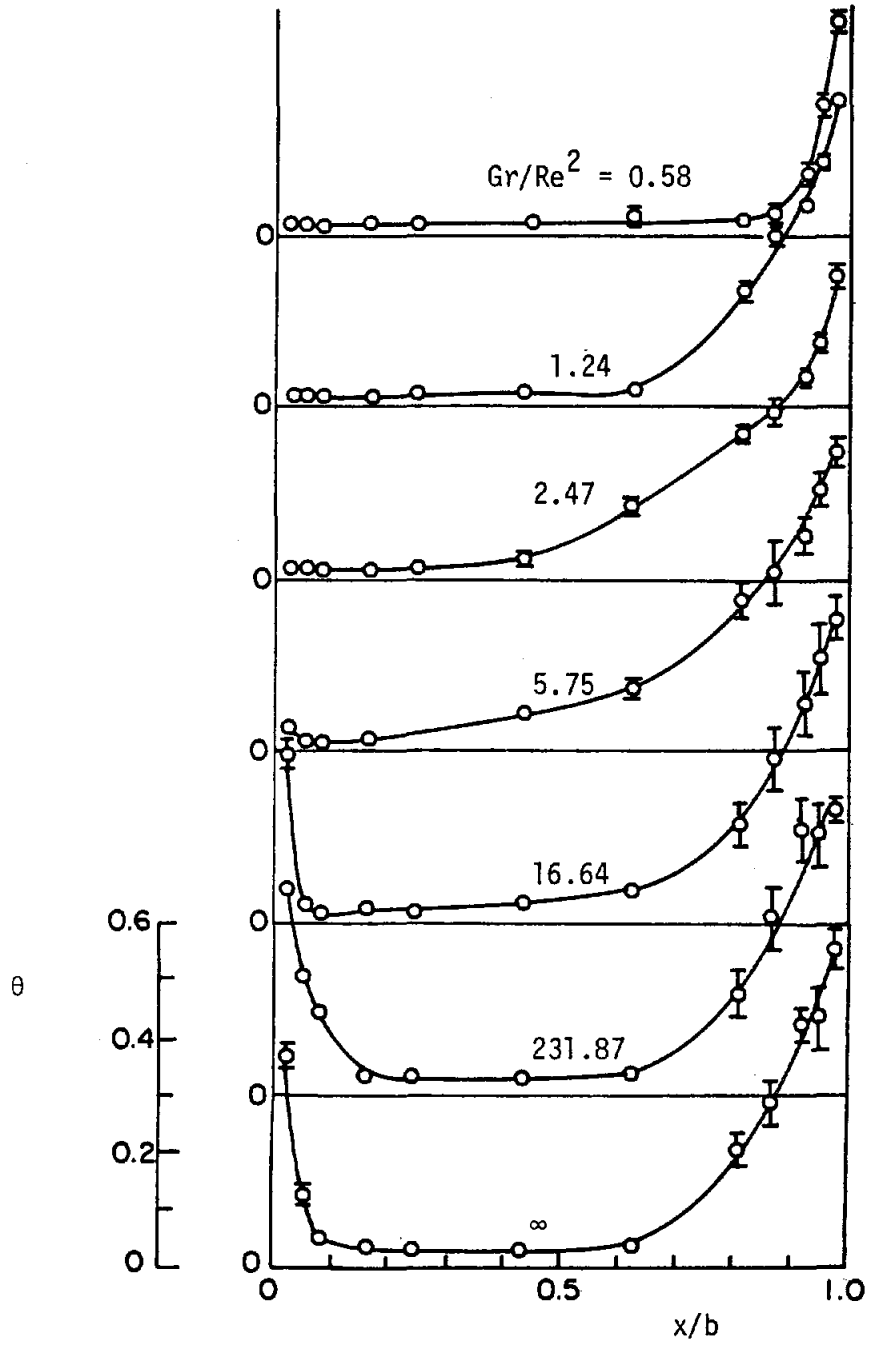

Figure 18 Cavity aperture plane temperature distributions in mixed convection regime for: a/b = 1.0, α = 20°, $\Delta T/T_\infty$ = 1.26, Gr = 4.28×10^7, T_∞ = 293.8°K.

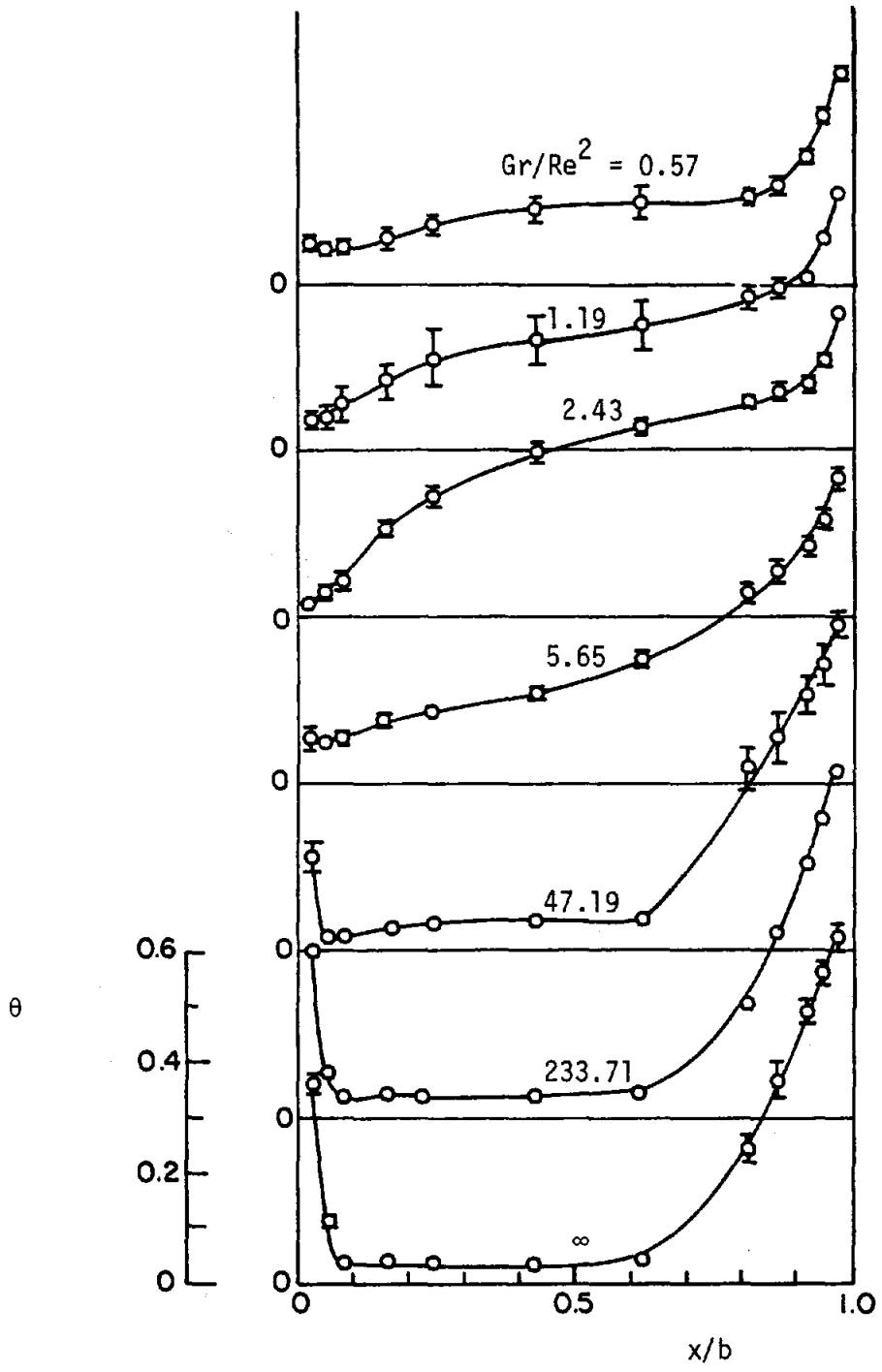

Figure 19 Cavity aperture plane temperature distributions in mixed convection regime for: a/b = 1, α = 45°, $\Delta T/T_\infty$ = 1.26, Gr = 4.27 × 10^7, T_∞ = 294.1°K.

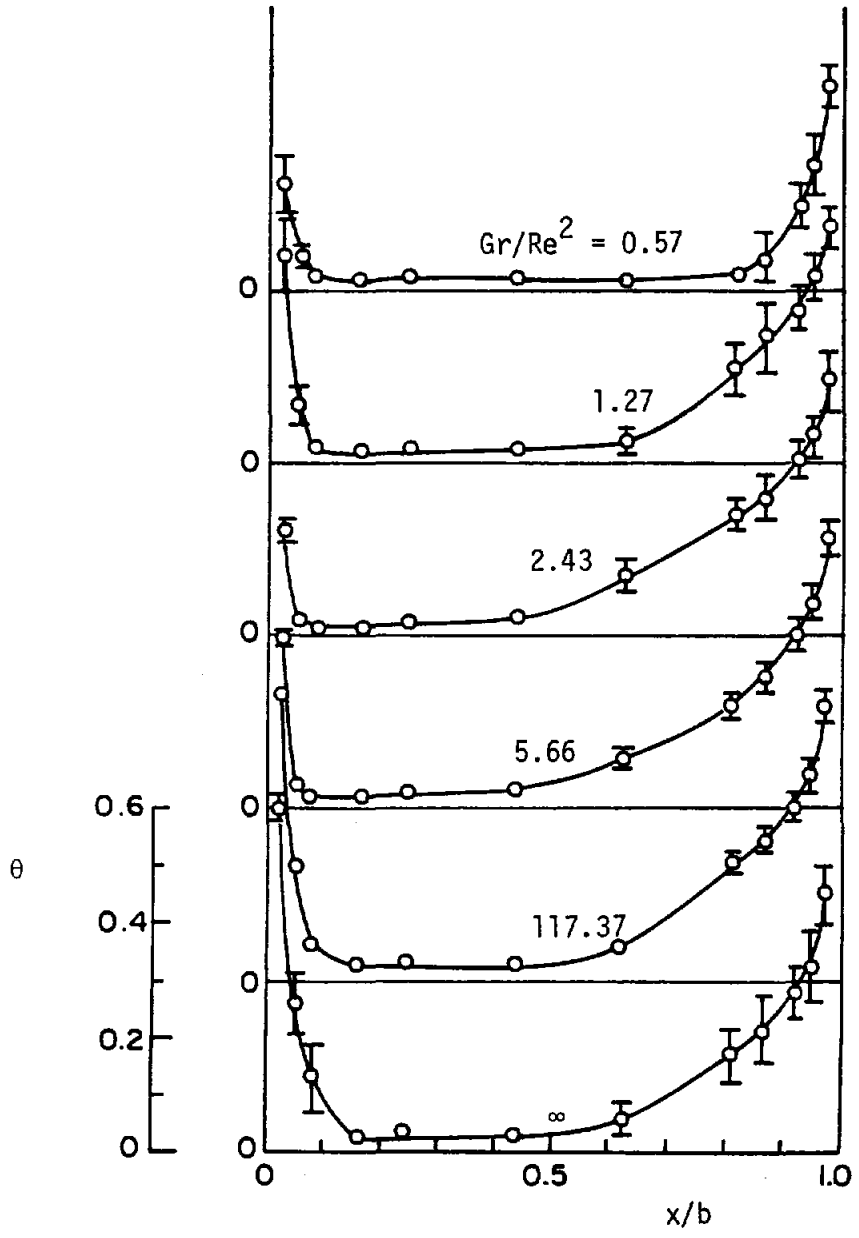

Figure 20 Cavity aperture plane temperature distributions in mixed convection regime for: a/b = 1.46, α = 0°, $\Delta T/T_\infty$ = 1.24, Gr = 4.20×10^7, T_∞ = 294.2°K.

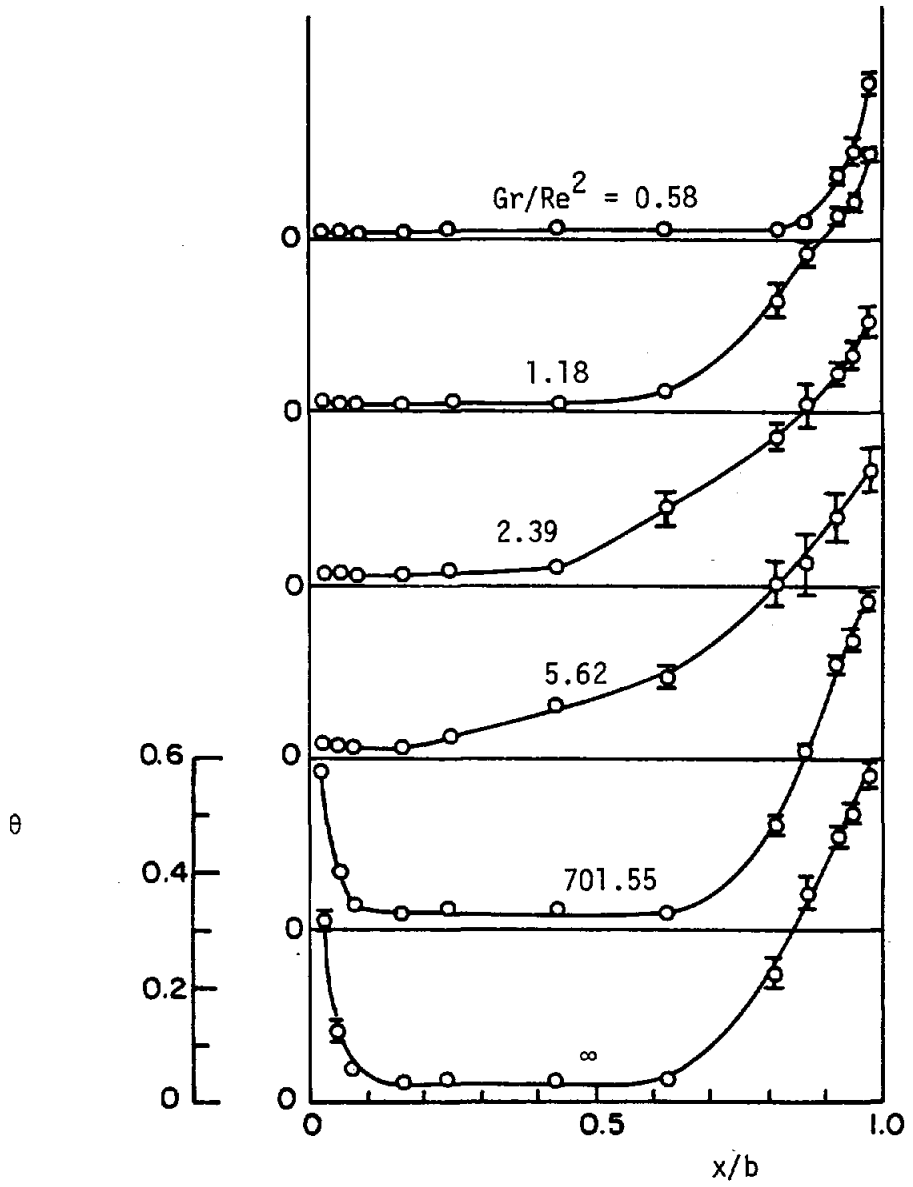

Figure 21 Cavity aperture plane temperature distributions in mixed convection regime for: a/b = 1.46, α = 20°, $\Delta T/T_\infty$ = 1.21, Gr = 4.09 × 10^7, T_∞ = 294.7°K.

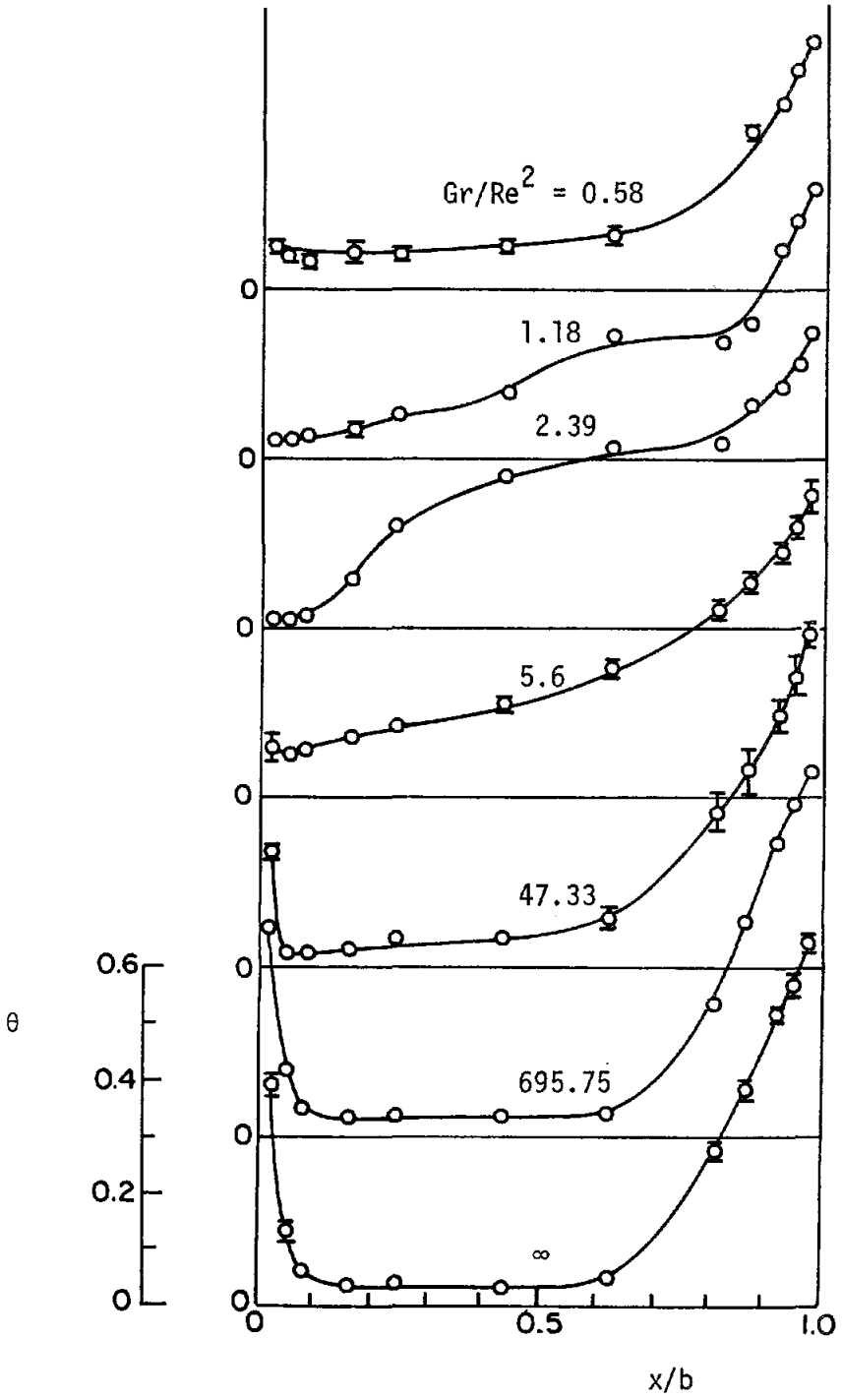

Figure 22 Cavity aperture plane temperature distributions in mixed convection regime for: a/b = 1.46, α = 45°, $\Delta T/T_\infty$ = 1.20, Gr = 4.07 × 10^7, T_∞ = 295.3°K.

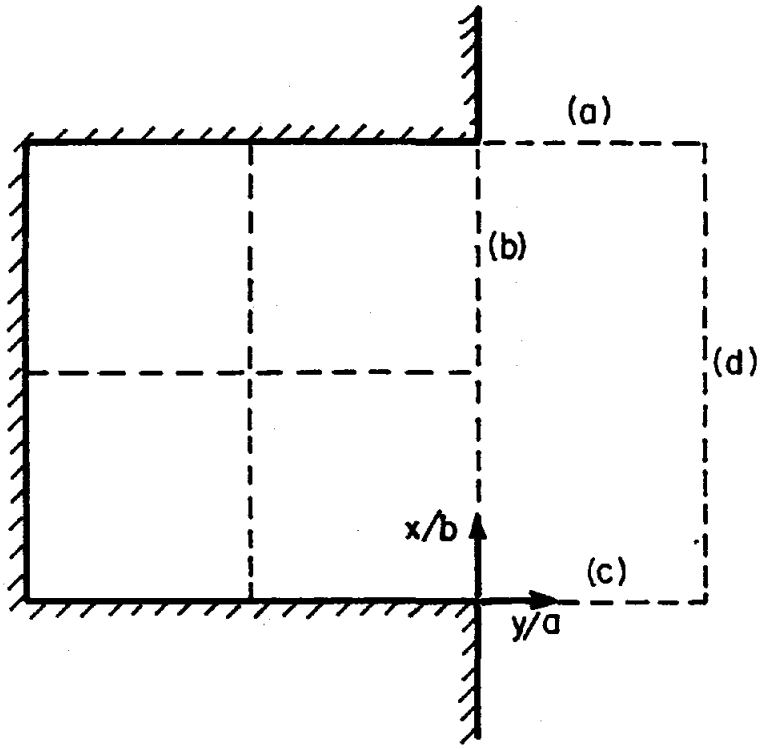

Figure 23 Positions at which laser-Doppler velocimeter and turbulent stress components were measured. These are shown as dashed lines in the figure. All locations on the cavity symmetry plane (z/(c/2) = 0.

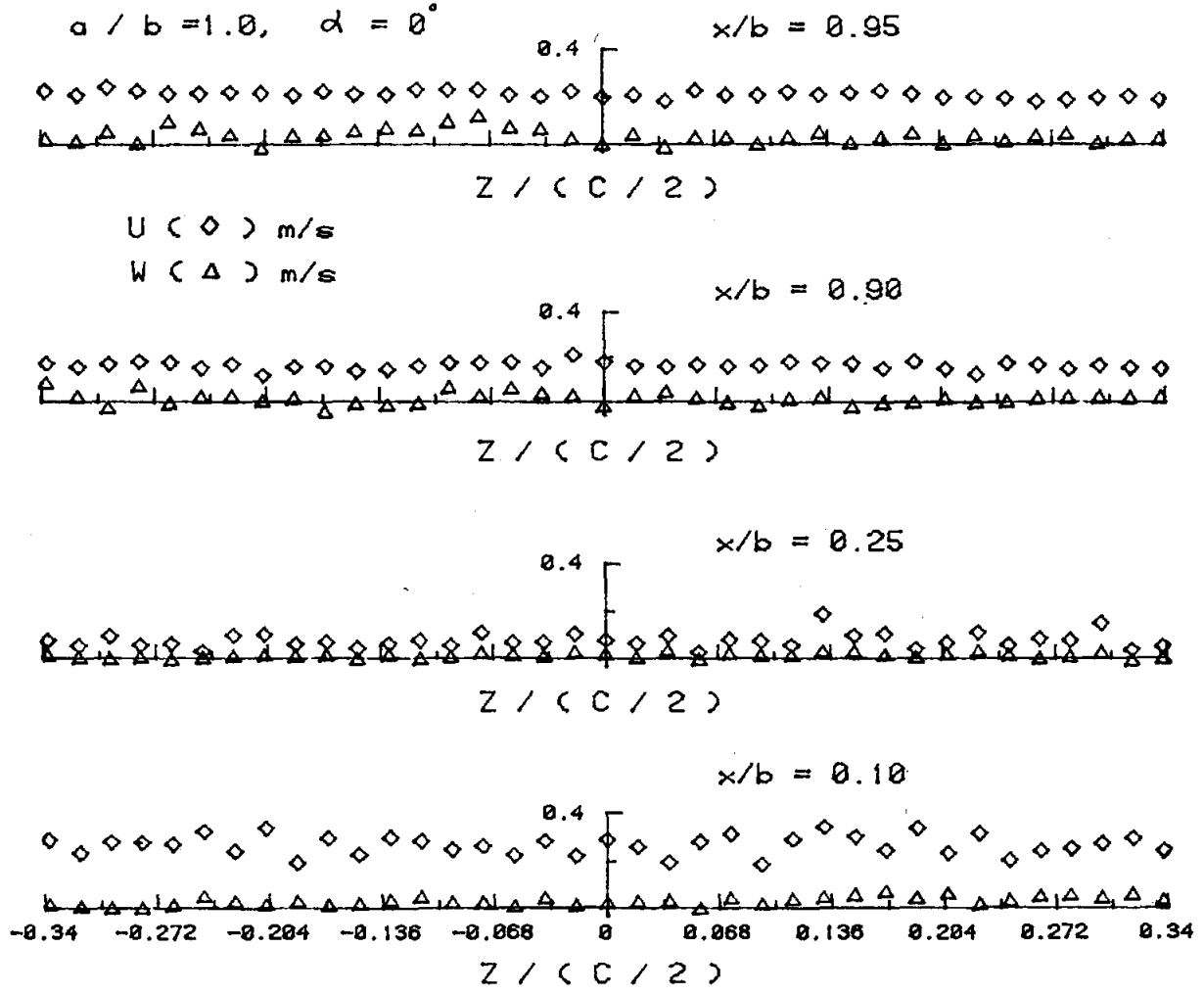

(a)

Figure 24 Spanwise symmetry check of mean components (a) and normal stresses (b) on the cavity aperture plane, y/a = 0.

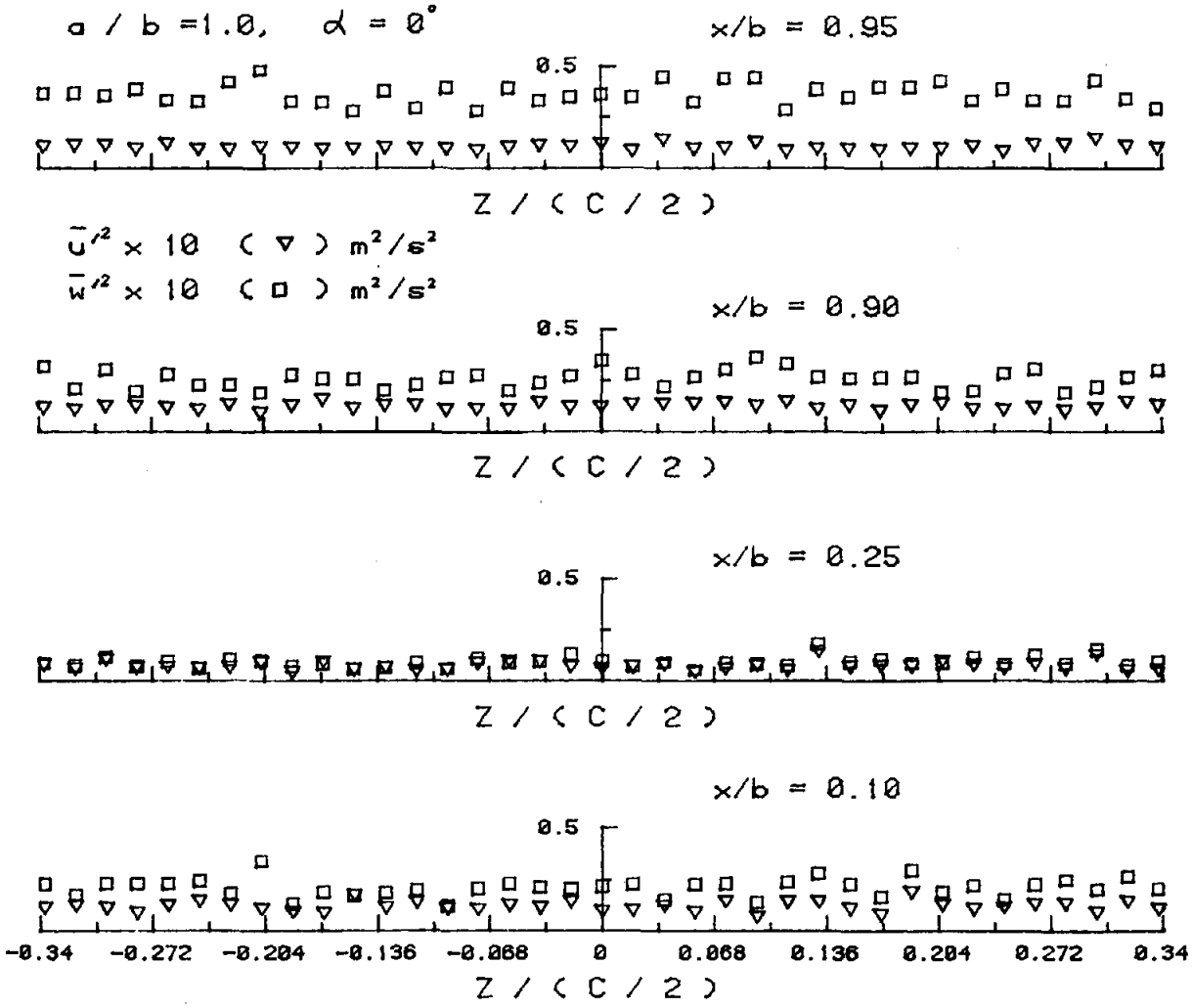

(b)

Figure 24 Spanwise symmetry check of mean components (a) and normal stresses (b) on the cavity aperture plane, y/a = 0.

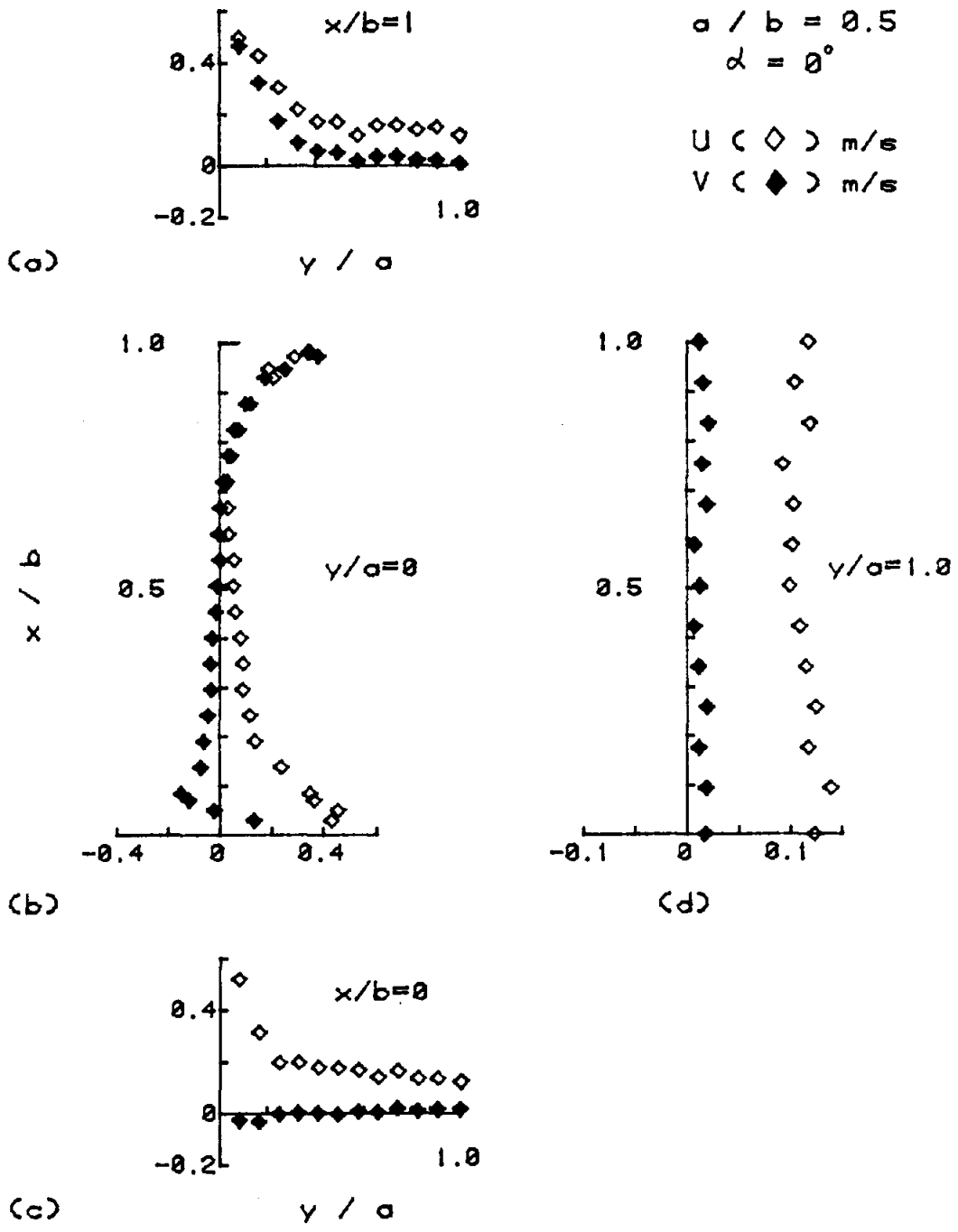

Figure 25a Mean velocity measurements on the cavity symmetry plane, $z/(c/2) = 0$, with $a/b = 0.5$ and $\alpha = 0°$. Measurement planes parenthesized.

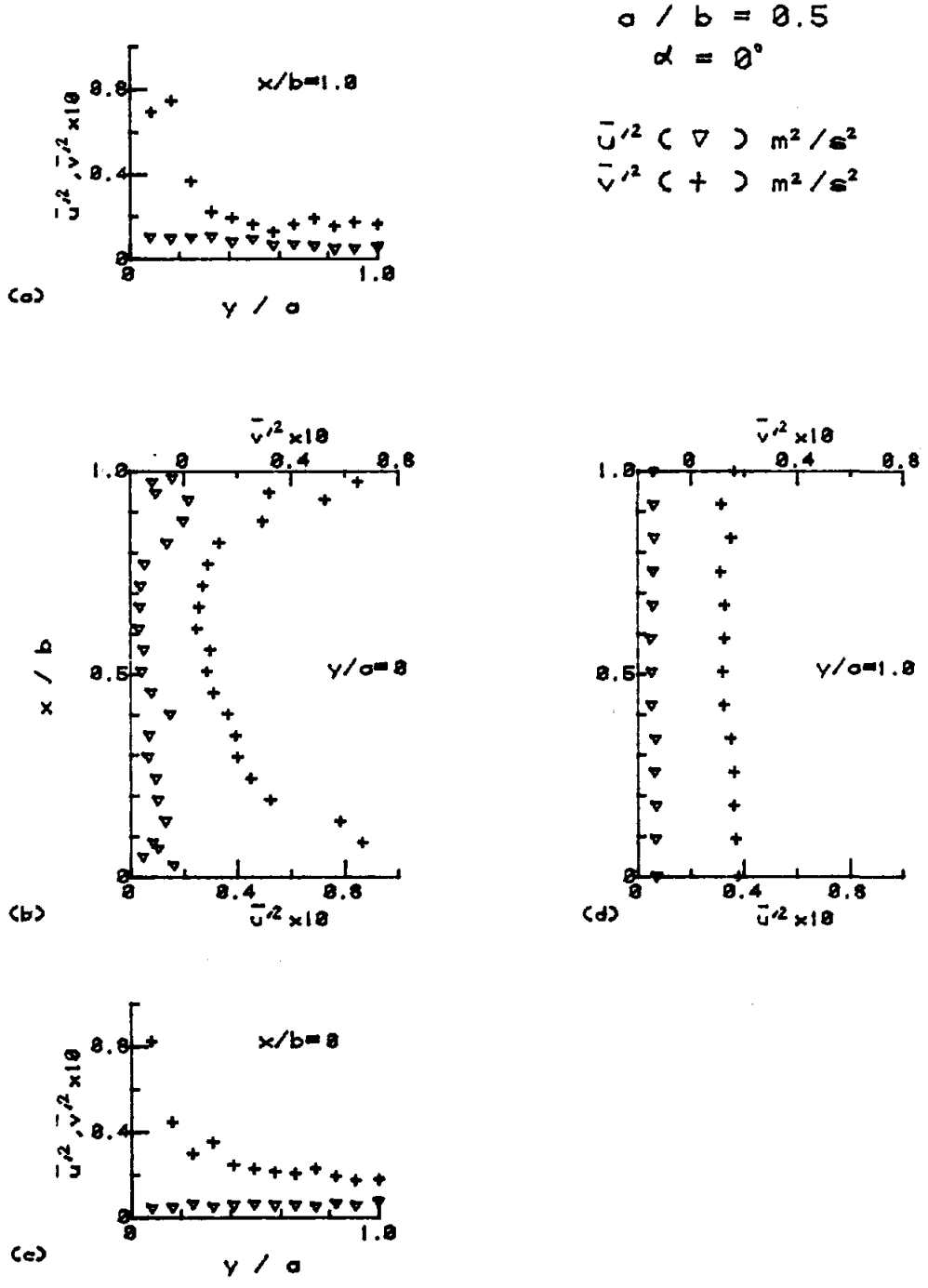

Figure 25b Normal stress measurements on the cavity symmetry plane, z/(c/2) = 0, with a/b = 0.5 and α = 0°. Measurement planes parenthesized.

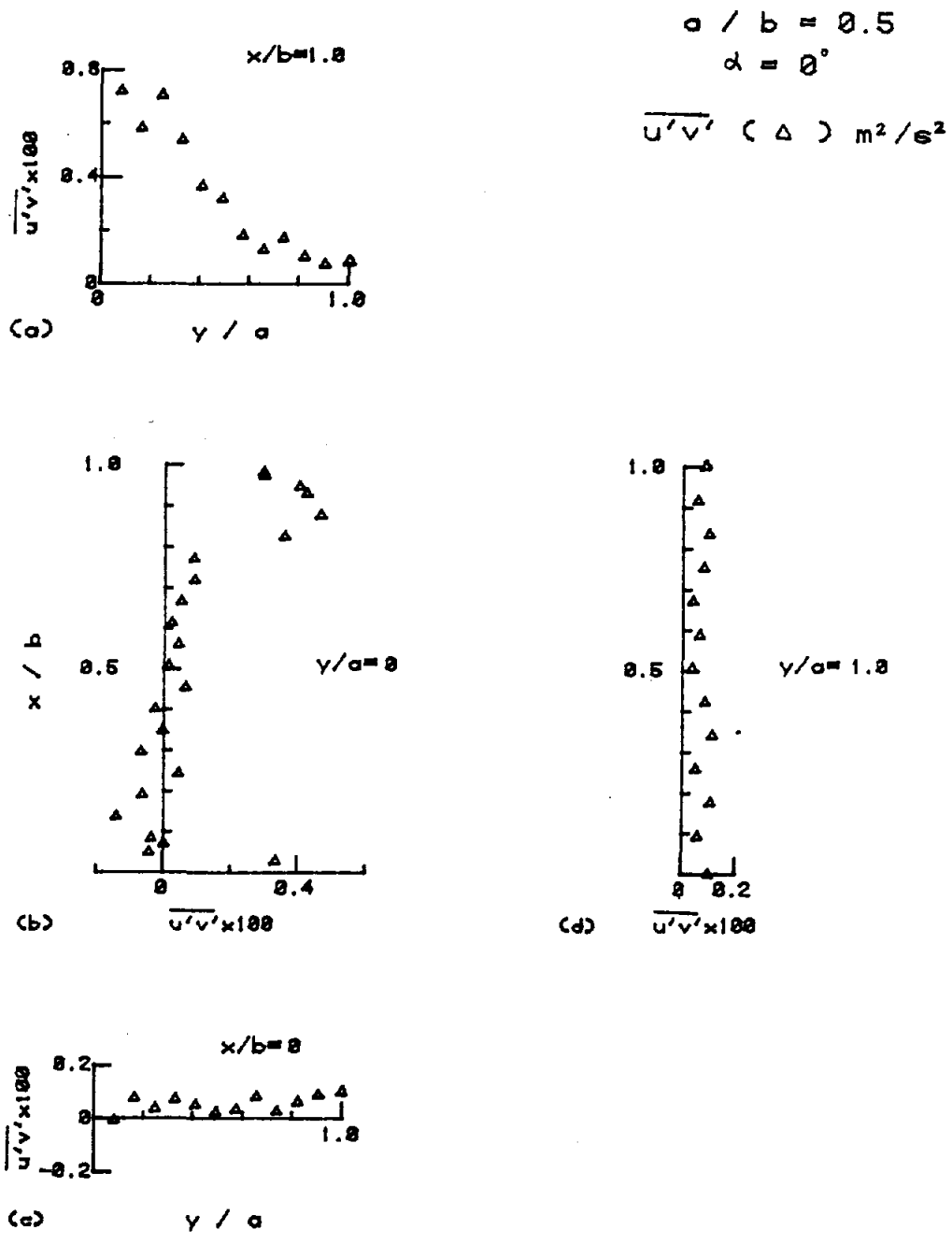

Figure 25c Shear stress measurements on the cavity symmetry plane, $z/(c/2) = 0$, with $a/b = 0.5$ and $\alpha = 0°$. Measurement planes parenthesized.

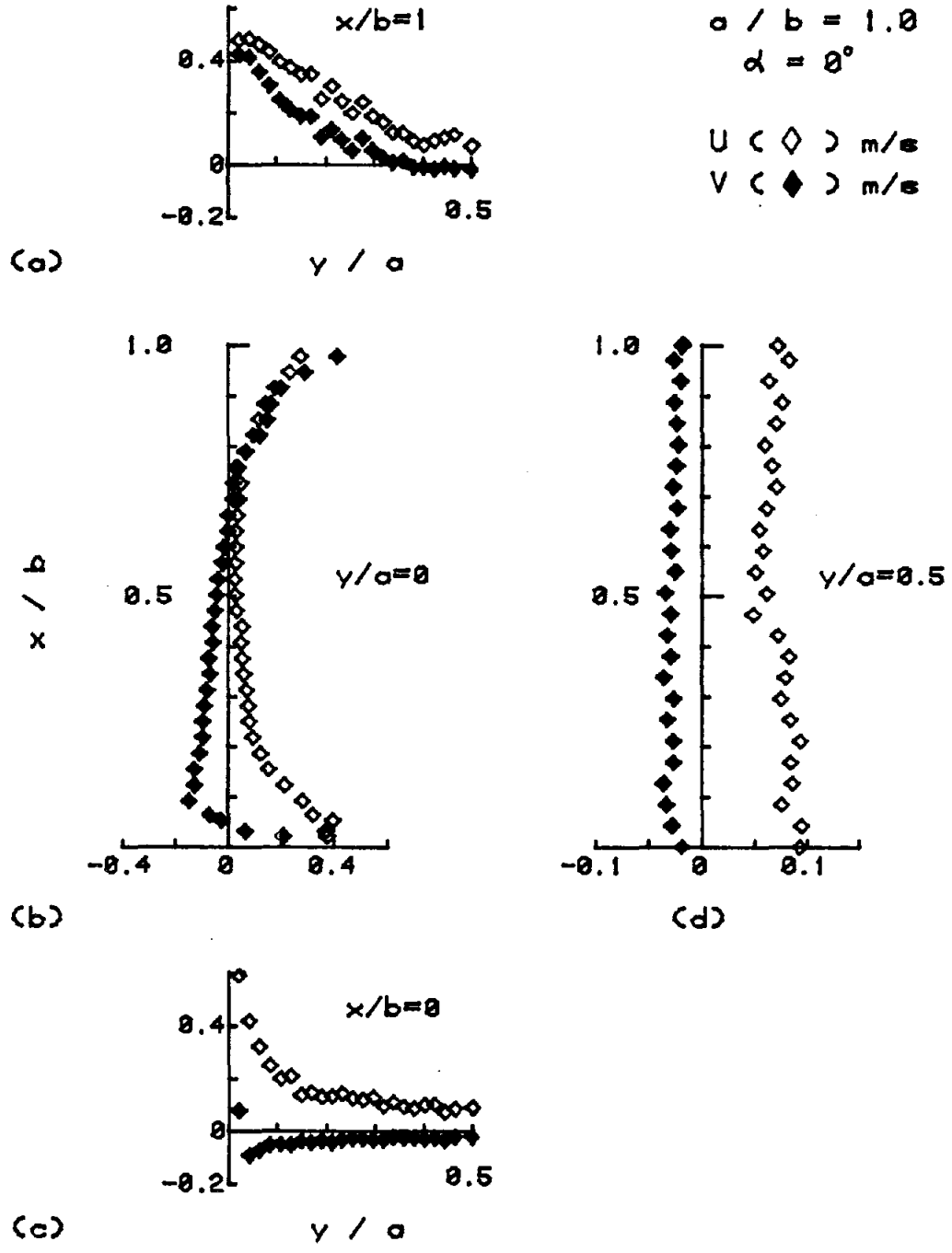

Figure 26a Mean velocity measurements on the cavity symmetry plane, $z/(c/2) = 0$, with $a/b = 1.0$ and $\alpha = 0°$. Measurement planes parenthesized.

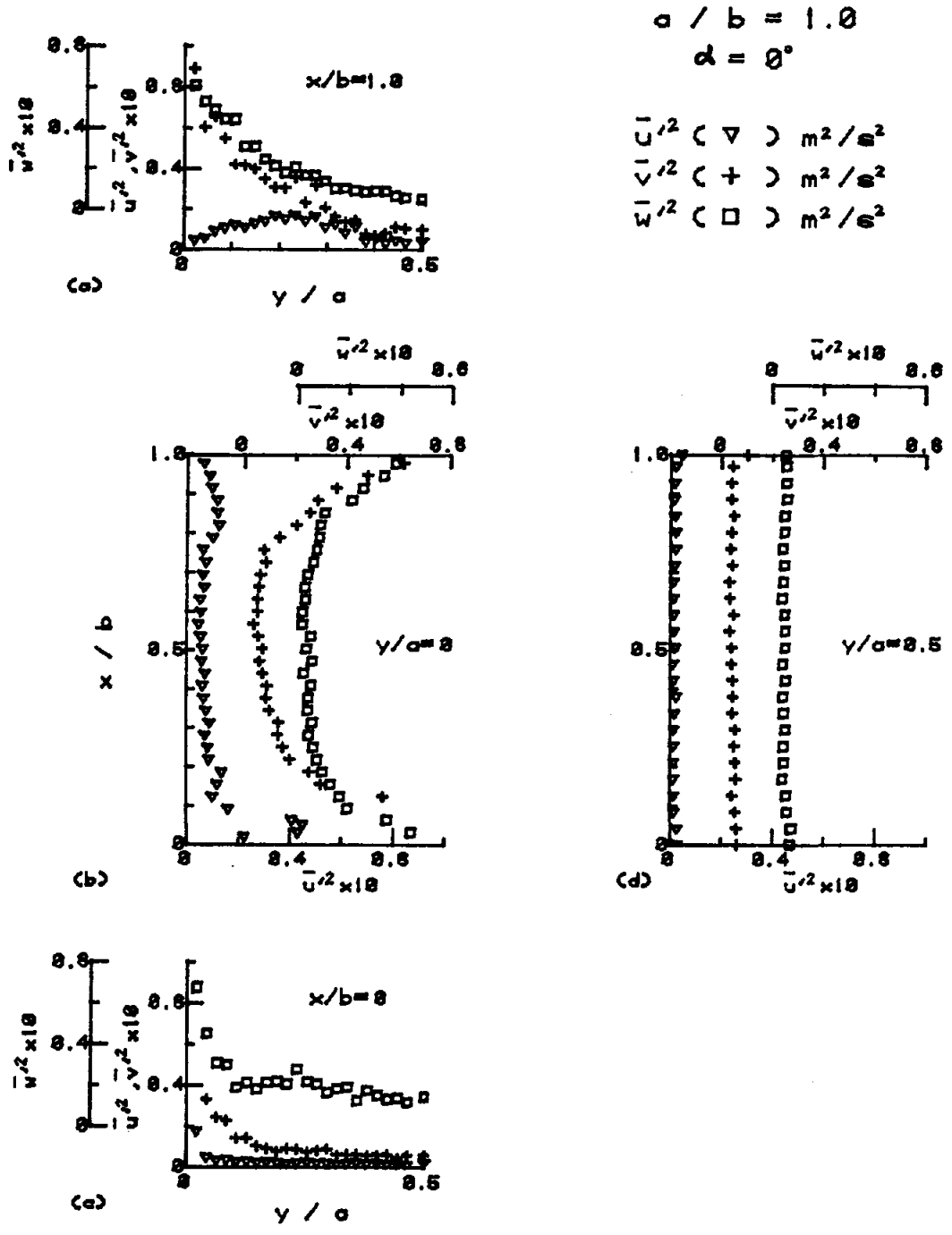

Figure 26b Normal stress measurements on the cavity symmetry plane, $z/(c/2) = 0$, with $a/b = 1.0$ and $\alpha = 0°$. Measurement planes parenthesized.

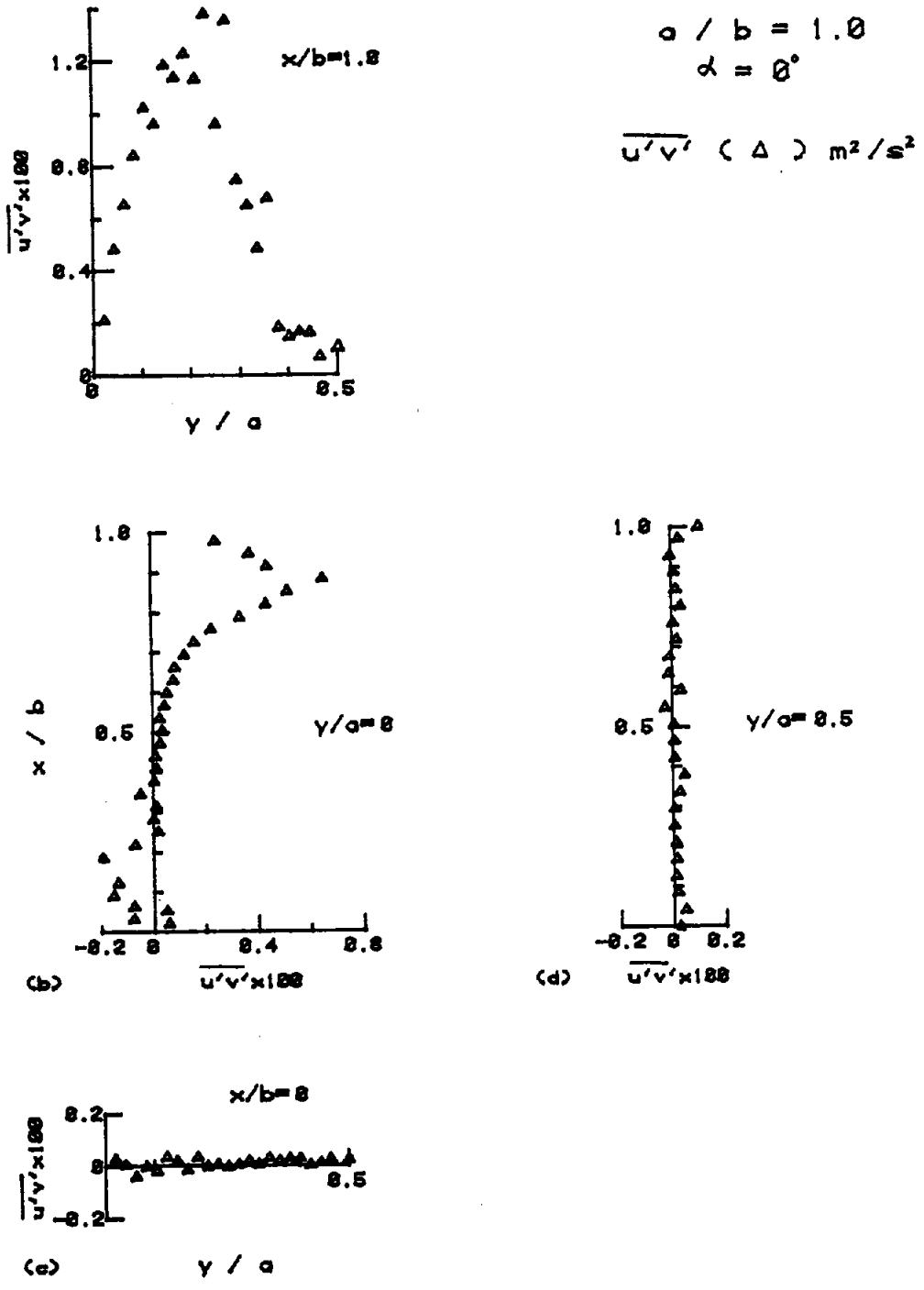

Figure 26c Shear stress measurements on the cavity symmetry plane, $z/(c/2) = 0$, with $a/b = 1.0$ and $\alpha = 0°$. Measurement planes parenthesized.

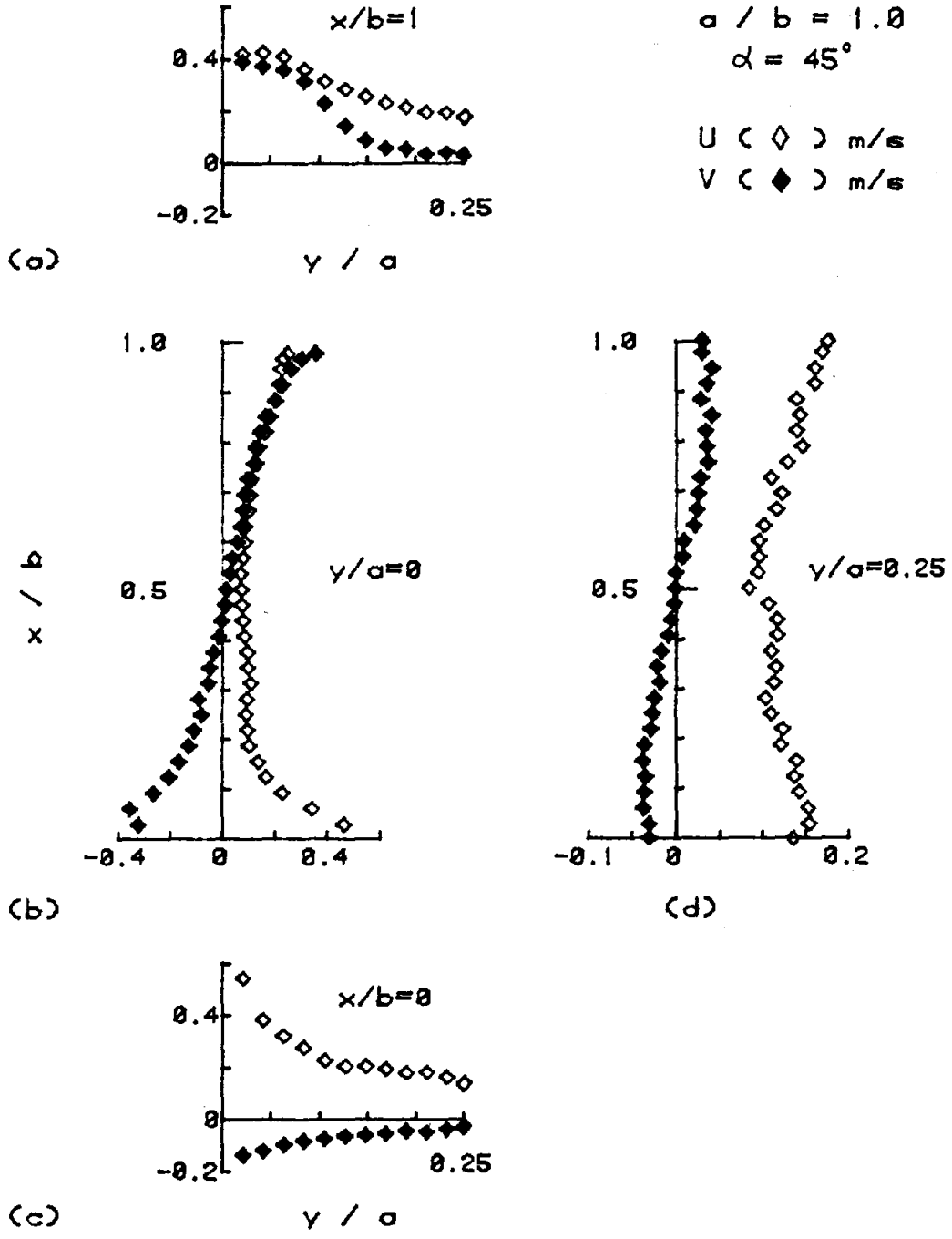

Figure 27a Mean velocity measurements on the cavity symmetry plane, $z/(c/2) = 0$, with $a/b = 1.0$ and $\alpha = 45°$. Measurement planes parenthesized.

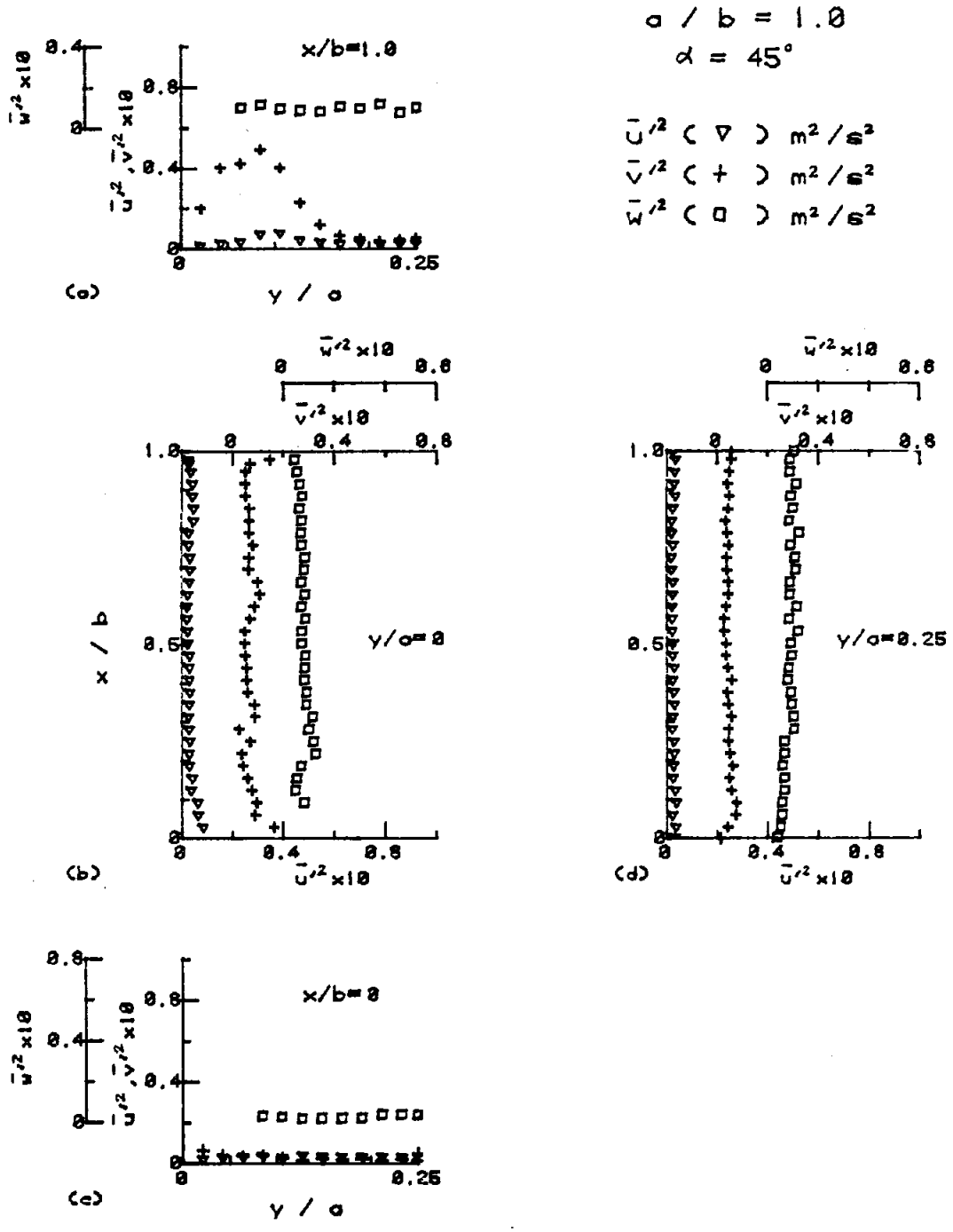

Figure 27b Normal stress measurements on the cavity symmetry plane, $z/(c/2) = 0$, with $a/b = 1.0$ and $\alpha = 45°$. Measurement planes parenthesized.

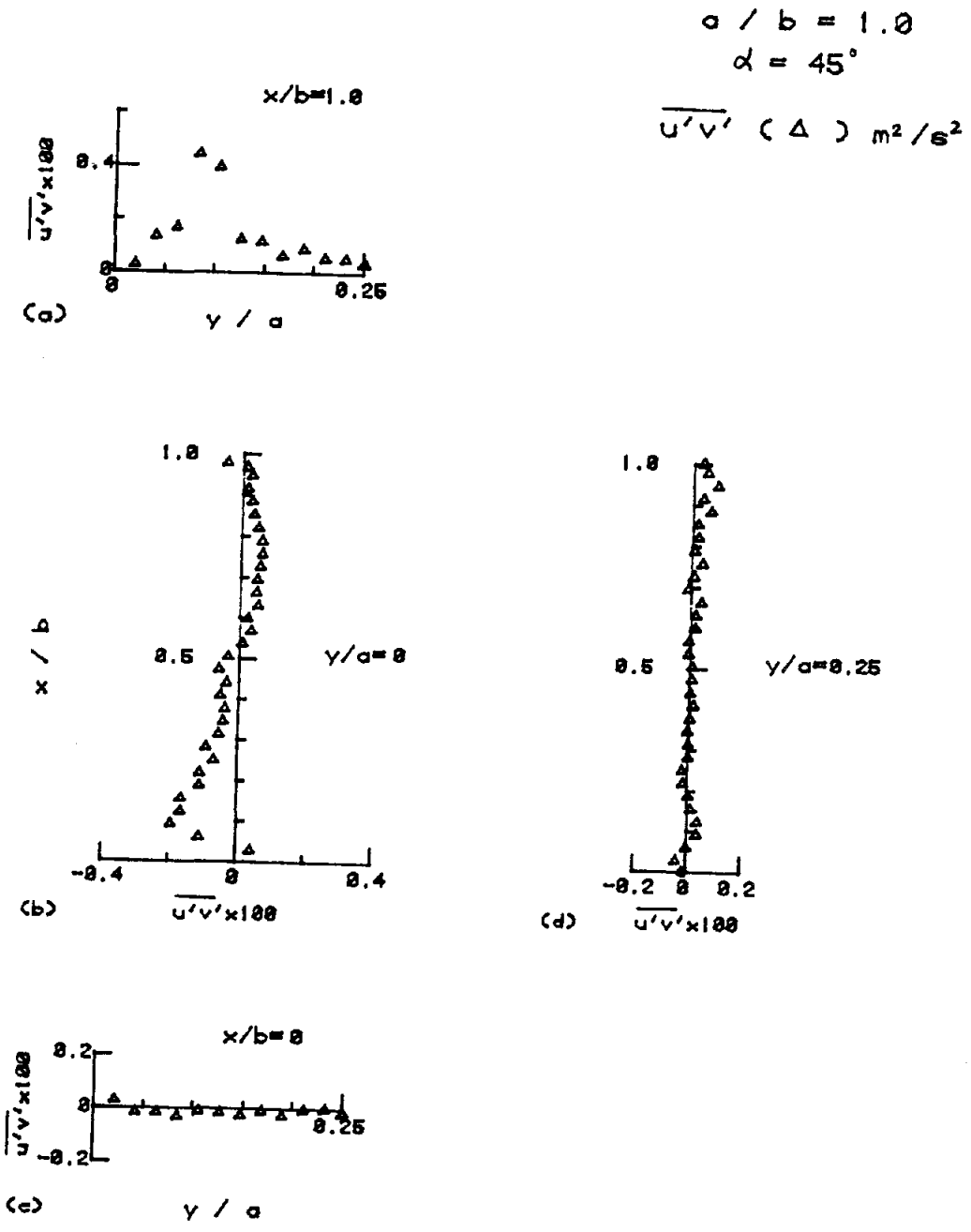

Figure 27c Shear stress measurements on the cavity symmetry plane, $z/(c/2) = 0$, with $a/b = 1.0$ and $\alpha = 45°$. Measurement planes parenthesized.

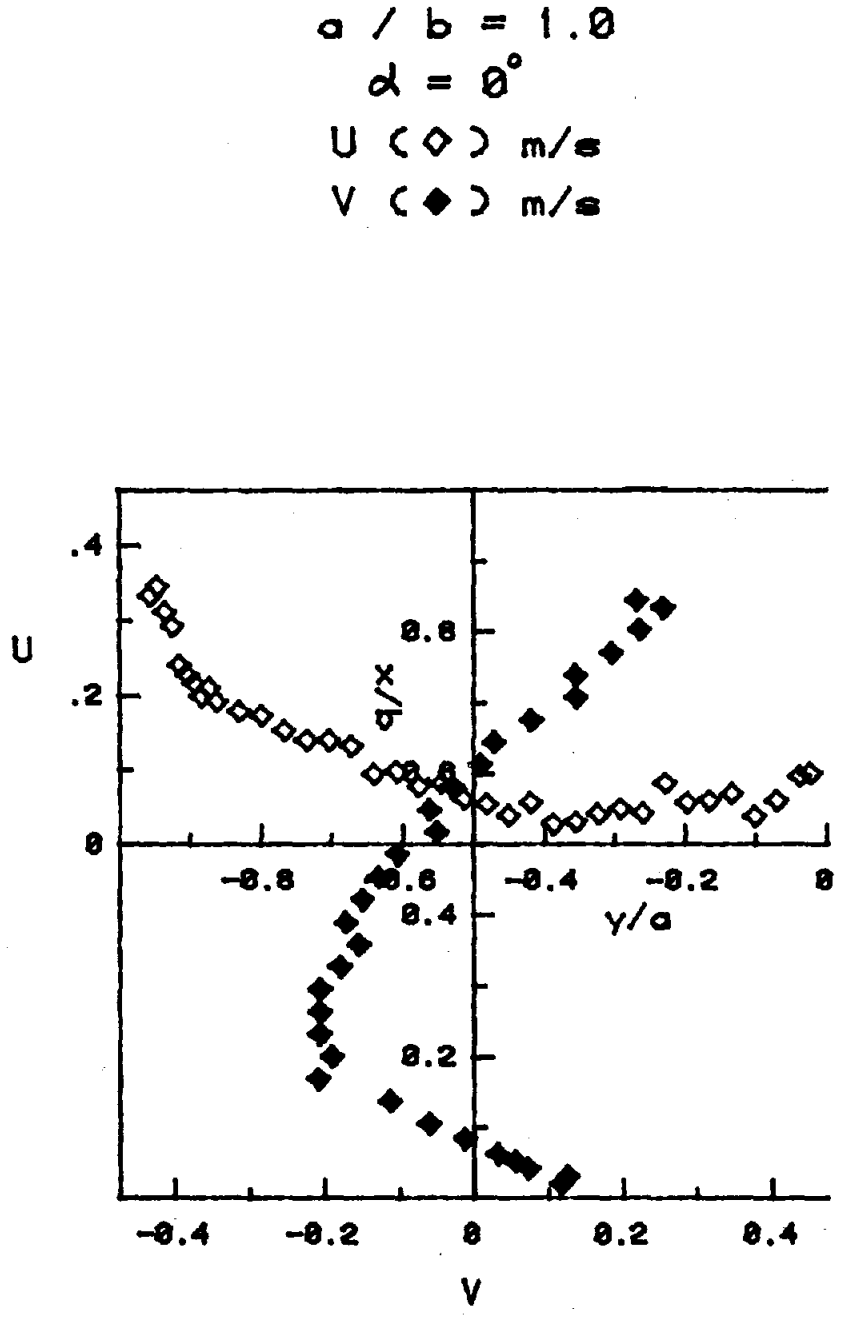

Figure 28a Mean velocity measurements inside the cavity on the symmetry plane, z/(c/2) = 0, with a/b = 1.0 and α = 0°; unweighted data. Measurements on planes shown.

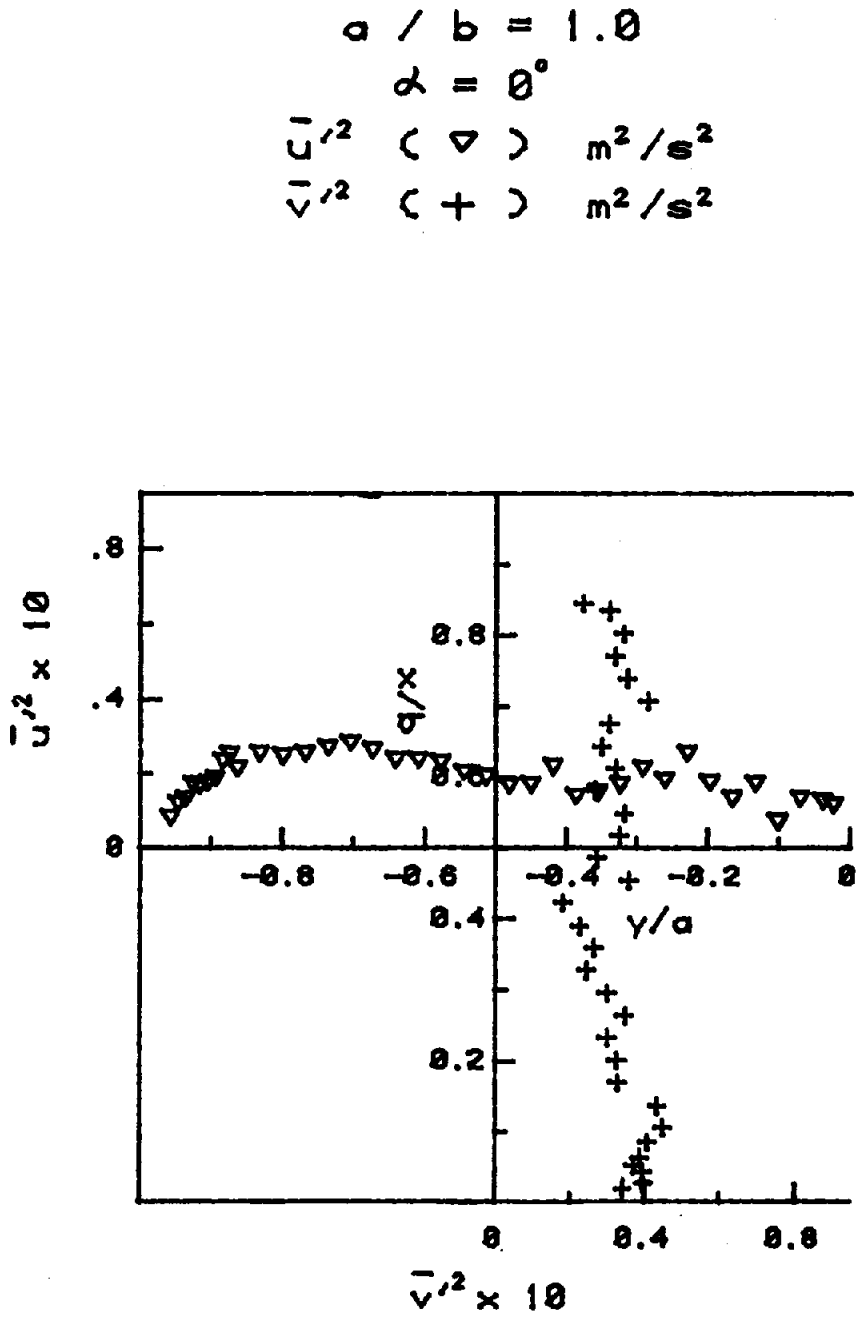

Figure 28b Normal stress measurements inside the cavity on the symmetry plane, z/(c/2) = 0, with a/b = 1.0 and α = 0°; unweighted data. Measurements on planes shown.

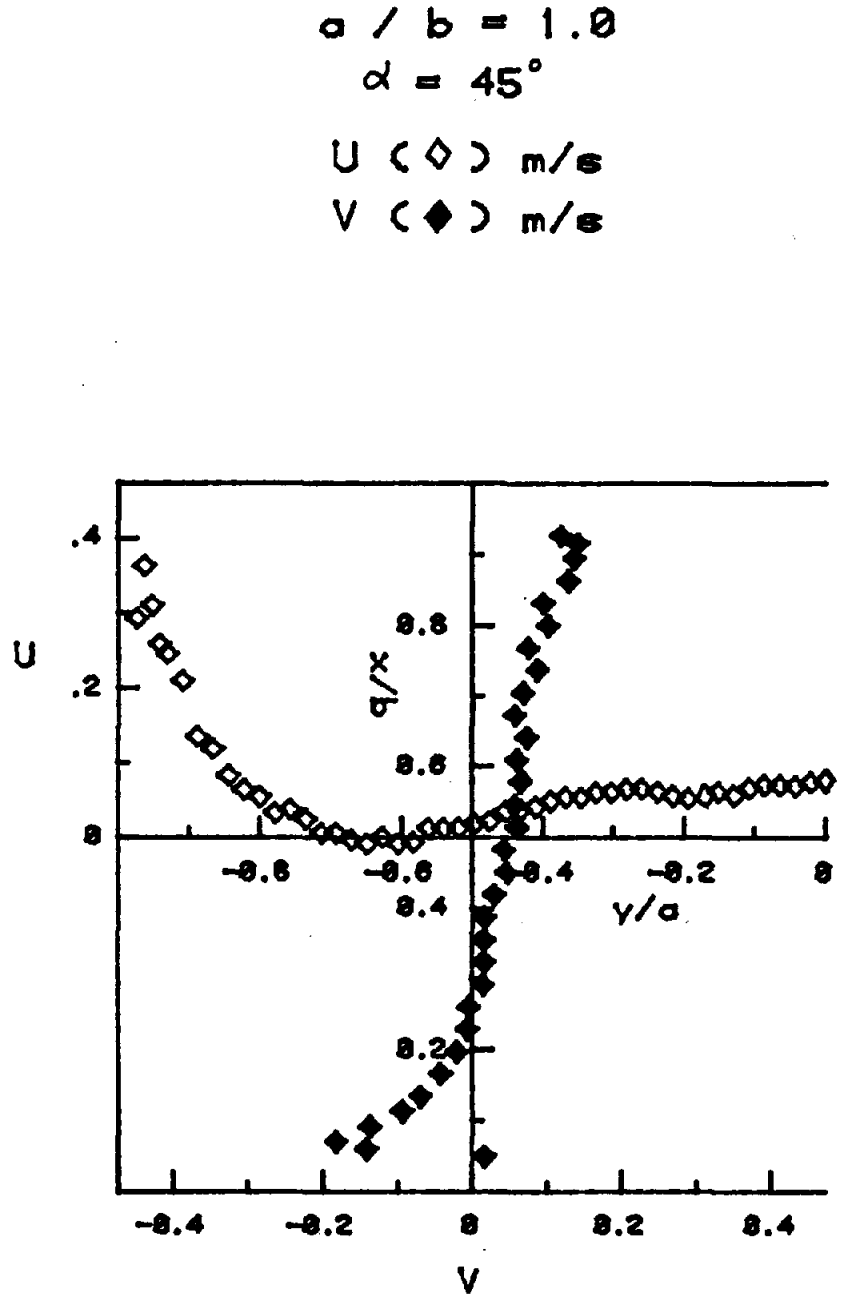

Figure 29a Mean velocity measurements inside the cavity on the symmetry plane, z/(c/2) = 0, with a/b = 1.0 and α = 45°. Measurements on planes shown.

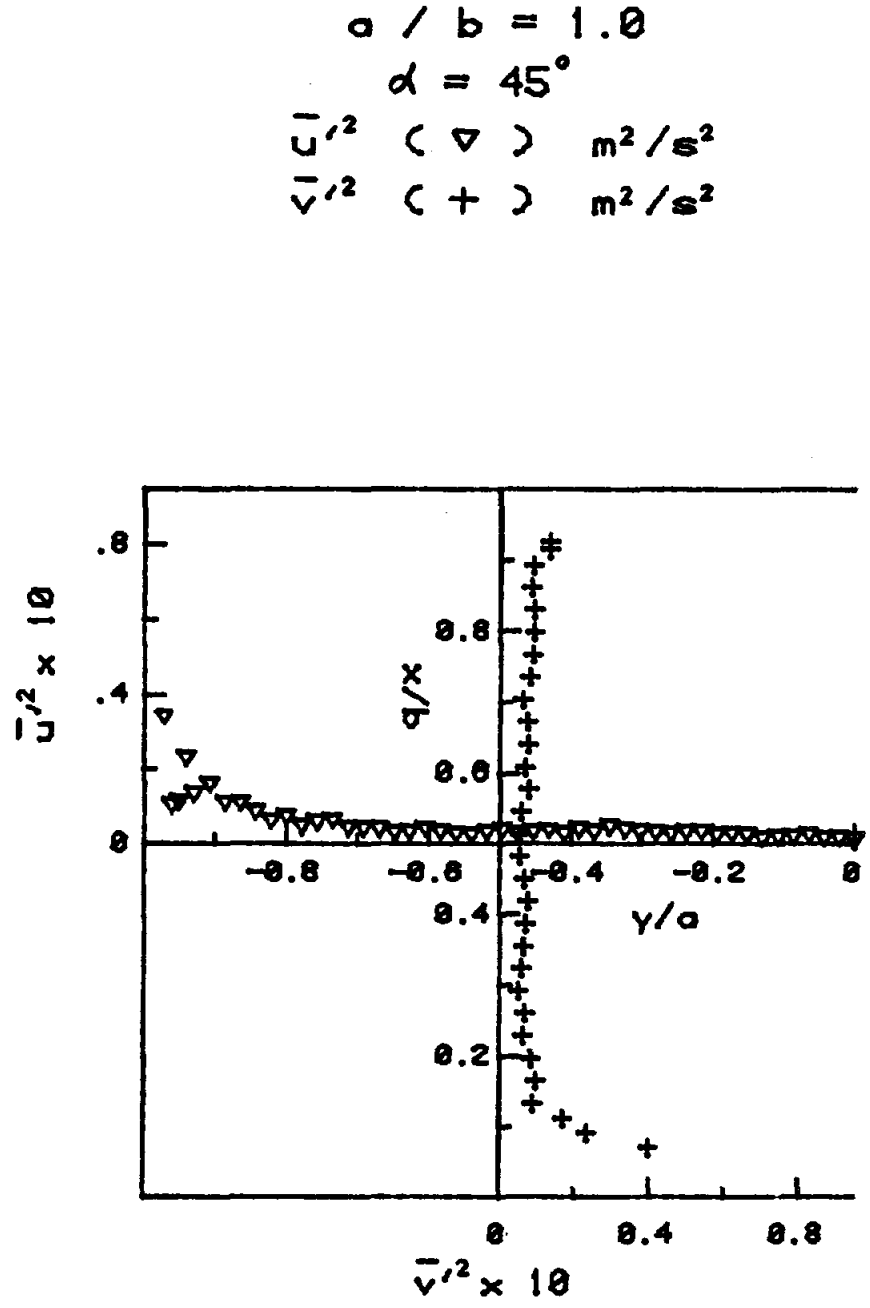

Figure 29b Normal stress measurements inside the cavity on the symmetry plane, z/(c/2) = 0, with a/b = 1.0 and α = 45°. Measurements on planes shown.

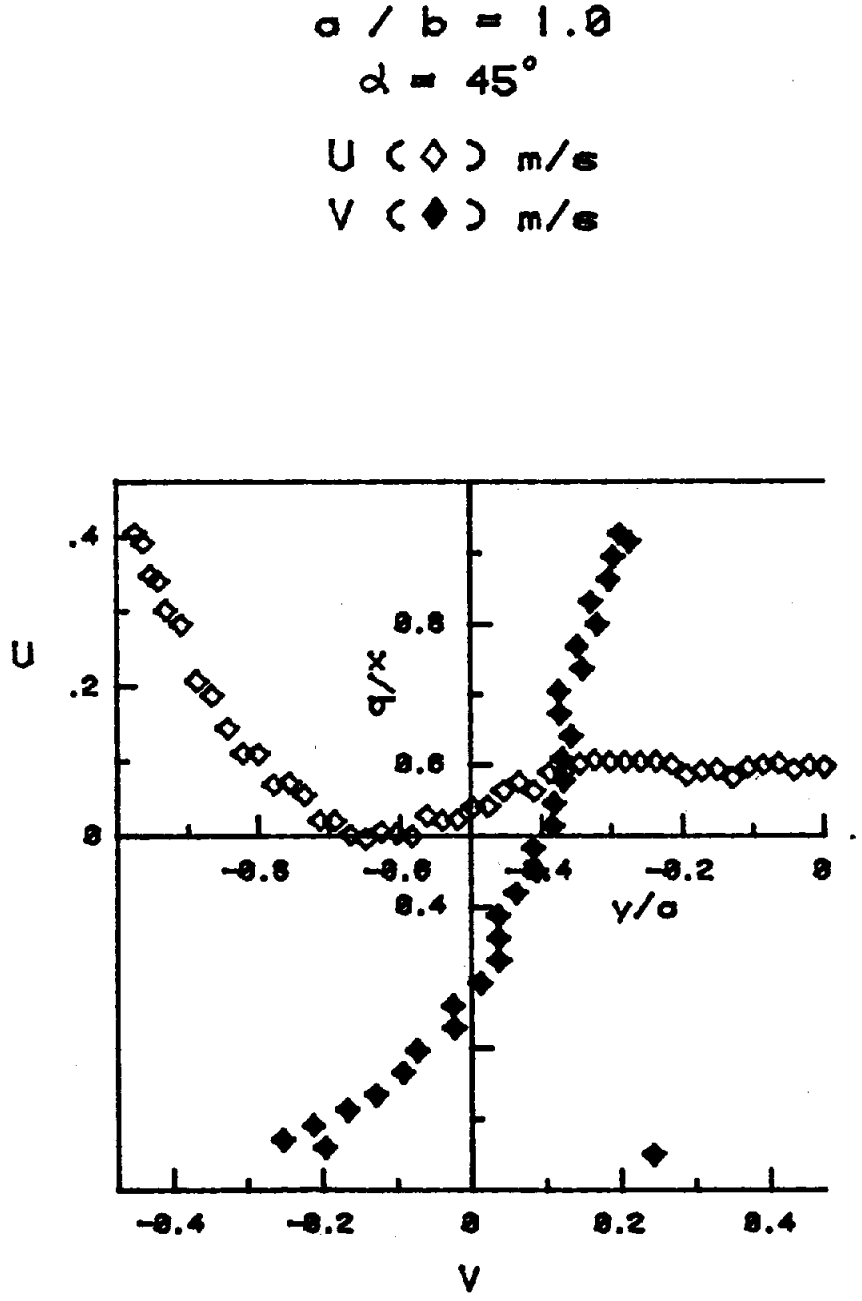

Figure 30a Mean velocity measurements inside the cavity on the symmetry plane, z/(c/2) = 0, with a/b = 1.0 and α = 45°; unweighted data. Measurements on planes shown.

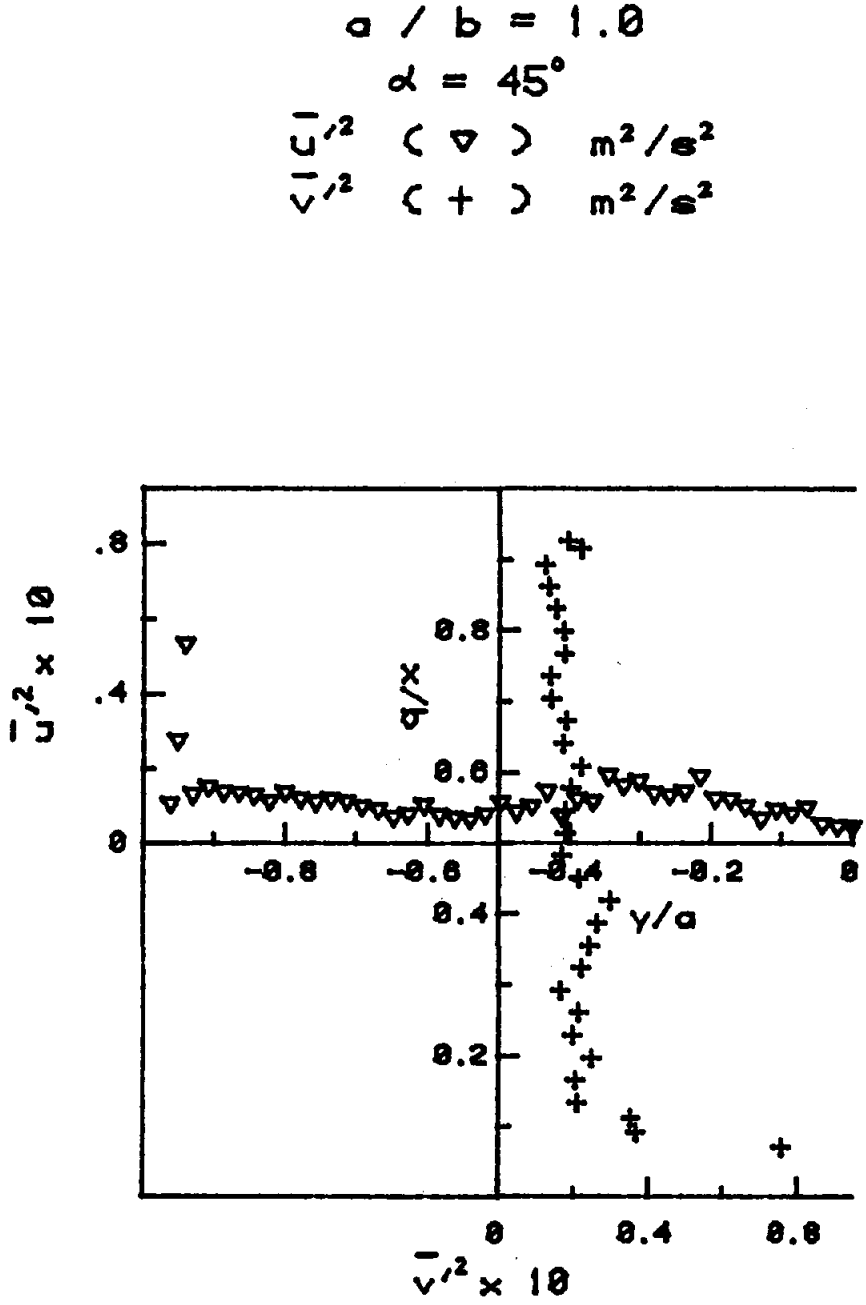

Figure 30b Normal stress (b) measurements inside the cavity on the symmetry plane, z/(c/2) = 0, with a/b = 1.0 and α = 45°; unweighted data. Measurements on planes shown.

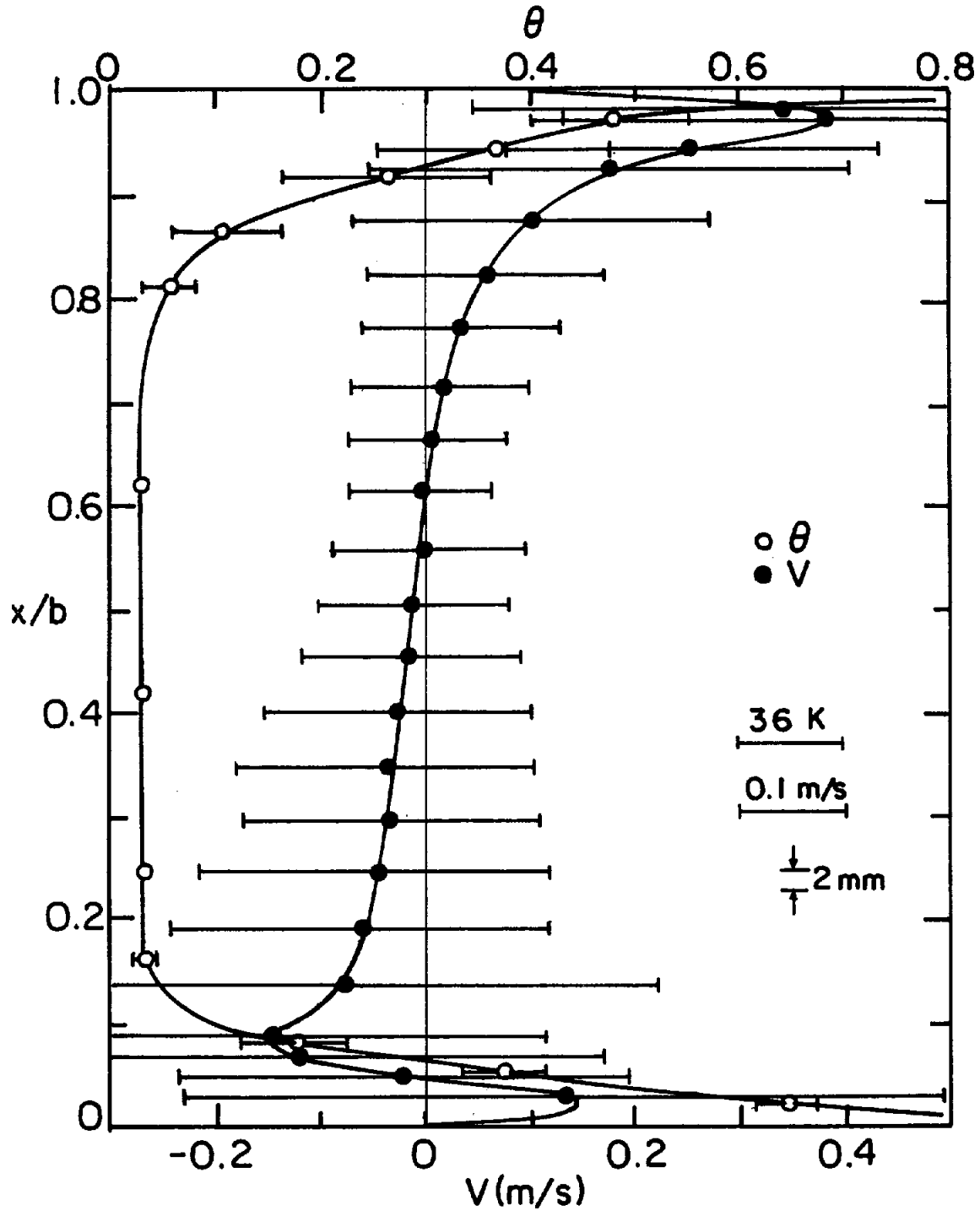

(a)

Figure 31 Measurements of θ and the V-velocity component (m/sec) in the cavity aperture plane with 2σ levels shown: (a) corresponds to a/b = 0.5, α = 0°; (b) corresponds to a/b = 1.0, α = 0°; (c) corresponds to a/b = 1, α = 45°; (d) is a composite of the V-velocity profiles.

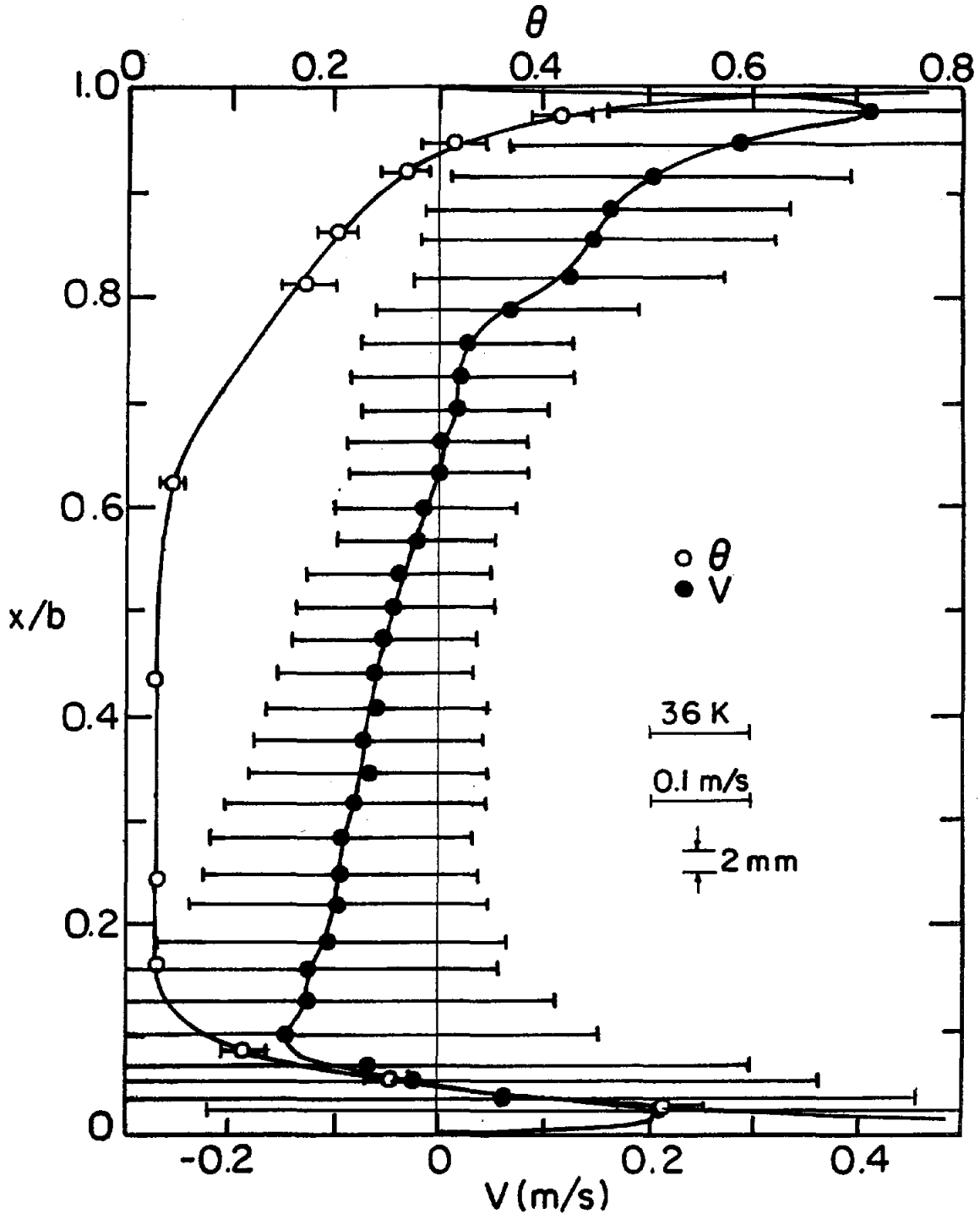

(b)

Figure 31 Measurements of θ and the V-velocity component (m/sec) in the cavity aperture plane with 2σ levels shown: (a) corresponds to a/b = 0.5, α = 0°; (b) corresponds to a/b = 1.0, α = 0°; (c) corresponds to a/b = 1, α = 45°; (d) is a composite of the V-velocity profiles.

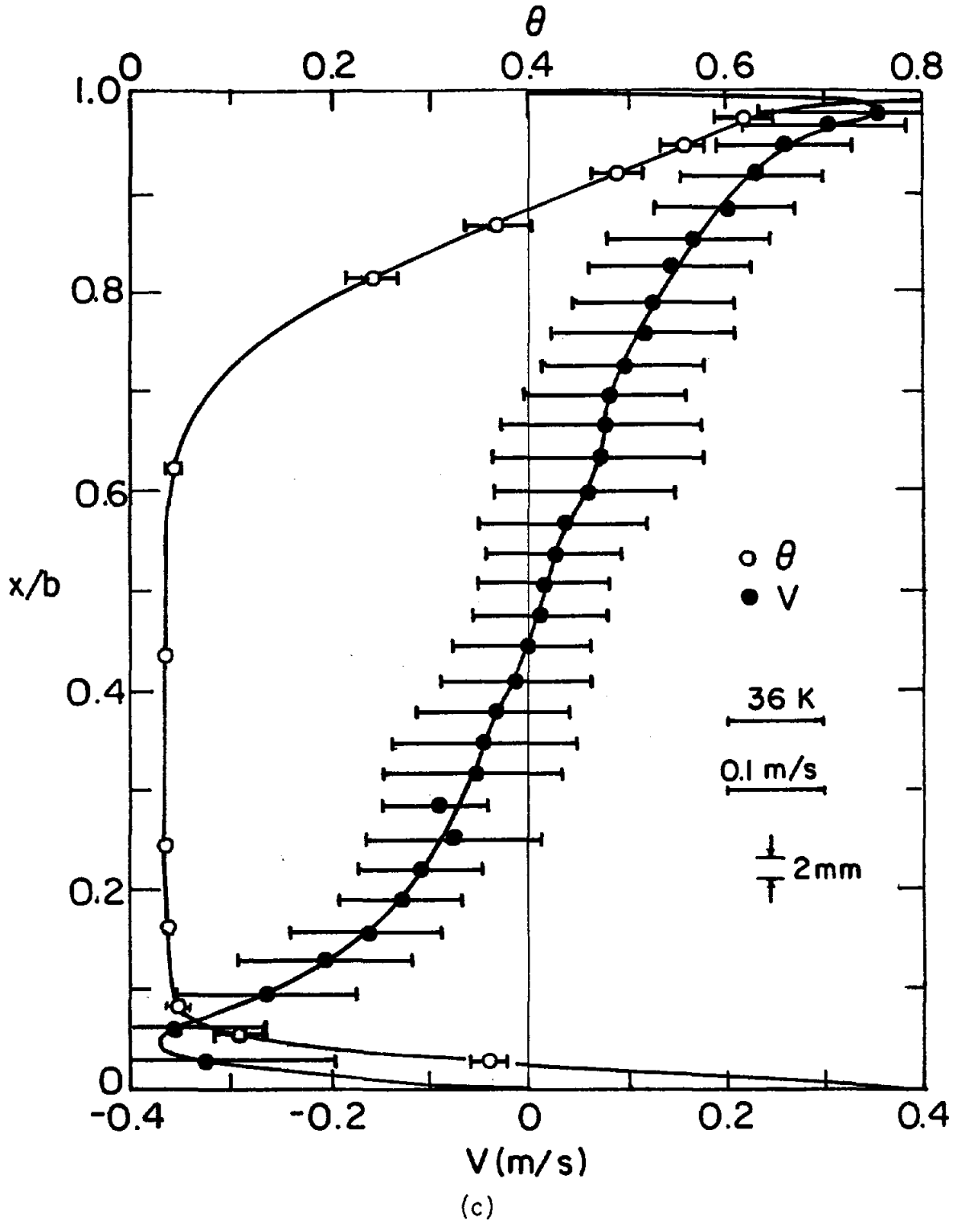

(c)

Figure 31 Measurements of θ and the V-velocity component (m/sec) in the cavity aperture plane with 2σ levels shown: (a) corresponds to a/b = 0.5, α = 0°; (b) corresponds to a/b = 1.0, α = 0°; (c) corresponds to a/b = 1, α = 45°; (d) is a composite of the V-velocity profiles.

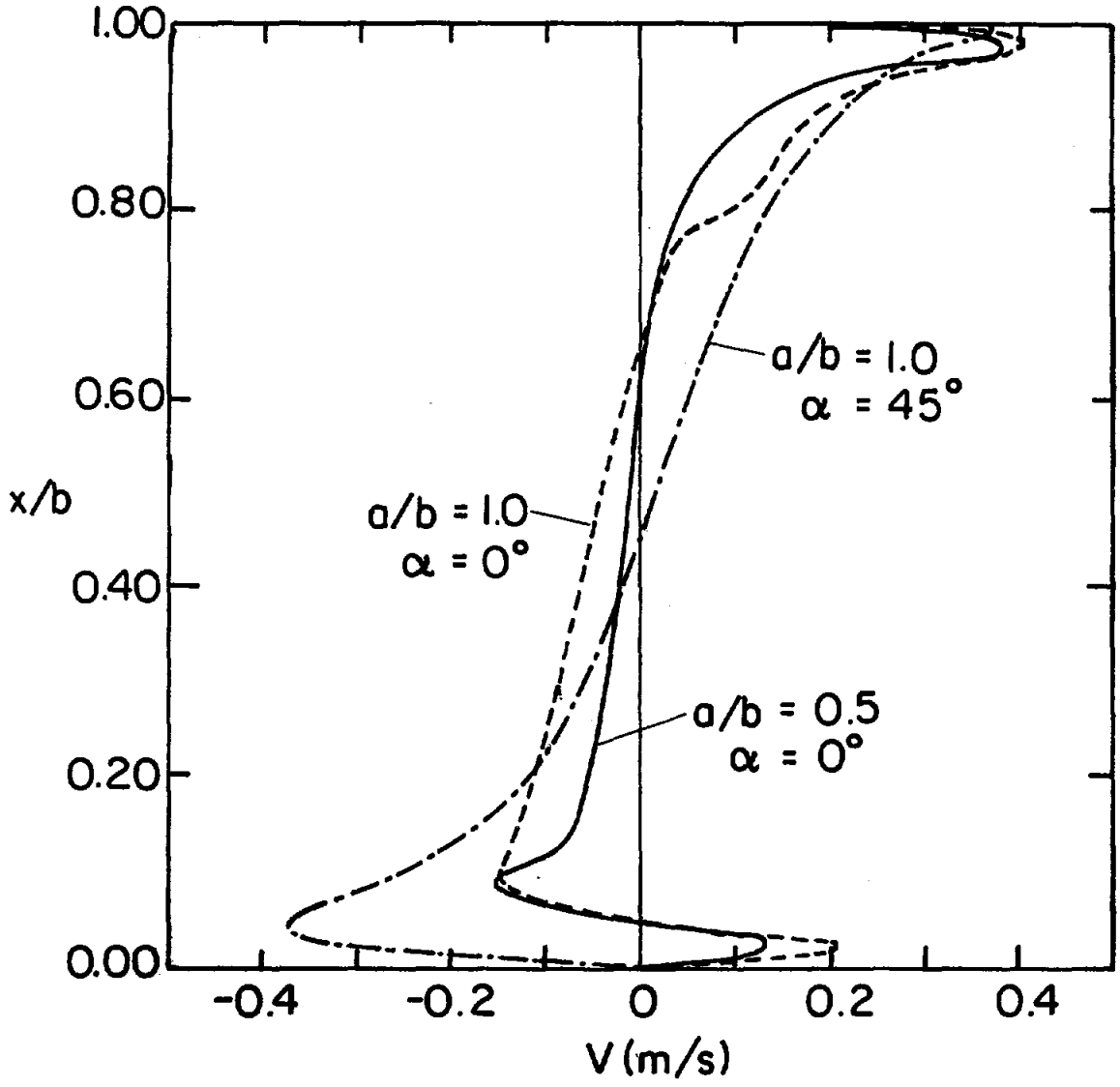

(d)

Figure 31 Measurements of θ and the V-velocity component (m/sec) in the cavity aperture plane with 2σ levels shown: (a) corresponds to a/b = 0.5, α = 0°; (b) corresponds to a/b = 1.0, α = 0°; (c) corresponds to a/b = 1, α = 45°; (d) is a composite of the V-velocity profiles.

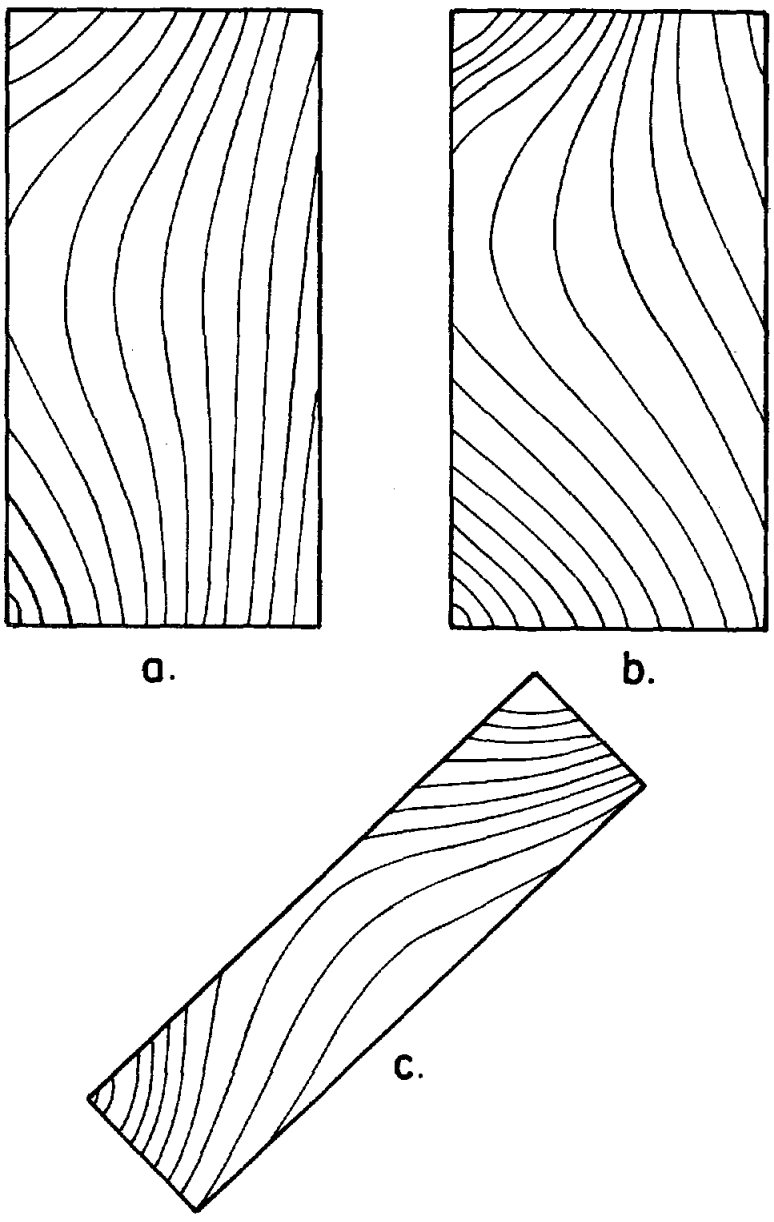

Figure 32 Streamlines of the mean flow in front of the cavity: (a) $a/b = 0.5$, $\alpha = 0°$; (b) $a/b = 1.0$, $\alpha = 0°$; (c) $a/b = 1.0$, $\alpha = 45°$.

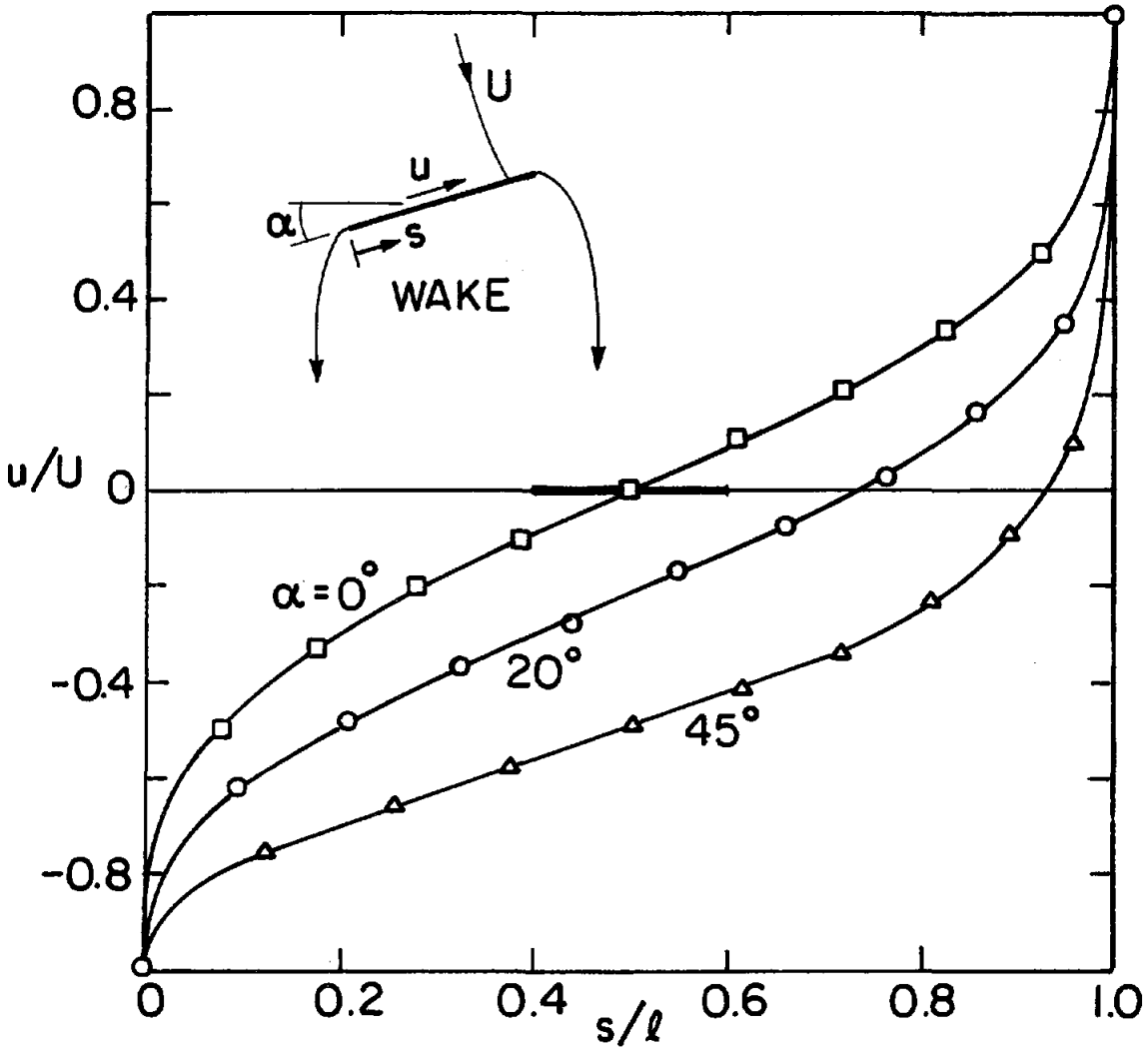

Figure 33 Potential flow along a flat plate inclined at an angle 90 - α with respect to the approaching wind.

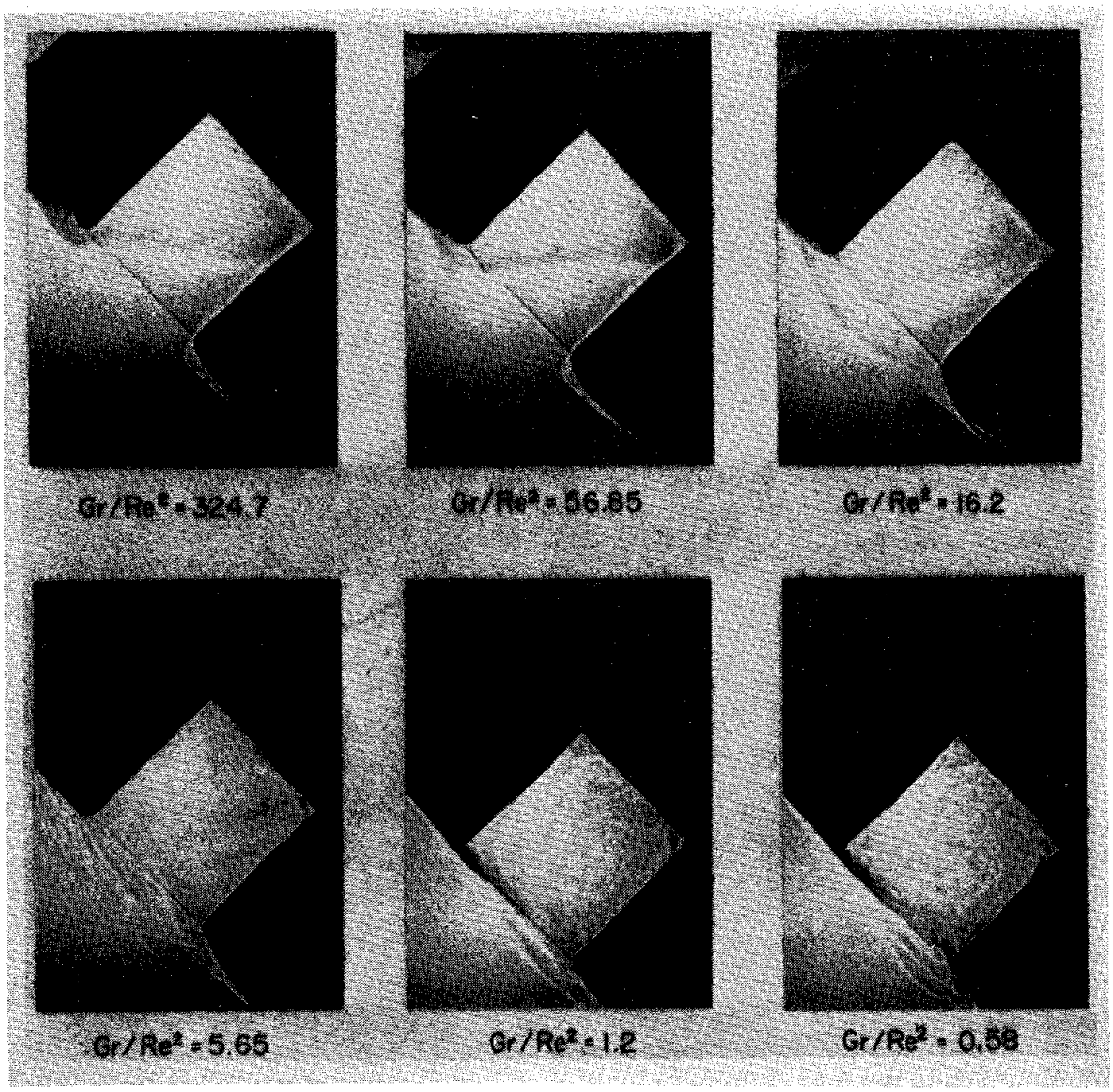

Figure 34a Shadowgraphs of heated cavity flows with a/b = 1.0 and α = 45° for different values of Gr/Re^2: $Gr \simeq 4.3 \times 10^7$, $\Delta T/T_\infty \simeq 1.26$.

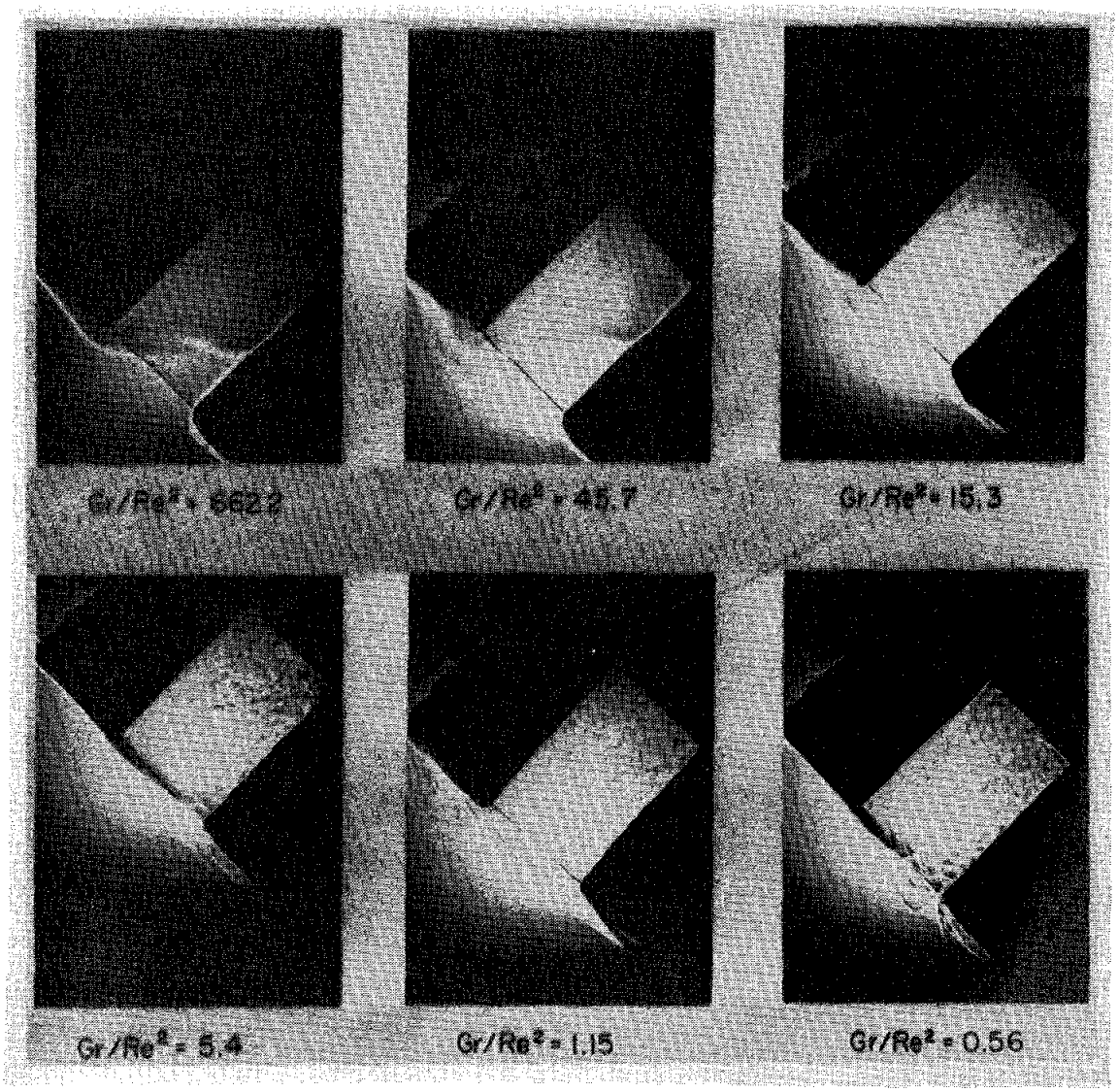

Figure 34b Shadowgraphs of heated cavity flows with a/b = 1.46 and α = 45° for different values of Gr/Re^2: $Gr \simeq 4.1 \times 10^7$, $\Delta T/T_\infty \simeq 1.20$.

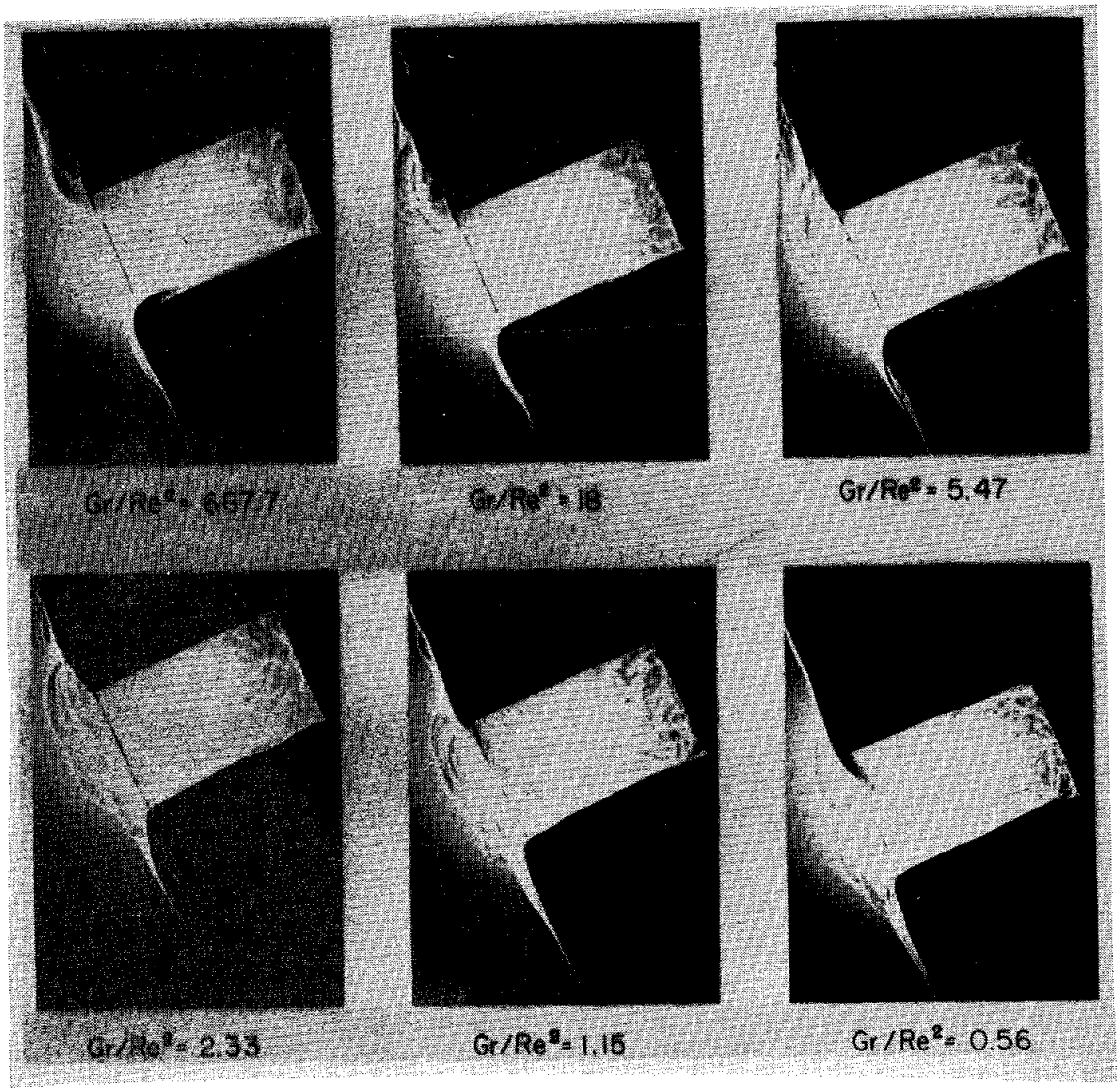

Figure 35 Shadowgraphs of heated cavity flows with a/b = 1.46 and α = 20° for different values of Gr/Re^2: $Gr \simeq 4.1 \times 10^7$, $\Delta T/T_\infty \simeq 1.21$.

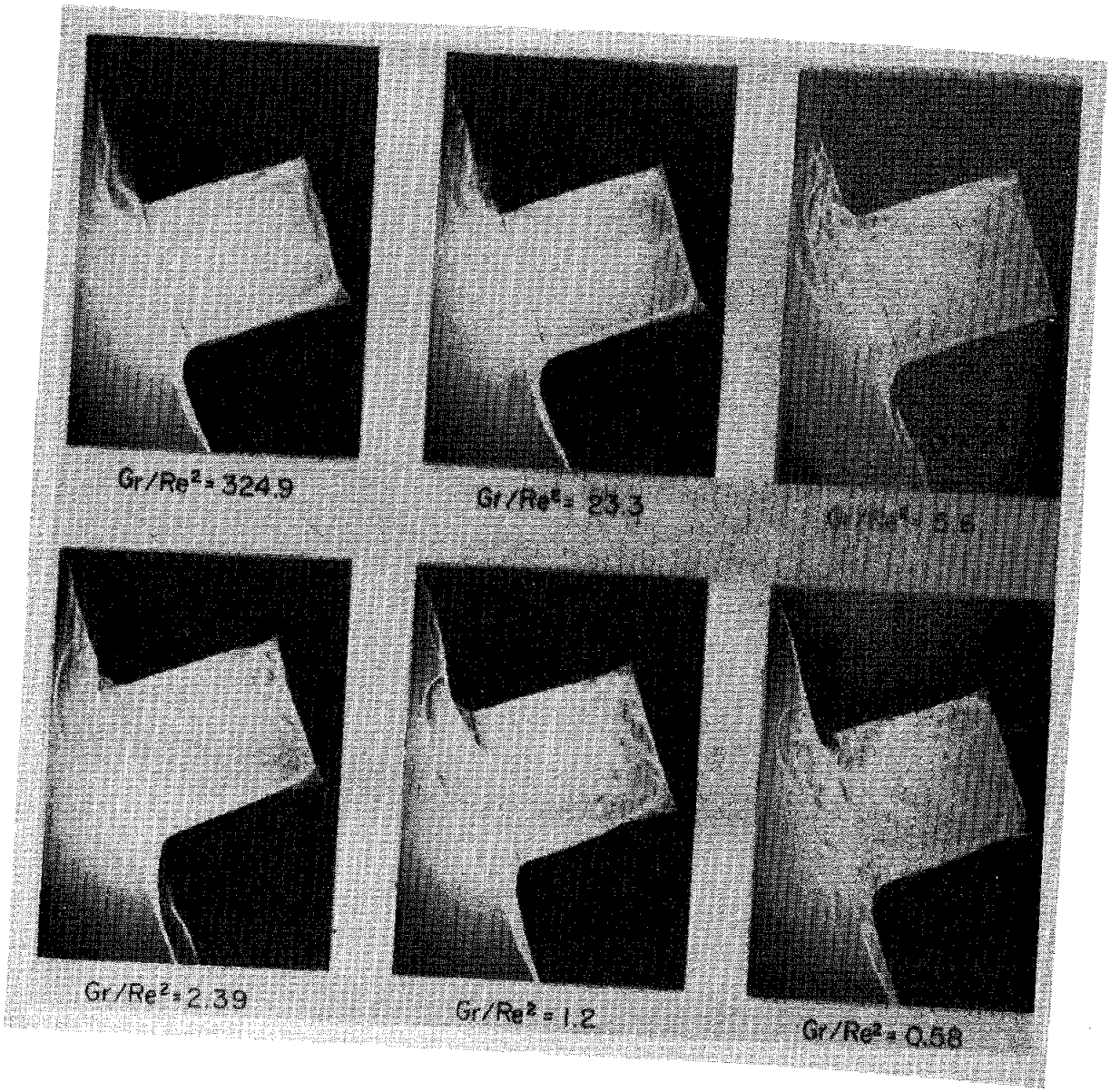

Figure 36 Shadowgraphs of heated cavity flows with a/b = 1.0 and α = 20° for different values of Gr/Re^2: $Gr \simeq 4.3 \times 10^7$, $\Delta T/T_\infty \simeq 1.26$.

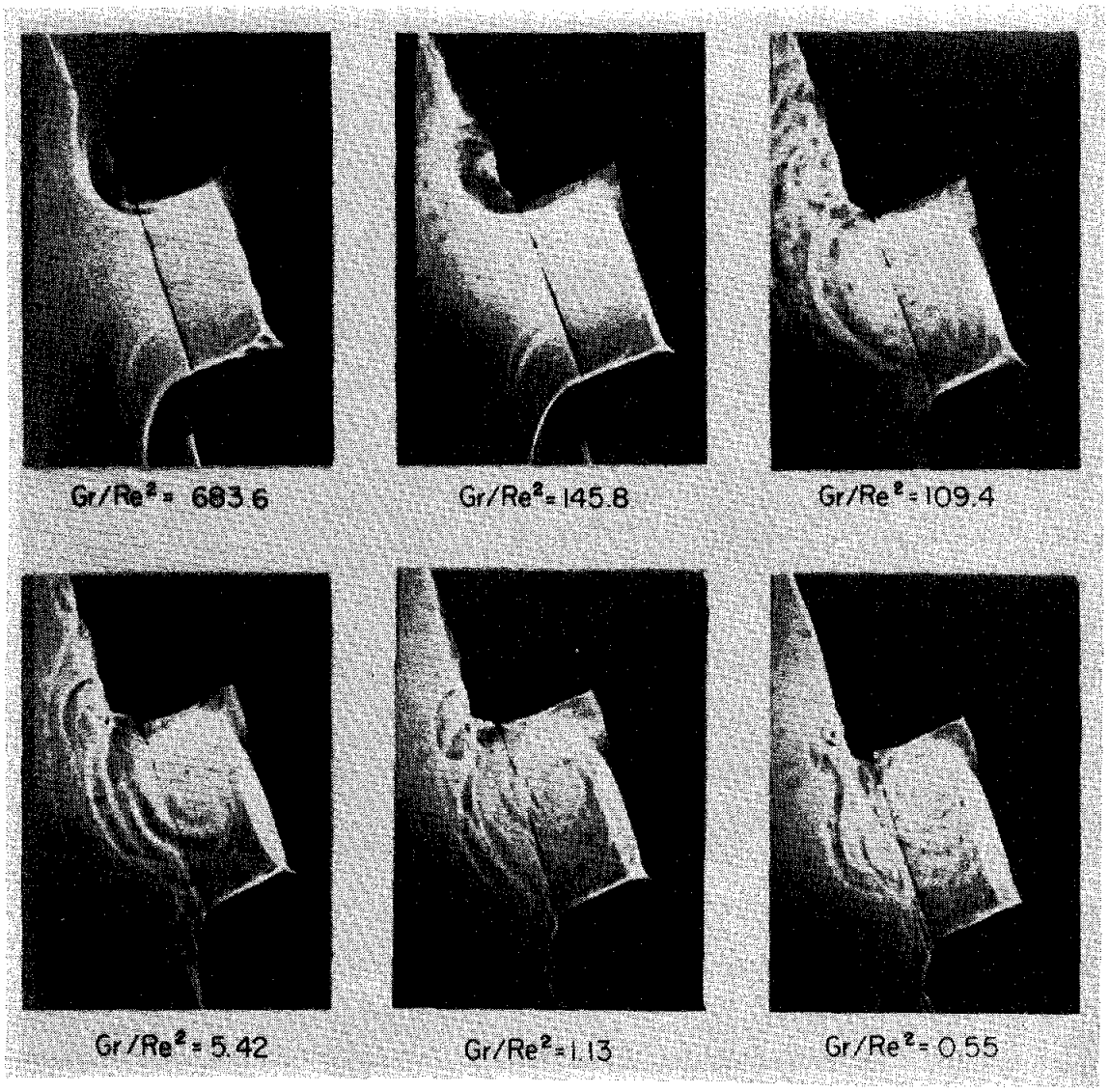

Figure 37 Shadowgraphs of heated cavity flows with a/b = 0.5 and α = 20° for different values of Gr/Re^2: $Gr \simeq 4.0 \times 10^7$, $\Delta T/T_\infty \simeq 1.18$.

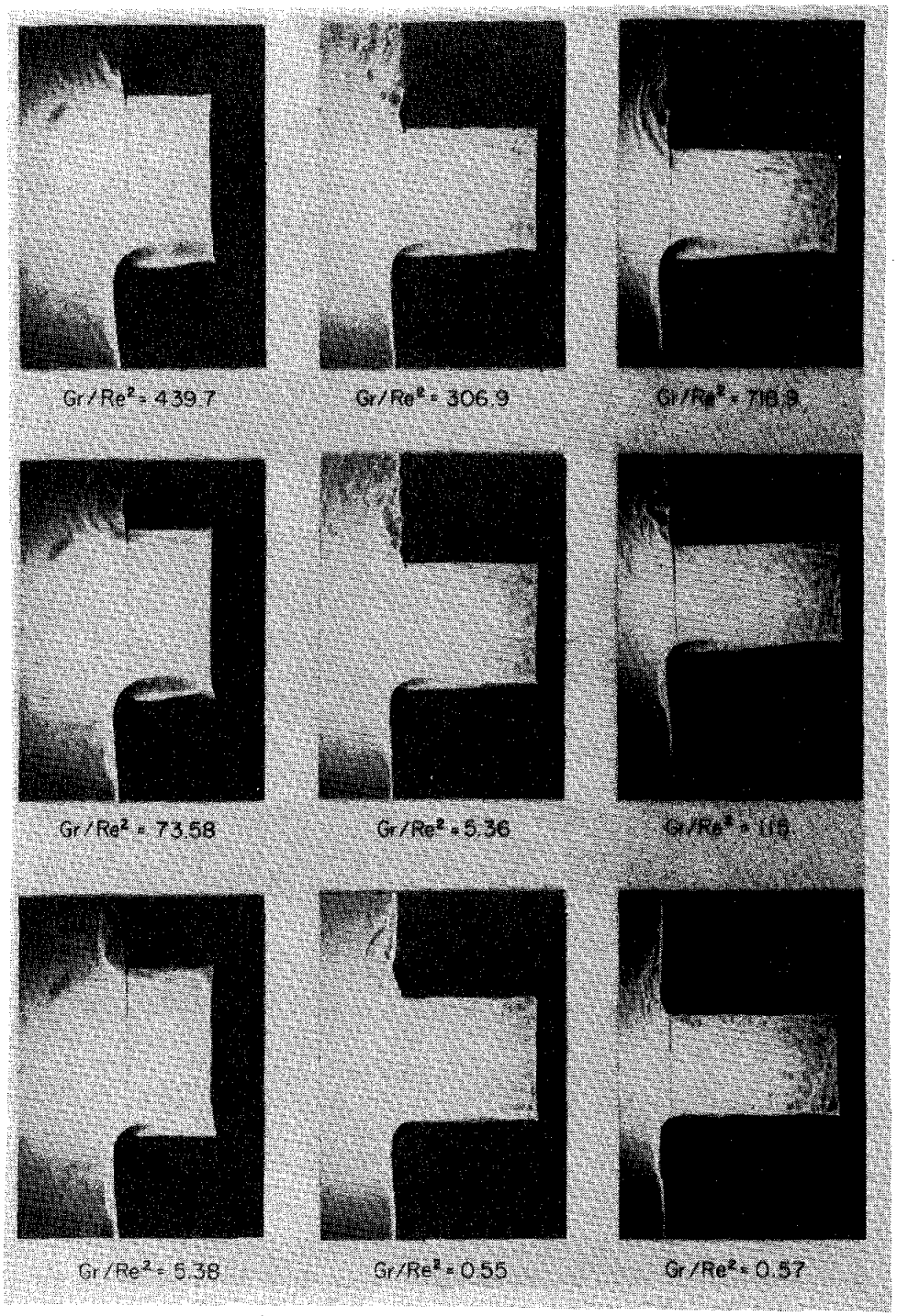

Figure 38 Shadowgraph of heated cavity flows with $\alpha = 0°$ and (from left to right) a/b = 0.5, 1.0 and 1.46 for different values of Gr/Re^2: $Gr \simeq 4.1 \times 10^7$, $\Delta T/T_\infty \simeq 1.2$ (average values).

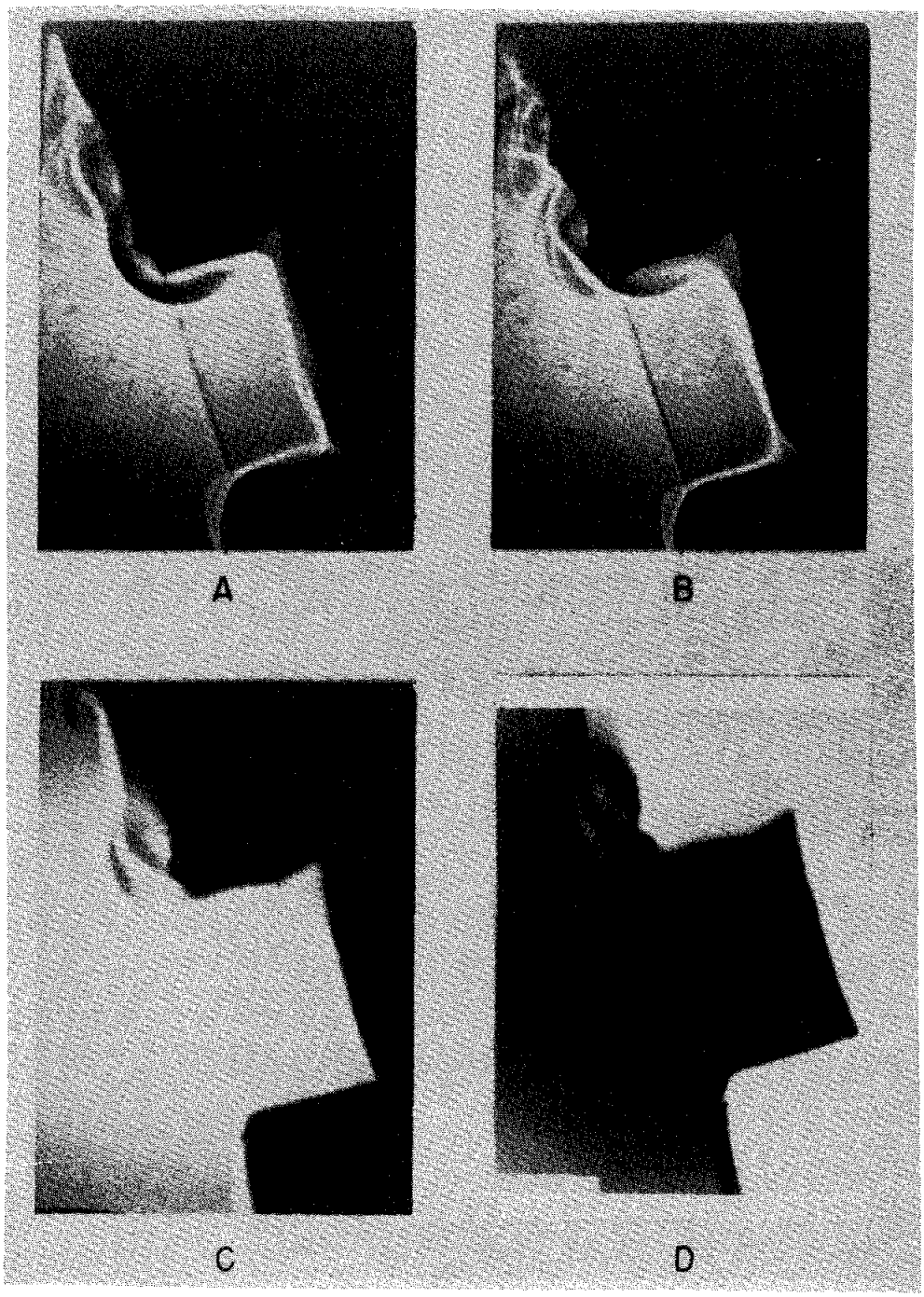

Figure 39 Large scale, coherent, low-frequency cavity flow pulsations frozen by stroboscopic pulsing of the point light source. Photographs are for different phases of a cycle for conditions indicated in Table 3.7.

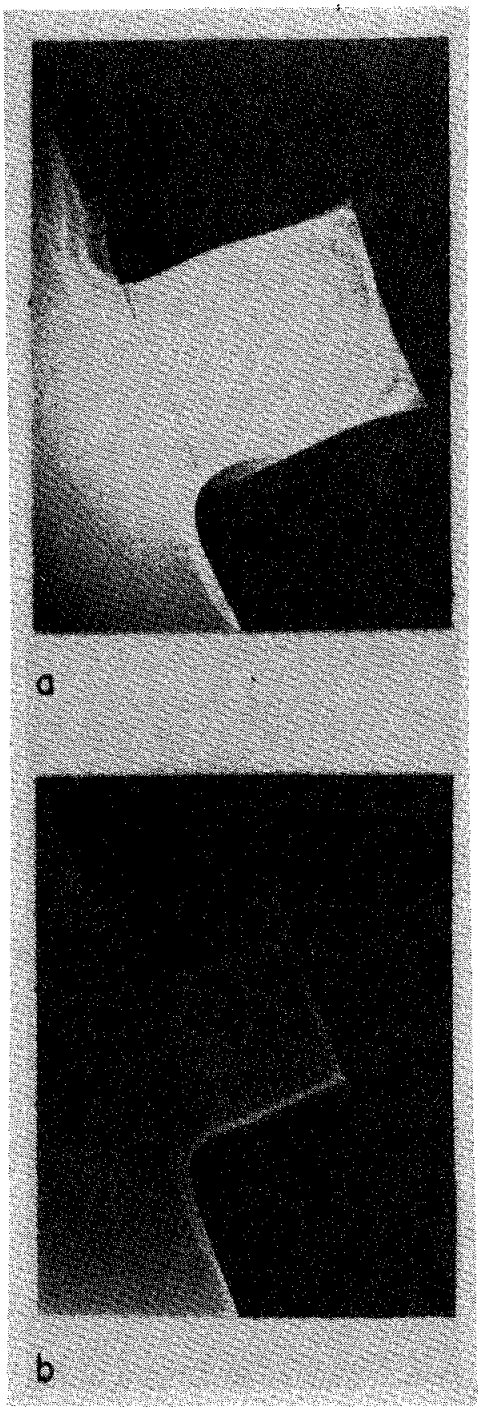

Figure 40 Large scale, coherent, low-frequency cavity flow pulsations frozen by high speed photography. Photographs are for conditions indicated in Table 3.7.

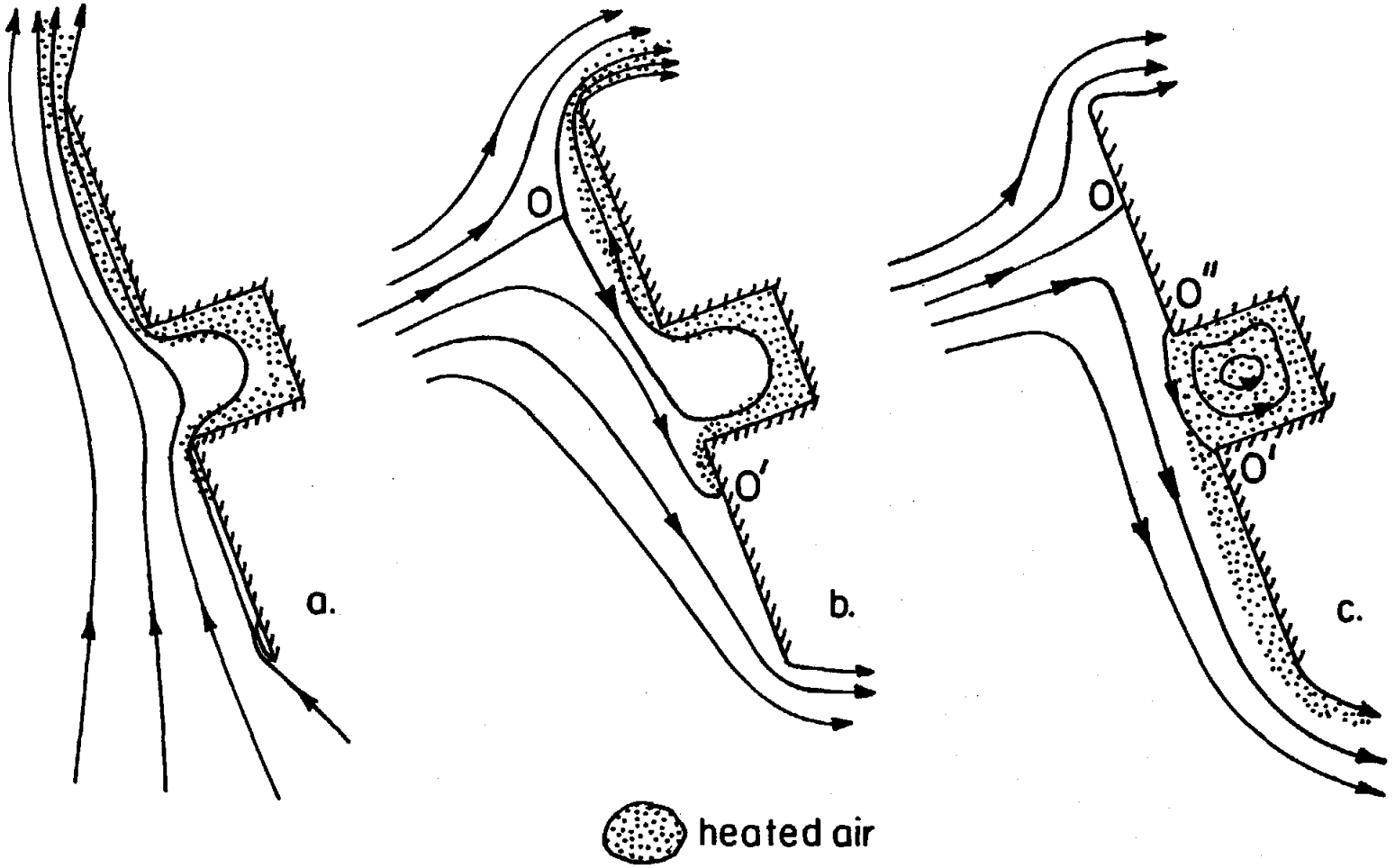

Figure 41 Qualitative options for two-dimensional free-forced flow
(a) No wind: $Gr/Re^2 = \infty$; (b) Weak wind: $10 < Gr/Re^2 < 500$;
(c) Strong wind: $Gr/Re^2 < 10$.

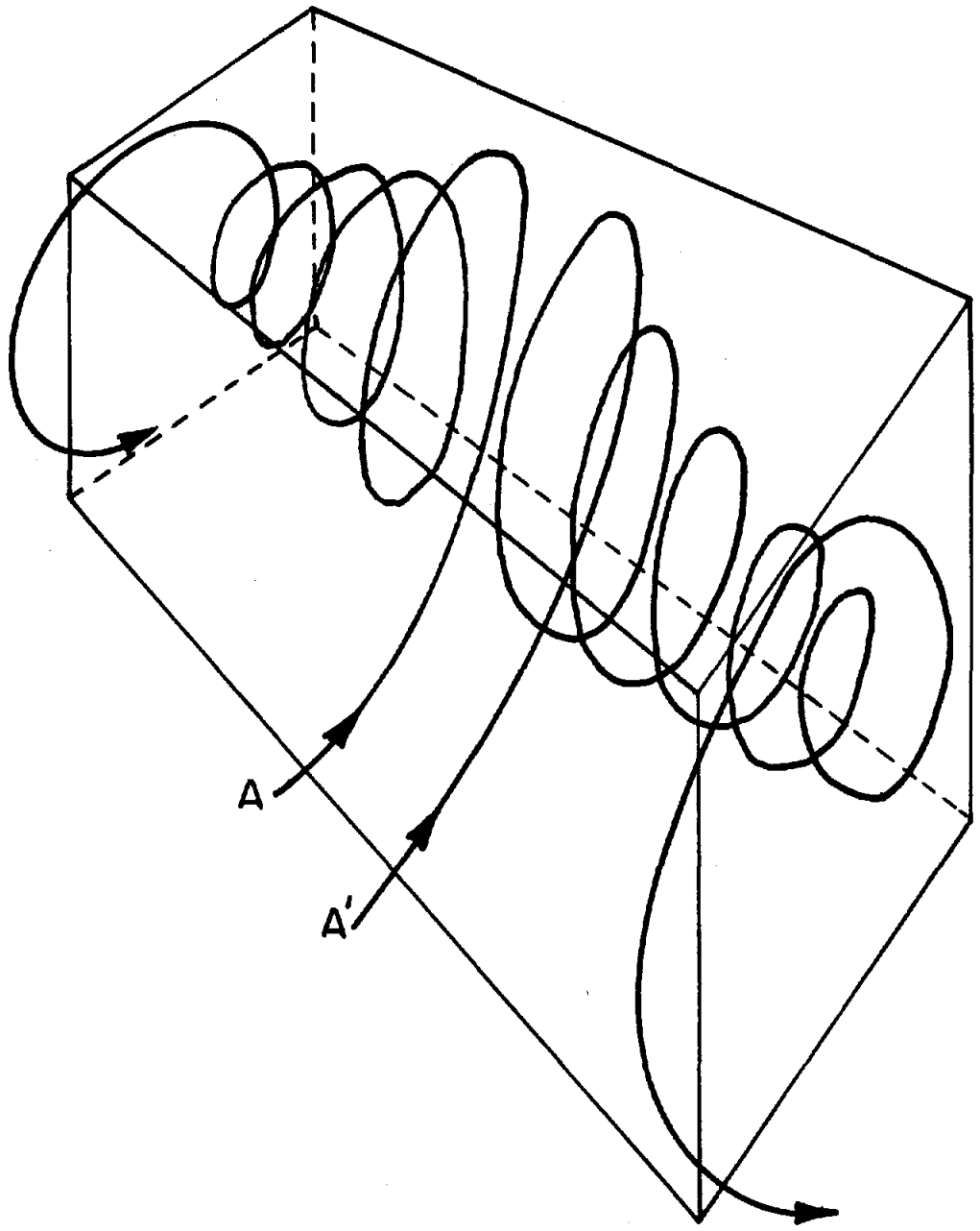

Figure 42 A three-dimensional interpretation of flow in the cavity for $Gr/Re^2 < 10$.

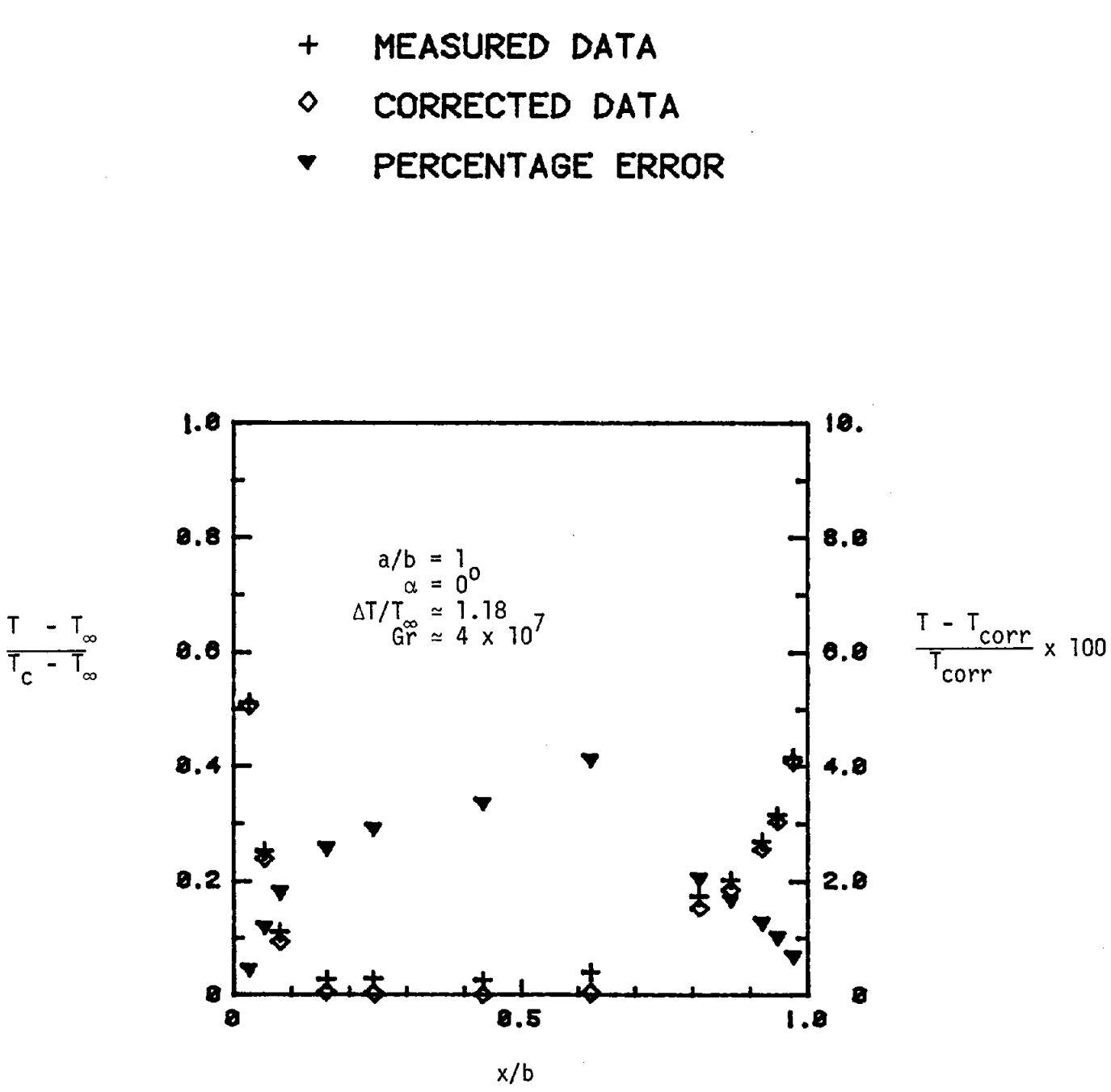

Figure 43 Comparison between aperture plane temperature measurements corrected and uncorrected for radiation error.

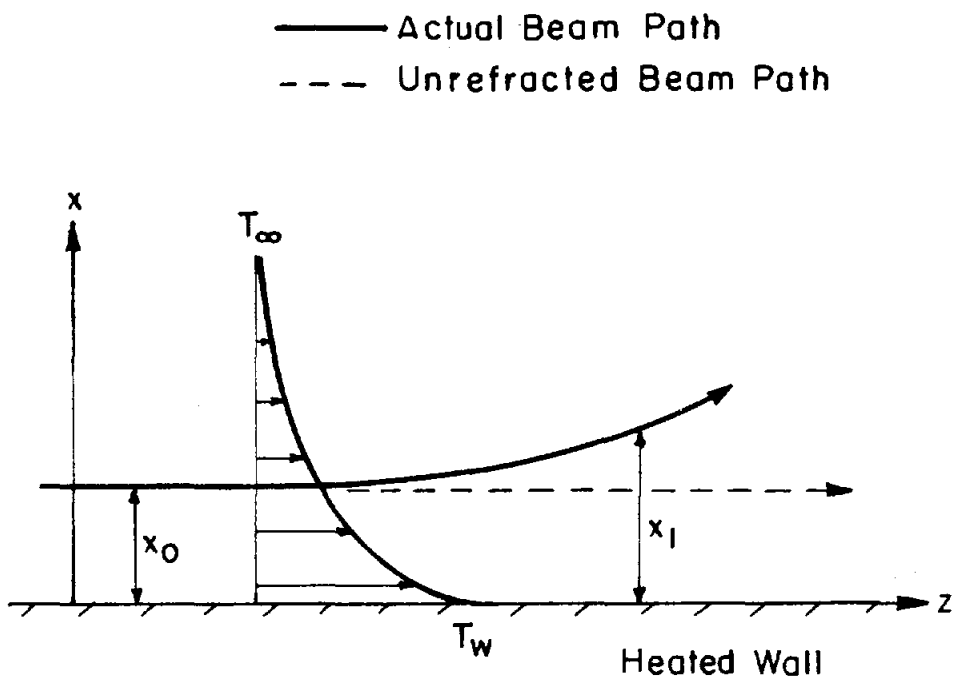

Figure 44 Systematic deflection of laser beam path due to the continuous mean variations in the index of refraction of air.

APPENDIX A

Weighted (W) and Unweighted (U) Measurements of Velocity and Turbulent Stress Components

U, V, W in [m/s]

$\overline{u'^2}$, $\overline{v'^2}$, $\overline{w'^2}$, $\overline{u'v'}$ in $[m^2/s^2]$

N is sample size

Weighted

a/b=1.0, α=0 , Free Convection (Re=0)

Tbot=400.8 ± 5.1 (C), Tbac=399.6 ± 5.0 (C)

Ttop=338.4 ± 3.3 (C), T_∞ =25 (C)

$\Delta T/T_\infty$ =1.19 , Gr=4.14 E7 , N = 1000

y/a=0.0, z/c=0.0

x/b	V	U	$\overline{v'^2}\times10$	$\overline{u'^2}\times10$	$\overline{u'v'}\times100$	W	$\overline{w'^2}\times10$
0.9789	0.4110	0.2735	0.6386	0.0640	0.2468	0.0760	0.409
0.9472	0.2885	0.2326	0.4990	0.0868	0.3752	0.0702	0.361
0.9155	0.2010	0.1777	0.3784	0.0960	0.4421	0.0529	0.282
0.8838	0.1631	0.1415	0.3047	0.1165	0.6539	0.0412	0.238
0.8521	0.1492	0.1176	0.2759	0.1181	0.5185	0.0244	0.134
0.8204	0.1219	0.0970	0.2228	0.1225	0.4367	0.0280	0.117
0.7887	0.0657	0.0647	0.1587	0.0990	0.3371	0.0229	0.112
0.7570	0.0278	0.0384	0.0985	0.0621	0.2287	0.0211	0.103
0.7253	0.0201	0.0465	0.1059	0.0728	0.1624	0.0192	0.09
0.6936	0.0199	0.0403	0.0846	0.0607	0.1241	0.0078	0.068
0.6619	0.0004	0.0360	0.0791	0.0665	0.0878	0.0121	0.059
0.6303	-0.0010	0.0301	0.0742	0.0505	0.0817	0.0047	0.06
0.5986	-0.0156	0.0306	0.0737	0.0541	0.0576	0.0026	0.048
0.5669	-0.0227	0.0265	0.0581	0.0445	0.0461	0.002	0.048
0.5352	-0.0390	0.0234	0.0772	0.0529	0.0275	0.0165	0.081
0.5035	-0.0427	0.0267	0.0926	0.0612	0.0380	-0.0034	0.064
0.4718	-0.0510	0.0310	0.0820	0.0570	0.0284	0.0110	0.087
0.4401	-0.0606	0.0523	0.0939	0.0716	0.0107	-0.0021	0.053
0.4084	-0.0569	0.0491	0.1122	0.0602	0.0149	0.0116	0.082
0.3767	-0.0727	0.0543	0.1081	0.0661	0.0052	0.0082	0.07
0.3450	-0.0678	0.0600	0.1207	0.0751	-0.0472	0.0158	0.068
0.3133	-0.0812	0.0692	0.1563	0.0880	0.0135	0.0158	0.085
0.2816	-0.0911	0.0759	0.1539	0.0714	0.0020	0.0155	0.074
0.2499	-0.0959	0.0795	0.1730	0.0819	0.0196	0.0165	0.091
0.2183	-0.0970	0.0943	0.2005	0.0868	-0.0692	0.0202	0.107
0.1866	-0.1071	0.1226	0.2756	0.1366	-0.1922	0.0225	0.128
0.1549	-0.1277	0.1531	0.3205	0.1187	-0.2131	0.0133	0.158
0.1232	-0.1274	0.2136	0.5616	0.1012	-0.1353	0.0456	0.195
0.0914	-0.1470	0.2820	0.8710	0.1620	-0.1530	0.0362	0.226
0.0634	-0.0698	0.3183	1.3477	0.4076	-0.0746	0.0806	0.378
0.0528	-0.0285	0.3930	1.4761	0.4486	0.0495		
0.0317	0.0629	0.3665	1.5209	0.4284	-0.0762	0.0947	0.470
0.0211	0.2082	0.3718	1.8094	0.2225	0.0579		

Weighted

a/b=1.0, α =0 , Free Convection (Re=0)

Tbot=400.8 ± 5.1 (C), Tbac=399.6 ± 5.0 (C)

Ttop=338.4 ± 3.3 (C), T_∞ =25 (C)

$\Delta T/T_\infty$ =1.19 , Gr=4.14 E7 , N = 1000

y/a=0.5, z/$\frac{c}{2}$=0.0

x/b	V	U	$\overline{v'^2}\times10$	$\overline{u'^2}\times10$	$\overline{u'v'}\times100$	W	$\overline{w'^2}\times10$
0.0000	-0.0186	0.0931	0.0597	0.0249	0.0218	0.0200	0.067
0.0423	-0.0288	0.0944	0.0575	0.0261	0.0447	0.0266	0.0727
0.0845	-0.0331	0.0761	0.0555	0.0157	0.0146	0.0195	0.0595
0.1268	-0.0363	0.0859	0.0429	0.0148	0.0082	0.0216	0.0540
0.1690	-0.0270	0.0844	0.0570	0.0129	0.0113	0.0082	0.0400
0.2113	-0.0271	0.0934	0.0525	0.0138	0.0081	0.0177	0.0456
0.2535	-0.0327	0.0834	0.0501	0.0119	0.0042	0.0085	0.0440
0.2958	-0.0269	0.0748	0.0529	0.0139	0.0053	0.0171	0.0519
0.3381	-0.0358	0.0794	0.0426	0.0164	0.0253	0.0152	0.0448
0.3803	-0.0292	0.0829	0.0449	0.0232	0.0427	0.0142	0.0413
0.4226	-0.0326	0.0720	0.0436	0.0140	0.0067	0.0195	0.0506
0.4648	-0.0295	0.0485	0.0377	0.0098	0.0058	0.0101	0.0406
0.5071	-0.0344	0.0615	0.0399	0.0175	0.0047	0.0141	0.0495
0.5493	-0.0254	0.0507	0.0312	0.0146	-0.0289	0.0647	0.0494
0.5916	-0.0287	0.0584	0.0466	0.0136	0.0321	0.0116	0.0476
0.6338	-0.0299	0.0546	0.0319	0.0126	-0.0145	0.0218	0.0376
0.6761	-0.0231	0.0616	0.0296	0.0119	-0.0107	0.0206	0.0423
0.7184	-0.0271	0.0709	0.0414	0.0157	0.0172	0.0159	0.0461
0.7606	-0.0241	0.0666	0.0334	0.0201	0.0032	0.0168	0.0404
0.8029	-0.0223	0.0598	0.0377	0.0202	0.0326	0.0137	0.0481
0.8451	-0.0235	0.0709	0.0484	0.0174	0.0156	0.0164	0.0455
0.8874	-0.0254	0.0767	0.0375	0.0130	0.0070	0.0107	0.0558
0.9296	-0.0199	0.0639	0.0375	0.0153	-0.0046	0.0176	0.0537
0.9718	-0.0262	0.0829	0.0423	0.0191	0.0276	0.0266	0.0531
0.9999	-0.0188	0.0721	0.1006	0.0437	0.1026	0.0080	0.051

Weighted

a/b=1.0, α=0 , Free Convection (Re=0)

Tbot=400.8 ± 5.1 (C), Tbac=399.6 ± 5.0 (C)

Ttop=338.4 ± 3.3 (C), T_∞ =25 (C)

$\Delta T/T_\infty$ =1.19 , Gr=4.14 E7 , N = 1000

x/b=1.0, z/c=0.0

y/a	V	U	$\overline{v'^2}\times10$	$\overline{u'^2}\times10$	$\overline{u'v'}\times100$	W	$\overline{w'^2}\times10$
0.5000	-0.0188	0.0721	0.1006	0.0437	0.1025	0.0080	0.0510
0.4648	-0.0141	0.1162	0.1064	0.0379	0.0690	0.0173	0.0562
0.4437	-0.0051	0.1047	0.1149	0.0496	0.1600	0.0184	0.0660
0.4226	-0.0154	0.0925	0.0841	0.0383	0.1628	0.0141	0.0898
0.4016	-0.0102	0.0762	0.0740	0.0584	0.1450	0.0231	0.0903
0.3805	-0.0111	0.0899	0.0808	0.0435	0.1805	0.0226	0.0858
0.3594	0.0145	0.1210	0.1482	0.1177	0.6723	0.0278	0.0934
0.3383	0.0086	0.1220	0.1384	0.0847	0.4820	0.0328	0.105
0.3172	0.0283	0.1645	0.1654	0.1279	0.6475	0.0277	0.103
0.2961	0.0568	0.1883	0.2115	0.1147	0.7432	0.0469	0.140
0.2750	0.1044	0.2427	0.3194	0.1686	1.3510	0.0385	0.168
0.2539	0.0559	0.1993	0.2345	0.1446	0.9572	0.0413	0.167
0.2328	0.0963	0.2446	0.3566	0.1750	1.3760	0.0453	0.208
0.2118	0.1379	0.3031	0.3053	0.1555	1.1310	0.0577	0.180
0.1907	0.1062	0.2533	0.3089	0.1702	1.2266	0.0559	0.214
0.1696	0.1867	0.3497	0.3495	0.1442	1.1372	0.0584	0.247
0.1485	0.1888	0.3477	0.4001	0.1318	1.1844	0.0516	0.308
0.1274	0.2126	0.3749	0.4165	0.1119	0.9599	0.0718	0.309
0.1063	0.2499	0.3954	0.4207	0.1251	1.0222	0.0516	0.441
0.0852	0.3064	0.4334	0.5488	0.1087	0.8397	0.0996	0.443
0.0641	0.3587	0.4618	0.6541	0.0932	0.6519	0.0836	0.486
0.0431	0.4142	0.4831	0.6036	0.0616	0.4830	0.0803	0.527
0.0220	0.4256	0.4773	0.8894	0.0495	0.2097	0.0835	0.608

Weighted

a/b=1.0, α=0 , Free Convection (Re=0)

Tbot=400.8 ± 5.1 (C), Tbac=399.6 ± 5.0 (C)

Ttop=338.4 ± 3.3 (C), T_∞ =25 (C)

$\Delta T/T_\infty$ =1.19 , Gr=4.14 E7 , N = 1000

x/b=0.0, z/c=0.0

y/a	V	U	$\overline{v'^2}\times10$	$\overline{u}^2\times10$	$\overline{u'v'}\times100$	W	$\overline{w'^2}\times10$
0.0211	0.0796	0.5911	1.3820	0.1762	0.0253	0.116	0.676
0.0422	-0.0903	0.4193	0.3333	0.0492	0.0045	0.0823	0.453
0.0633	-0.0706	0.3221	0.2442	0.0348	-0.0398	0.0358	0.309
0.0844	-0.0501	0.2495	0.2299	0.0389	-0.0002	0.0344	0.299
0.1055	-0.0481	0.2008	0.1424	0.0276	-0.0190	0.0105	0.191
0.1266	-0.0505	0.2105	0.1441	0.0327	0.0350	0.0107	0.215
0.1477	-0.0360	0.1378	0.1030	0.0254	0.0180	0.0239	0.183
0.1687	-0.0406	0.1477	0.0939	0.0277	-0.0136	0.0186	0.217
0.1898	-0.0346	0.1300	0.0783	0.0256	0.0342	0.0218	0.221
0.2109	-0.0399	0.1334	0.0932	0.0199	-0.0004	0.0262	0.208
0.2320	-0.0308	0.1440	0.0882	0.0235	0.0074	0.0423	0.279
0.2531	-0.0256	0.1272	0.0748	0.0288	-0.0013	0.0301	0.219
0.2742	-0.0278	0.1206	0.0853	0.0213	0.0055	0.0299	0.208
0.2953	-0.0302	0.1309	0.0909	0.0230	0.0195	0.0230	0.167
0.3164	-0.0290	0.0972	0.0609	0.0177	0.0062	0.0193	0.186
0.3375	-0.0227	0.1110	0.0654	0.0184	0.0275	0.0250	0.193
0.3585	-0.0244	0.0936	0.0648	0.0236	0.0188	0.0157	0.130
0.3796	-0.0238	0.0881	0.0604	0.0183	0.0268	0.0298	0.177
0.4007	-0.0277	0.1009	0.0612	0.0207	0.0266	0.0129	0.155
0.4218	-0.0247	0.1043	0.0644	0.0156	0.0024	0.0340	0.134
0.4429	-0.0321	0.0740	0.0474	0.0177	0.0121	0.0175	0.141
0.4640	-0.0198	0.0867	0.0596	0.0117	0.0238	0.0135	0.121
0.5000	-0.0186	0.0931	0.0597	0.0249	0.0218	0.0200	0.147

Weighted

a/b=1.0, α=0 , Free Convection (Re=0)

Tbot=400.8 ± 5.7 (C), Tbac=403.4 ±4.5 (C)

Ttop=336.8 ± 4.0 (C), T_∞ =26 (C)

$\Delta T/T_\infty$ =1.184 , Gr=4.15 E7 , N = 1000

x/b=0.95, y/a=0.0

z/(c/2)	W	U	$\overline{w}^2$ x10	$\overline{u'^2}$ x10	$\overline{u'w'}$x100
0.3375	0.0211	0.1892	0.2918	0.1059	0.1941
0.3187	0.0227	0.2040	0.3383	0.1153	0.0573
0.3000	0.0015	0.1968	0.4302	0.1517	0.2336
0.2812	0.0395	0.1872	0.3313	0.1219	0.1612
0.2625	0.0316	0.1822	0.3298	0.1218	0.1000
0.2437	0.0115	0.1950	0.3863	0.0881	0.0149
0.2250	0.0334	0.1967	0.3307	0.1132	0.1852
0.2062	-0.0010	0.1972	0.4264	0.1019	0.0365
0.1875	0.0442	0.2114	0.3978	0.1008	0.0326
0.1687	0.0236	0.2254	0.3986	0.0959	0.0390
0.1500	0.0038	0.2156	0.3491	0.0991	0.1007
0.1312	0.0453	0.2063	0.3878	0.1019	0.1284
0.1125	0.0253	0.2193	0.2850	0.0899	0.0760
0.0937	-0.0028	0.2063	0.4425	0.1334	0.4474
0.0750	0.0248	0.2075	0.4399	0.1061	0.0150
0.0562	0.0235	0.2250	0.3242	0.1010	0.2352
0.0375	-0.0126	0.1813	0.4483	0.1465	0.4344
0.0187	0.0384	0.2081	0.3480	0.0903	0.1727
0.0000	-0.0037	0.1978	0.3600	0.1260	0.0970
-0.0187	0.0198	0.2209	0.3486	0.1140	0.1170
-0.0375	0.0618	0.2013	0.3285	0.1188	0.2715
-0.0562	0.0665	0.2095	0.3913	0.1068	0.0521
-0.0750	0.1172	0.2313	0.2785	0.0920	-0.0299
-0.0937	0.0916	0.2300	0.3951	0.1041	0.2533
-0.1125	0.0554	0.2285	0.2924	0.1024	0.0481
-0.1312	0.0647	0.2100	0.3771	0.1066	0.2202
-0.1500	0.0509	0.2107	0.2766	0.1007	0.0737
-0.1687	0.0379	0.2231	0.3222	0.1020	0.1795
-0.1875	0.0323	0.2064	0.3257	0.1080	0.1444
-0.2062	-0.0209	0.2134	0.4833	0.1129	0.2117
-0.2250	0.0373	0.2176	0.4212	0.0966	0.2419
-0.2437	0.0628	0.2123	0.3255	0.1030	0.0465
-0.2625	0.0905	0.2138	0.3347	0.1277	0.1200
-0.2812	0.0005	0.2233	0.3904	0.1038	0.0753
-0.3000	0.0468	0.2376	0.3561	0.1238	0.1022
-0.3187	0.0108	0.2059	0.3686	0.1224	0.2179
-0.3375	0.0195	0.2223	0.3654	0.1164	0.1272

Weighted

a/b=1.0, α=0 , Free Convection (Re=0)

Tbot=400.8 ± 5.7 (C), Tbac=403.4 ± 4.5 (C)

Ttop=336.8 ± 4.0 (C), T_∞ =26 (C)

$\Delta T/T_\infty$ =1.184 , Gr=4.15 E7 , N = 1000

x/b=0.90, y/a=0.0

z/(c/2)	W	U	$\overline{w'^2}\times10$	$\overline{u'^2}\times10$	$\overline{u'w'}\times100$
-0.3375	0.0774	0.1706	0.3178	0.1227	0.0767
-0.3187	0.0183	0.1555	0.2110	0.1148	0.1474
-0.3000	-0.0314	0.1672	0.3043	0.1319	-0.0579
-0.2812	0.0644	0.1806	0.1972	0.1318	0.2098
-0.2625	-0.0095	0.1764	0.2809	0.1233	0.2008
-0.2437	0.0166	0.1503	0.2295	0.1118	0.2196
-0.2250	0.0188	0.1671	0.2280	0.1395	0.1244
-0.2062	-0.0026	0.1158	0.1917	0.0960	0.1043
-0.1875	0.0108	0.1561	0.2787	0.1351	0.0749
-0.1687	-0.0457	0.1593	0.2573	0.1637	0.0265
-0.1500	-0.0119	0.1366	0.2554	0.1187	0.1348
-0.1312	-0.0178	0.1449	0.1982	0.1360	0.0566
-0.1125	-0.0133	0.1578	0.2296	0.1337	0.0237
-0.0937	0.0602	0.1754	0.2680	0.1132	0.1476
-0.0750	0.0219	0.1741	0.2761	0.1188	0.2534
-0.0562	0.0546	0.1770	0.1986	0.1125	0.0701
-0.0375	0.0317	0.1508	0.2383	0.1498	0.1657
-0.0187	0.0214	0.2075	0.2716	0.1228	0.1441
0.0000	-0.0233	0.1764	0.3463	0.1269	0.2209
0.0187	0.0256	0.1599	0.2811	0.1393	0.1147
0.0375	0.0378	0.1560	0.2225	0.1454	0.1850
0.0562	0.0124	0.1646	0.2693	0.1457	-0.0907
0.0750	-0.0079	0.1581	0.3033	0.1503	0.1403
0.0937	-0.0224	0.1621	0.3634	0.1309	-0.0553
0.1125	0.0093	0.1771	0.3324	0.1529	0.2250
0.1312	0.0146	0.1689	0.2646	0.1150	0.0303
0.1500	-0.0261	0.1696	0.2614	0.1337	0.1318
0.1687	-0.0110	0.1483	0.2621	0.1079	0.0116
0.1875	-0.0060	0.1793	0.2671	0.1367	0.0843
0.2062	0.0099	0.1467	0.1938	0.1431	0.0786
0.2250	-0.0075	0.1189	0.1977	0.1167	-0.1357
0.2437	-0.0028	0.1711	0.2835	0.1145	0.0484
0.2625	0.0119	0.1646	0.3029	0.1227	0.1545
0.2812	0.0144	0.1452	0.1920	0.1083	0.0676
0.3000	0.0182	0.1616	0.2187	0.1216	0.1903
0.3187	0.0157	0.1524	0.2654	0.1531	0.2442
0.3375	0.0160	0.1460	0.3018	0.1330	0.2533

Weighted

a/b=1.0, α=0 , Free Convection (Re=0)

Tbot=400.8 ± 5.7 (C), Tbac=403.4 ± 4.5 (C)

Ttop=336.8 ± 4.0 (C), T_∞ =26 (C)

$\Delta T/T_\infty$ =1.184 , Gr=4.15 E7 , N = 1000

x/b=0.25, y/a=0.0

z/(c/2)	W	U	$\overline{w}^2$ x10	$\overline{u}'^2$ x10	$\overline{u'w'}$x100
0.3375	-0.0031	0.0525	0.0909	0.0600	-0.0474
0.3187	-0.0111	0.0387	0.0765	0.0537	0.0128
0.3000	0.0219	0.1494	0.1506	0.1337	0.0927
0.2812	0.0043	0.0771	0.0817	0.0643	0.0648
0.2625	-0.0024	0.0853	0.1253	0.0872	0.1406
0.2437	0.0095	0.0572	0.0800	0.0635	0.0693
0.2250	0.0258	0.1085	0.1118	0.0858	0.0555
0.2062	0.0137	0.0686	0.0830	0.1039	0.1197
0.1875	0.0011	0.0419	0.0831	0.0755	0.0146
0.1687	0.0122	0.1066	0.1052	0.0809	0.0421
0.1500	0.0252	0.0984	0.0915	0.0772	0.0311
0.1312	0.0250	0.1857	0.1794	0.1511	0.3831
0.1125	0.0079	0.0567	0.0768	0.0581	0.0240
0.0937	0.0081	0.0752	0.0820	0.0832	0.1304
0.0750	0.0199	0.0836	0.0897	0.0656	0.0876
0.0562	-0.0090	0.0289	0.0520	0.0502	0.0169
0.0375	0.0292	0.0969	0.0899	0.0884	0.1583
0.0187	-0.0012	0.0654	0.0718	0.0736	0.0104
0.0000	0.0146	0.0776	0.0933	0.0647	0.1436
-0.0187	0.0242	0.1057	0.1290	0.0776	0.1921
-0.0375	0.0050	0.0706	0.0926	0.1020	0.0680
-0.0562	0.0126	0.0693	0.0877	0.1041	-0.0003
-0.0750	0.0218	0.1106	0.1093	0.0914	0.0530
-0.0937	0.0044	0.0558	0.0616	0.0617	-0.0153
-0.1125	-0.0047	0.0750	0.0886	0.0534	0.0560
-0.1312	0.0112	0.0629	0.0648	0.0721	0.0535
-0.1500	-0.0059	0.0443	0.0590	0.0618	0.0392
-0.1687	0.0074	0.0689	0.0815	0.1013	0.1256
-0.1875	0.0060	0.0627	0.0709	0.0469	0.0741
-0.2062	0.0073	0.1004	0.0997	0.0970	0.1099
-0.2250	0.0048	0.0975	0.1009	0.0723	0.0749
-0.2437	-0.0019	0.0307	0.0607	0.0649	0.0421
-0.2625	-0.0092	0.0640	0.0967	0.0728	-0.0011
-0.2812	0.0006	0.0564	0.0709	0.0717	-0.0323
-0.3000	-0.0041	0.0936	0.1160	0.1128	-0.0543
-0.3187	0.0001	0.0549	0.0763	0.0659	0.0100
-0.3375	0.0082	0.0763	0.0854	0.0868	0.1173

Weighted

a/b=1.0, α=0 , Free Convection (Re=0)

Tbot=400.8 ± 5.7 (C), Tbac=403.4 ± 4.5 (C)

Ttop=336.8 ± 4.0 (C), T_∞ =26 (C)

$\Delta T/T_\infty$ =1.184 , Gr=4.15 E7 , N = 1000

x/b=0.10, y/a=0.0

z/(c/2)	W	U	$\overline{w'^2}$ x10	$\overline{u'^2}$ x10	$\overline{u'w'}$ x100
-0.3375	0.0081	0.2866	0.2293	0.1180	0.1015
-0.3187	0.0021	0.2307	0.1748	0.1278	0.1536
-0.3000	-0.0043	0.2778	0.2319	0.1164	0.1456
-0.2812	-0.0036	0.2758	0.2315	0.0945	0.0454
-0.2625	0.0084	0.2705	0.2319	0.1337	0.2316
-0.2437	0.0437	0.3210	0.2469	0.1532	0.0512
-0.2250	0.0221	0.2393	0.1822	0.1324	0.0525
-0.2062	0.0067	0.3341	0.3388	0.1106	0.1022
-0.1875	0.0219	0.1914	0.1281	0.0981	0.1141
-0.1687	0.0071	0.2962	0.1908	0.0898	0.0163
-0.1500	0.0127	0.2242	0.1726	0.1777	0.2008
-0.1312	0.0278	0.2960	0.1852	0.1165	0.0643
-0.1125	0.0395	0.2805	0.1998	0.1455	0.1850
-0.0937	0.0203	0.2450	0.1206	0.1158	0.0824
-0.0750	0.0201	0.2620	0.2069	0.1124	0.0932
-0.0562	0.0026	0.2221	0.2299	0.1311	0.2348
-0.0375	0.0378	0.2831	0.2127	0.1194	0.0136
-0.0187	0.0096	0.2217	0.2050	0.1474	0.2390
0.0000	0.0179	0.2891	0.2168	0.1012	0.0214
0.0187	0.0233	0.2592	0.2277	0.1068	0.0614
0.0375	0.0245	0.1923	0.1520	0.1283	0.1181
0.0562	-0.0073	0.2792	0.2290	0.0980	0.1224
0.0750	0.0381	0.3132	0.2315	0.1517	0.0975
0.0937	0.0110	0.1842	0.1365	0.0750	0.0606
0.1125	0.0307	0.2896	0.2395	0.1481	0.1282
0.1312	0.0407	0.3399	0.2787	0.1475	-0.0253
0.1500	0.0518	0.3013	0.2291	0.1142	0.0023
0.1687	0.0641	0.2441	0.1653	0.0839	-0.0266
0.1875	0.0374	0.3358	0.2919	0.1961	0.2672
0.2062	0.0548	0.2319	0.1899	0.1333	0.1688
0.2250	0.0125	0.3126	0.2207	0.1136	0.1177
0.2437	0.0272	0.2008	0.1522	0.1230	-0.0492
0.2625	0.0459	0.2418	0.2231	0.1350	0.0937
0.2812	0.0498	0.2497	0.2473	0.1397	-0.0710
0.3000	0.0389	0.2717	0.2004	0.0954	0.0165
0.3187	0.0546	0.2949	0.2629	0.1511	0.0932
0.3375	0.0285	0.2404	0.2025	0.1101	0.1383

Unweighted

a/b=1.0, α=0 , Free Convection (Re=0)

Tbot=400.8 ± 5.1 (C), Tbac=399.6 ± 5.0 (C)

Ttop=338.4 ± 3.3 (C), T_∞ =25 (C)

$\Delta T/T_\infty$ =1.19 , Gr=4.14 E7 , N = 1000

y/a=0.0, z/c=0.0

x/b	V	U	$\overline{v'^2}\times10$	$\overline{u'^2}\times10$	$\overline{u'v'}\times100$	W	$\overline{w'^2}\times10$
0.9789	0.4984	0.2850	0.6627	0.0818	0.1409	0.1090	0.526
0.9472	0.3632	0.2530	0.6302	0.1069	0.1854	0.1080	0.538
0.9155	0.2763	0.2117	0.6340	0.1205	0.1146	0.0911	0.480
0.8838	0.2619	0.1939	0.4537	0.1781	0.2961	0.0850	0.448
0.8521	0.2486	0.1716	0.4518	0.1924	0.1453	0.0793	0.371
0.8204	0.2172	0.1631	0.3930	0.3556	0.0576	0.0729	0.295
0.7887	0.1593	0.1397	0.4101	0.2762	0.1319	0.0774	0.349
0.7570	0.1207	0.1175	0.4009	0.2434	0.4061	0.0871	0.450
0.7253	0.0937	0.1215	0.3995	0.2805	0.2152	0.0803	0.392
0.6936	0.0879	0.1127	0.3724	0.2641	0.1135	0.0670	0.302
0.6619	0.0545	0.1075	0.3570	0.2972	0.0151	0.0550	0.265
0.6303	0.0413	0.0828	0.3487	0.2366	0.1370	0.0546	0.327
0.5986	0.0215	0.0884	0.3513	0.2239	0.1788	0.0510	0.290
0.5669	0.0033	0.0759	0.2600	0.2175	0.1995	0.0509	0.348
0.5352	-0.0146	0.0732	0.3403	0.2460	0.1324	0.0806	0.381
0.5035	-0.0246	0.0719	0.3456	0.2495	0.0211	0.0428	0.336
0.4718	-0.0366	0.0764	0.2735	0.2461	0.1314	0.0675	0.406
0.4401	-0.0542	0.1022	0.2756	0.2524	0.0768	0.0356	0.278
0.4084	-0.0403	0.0891	0.3089	0.1766	0.1195	0.0664	0.359
0.3767	-0.0684	0.0965	0.2829	0.1885	0.1303	0.0577	0.331
0.3450	-0.0644	0.1097	0.2738	0.2515	-0.0564	0.0620	0.273
0.3133	-0.0750	0.1169	0.3691	0.2415	0.1203	0.0605	0.322
0.2816	-0.0876	0.1135	0.3317	0.1838	0.0822	0.0734	0.319
0.2499	-0.0975	0.1202	0.3279	0.2023	0.1506	0.0575	0.282
0.2183	-0.0988	0.1347	0.3362	0.1955	-0.0802	0.0650	0.343
0.1866	-0.1193	0.1777	0.4203	0.3395	-0.1107	0.0597	0.302
0.1549	-0.1424	0.1936	0.4445	0.2096	-0.2729	0.0503	0.369
0.1232	-0.1410	0.2393	0.8018	0.1391	-0.1696	0.0846	0.390
0.0914	-0.1765	0.3090	0.9734	0.1353	-0.1968	0.0614	0.359
0.0634	-0.1080	0.3700	2.1600	0.4340	0.0158	0.1150	0.532
0.0528	-0.0434	0.4500	2.5000	0.3810	0.1920		
0.0317	0.0819	0.4290	2.5200	0.3720	-0.3970	0.1430	0.633
0.0211	0.2810	0.3980	2.8600	0.2660	-0.1240		

Unweighted

a/b=1.0, α=0 , Free Convection (Re=0)

Tbot=400.8 ±5.1 (C), Tbac=399.6 ± 5.0 (C)

Ttop=338.4 ±3.3 (C), T_∞ =25 (C)

$\Delta T/T_\infty$ =1.19 , Gr=4.14 E7 , N = 1000

y/a=0.5, z/c=0.0

x/b	V	U	$\overline{v'^2}$ x10	$\overline{u'^2}$ x10	$\overline{u'v'}$ x100	W	$\overline{w'^2}$ x10
0.0000	-0.0019	0.1143	0.1998	0.0764	0.0587	0.0672	0.430
0.0423	-0.0132	0.1134	0.1526	0.0374	0.0547	0.0621	0.263
0.0845	-0.0186	0.0904	0.1848	0.0397	0.0595	0.0631	0.216
0.1268	-0.0286	0.0979	0.1146	0.0296	-0.0074	0.0630	0.228
0.1690	-0.0121	0.0955	0.1745	0.0288	0.0479	0.0401	0.195
0.2113	-0.0140	0.1046	0.1466	0.0287	0.0073	0.0518	0.198
0.2535	-0.0197	0.0927	0.1363	0.0208	-0.0012	0.0359	0.187
0.2958	-0.0070	0.0878	0.1906	0.0271	0.0175	0.0560	0.217
0.3381	-0.0276	0.0929	0.1112	0.0297	0.0412	0.0532	0.208
0.3803	-0.0174	0.1012	0.1233	0.0365	0.0609	0.0473	0.187
0.4226	-0.0273	0.0854	0.1129	0.0282	0.0360	0.0565	0.234
0.4648	-0.0182	0.0587	0.1406	0.0219	0.0262	0.0504	0.205
0.5071	-0.0248	0.0787	0.1216	0.0369	-0.0093	0.0548	0.222
0.5493	-0.0187	0.0702	0.1262	0.0288	-0.0277	0.0367	0.257
0.5916	-0.0152	0.0700	0.1540	0.0205	0.0695	0.0521	0.226
0.6338	-0.0250	0.0688	0.0999	0.0231	-0.0221	0.0526	0.169
0.6761	-0.0200	0.0761	0.0820	0.0206	0.0095	0.0553	0.183
0.7184	-0.0147	0.0865	0.1326	0.0280	0.0459	0.0564	0.237
0.7606	-0.0152	0.0875	0.1143	0.0480	0.0110	0.0503	0.181
0.8029	-0.0085	0.0799	0.1267	0.0392	0.0738	0.0493	0.232
0.8451	-0.0082	0.0872	0.1605	0.1380	-0.0178	0.0483	0.205
0.8874	-0.0169	0.0889	0.1095	0.0227	0.0038	0.0454	0.207
0.9296	-0.0106	0.0794	0.1262	0.0203	-0.0078	0.0586	0.246
0.9718	-0.0146	0.1003	0.1124	0.0327	0.0745	0.0661	0.210
0.9999	0.0099	0.1120	0.3434	0.1283	0.2841	0.0379	0.195

Unweighted

a/b=1.0, α=0 , Free Convection (Re=0)

Tbot=400.8 ± 5.1 (C), Tbac=399.6 ± 5.0 (C)

Ttop=338.4 ±3.3 (C), T_∞ =25 (C)

$\Delta T/T_\infty$ =1.19 , Gr=4.14 E7 , N = 1000

x/b=1.0, $z/\frac{c}{2}$=0.0

y/a	V	U	$\overline{v}^2$ x10	$\overline{u}'^2$ x10	$\overline{u'v'}$x100	W	$\overline{w}'^2$ x10
0.5000	0.0099	0.1120	0.3434	0.1283	0.2841	0.0379	0.195
0.4648	0.0037	0.1434	0.2957	0.0679	0.2127	0.0487	0.222
0.4437	0.0212	0.1419	0.3667	0.1124	0.3817	0.0513	0.210
0.4226	0.0108	0.1262	0.2505	0.1961	0.5091	0.0473	0.274
0.4016	0.0170	0.1348	0.2914	0.1504	0.6541	0.0609	0.252
0.3805	0.0141	0.1304	0.2315	0.0902	0.6262	0.0661	0.256
0.3594	0.0781	0.2058	0.3297	0.1906	1.3146	0.0569	0.214
0.3383	0.0507	0.1838	0.4084	0.1842	1.2775	0.0616	0.247
0.3172	0.0796	0.2349	0.3021	0.1796	0.9418	0.0607	0.259
0.2961	0.1175	0.2471	0.3944	0.1574	1.0992	0.0747	0.295
0.2750	0.1841	0.3105	0.4581	0.1638	1.3210	0.0661	0.311
0.2539	0.1221	0.2699	0.4136	0.1703	1.2973	0.0609	0.297
0.2328	0.1769	0.3144	0.5135	0.1711	1.3474	0.0778	0.383
0.2118	0.1976	0.3544	0.3891	0.1682	1.1727	0.0839	0.301
0.1907	0.1796	0.3196	0.4301	0.1656	1.2167	0.0887	0.357
0.1696	0.2432	0.3907	0.4050	0.1184	0.8949	0.0850	0.395
0.1485	0.2519	0.3864	0.4593	0.1237	1.0891	0.0786	0.483
0.1274	0.2651	0.4054	0.5479	0.1048	0.8378	0.0977	0.429
0.1063	0.3019	0.4275	0.4782	0.1090	0.8142	0.0736	0.571
0.0852	0.3515	0.4566	0.6800	0.0886	0.6642	0.1310	0.584
0.0641	0.4074	0.4797	0.7578	0.0845	0.5438	0.1160	0.655
0.0431	0.4512	0.4943	0.6634	0.0598	0.4116	0.1280	0.804
0.0220	0.4702	0.4841	1.0327	0.0541	0.2077	0.1350	0.918

Unweighted

a/b=1.0, α =0 , Free Convection (Re=0)

Tbot=400.8 ± 5.1 (C), Tbac=399.6 ± 5.0 (C)

Ttop=338.4 ± 3.3 (C), T_∞ =25 (C)

$\Delta T/T_\infty$ =1.19 , Gr=4.14 E7 , N = 1000

x/b=0.0, $z/\frac{c}{2}$=0.0

y/a	V	U	$\overline{v'^2}$ x10	$\overline{u'^2}$ x10	$\overline{u'v'}$ x100	W	$\overline{w'^2}$ x10
0.0211	0.1231	0.6047	1.6143	0.1103	0.0167	0.157	0.866
0.0422	-0.0806	0.4295	0.4333	0.0539	0.0003	0.108	0.579
0.0633	-0.0599	0.3310	0.3313	0.0428	-0.0707	0.0585	0.464
0.0844	-0.0359	0.2624	0.3553	0.0624	-0.0116	0.0646	0.485
0.1055	-0.0318	0.2121	0.2400	0.0356	-0.0414	0.0321	0.327
0.1266	-0.0377	0.2233	0.2493	0.0537	0.0433	0.0417	0.398
0.1477	-0.0163	0.1526	0.2324	0.0542	0.0753	0.0489	0.350
0.1687	-0.0279	0.1634	0.2021	0.0484	-0.0066	0.0571	0.457
0.1898	-0.0249	0.1978	0.2286	0.0418	0.0605	0.0583	0.471
0.2109	-0.0228	0.1453	0.2268	0.0459	-0.0014	0.0608	0.488
0.2320	-0.0164	0.1581	0.1945	0.0460	-0.0107	0.0826	0.622
0.2531	-0.0098	0.1462	0.1873	0.0380	-0.0076	0.0807	0.577
0.2742	-0.0111	0.1352	0.2113	0.0508	-0.0015	0.0756	0.479
0.2953	-0.0136	0.1452	0.2246	0.0493	0.0504	0.0686	0.469
0.3164	-0.0126	0.1117	0.1691	0.0396	0.0130	0.0633	0.452
0.3375	-0.0072	0.1648	0.2240	0.0427	-0.0062	0.0640	0.478
0.3585	-0.0024	0.1127	0.1830	0.1608	0.0452	0.0515	0.359
0.3796	-0.0024	0.1042	0.1988	0.0407	0.0604	0.0766	0.434
0.4007	-0.0140	0.1140	0.1544	0.0625	0.0568	0.0536	0.432
0.4218	-0.0064	0.1162	0.1768	0.0345	0.0073	0.0789	0.354
0.4429	-0.0194	0.0905	0.1454	0.0594	-0.0057	0.0634	0.382
0.4640	-0.0036	0.0964	0.1850	0.0252	0.0530	0.0528	0.330
0.5000	-0.0019	0.1143	0.1998	0.0764	0.0587	0.0672	0.430

Unweighted

a/b=1.0, α=0 , Free Convection (Re=0)

Tbot=400.8 ± 5.7 (C), Tbac=403.4 ± 4.5 (C)

Ttop=336.8 ± 4.0 (C), T_∞ =26 (C)

$\Delta T/T_\infty$ =1.184 , Gr=4.15 E7 , N = 1000

x/b=0.95, y/a=0.0

z/(c/2)	W	U	$\overline{w}^2$ x10	$\overline{u}^2$ x10	$\overline{u'w'}$x100
0.3375	0.0436	0.2280	0.5002	0.1523	0.2844
0.3187	0.0425	0.2417	0.5734	0.1807	0.1093
0.3000	0.0168	0.2384	0.7072	0.1931	0.3585
0.2812	0.0683	0.2323	0.5991	0.1642	0.1138
0.2625	0.0542	0.2256	0.6139	0.1972	0.1510
0.2437	0.0244	0.2209	0.5979	0.1231	0.1158
0.2250	0.0594	0.2341	0.5484	0.2023	0.2275
0.2062	0.0129	0.2264	0.6920	0.1434	0.0347
0.1875	0.0621	0.2385	0.5587	0.1533	-0.0439
0.1687	0.0377	0.2520	0.5844	0.1325	0.0122
0.1500	0.0218	0.2466	0.5592	0.1508	0.1561
0.1312	0.0694	0.2356	0.5961	0.1436	0.1866
0.1125	0.0447	0.2489	0.4596	0.1305	-0.0387
0.0937	0.0151	0.2430	0.7144	0.1747	0.7623
0.0750	0.0585	0.2359	0.6685	0.1632	-0.0307
0.0562	0.0444	0.2563	0.4913	0.1477	0.2623
0.0375	-0.0077	0.2226	0.7674	0.2022	0.7664
0.0187	0.0656	0.2381	0.5596	0.1282	0.1668
0.0000	0.0082	0.2404	0.5918	0.1873	0.0619
-0.0187	0.0322	0.2531	0.5271	0.1887	0.1461
-0.0375	0.1040	0.2464	0.5460	0.1564	0.2774
-0.0562	0.0913	0.2367	0.5883	0.1580	-0.0104
-0.0750	0.1511	0.2568	0.4019	0.1435	-0.1014
-0.0937	0.1292	0.2599	0.5606	0.1509	0.2456
-0.1125	0.0786	0.2622	0.4610	0.1496	0.0560
-0.1312	0.1095	0.2433	0.5882	0.1636	0.1559
-0.1500	0.0708	0.2464	0.4820	0.1637	0.0073
-0.1687	0.0656	0.2569	0.5330	0.1623	0.1818
-0.1875	0.0499	0.2423	0.5224	0.1624	0.1850
-0.2062	-0.0136	0.2414	0.7448	0.1864	0.2986
-0.2250	0.0654	0.2462	0.6472	0.1515	0.2210
-0.2437	0.0910	0.2411	0.4769	0.1554	0.0028
-0.2625	0.1259	0.2508	0.4810	0.1876	-0.0089
-0.2812	0.0072	0.2536	0.6413	0.1543	0.2293
-0.3000	0.0694	0.2743	0.5249	0.1689	0.0407
-0.3187	0.0366	0.2430	0.6000	0.2022	0.2634
-0.3375	0.0290	0.2583	0.5602	0.1826	0.0981

Unweighted

a/b=1.0, α=0 , Free Convection (Re=0)

Tbot=400.8 ± 5.7 (C), Tbac=403.4 ± 4.5 (C)

Ttop=336.8 ± 4.0 (C), T_∞ =26 (C)

$\Delta T/T_\infty$ =1.184 , Gr=4.15 E7 , N = 1000

x/b=0.90, y/a=0.0

z/(c/2)	W	U	$\overline{w}^2$ x10	$\overline{u'}^2$ x10	$\overline{u'w'}$ x100
-0.3375	0.1254	0.2125	0.4991	0.1881	-0.1914
-0.3187	0.0455	0.2111	0.4353	0.1945	0.1785
-0.3000	-0.0320	0.2118	0.5569	0.2117	-0.0120
-0.2812	0.1043	0.2354	0.3768	0.2156	0.1611
-0.2625	0.0096	0.2231	0.4947	0.1786	0.3380
-0.2437	0.0517	0.1992	0.4479	0.2037	0.2033
-0.2250	0.0481	0.2317	0.4609	0.2186	0.0344
-0.2062	0.0127	0.1678	0.4605	0.2114	0.1937
-0.1875	0.0334	0.2158	0.5730	0.2532	-0.0265
-0.1687	-0.0557	0.2204	0.4641	0.2682	0.3239
-0.1500	0.0010	0.1890	0.5259	0.2223	0.0778
-0.1312	-0.0058	0.2121	0.4095	0.2175	0.0939
-0.1125	-0.0000	0.2182	0.4628	0.1943	-0.0059
-0.0937	0.1052	0.2165	0.4526	0.1865	0.2557
-0.0750	0.0529	0.2219	0.5074	0.1770	0.3182
-0.0562	0.0871	0.2212	0.3712	0.1676	-0.0923
-0.0375	0.0585	0.2134	0.4584	0.2229	0.1827
-0.0187	0.0466	0.2490	0.4329	0.1997	0.1322
0.0000	-0.0147	0.2183	0.5799	0.2029	0.3931
0.0187	0.0513	0.2158	0.4926	0.2084	0.1068
0.0375	0.0759	0.2271	0.4580	0.2241	0.0219
0.0562	0.0207	0.2255	0.5390	0.2233	-0.1419
0.0750	0.0122	0.2179	0.6084	0.2343	0.0894
0.0937	-0.0183	0.2115	0.5986	0.1813	0.0109
0.1125	0.0279	0.2269	0.5527	0.2069	0.3344
0.1312	0.0504	0.2131	0.4820	0.2042	-0.1220
0.1500	-0.0128	0.2266	0.5054	0.2329	0.1981
0.1687	-0.0043	0.1945	0.5123	0.1975	0.1174
0.1875	0.0145	0.2286	0.4735	0.2045	0.2231
0.2062	0.0296	0.2146	0.3809	0.2652	0.0245
0.2250	-0.0048	0.1869	0.4800	0.2330	-0.2347
0.2437	0.0167	0.2170	0.5126	0.1844	0.0209
0.2625	0.0360	0.2083	0.5099	0.2139	0.0494
0.2812	0.0376	0.1981	0.3846	0.2246	0.1294
0.3000	0.0486	0.2123	0.3907	0.2082	0.2440
0.3187	0.0413	0.2087	0.5252	0.2373	0.2219
0.3375	0.0358	0.1935	0.5303	0.2074	0.3048

Unweighted

a/b=1.0, α=0 , Free Convection (Re=0)

Tbot=400.8 ± 5.7 (C), Tbac=403.4 ± 4.5 (C)

Ttop=336.8 ± 4.0 (C), T_∞ =26 (C)

$\Delta T/T_\infty$ =1.184 , Gr=4.15 E7 , N = 1000

x/b=0.25, y/a=0.0

z/(c/2)	W	U	$\overline{w}^2$ x10	$\overline{u'}^2$ x10	$\overline{u'w'}$ x100
0.3375	0.0182	0.1187	0.4420	0.2214	-0.2756
0.3187	0.0176	0.1003	0.3800	0.2594	-0.0444
0.3000	0.0556	0.2247	0.3881	0.2396	-0.1072
0.2812	0.0361	0.1366	0.3599	0.2586	0.2414
0.2625	0.0433	0.1531	0.4299	0.2143	0.0804
0.2437	0.0393	0.1158	0.3428	0.2220	0.1659
0.2250	0.0578	0.1699	0.3398	0.1979	0.0675
0.2062	0.0584	0.1653	0.3800	0.3016	-0.0815
0.1875	0.0325	0.1170	0.3732	0.2547	-0.1973
0.1687	0.0413	0.1578	0.3003	0.2232	0.0036
0.1500	0.0535	0.1586	0.3101	0.2476	0.0147
0.1312	0.0603	0.2536	0.3865	0.2147	0.4376
0.1125	0.0369	0.1219	0.3408	0.1987	0.0535
0.0937	0.0520	0.1477	0.3050	0.2263	0.0820
0.0750	0.0576	0.1424	0.3218	0.2037	0.0736
0.0562	0.0135	0.0984	0.3051	0.2841	0.0270
0.0375	0.0715	0.1655	0.2715	0.2418	-0.0196
0.0187	0.0240	0.1458	0.3676	0.2589	-0.0388
0.0000	0.0663	0.1393	0.3559	0.2157	0.2271
-0.0187	0.0745	0.1605	0.3967	0.2112	0.2501
-0.0375	0.0441	0.1720	0.4602	0.2978	0.0215
-0.0562	0.0446	0.1657	0.3707	0.2465	-0.1398
-0.0750	0.0609	0.1777	0.3792	0.1997	0.0126
-0.0937	0.0340	0.1295	0.3101	0.2460	-0.0851
-0.1125	0.0361	0.1266	0.3444	0.1966	0.0911
-0.1312	0.0433	0.1334	0.2261	0.1929	-0.0144
-0.1500	0.0253	0.1247	0.3354	0.2405	0.1831
-0.1687	0.0546	0.1699	0.3445	0.4371	0.1152
-0.1875	0.0461	0.1137	0.3175	0.1893	0.1176
-0.2062	0.0387	0.1710	0.3108	0.2478	0.0863
-0.2250	0.0383	0.1547	0.3183	0.1887	0.0464
-0.2437	0.0368	0.1118	0.3665	0.2994	0.1185
-0.2625	0.0141	0.1312	0.3991	0.2291	-0.0585
-0.2812	0.0288	0.1401	0.3475	0.2506	-0.1386
-0.3000	0.0225	0.1809	0.4278	0.2737	-0.2980
-0.3187	0.0323	0.1264	0.3569	0.2636	-0.0331
-0.3375	0.0554	0.1523	0.3148	0.2692	0.0136

Unweighted

a/b=1.0, α=0 , Free Convection (Re=0)

Tbot=400.8 ± 5.7 (C), Tbac=403.4 ± 4.5 (C)

Ttop=336.8 ± 4.0 (C), T_∞ =26 (C)

$\Delta T/T_\infty$ =1.184 , Gr=4.15 E7 , N = 1000

x/b=0.10, y/a=0.0

z/(c/2)	W	U	$\overline{w}^2$ x10	$\overline{u}^2$ x10	$\overline{u'w'}$x100
-0.3375	0.0305	0.3222	0.3646	0.1458	0.0653
-0.3187	0.0280	0.2782	0.3481	0.1760	0.1330
-0.3000	0.0197	0.3110	0.3865	0.1488	0.0848
-0.2812	0.0156	0.3059	0.3870	0.1152	-0.0061
-0.2625	0.0367	0.3134	0.4416	0.1809	0.2641
-0.2437	0.0711	0.3634	0.4213	0.1688	0.0367
-0.2250	0.0478	0.2873	0.3325	0.1819	-0.0755
-0.2062	0.0329	0.3596	0.5537	0.1318	0.0531
-0.1875	0.0514	0.2382	0.2921	0.1771	0.1155
-0.1687	0.0222	0.3226	0.3023	0.1149	-0.0276
-0.1500	0.0389	0.2905	0.3253	0.2450	0.2080
-0.1312	0.0511	0.3320	0.3086	0.1280	-0.0223
-0.1125	0.0670	0.3283	0.3706	0.1612	0.2242
-0.0937	0.0339	0.2891	0.2326	0.1601	0.0873
-0.0750	0.0453	0.2986	0.3775	0.1652	0.0655
-0.0562	0.0344	0.2718	0.4450	0.2193	0.2523
-0.0375	0.0627	0.3194	0.3624	0.1519	-0.0157
-0.0187	0.0464	0.2817	0.4294	0.2056	0.2487
0.0000	0.0367	0.3202	0.3621	0.1303	-0.0523
0.0187	0.0433	0.2931	0.4062	0.1394	0.0551
0.0375	0.0536	0.2519	0.3522	0.1985	0.1346
0.0562	0.0113	0.3071	0.3861	0.1254	0.1062
0.0750	0.0617	0.3576	0.4093	0.1384	0.1749
0.0937	0.0352	0.2189	0.2849	0.1326	0.0572
0.1125	0.0580	0.3343	0.4104	0.1601	0.0328
0.1312	0.0573	0.3751	0.4553	0.1480	-0.0384
0.1500	0.0684	0.3351	0.4101	0.1437	-0.0323
0.1687	0.0885	0.2741	0.3052	0.1161	-0.0371
0.1875	0.0690	0.3902	0.4900	0.1793	0.1664
0.2062	0.0883	0.2808	0.3812	0.1734	0.1417
0.2250	0.0352	0.3439	0.3577	0.1209	0.1067
0.2437	0.0460	0.2547	0.3135	0.2136	-0.1306
0.2625	0.0751	0.2923	0.4338	0.1795	0.0041
0.2812	0.0747	0.2964	0.5172	0.1590	-0.2305
0.3000	0.0611	0.3016	0.3826	0.1347	-0.0120
0.3187	0.0801	0.3358	0.4538	0.1717	0.2026
0.3375	0.0530	0.2777	0.3334	0.1410	-0.0008

Unweighted

a/b=1.0, α=0 , Free Convection (Re=0)

Tbot=398.2 ±5.2 (C), Tbac=402.9 ± 2.2 (C)

Ttop=339.1 ±1.9 (C), T_∞ =26 (C)

$\Delta T/T_\infty$ =1.184 , Gr=4.1 E7 , N = 500

y/a=-0.5, z/$\frac{c}{2}$=0.0

x/b	V	$\overline{v^2}$ x10
0.0211	0.1167	0.3313
0.0317	0.1259	0.3972
0.0423	0.0728	0.3951
0.0528	0.0557	0.3702
0.0634	0.0313	0.3864
0.0845	-0.0126	0.4097
0.1056	-0.0604	0.4490
0.1373	-0.1123	0.4344
0.1690	-0.2087	0.3271
0.2007	-0.1894	0.3250
0.2324	-0.2066	0.2978
0.2641	-0.2057	0.3453
0.2958	-0.2057	0.2983
0.3275	-0.1786	0.2445
0.3592	-0.1531	0.2643
0.3909	-0.1709	0.2243
0.4226	-0.1487	0.1802
0.4543	-0.1270	0.3576
0.4859	-0.1017	0.2708
0.5176	-0.0495	0.3312
0.5493	-0.0593	0.3434
0.5810	-0.0287	0.2658
0.6127	0.0086	0.3211
0.6444	0.0276	0.2825
0.6761	0.0766	0.3035
0.7078	0.1371	0.4094
0.7395	0.1363	0.3511
0.7712	0.1847	0.3176
0.8029	0.2221	0.3430
0.8346	0.2541	0.3059
0.8451	0.2183	0.2319

Unweighted

a/b=1.0, α=0 , Free Convection (Re=0)

Tbot=398.2 ±5.2 (C), Tbac=402.9 ± 2.2 (C)

Ttop=339.1 ±1.9 (C), T_∞ =26 (C)

$\Delta T/T_\infty$ =1.184 , Gr=4.1 E7 , N = 500

x/b=0.5, z/c=0.0

y/a	$\overline{U}^2$	$\overline{u'^2}\times10$
-0.9577	0.3331	0.0863
-0.9472	0.3454	0.1242
-0.9366	0.3111	0.1370
-0.9261	0.2925	0.1774
-0.9155	0.2403	0.1743
-0.9049	0.2275	0.1806
-0.8944	0.2164	0.1917
-0.8838	0.1982	0.2384
-0.8732	0.2100	0.2561
-0.8627	0.1920	0.2189
-0.8310	0.1793	0.2595
-0.7993	0.1729	0.2501
-0.7676	0.1526	0.2589
-0.7359	0.1394	0.2749
-0.7042	0.1392	0.2879
-0.6725	0.1325	0.2663
-0.6408	0.0939	0.2418
-0.6091	0.0975	0.2408
-0.5774	0.0777	0.2340
-0.5457	0.0809	0.2069
-0.5141	0.0610	0.1947
-0.4824	0.0541	0.1717
-0.4507	0.0392	0.1742
-0.4190	0.0558	0.2226
-0.3873	0.0275	0.1434
-0.3556	0.0302	0.1537
-0.3239	0.0406	0.1742
-0.2922	0.0477	0.2187
-0.2605	0.0421	0.1863
-0.2288	0.0821	0.2594
-0.1971	0.0558	0.1803
-0.1654	0.0591	0.1369
-0.1337	0.0679	0.1782
-0.1020	0.0384	0.0751
-0.0704	0.0582	0.1382
-0.0387	0.0920	0.1301
-0.0232	0.0952	0.1202

Weighted

a/b=1.0, α =45 , Free Convection (Re=0)

Tbot=397.8 ± 6.6 (C), Tbac=401.1 ± 5.0 (C)

Ttop=337.7 ± 4.1 (C), T_∞ =24 (C)

$\Delta T/T_\infty$ =1.19 , Gr=4.2 E7 , N = 1000

y/a=0.0, z/c=0.0

x/b	V	U	$\overline{v}^2$ x10	$\overline{u'^2}$ x10	$\overline{u'v'}$ x100	W	$\overline{w}^2$ x10
0.9789	0.3560	0.2500	0.1470	0.0246	-0.0455	-0.0302	0.0448
0.9683	0.3017	0.2305	0.0692	0.0262	0.0136		
0.9472	0.2613	0.2244	0.0498	0.0333	0.0295	-0.0203	0.0544
0.9155	0.2284	0.2155	0.0518	0.0397	0.0174	-0.0147	0.0669
0.8838	0.2001	0.2009	0.0524	0.0396	0.0317	-0.0096	0.0763
0.8522	0.1651	0.1810	0.0679	0.0475	0.0378	-0.0025	0.0657
0.8205	0.1437	0.1639	0.0660	0.0461	0.0507	-0.0005	0.0731
0.7888	0.1234	0.1371	0.0661	0.0269	0.0638	0.0027	0.0699
0.7571	0.1178	0.1284	0.0815	0.0279	0.0650	0.0059	0.0732
0.7254	0.0951	0.1112	0.0647	0.0319	0.0588	0.0014	0.0847
0.6938	0.0811	0.1030	0.0638	0.0318	0.0514	0.0032	0.0819
0.6621	0.0774	0.0987	0.0991	0.0291	0.0503	0.0057	0.0697
0.6304	0.0718	0.0862	0.1078	0.0228	0.0561	0.0088	0.0857
0.5987	0.0564	0.0835	0.0859	0.0200	0.0265	-0.0008	0.0711
0.5670	0.0364	0.0776	0.0698	0.0188	0.0355	0.0058	0.0873
0.5354	0.0290	0.0693	0.0484	0.0221	0.0100	-0.0091	0.0742
0.5037	0.0152	0.0709	0.0493	0.0228	-0.0319	-0.0078	0.0731
0.4720	0.0111	0.0734	0.0502	0.0291	-0.0580	-0.0121	0.0877
0.4403	-0.0019	0.0786	0.0562	0.0287	-0.0344	-0.0146	0.0840
0.4086	-0.0145	0.0831	0.0556	0.0290	-0.0529	-0.0137	0.0833
0.3767	-0.0330	0.0945	0.0585	0.0293	-0.0383	-0.0073	0.0894
0.3450	-0.0473	0.0982	0.0858	0.0272	-0.0428	0.0007	0.0898
0.3134	-0.0534	0.1064	0.0886	0.0254	-0.0546	-0.0089	0.116
0.2817	-0.0902	0.0936	0.0257	0.0261	-0.0924	-0.0049	0.0994
0.2500	-0.0785	0.0907	0.0698	0.0293	-0.0683	-0.0057	0.119
0.2183	-0.1087	0.0935	0.0359	0.0272	-0.1094	-0.0001	0.128
0.1867	-0.1279	0.1003	0.0407	0.0268	-0.1089	-0.009	0.0692
0.1550	-0.1652	0.1370	0.0592	0.0401	-0.1631	-0.0152	0.0533
0.1233	-0.2058	0.1659	0.0760	0.0352	-0.1630	-0.0335	0.0465
0.0916	-0.2637	0.2285	0.0938	0.0614	-0.1947	-0.0165	0.0803
0.0599	-0.3549	0.3429	0.0884	0.0630	-0.1095		
0.0281	-0.3233	0.4623	0.1627	0.0830	0.0426		

Weighted

a/b=1.0, α=45 , Free Convection (Re=0)

Tbot=397.8 ± 6.6 (C), Tbac=401.1 ± 5.0 (C)

Ttop=337.7 ± 4.1 (C), T_∞ =24 (C)

$\Delta T/T_\infty$ =1.19 , Gr=4.2 E7 , N = 1000

w/a=0.25, z/$\overline{c}$=0.0

x/b	V	U	$\overline{v'^2}$ x10	$\overline{u'^2}$ x10	$\overline{u'v'}$ x100	W	$\overline{w'^2}$ x10
0.0000	-0.0303	0.1358	0.0128	0.0305	-0.0166	-0.0264	0.0373
0.0281	-0.0309	0.1535	0.0409	0.0342	-0.0404	0.0152	0.0492
0.0598	-0.0371	0.1525	0.0723	0.0208	-0.0021	-0.0028	0.0570
0.0915	-0.0361	0.1421	0.0751	0.0358	0.0364	0.0064	0.0559
0.1231	-0.0351	0.1362	0.0551	0.0327	0.0377	-0.0013	0.0668
0.1548	-0.0374	0.1386	0.0467	0.0241	0.0139	0.0008	0.0677
0.1865	-0.0360	0.1208	0.0614	0.0260	0.0035	-0.0140	0.0585
0.2182	-0.0290	0.1227	0.0491	0.0286	-0.0169	-0.0161	0.0661
0.2499	-0.0265	0.1098	0.0444	0.0267	-0.0211	-0.0208	0.0658
0.2815	-0.0244	0.1030	0.0453	0.0216	0.0000	-0.0149	0.104
0.3132	-0.0186	0.1127	0.0549	0.0241	-0.0006	-0.0207	0.103
0.3449	-0.0216	0.1147	0.0441	0.0296	-0.0027	-0.0019	0.0939
0.3766	-0.0169	0.1098	0.0404	0.0267	0.0048	-0.0016	0.0918
0.4083	-0.0092	0.1166	0.0569	0.0232	0.0155	-0.0081	0.0792
0.4399	-0.0059	0.1160	0.0425	0.0298	0.0034	-0.0375	0.0836
0.4716	-0.0022	0.1064	0.0342	0.0241	0.0095	-0.0203	0.0946
0.5033	-0.0016	0.0833	0.0353	0.0247	0.0091	-0.0034	0.0926
0.5350	0.0001	0.0943	0.0274	0.0217	-0.0080	-0.0008	0.120
0.5667	0.0073	0.0955	0.0277	0.0210	-0.0051	-0.0071	0.0844
0.5983	0.0084	0.0950	0.0341	0.0209	0.0158	-0.0160	0.114
0.6300	0.0210	0.1018	0.0441	0.0236	0.0191	-0.0071	0.0882
0.6619	0.0239	0.1161	0.0431	0.0247	0.0402	-0.0179	0.0883
0.6936	0.0249	0.1219	0.0382	0.0193	-0.0120	-0.0180	0.110
0.7253	0.0285	0.1097	0.0371	0.0185	0.0103	0.0008	0.106
0.7570	0.0368	0.1287	0.0453	0.0248	0.0391	-0.0167	0.0902
0.7887	0.0351	0.1454	0.0402	0.0216	0.0084	-0.0198	0.125
0.8203	0.0343	0.1391	0.0331	0.0203	0.0216	-0.0095	0.0849
0.8520	0.0408	0.1433	0.0432	0.0247	0.0196	-0.0237	0.0988
0.8837	0.0285	0.1390	0.0489	0.0351	0.0672	-0.0105	0.0937
0.9154	0.0362	0.1608	0.0430	0.0315	0.0375	0.0056	0.116
0.9471	0.0416	0.1608	0.0470	0.0314	0.0905	0.0052	0.0865
0.9787	0.0298	0.1692	0.0552	0.0345	0.0518	-0.0043	0.0874
1.0000	0.0306	0.1754	0.0521	0.0248	0.0338	-0.0017	0.103

Weighted

a/b=1.0, α=45 , Free Convection (Re=0)

Tbot=397.6 ± 6.7 (C), Tbac=397.1 ± 9.3 (C)

Ttop=334.9 ± 5.5 (C), T_∞ =24 (C)

$\Delta T/T_\infty$ =1.186 , Gr=4.2 E7 , N = 500

y/a=-0.5, z/c=0.0

x/b	$\overline{V}$	$\overline{v'^2}$ x10
0.0493	0.0161	1.6393
0.0598	-0.1411	0.7848
0.0703	-0.1817	0.3991
0.0915	-0.1363	0.2319
0.1126	-0.0946	0.1687
0.1338	-0.0699	0.0876
0.1655	-0.0429	0.0973
0.1972	-0.0207	0.0827
0.2288	-0.0067	0.0628
0.2605	-0.0045	0.0688
0.2922	0.0141	0.0497
0.3239	0.0155	0.0584
0.3555	0.0155	0.0635
0.3872	0.0155	0.0685
0.4189	0.0284	0.0745
0.4506	0.0458	0.0651
0.4823	0.0420	0.0526
0.5139	0.0601	0.0513
0.5456	0.0561	0.0565
0.5773	0.0641	0.0745
0.6091	0.0599	0.0681
0.6408	0.0731	0.0738
0.6725	0.0560	0.0729
0.7042	0.0672	0.0601
0.7358	0.0863	0.0786
0.7675	0.0742	0.0855
0.7992	0.1013	0.0920
0.8309	0.0947	0.0908
0.8626	0.1289	0.0840
0.8942	0.1368	0.0870
0.9155	0.1415	0.1319
0.9260	0.1187	0.1315

Weighted

a/b=1.0, α=45 , Free Convection (Re=0)

Tbot=397.8 ± 6.6 (C), Tbac=401.1 ± 5.0 (C)

Ttop=337.7 ± 4.1 (C), T_∞ =24 (C)

$\Delta T/T_\infty$ =1.19 , Gr=4.2 E7 , N = 1000

x/b=0.0, z/c=0.0

y/a	V	U	$\overline{v'^2}$ x10	$\overline{u'^2}$ x10	$\overline{u'v'}$ x100	W	$\overline{w'^2}$ x10
0.0211	-0.1356	0.5436	0.0646	0.0184	0.0265		
0.0423	-0.1190	0.3827	0.0398	0.0280	-0.0139		
0.0635	-0.0963	0.3217	0.0330	0.0313	-0.0156		
0.0846	-0.0810	0.2778	0.0379	0.0361	-0.0297	-0.0116	0.0324
0.1058	-0.0727	0.2280	0.0238	0.0262	-0.0096	-0.0192	0.0278
0.1269	-0.0632	0.2062	0.0139	0.0374	-0.0148	-0.0227	0.0213
0.1481	-0.0581	0.2056	0.0215	0.0320	-0.0248	-0.0147	0.0229
0.1692	-0.0522	0.1951	0.0155	0.0306	-0.0079	-0.0223	0.0223
0.1904	-0.0439	0.1790	0.0234	0.0306	-0.0243	-0.0288	0.0250
0.2116	-0.0483	0.1812	0.0143	0.0315	-0.0013	-0.0199	0.0386
0.2327	-0.0371	0.1645	0.0194	0.0290	0.0019	-0.0280	0.0400
0.2500	-0.0303	0.1358	0.0128	0.0305	-0.0165	-0.0264	0.0373

x/b=1.0, z/c=0.0

y/a	V	U	$\overline{v'^2}$ x10	$\overline{u'^2}$ x10	$\overline{u'v'}$ x100	W	$\overline{w'^2}$ x10
0.2500	0.0306	0.1754	0.0521	0.0248	0.0338	-0.0017	0.103
0.2324	0.0397	0.1944	0.0453	0.0246	0.0528	-0.0206	0.0768
0.2112	0.0343	0.1955	0.0380	0.0207	0.0557	-0.0130	0.119
0.1901	0.0524	0.2131	0.0518	0.0313	0.0880	-0.0109	0.0985
0.1689	0.0595	0.2329	0.0668	0.0236	0.0606	0.0080	0.108
0.1478	0.0889	0.2576	0.1205	0.0356	0.1163	0.0119	0.0818
0.1266	0.1449	0.2844	0.2305	0.0436	0.1244	0.0200	0.0884
0.1054	0.2309	0.3158	0.4026	0.0801	0.3929	0.0006	0.0950
0.0843	0.3162	0.3616	0.4924	0.0718	0.4408	0.0012	0.117
0.0631	0.3595	0.4089	0.4227	0.0329	0.1672	0.0062	0.101
0.0420	0.3709	0.4254	0.4012	0.0283	0.1335		
0.0208	0.3893	0.4198	0.2001	0.0149	0.0266		

Weighted

a/b=1.0, α =45 , Free Convection (Re=0)

Tbot=397.6 ±6.7 (C), Tbac=397.1 ± 9.3 (C)

Ttop=334.9 ± 5.5 (C), T_∞ =24 (C)

$\Delta T/T_\infty$ =1.186 , Gr=4.2 E7 , N = 500

x/b=0.5, z/c=0.0

y/a	$\overline{U}$	$\overline{u'^2}\times 10$	y/a	$\overline{U}$	$\overline{u'^2}\times 10$
-0.9733	0.2933	0.3593	-0.2162	0.0545	0.0352
-0.9624	0.3628	0.1055	-0.1946	0.0513	0.0279
-0.9517	0.3104	0.1164	-0.1729	0.0547	0.0307
-0.9409	0.2584	0.2338	-0.1513	0.0607	0.0278
-0.9300	0.2457	0.1382	-0.1296	0.0558	0.0186
-0.9084	0.2095	0.1621	-0.1080	0.0661	0.0222
-0.8867	0.1341	0.1139	-0.0863	0.0696	0.0224
-0.8652	0.1183	0.1116	-0.0649	0.0690	0.0272
-0.8435	0.0821	0.0888	-0.0432	0.0683	0.0188
-0.8219	0.0631	0.0651	-0.0216	0.0727	0.0211
-0.8002	0.0535	0.0768	-0.0001	0.0753	0.0157
-0.7786	0.0322	0.0497			
-0.7570	0.0366	0.0627			
-0.7354	0.0242	0.0669			
-0.7137	0.0052	0.0468			
-0.6921	0.0052	0.0460			
-0.6705	-0.0040	0.0417			
-0.6488	-0.0095	0.0338			
-0.6273	-0.0004	0.0366			
-0.6056	-0.0093	0.0447			
-0.5840	-0.0072	0.0352			
-0.5623	0.0117	0.0309			
-0.5407	0.0117	0.0277			
-0.5190	0.0120	0.0344			
-0.4974	0.0176	0.0405			
-0.4758	0.0210	0.0314			
-0.4542	0.0341	0.0368			
-0.4325	0.0368	0.0397			
-0.4109	0.0399	0.0299			
-0.3892	0.0482	0.0417			
-0.3676	0.0535	0.0352			
-0.3459	0.0526	0.0498			
-0.3243	0.0594	0.0408			
-0.3026	0.0602	0.0345			
-0.2811	0.0637	0.0326			
-0.2595	0.0643	0.0309			
-0.2378	0.0602	0.0360			

Unweighted

a/b=1.0, α =45 , Free Convection (Re=0)

Tbot=397.8 ± 6.6 (C), Tbac=401.1 ± 5.0 (C)

Ttop=337.7 ± 4.1 (C), T_∞ =24 (C)

$\Delta T/T_\infty$ =1.19 , Gr=4.2 E7 , , N = 1000

y/a=0.0, z/c=0.0

x/b	V	U	$\overline{v}^2$ x10	$\overline{u'^2}$ x10	$\overline{u'v'}$ x100	W	$\overline{w'^2}$ x10
0.9789	0.3770	0.2550	0.1850	0.0382	0.0104	-0.0116	0.187
0.9683	0.3140	0.2355	0.0965	0.0436	-0.0054		
0.9472	0.2738	0.2326	0.0847	0.0622	0.0333	0.0141	0.228
0.9155	0.2411	0.2258	0.0823	0.0639	-0.0092	0.0272	0.318
0.8838	0.2153	0.2128	0.0989	0.0760	0.0246	0.0517	0.394
0.8522	0.1855	0.1979	0.1314	0.1058	-0.0178	0.0489	0.350
0.8205	0.1681	0.1830	0.1344	0.1016	0.0049	0.0560	0.359
0.7888	0.1538	0.1510	0.1764	0.0588	0.0879	0.0669	0.425
0.7571	0.1532	0.1430	0.2014	0.0544	0.0643	0.0635	0.368
0.7254	0.1273	0.1310	0.1674	0.0708	0.0011	0.0636	0.458
0.6938	0.1190	0.1241	0.2153	0.0739	0.0164	0.0717	0.465
0.6621	0.1303	0.1187	0.3030	0.0596	-0.0378	0.0621	0.360
0.6304	0.1386	0.1029	0.3647	0.0414	0.0468	0.0795	0.438
0.5987	0.1084	0.0995	0.2906	0.0365	0.0084	0.0507	0.330
0.5670	0.0814	0.0937	0.2643	0.0325	0.0304	0.0685	0.434
0.5354	0.0594	0.0901	0.2102	0.0466	0.0605	0.0441	0.410
0.5037	0.0408	0.0903	0.1793	0.0409	-0.0803	0.0426	0.377
0.4720	0.0337	0.0997	0.1840	0.0640	-0.0933	0.0440	0.454
0.4403	0.0201	0.1047	0.2183	0.0609	0.0074	0.0387	0.390
0.4086	0.0030	0.1090	0.1982	0.0592	-0.0880	0.0347	0.417
0.3767	-0.0203	0.1180	0.1586	0.0502	-0.0198	0.0464	0.426
0.3450	-0.0286	0.1186	0.2482	0.0400	0.0157	0.0675	0.422
0.3134	-0.0404	0.1246	0.2138	0.0371	-0.0615	0.0571	0.540
0.2817	-0.1006	0.1123	0.2666	0.0446	0.0611	0.0554	0.487
0.2500	-0.0747	0.1112	0.1620	0.0491	-0.0521	0.0613	0.598
0.2183	-0.1214	0.1116	0.0463	0.0406	-0.0898	0.0867	0.663
0.1867	-0.1387	0.1157	0.0572	0.0396	-0.0972	0.0267	0.296
0.1550	-0.1762	0.1548	0.0693	0.0540	-0.1469	0.0529	0.211
0.1233	-0.2159	0.1784	0.0773	0.0358	-0.1539	0.0276	0.143
0.0916	-0.2741	0.2441	0.0878	0.0708	-0.1948	0.0377	0.448
0.0599	-0.3617	0.3525	0.0813	0.0664	-0.0962		
0.0281	-0.3279	0.4633	0.1658	0.0087	0.0459		

Unweighted

a/b=1.0, α=45 , Free Convection (Re=0)

Tbot=397.8 ±6.6 (C), Tbac=401.1 ±5.0 (C)

Ttop=337.7 ±4.1 (C), T_∞ =24 (C)

$\Delta T/T_\infty$ =1.19 , Gr=4.2 E7 , N = 1000

y/a=0.25, z/$\frac{c}{2}$=0.0

x/b	V	U	$\overline{v'^2}\times10$	$\overline{u'^2}\times10$	$\overline{u'v'}\times100$	W	$\overline{w'^2}\times10$
0.0000	-0.0313	0.1563	0.0199	0.0314	-0.0067	-0.0146	0.151
0.0281	-0.0268	0.1733	0.0914	0.0343	-0.0297	0.0643	0.291
0.0598	-0.0246	0.1644	0.1909	0.0301	-0.0018	0.0448	0.306
0.0915	-0.0179	0.1639	0.1928	0.0507	0.1252	0.0554	0.303
0.1231	-0.0239	0.1545	0.1236	0.0474	0.0458	0.0530	0.381
0.1548	-0.0295	0.1530	0.0967	0.0430	0.0173	0.0596	0.393
0.1865	-0.0183	0.1380	0.1882	0.0388	0.0002	0.0300	0.323
0.2182	-0.0172	0.1420	0.1195	0.0482	-0.0433	0.0254	0.388
0.2499	-0.0170	0.1290	0.1206	0.0304	-0.0459	0.0159	0.345
0.2815	-0.0122	0.1194	0.1240	0.0340	-0.0234	0.0486	0.575
0.3132	0.0013	0.1306	0.1799	0.0320	-0.0005	0.0377	0.550
0.3449	-0.0105	0.1369	0.1213	0.0538	0.0156	0.0593	0.529
0.3766	-0.0073	0.1301	0.1125	0.0423	0.0411	0.0610	0.533
0.4083	0.0130	0.1338	0.1683	0.0306	0.0042	0.0460	0.430
0.4399	0.0086	0.1387	0.1176	0.0427	-0.0213	-0.0107	0.389
0.4716	0.0111	0.1256	0.1039	0.0321	0.0308	0.0331	0.524
0.5033	0.0147	0.1050	0.1388	0.0992	0.0248	0.0546	0.486
0.5350	0.0090	0.1130	0.0855	0.0325	-0.0359	0.0781	0.725
0.5667	0.0184	0.1137	0.0757	0.0321	-0.0206	0.0405	0.499
0.5983	0.0237	0.1133	0.0920	0.0294	0.0080	0.0368	0.580
0.6300	0.0438	0.1222	0.1378	0.0442	-0.0068	0.0529	0.464
0.6619	0.0439	0.1350	0.1164	0.0418	0.0241	0.0328	0.443
0.6936	0.0390	0.1356	0.0958	0.0323	-0.0296	0.0388	0.543
0.7253	0.0451	0.1241	0.1054	0.0395	-0.0041	0.0522	0.633
0.7570	0.0563	0.1460	0.1130	0.0332	0.0773	0.0366	0.550
0.7887	0.0488	0.1588	0.0944	0.0367	0.0081	0.0403	0.636
0.8203	0.0462	0.1523	0.0670	0.0258	0.0014	0.0438	0.502
0.8520	0.0553	0.1587	0.0938	0.0295	-0.0092	0.0279	0.536
0.8837	0.0503	0.1627	0.2315	0.0642	0.1326	0.0454	0.526
0.9154	0.0494	0.1792	0.0869	0.0622	0.0619	0.0723	0.063
0.9471	0.0576	0.1792	0.0942	0.0576	0.0791	0.0666	0.460
0.9787	0.0474	0.1886	0.1363	0.0689	0.0410	0.0439	0.511
1.0000	0.0454	0.1887	0.1082	0.0470	0.0297	0.0531	0.523

Unweighted

a/b=1.0, α=45 , Free Convection (Re=0)

Tbot=397.6 ± 6.7 (C), Tbac=397.1 ± 9.3 (C)

Ttop=334.9 ± 5.5 (C), T_∞ =24 (C)

$\Delta T/T_\infty$ =1.186 , Gr=4.2 E7 , N = 500

y/a=-0.5, z/c=0.0

x/b	$\overline{v}^2$	$\overline{v'^2}_{x10}$
0.0493	0.2432	4.8618
0.0598	-0.1969	2.0763
0.0703	-0.2536	0.7575
0.0915	-0.2123	0.3677
0.1126	-0.1666	0.3544
0.1338	-0.1289	0.2106
0.1655	-0.0921	0.2056
0.1972	-0.0728	0.2468
0.2288	-0.0227	0.1967
0.2605	-0.0248	0.2149
0.2922	0.0116	0.1656
0.3239	0.0368	0.2203
0.3555	0.0364	0.2427
0.3872	0.0359	0.2651
0.4189	0.0597	0.2976
0.4506	0.0876	0.2158
0.4823	0.0833	0.1687
0.5139	0.1095	0.1788
0.5456	0.1112	0.1765
0.5773	0.1240	0.1920
0.6091	0.1221	0.2219
0.6408	0.1343	0.1718
0.6725	0.1189	0.1814
0.7042	0.1179	0.1400
0.7358	0.1492	0.1371
0.7675	0.1426	0.1740
0.7992	0.1696	0.1703
0.8309	0.1609	0.1498
0.8626	0.1853	0.1326
0.8942	0.1915	0.1205
0.9155	0.2124	0.2184
0.9260	0.2000	0.1825

Unweighted

a/b=1.0, α =45 , Free Convection (Re=0)

Tbot=397.8 ± 6.6 (C), Tbac=401.1 ± 5.0 (C)

Ttop=337.7 ± 4.1 (C), T_∞ =24 (C)

$\Delta T/T_\infty$ =1.19 , Gr=4.2 E7 , N = 1000

x/b=0.0, z/c=0.0

y/a	V	U	$\overline{v}^2 \times 10$	$\overline{u}^2 \times 10$	$\overline{u'v'} \times 100$	W	$\overline{w}^2 \times 10$
0.0211	-0.1347	0.5467	0.0706	0.0195	0.0285		
0.0423	-0.1184	0.3895	0.0488	0.0301	-0.0128		
0.0635	-0.0949	0.3309	0.0468	0.0323	-0.0096		
0.0846	-0.0791	0.2897	0.0563	0.0371	-0.0237	-0.0050	0.174
0.1058	-0.0713	0.2387	0.0452	0.0267	0.0118	-0.0115	0.101
0.1269	-0.0638	0.2225	0.0184	0.0358	-0.0000	-0.0200	0.073
0.1481	-0.0570	0.2200	0.0403	0.0351	-0.0176	-0.0105	0.0623
0.1692	-0.0523	0.2093	0.0213	0.0332	-0.0037	-0.0266	0.0452
0.1904	-0.0429	0.1949	0.0457	0.0417	-0.0199	0.0243	0.0779
0.2116	-0.0487	0.1968	0.0190	0.0329	0.0033	-0.0016	0.169
0.2327	-0.0358	0.1801	0.0304	0.0336	0.0051	-0.0116	0.161
0.2500	-0.0313	0.1563	0.0199	0.0314	-0.0067	-0.0146	0.151

x/b=1.0, z/c=0.0

y/a	V	U	$\overline{v}^2 \times 10$	$\overline{u}^2 \times 10$	$\overline{u'v'} \times 100$	W	$\overline{w}^2 \times 10$
0.2500	0.0454	0.1887	0.1082	0.0470	0.0297	0.0531	0.523
0.2324	0.0520	0.2067	0.0846	0.0360	0.0440	0.0251	0.439
0.2112	0.0451	0.2058	0.0696	0.0310	0.0656	0.0392	0.660
0.1901	0.0670	0.2275	0.0999	0.0574	0.0839	0.0424	0.533
0.1689	0.0763	0.2426	0.1321	0.0352	0.0468	0.0809	0.569
0.1478	0.1115	0.2708	0.2192	0.0501	0.1185	0.0661	0.445
0.1266	0.1817	0.2972	0.3856	0.0454	0.0846	0.0992	0.492
0.1054	0.2886	0.3376	0.5751	0.0609	0.1906	0.0653	0.558
0.0843	0.3712	0.3779	0.6022	0.0436	0.1464	0.0833	0.644
0.0631	0.3938	0.4157	0.5430	0.0338	0.1398	0.0761	0.493
0.0420	0.4021	0.4306	0.5234	0.0298	0.1030		
0.0208	0.4051	0.4218	0.2362	0.0167	0.0189		

Unweighted

a/b=1.0, α =45 , Free Convection (Re=0)

Tbot=397.6 ± 6.7 (C), Tbac=397.1 ± 9.3 (C)

Ttop=334.9 ± 5.5 (C), T_∞ =24 (C)

$\Delta T/T_\infty$ =1.186 , Gr=4.2 E7 , N = 500

x/b=0.5, z/c=0.0

y/a	$\overline{U}^2$	$\overline{u'^2}$ x10	y/a	$\overline{U}^2$	$\overline{u'^2}$ x10
-0.9733	0.4043	0.9486	-0.2162	0.0949	0.1800
-0.9624	0.3919	0.1071	-0.1946	0.0809	0.1202
-0.9517	0.3479	0.2777	-0.1729	0.0861	0.1163
-0.9409	0.3408	0.5333	-0.1513	0.0883	0.0988
-0.9300	0.3017	0.1311	-0.1296	0.0772	0.0658
-0.9084	0.2826	0.1528	-0.1080	0.0914	0.0914
-0.8867	0.2075	0.1378	-0.0863	0.0945	0.0804
-0.8652	0.1880	0.1360	-0.0649	0.0965	0.0960
-0.8435	0.1437	0.1305	-0.0432	0.0878	0.0515
-0.8219	0.1099	0.1133	-0.0216	0.0935	0.0462
-0.8002	0.1095	0.1374	-0.0001	0.0916	0.0426
-0.7786	0.0686	0.1191			
-0.7570	0.0709	0.1110			
-0.7354	0.0541	0.1198			
-0.7137	0.0205	0.1130			
-0.6921	0.0197	0.0994			
-0.6705	0.0004	0.0914			
-0.6488	-0.0043	0.0716			
-0.6273	0.0052	0.0789			
-0.6056	0.0021	0.1034			
-0.5840	-0.0011	0.0754			
-0.5623	0.0263	0.0688			
-0.5407	0.0197	0.0652			
-0.5190	0.0212	0.0787			
-0.4974	0.0380	0.1088			
-0.4758	0.0390	0.0830			
-0.4542	0.0600	0.1005			
-0.4325	0.0718	0.1386			
-0.4109	0.0598	0.0714			
-0.3892	0.0844	0.1187			
-0.3676	0.0851	0.1118			
-0.3459	0.0958	0.1813			
-0.3243	0.1013	0.1557			
-0.3026	0.0990	0.1666			
-0.2811	0.0993	0.1334			
-0.2595	0.0992	0.1283			
-0.2378	0.0993	0.1395			

Weighted

a/b=0.5, α =0 , Free Convection (Re=0)

Tbot=399.5 ±4.3 (C), Tbac=400.6 ± 2.9 (C)

Ttop=341.8 ± 2.4 (C), T_∞ =24.5 (C)

$\Delta T/T_\infty$ =1.2 , Gr=4.2 E7 , N = 1000

y/a=0.0, z/c=0.0

x/b	V	U	$\overline{v'^2}\times 10$	$\overline{u'^2}\times 10$	$\overline{u'v'}\times 100$
0.9825	0.3448	0.3511	0.9121	0.1576	0.2958
0.9736	0.3805	0.2896	0.6453	0.0799	0.2973
0.9472	0.2524	0.1914	0.3140	0.0924	0.4027
0.9296	0.1761	0.2089	0.5254	0.2174	0.4241
0.8768	0.1028	0.1201	0.2932	0.1975	0.4654
0.8240	0.0594	0.0727	0.1324	0.1368	0.3591
0.7712	0.0338	0.0430	0.0896	0.0526	0.0890
0.7184	0.0166	0.0309	0.0701	0.0372	0.0906
0.6655	0.0031	0.0320	0.0556	0.0339	0.0496
0.6127	-0.0043	0.0356	0.0475	0.0303	0.0213
0.5599	0.0017	0.0558	0.0967	0.0478	0.0417
0.5071	-0.0112	0.0514	0.0845	0.0400	0.0161
0.4543	-0.0123	0.0627	0.1104	0.0766	0.0661
0.4014	-0.0276	0.0811	0.1613	0.1480	-0.0245
0.3486	-0.0356	0.0912	0.1917	0.0679	-0.0028
0.2958	-0.0328	0.0891	0.1973	0.0640	-0.0663
0.2430	-0.0468	0.1156	0.2483	0.0930	0.0445
0.1902	-0.0622	0.1383	0.3203	0.1001	-0.0635
0.1373	-0.0735	0.2361	0.8804	0.1293	-0.1405
0.0845	-0.1494	0.3477	0.6654	0.0816	-0.0356
0.0704	-0.1199	0.3623	0.8113	0.1014	0.0004
0.0493	-0.0222	0.4552	0.4378	0.0440	-0.0409
0.0289	0.1320	0.4290	1.290	0.1590	0.3380

Weighted

a/b=0.5, α=0 , Free Convection (Re=0)

Tbot=399.5 ± 4.3 (C), Tbac=400.6 ± 2.9 (C)

Ttop=341.8 ± 2.4 (C), T_∞ =24.5 (C)

$\Delta T/T_\infty$ =1.2 , Gr=4.2 E7 , N = 1000

y/a=1.0, z/c=0.0

x/b	V	U	$\overline{v'^2}\times 10$	$\overline{u'^2}\times 10$	$\overline{u'v'}\times 100$
1.0000	0.0116	0.1177	0.1612	0.0559	0.0822
0.9175	0.0156	0.1049	0.1138	0.0600	0.0536
0.8351	0.0205	0.1194	0.1519	0.0624	0.0969
0.7526	0.0142	0.0932	0.1115	0.0580	0.0773
0.6702	0.0192	0.1038	0.1279	0.0560	0.0367
0.5877	0.0067	0.1022	0.1260	0.0474	0.0623
0.5053	0.0124	0.0998	0.1186	0.0524	0.0364
0.4228	0.0072	0.1098	0.1240	0.0521	0.0847
0.3404	0.0114	0.1155	0.1505	0.0655	0.1136
0.2579	0.0190	0.1247	0.1629	0.0618	0.0492
0.1755	0.0117	0.1178	0.1621	0.0698	0.1068
0.0930	0.0186	0.1391	0.1692	0.0659	0.0577
0.0000	0.0171	0.1237	0.1795	0.0726	0.0993

x/b=1.0, z/c=0.0

y/a	V	U	$\overline{v'^2}\times 10$	$\overline{u'^2}\times 10$	$\overline{v'u'}\times 100$
0.0823	0.4660	0.4980	0.6941	0.1046	0.7205
0.1647	0.3246	0.4271	0.7465	0.0988	0.5808
0.2470	0.1747	0.3043	0.3671	0.1030	0.7039
0.3294	0.0903	0.2185	0.2225	0.1071	0.5365
0.4117	0.0584	0.1718	0.1950	0.0804	0.3635
0.4941	0.0521	0.1707	0.1638	0.0953	0.3168
0.5764	0.0198	0.1190	0.1280	0.0654	0.1798
0.6588	0.0363	0.1580	0.1650	0.0706	0.1261
0.7411	0.0366	0.1576	0.1920	0.0624	0.1689
0.8234	0.0214	0.1398	0.1539	0.0478	0.1004
0.9058	0.0215	0.1510	0.1721	0.0492	0.0736
1.0000	0.0116	0.1177	0.1612	0.0559	0.0822

Weighted

a/b=0.5, α =0 , Free Convection (Re=0)

Tbot=399.5 ± 4.3 (C), Tbac=400.6 ± 2.9 (C)

Ttop=341.8 ± 2.4 (C), T_∞ =24.5 (C)

$\Delta T/T_\infty$ =1.2 , Gr=4.2 E7 , N = 1000

x/b=0.0, z/c=0.0

y/a	$\overline{V}$	U	$\overline{v'^2}$ x10	$\overline{u'^2}$ x10	$\overline{u'v'}$x100
1.0000	0.0171	0.1237	0.1795	0.0726	0.0993
0.9059	0.0179	0.1375	0.1755	0.0564	0.0882
0.8235	0.0109	0.1372	0.1947	0.0677	0.0630
0.7412	0.0200	0.1650	0.2311	0.0524	0.0264
0.6589	0.0054	0.1408	0.2057	0.0588	0.0815
0.5765	0.0091	0.1690	0.2158	0.0576	0.0337
0.4942	-0.0010	0.1775	0.2303	0.0625	0.0237
0.4118	0.0036	0.1792	0.2471	0.0582	0.0517
0.3295	0.0026	0.1992	0.3542	0.0514	0.0724
0.2471	-0.0015	0.1977	0.2997	0.0632	0.0374
0.1648	-0.0302	0.3146	0.4481	0.0467	0.0760
0.0824	-0.0254	0.5190	0.8276	0.0458	-0.0071

Unweighted

a/b=0.5, α =0 , Free Convection (Re=0)

Tbot=399.5 ± 4.3 (C), Tbac=400.6 ± 2.9 (C)

Ttop=341.8 ± 2.4 (C), T_∞ =24.5 (C)

$\Delta T/T_\infty$ =1.2 , Gr=4.2 E7 , N = 1000

y/a=0.0, z/c=0.0

x/b	V	U	$\overline{v'^2}\times 10$	$\overline{u'^2}\times 10$	$\overline{u'v'}\times 100$
0.9825	0.4138	0.3721	1.1562	0.1647	0.1424
0.9736	0.4592	0.3044	0.7974	0.1070	0.2710
0.9472	0.3184	0.2199	0.4120	0.1404	0.3221
0.9296	0.2417	0.2677	1.0169	0.3232	-0.0037
0.8768	0.1776	0.2147	0.7406	0.3818	0.2133
0.8240	0.1444	0.1815	0.4593	0.3852	0.2467
0.7712	0.0891	0.0990	0.4445	0.2243	0.2117
0.7184	0.0803	0.0820	0.4162	0.1745	0.1697
0.6655	0.0487	0.0843	0.3339	0.1788	0.1349
0.6127	0.0246	0.0811	0.2996	0.1611	0.1091
0.5599	0.0579	0.1060	0.4186	0.2598	-0.0222
0.5071	0.0117	0.0964	0.3926	0.1594	-0.0785
0.4543	0.0255	0.1403	0.4610	0.2342	0.1967
0.4014	-0.0087	0.0830	0.5686	0.4231	0.2196
0.3486	-0.0152	0.1395	0.5601	0.1455	-0.0032
0.2958	-0.0112	0.1337	0.5864	0.1585	-0.1996
0.2430	-0.0315	0.1633	0.5523	0.1900	0.1013
0.1902	-0.0525	0.1838	0.6548	0.1612	-0.0151
0.1373	-0.1254	0.2701	1.7507	0.1596	-0.1785
0.0845	-0.1547	0.3643	0.8365	0.0887	-0.0014
0.0704	-0.1232	0.3817	1.0226	0.1045	0.0018
0.0493	-0.0195	0.4637	0.5718	0.0467	-0.0590
0.0289	0.1710	0.4360	1.3800	0.1360	0.2760

Unweighted

a/b=0.5, α=0 , Free Convection (Re=0)

Tbot=399.5 ± 4.3 (C), Tbac=400.6 ± 2.9 (C)

Ttop=341.8 ± 2.4 (C), T_∞=24.5 (C)

$\Delta T/T_\infty$ =1.2 , Gr=4.2 E7 , N = 1000

y/a=1.0, z/c=0.0

x/b	$\overline{V}$	U	$\overline{v^2}$ x10	$\overline{u^2}$ x10	$\overline{u'v'}$x100
1.0000	0.0527	0.1533	0.4319	0.1465	0.0021
0.9175	0.0510	0.1495	0.3341	0.2971	-0.0286
0.8351	0.0633	0.1605	0.4114	0.1843	0.1027
0.7526	0.0570	0.1415	0.3545	0.1938	0.0161
0.6702	0.0539	0.1455	0.3853	0.1439	-0.1786
0.5877	0.0429	0.1377	0.3896	0.1374	0.0157
0.5053	0.0404	0.1390	0.3831	0.1653	-0.0019
0.4228	0.0379	0.1478	0.3537	0.1535	0.0766
0.3404	0.0571	0.1618	0.4321	0.1755	0.1948
0.2579	0.0483	0.1628	0.4349	0.1541	0.0201
0.1755	0.0545	0.1640	0.4655	0.1538	0.0535
0.0930	0.0466	0.1757	0.4060	0.1805	0.0266
0.0000	0.0552	0.1699	0.5552	0.1846	-0.0329

x/b=1.0, z/c=0.0

y/a	$\overline{V}$	U	$\overline{v^2}$ x10	$\overline{u^2}$ x10	$\overline{u'v'}$x100
0.0823	0.5210	0.5144	0.7010	0.0934	0.5029
0.1647	0.3739	0.4455	0.9187	0.1100	0.6040
0.2470	0.2324	0.3377	0.5129	0.1203	0.7102
0.3294	0.1444	0.2640	0.3583	0.1376	0.5618
0.4117	0.1103	0.2143	0.3932	0.1181	0.4965
0.4941	0.0968	0.2196	0.3071	0.1276	0.3435
0.5764	0.0637	0.1636	0.3570	0.1336	0.2393
0.6588	0.0655	0.1957	0.3969	0.1439	0.0608
0.7411	0.0762	0.1920	0.4627	0.1316	0.2971
0.8234	0.0550	0.1686	0.3865	0.1027	0.0948
0.9058	0.0542	0.1782	0.4010	0.1226	0.0622
1.0000	0.0527	0.1533	0.4319	0.1465	0.0021

Unweighted

a/b=0.5, α=0 , Free Convection (Re=0)

Tbot=399.5 ± 4.3 (C), Tbac=400.6 ± 2.9 (C)

Ttop=341.8 ± 2.4 (C), T_∞ =24.5 (C)

$\Delta T/T_\infty$ =1.2 , Gr=4.2 E7 , N = 1000

x/b=0.0, $z/\frac{c}{2}$=0.0

y/a	V	U	$\overline{v'^2}\times10$	$\overline{u'^2}\times10$	$\overline{u'v'}\times100$
1.0000	0.0552	0.1699	0.5552	0.1846	-0.0329
0.9059	0.0475	0.1703	0.4324	0.1160	0.1306
0.8235	0.0437	0.1776	0.5196	0.1171	0.0033
0.7412	0.0529	0.1904	0.4968	0.1005	-0.0619
0.6589	0.0416	0.1756	0.5253	0.1176	0.1351
0.5765	0.0418	0.1967	0.4769	0.1173	0.0262
0.4942	0.0264	0.2069	0.4790	0.1147	-0.0902
0.4118	0.0318	0.2064	0.5170	0.0955	0.0519
0.3295	0.0370	0.2192	0.7096	0.0881	0.1518
0.2471	0.0229	0.2237	0.5514	0.0978	-0.0041
0.1648	-0.0029	0.3274	0.6684	0.0604	0.0842
0.0824	-0.0113	0.5259	1.0556	0.0486	-0.0792

APPENDIX B

Measurements of Temperature

$$\theta = \frac{T - T_\infty}{\Delta T}$$

SD is the standard deviation in degrees K

N is the sample size

a/b=0.5, α=0 , Free Convection (Re=0)

Tbot=400.3 ± 3.7 (C), Tbac=402.8 ± 4.9 (C)

Ttop=310.7 ± 2.1 (C), T_∞ =22.5 (C)

$\Delta T/T_\infty$ =1.18 , Gr=4 E7 , N = 50

y/a=0.0, $z/\frac{c}{2}$=0.0

x/b		SD(K)
.0254	.6448	9.1
.0525	.3744	14.5
.0797	.1746	17.5
.1610	.0315	3.6
.2424	.0315	0.6
.4322	.0301	0.4
.6220	.0290	0.6
.8119	.0585	9.8
.8661	.1067	18.1
.9203	.2626	34.8
.9475	.3667	39.6
.9746	.4799	24.9

a/b=0.5, α=0

Tbot=401.6 ± 3.5 (C), Tbac=405.2 ± 4.9 (C)

Ttop=317.1 ± 2.1 (C), T_∞ =23.0 (C)

$\Delta T/T_\infty$ =1.19 , Gr=4.03 E7, Gr/Re**2=459.78

y/a=0.0, $z/\frac{c}{2}$=0.0

x/b		SD(K)
.0254	.6186	1.3
.0525	.3450	2.2
.0797	.1396	1.4
.1610	.0284	0
.2424	.0319	0.4
.4322	.0313	0
.6220	.0284	0
.8119	.0924	3.6
.8661	.1180	8.3
.9203	.1687	7.8
.9475	.2659	13.6
.9746	.4272	8.9

a/b=0.5, α=0

Tbot=402.1 ± 3.7 (C), Tbac=405.4 ± 4.7 (C)

Ttop=318.8 ± 2.1 (C), T_∞ =23.0 (C)

$\Delta T/T_\infty$ =1.19 , Gr=4.03 E7, Gr/Re**2=75.4

y/a=0.0, z/c/2=0.0, N = 50

x/b	θ	SD(K)
.0254	.5743	2.0
.0525	.2911	2.4
.0797	.1033	1.4
.1610	.0278	0.4
.2424	.0341	0
.4322	.0321	0.4
.6220	.0289	0.4
.8119	.0463	2.5
.8661	.1016	8.1
.9203	.1825	3.8
.9475	.2738	4.1
.9746	.4458	5.6

a/b=0.5, α=0

Tbot=401.9 ± 3.7 (C), Tbac=405.2 ± 4.5 (C)

Ttop=319.2 ± 2.1 (C), T_∞ =23.0 (C)

$\Delta T/T_\infty$ =1.19 , Gr=4.03 E7, Gr/Re**2=7.53

y/a=0.0, z/c/2=0.0, N = 50

x/b	θ	SD(K)
.0254	.4492	6.0
.0525	.1586	5.4
.0797	.0363	1.6
.1610	.0227	0
.2424	.0295	0.5
.4322	.0264	0.4
.6220	.0227	0
.8119	.0375	1.7
.8661	.1215	8.0
.9203	.2409	6.9
.9475	.3578	7.9
.9746	.5082	8.2

a/b=0.5, α=0

Tbot=401.6 ± 3.5 (C), Tbac=405.1 ± 4.7 (C)

Ttop=318.5 ± 2.1 (C), T_∞ =23.0 (C)

$\Delta T/T_\infty$ =1.19 , Gr=4.03 E7, Gr/Re**2=5.55

y/a=0.0, z/$\frac{c}{2}$=0.0, N = 50

x/b	θ	SD(K)
.0254	.4147	7.1
.0525	.1210	6.0
.0797	.0275	0.8
.1610	.0227	0
.2424	.0287	0.3
.4322	.0256	0
.6220	.0224	0.3
.8119	.0375	2.5
.8661	.1213	6.6
.9203	.2539	5.8
.9475	.3976	13.0
.9746	.5351	6.8

a/b=0.5, α =0

Tbot=402.6 ± 3.8 (C), Tbac=404.3± 4.7 (C)

Ttop=317.3 ± 1.9 (C), T_∞ =23.0 (C)

$\Delta T/T_\infty$ =1.19 , Gr=4.03 E7, Gr/Re**2=2.38

y/a=0.0, z/$\frac{c}{2}$=0.0, N = 50

x/b	θ	SD(K)
.0254	.3344	7.1
.0525	.0745	3.8
.0797	.0227	0
.1610	.0227	0
.2424	.0281	0.3
.4322	.0227	0
.6220	.0199	0
.8119	.0245	1.2
.8661	.0873	6.9
.9203	.2150	4.9
.9475	.3267	7.8
.9746	.4765	5.8

a/b=0.5, α=0

Tbot=401.7 ± 4.0 (C), Tbac=403.8 ± 4.5 (C)

Ttop=313.3 ± 2.4 (C), T_∞ =23.0 (C)

$\Delta T/T_\infty$ =1.18 , Gr=4 E7, Gr/Re**2=1.15

y/a=0.0, $z/\frac{c}{2}$=0.0, N = 50

x/b	θ	SD(K)
.0254	.1115	4.4
.0525	.0229	0.3
.0797	.0191	0.5
.1610	.0174	0.4
.2424	.0229	0
.4322	.0229	0
.6220	.0191	0.4
.8119	.0217	0.9
.8661	.0483	7.5
.9203	.1375	13.2
.9475	.2375	20.4
.9746	.3447	17.9

a/b=0.5, α=0

Tbot=400.5 ± 4.7 (C), Tbac=402.5 ± 4.3 (C)

Ttop=306.3 ± 3.0 (C), T_∞ =23.0 (C)

$\Delta T/T_\infty$ =1.17 , Gr=3.97 E7, Gr/Re**2=0.56

y/a=0.0, $z/\frac{c}{2}$=0.0, N = 50

x/b	θ	SD(K)
.0254	.0753	7.7
.0525	.0225	1.0
.0797	.0187	0.5
.1610	.0185	0.6
.2424	.0231	0
.4322	.0202	0
.6220	.0173	0
.8119	.0213	0.6
.8661	.0396	7.3
.9203	.0830	11.9
.9475	.1422	19.2
.9746	.1597	19.3

a/b=0.5, α=20 , Free Convection (Re=0)

Tbot=402.6 ± 4.0 (C), Tbac=399.5 ± 5.5 (C)

Ttop=317.4 ± 1.7 (C), T_∞ =23.0 (C)

$\Delta T/T_\infty$ =1.18 , Gr=4.0 E7

y/a=0.0, z/c=0.0 , N = 50

x/b	$\overline{\theta}$	SD(K)
.0254	.5017	16.1
.0525	.2119	13.8
.0797	.1017	11.0
.1610	.0334	3.5
.2424	.0357	1.2
.4322	.0334	0.9
.6220	.0317	1.0
.8119	.0922	10.6
.8661	.1628	20.4
.9203	.2893	24.1
.9475	.3761	26.4
.9746	.4846	19.9

a/b=0.5, α=20

Tbot=402.0 ±3.7 (C), Tbac=398.9 ± 5.0 (C)

Ttop=318.5 ±2.1 (C), T_∞ =22.0 (C)

$\Delta T/T_\infty$ =1.19 , Gr=4.03 E7, Gr/Re**2=110.39

y/a=0.0, z/c=0.0, N = 50

x/b	$\overline{\theta}$	SD(K)
.0254	.4287	0.5
.0525	.1532	0.5
.0797	.0541	0
.1610	.0313	0
.2424	.0370	0
.4322	.0367	0.3
.6220	.0342	0
.8119	.0456	0
.8661	.0758	1.0
.9203	.2156	1.3
.9475	.3677	0.9
.9746	.5443	0.8

a/b=0.5, α=20

Tbot=401.9 ± 3.9 (C), Tbac=398.8 ± 5.1 (C)

Ttop=317.6 ± 2.1 (C), T_∞ =21.5 (C)

$\Delta T/T_\infty$ =1.19 , Gr=4.03 E7, Gr/Re**2=43.12

y/a=0.0, z/c=0.0, N = 50

x/b	$\bar{\theta}$	SD(K)
.0254	.4130	0.5
.0525	.1503	0.6
.0797	.0529	0.3
.1610	.0299	0
.2424	.0379	0.4
.4322	.0344	0.5
.6220	.0299	0
.8119	.0697	1.7
.8661	.1634	17.4
.9203	.2491	3.9
.9475	.3792	2.2
.9746	.5519	1.3

a/b=0.5, α=20

Tbot=401.3 ± 4.0 (C), Tbac=397.8 ± 5.1 (C)

Ttop=316.3 ± 1.8 (C), T_∞ =22.5 (C)

$\Delta T/T_\infty$ =1.18 , Gr=4 E7, Gr/Re**2=16.19

y/a=0.0, z/c=0.0, N = 50

x/b	$\bar{\theta}$	SD(K)
.0254	.0667	7.3
.0525	.0206	1.0
.0797	.0203	1.2
.1610	.0404	4.9
.2424	.0819	4.8
.4322	.0962	4.4
.6220	.0842	4.0
.8119	.0716	4.0
.8661	.1039	15.1
.9203	.2932	24.7
.9475	.4635	27.2
.9746	.6175	17.9

a/b=0.5, α=20

Tbot=400.7 ± 4.1 (C), Tbac=397.1 ± 5.0 (C)

Ttop=315.3 ± 1.9 (C), T_∞ =23.0 (C)

$\Delta T/T_\infty$ =1.18 , Gr=4 E7, Gr/Re**2=5.65

y/a=0.0, $z/\frac{c}{2}$=0.0, N = 50

x/b	θ	SD(K)
.0254	.0339	4.2
.0525	.0187	0.7
.0797	.0195	1.1
.1610	.0566	6.5
.2424	.1063	5.2
.4322	.1172	3.0
.6220	.1086	2.6
.8119	.0989	6.7
.8661	.2009	23.6
.9203	.4546	16.4
.9475	.5807	16.8
.9746	.6730	11.1

a/b=0.5, α=20

Tbot=400.2 ± 4.9 (C), Tbac=396.2 ± 4.9 (C)

Ttop=314.0 ± 2.0 (C), T_∞ =23.0 (C)

$\Delta T/T_\infty$ =1.17 , Gr=3.97 E7, Gr/Re**2=2.35

y/a=0.0, $z/\frac{c}{2}$=0.0, N = 50

x/b	θ	SD(K)
.0254	.0187	4.4
.0525	.0202	0
.0797	.0199	1.5
.1610	.0256	3.5
.2424	.0622	7.3
.4322	.1625	4.6
.6220	.1544	7.0
.8119	.2247	14.8
.8661	.3748	19.3
.9203	.5203	28.9
.9475	.5995	9.6
.9746	.6356	6.4

a/b=0.5, α =20

Tbot=400.0 ± 5.3 (C), Tbac=395.9 ± 5.2 (C)

Ttop=313.1 ± 1.8 (C), T_∞ =23.0 (C)

$\Delta T/T_\infty$ =1.17 , Gr=3.97 E7, Gr/Re**2=1.15

y/a=0.0, $z/\frac{c}{2}$=0.0, N = 50

x/b	θ	SD(K)
.0254	.0211	0.5
.0525	.0205	0.2
.0797	.0173	0
.1610	.0173	0.4
.2424	.0208	0.6
.4322	.0588	7.5
.6220	.1762	8.2
.8119	.2818	11.9
.8661	.3513	20.6
.9203	.4318	9.0
.9475	.4575	11.7
.9746	.5359	7.7

a/b=0.5, α =20

Tbot=399.1 ± 5.4 (C), Tbac=397.3 ± 5.4 (C)

Ttop=307.8 ± 1.9 (C), T_∞ =23.0 (C)

$\Delta T/T_\infty$ =1.17 , Gr=3.97 E7, Gr/Re**2=0.56

y/a=0.0, $z/\frac{c}{2}$=0.0, N = 50

x/b	θ	SD(K)
.0254	.0171	0.3
.0525	.0200	0.3
.0797	.0174	0.2
.1610	.0183	2.4
.2424	.0206	0.5
.4322	.0188	0.9
.6220	.0536	9.5
.8119	.0823	11.6
.8661	.1272	15.1
.9203	.2083	10.5
.9475	.2904	9.9
.9746	.4034	5.8

a/b=0.5, α=45 , Free Convection (Re=0)

Tbot=400.5 ± 3.9 (C), Tbac=401.8± 5.1 (C)

Ttop=320.7 ± 2.2 (C), T_∞ =20.5 (C)

$\Delta T/T_\infty$ =1.2 , Gr=4.06 E7

y/a=0.0, z/c=0.0, N = 50
2

x/b	θ	SD(K)
.0254	.2764	3.7
.0525	.1003	3.1
.0797	.0520	2.4
.1610	.0317	0.6
.2424	.0382	0.6
.4322	.0384	0.7
.6220	.0469	1.9
.8119	.2903	12.8
.8661	.3666	16.3
.9203	.5031	13.0
.9475	.5820	14.0
.9746	.6583	14.4

a/b=0.5, α=45

Tbot=400.5 ± 3.9 (C), Tbac=402.7 ± 6.3 (C)

Ttop=322.1 ± 2.1 (C), T_∞ =20.5 (C)

$\Delta T/T_\infty$ =1.21 , Gr=4.1 E7, Gr/Re**2=274.04

y/a=0.0, z/c=0.0, N = 50
2

x/b	θ	SD(K)
.0254	.2524	0.7
.0525	.0821	0.6
.0797	.0378	0.2
.1610	.0321	0.3
.2424	.0389	0.5
.4322	.0381	0
.6220	.0358	0.4
.8119	.1864	3.6
.8661	.3590	3.8
.9203	.5099	1.9
.9475	.6097	1.9
.9746	.6873	0.8

a/b=0.5, α=45

Tbot=400.6 ± 3.9 (C), Tbac=401.8± 5.1 (C)

Ttop=322.3 ± 2.1 (C), T_∞ =20.5 (C)

$\Delta T/T_\infty$ =1.21 , Gr=4.1 E7, Gr/Re**2=54.89

y/a=0.0, z/c=0.0, N = 50

x/b	$\overline{\theta^2}$	SD(K)
.0254	.2046	6.5
.0525	.0322	1.2
.0797	.0240	0.3
.1610	.0319	1.4
.2424	.0446	1.5
.4322	.0522	1.3
.6220	.0821	3.4
.8119	.3124	9.8
.8661	.4058	11.0
.9203	.5519	9.2
.9475	.6354	6.3
.9746	.6888	9.2

a/b=0.5, α=45

Tbot=400.3 ±4.3 (C), Tbac=401.7 ± 5.2 (C)

Ttop=321.3 ±1.9 (C), T_∞ =21.0 (C)

$\Delta T/T_\infty$ =1.2 , Gr=4.06 E7, Gr/Re**2=19.49

y/a=0.0, z/c=0.0, N = 100

x/b	$\overline{\theta^2}$	SD(K)
.0254	.0611	7.1
.0525	.0337	2.6
.0797	.0379	1.9
.1610	.0535	2.0
.2424	.0676	1.9
.4322	.0908	2.8
.6220	.1336	4.4
.8119	.3350	12.2
.8661	.4103	14.9
.9203	.5255	7.9
.9475	.5897	11.2
.9746	.6551	6.6

a/b=0.5, α=45

Tbot=399.9 ± 4.9 (C), Tbac=401.0 ± 5.2 (C)

Ttop=319.5 ± 2.0 (C), T_∞ =21.0 (C)

$\Delta T/T_\infty$ =1.2 , Gr=4.06 E7, Gr/Re**2=5.5

y/a=0.0, z/c=0.0, N = 100

x/b	θ	SD(K)
.0254	.0936	9.8
.0525	.0896	6.5
.0797	.0948	4.6
.1610	.1126	5.8
.2424	.1384	4.5
.4322	.1807	4.5
.6220	.2746	7.2
.8119	.3591	7.1
.8661	.4173	13.1
.9203	.5098	8.2
.9475	.5679	10.7
.9746	.6270	6.7

a/b=0.5, α=45

Tbot=399.5 ± 5.6 (C), Tbac=400.5 ± 4.8 (C)

Ttop=317.8 ± 1.8 (C), T_∞ =21.0 (C)

$\Delta T/T_\infty$ =1.19 , Gr=4.03 E7, Gr/Re**2=2.35

y/a=0.0, z/c=0.0, N = 100

x/b	θ	SD(K)
.0254	.0654	7.0
.0525	.0933	8.4
.0797	.1212	10.6
.1610	.1883	13.6
.2424	.2541	7.6
.4322	.2834	6.5
.6220	.3209	7.6
.8119	.2714	10.2
.8661	.3624	10.5
.9203	.4083	6.9
.9475	.4404	8.5
.9746	.5144	8.2

a/b=0.5, α =45

Tbot=398.3 ± 6.2 (C), Tbac=398.0 ± 4.9 (C)

Ttop=311.4 ± 2.1 (C), T_∞ =21.5 (C)

$\Delta T/T_\infty$ =1.18 , Gr=4 E7, Gr/Re**2=1.16

y/a=0.0, z/c=0.0, N = 100

x/b	θ	SD(K)
.0254	.0693	7.2
.0525	.0742	8.0
.0797	.0774	8.5
.1610	.1113	12.5
.2424	.1427	12.3
.4322	.2053	12.8
.6220	.2261	9.0
.8119	.1579	9.2
.8661	.2272	7.1
.9203	.3445	4.8
.9475	.4049	5.8
.9746	.4938	5.1

a/b=1.0, α=0 , Free Convection (Re=0)

Tbot=399.5 ± 5.8 (C), Tbac=400.1 ± 6.2 (C)

Ttop=327.2 ± 4.6 (C), T_∞ =24.5 (C)

$\Delta T/T_\infty$ =1.18 , Gr=4.0 E7 , N = 50

y/a=0.0, $z/\frac{c}{2}$=0.0

x/b	θ	SD(K)
.0254	.5118	15.8
.0525	.2518	12.9
.0797	.1105	12.5
.1610	.0276	2.2
.2424	.0285	1.3
.4322	.0262	0.5
.6220	.0410	8.1
.8119	.1735	19.9
.8661	.2019	17.9
.9203	.2692	12.9
.9475	.3156	19.7
.9746	.4164	19.0

a/b=1.0, α=0

Tbot=400.3 ± 5.4 (C), Tbac=402 ± 5.8 (C)

Ttop=334.5 ± 4.5 (C), T_∞ =24.5 (C), N =100

$\Delta T/T_\infty$ =1.19, Gr=4.03 E7, Gr/Re**2=225.29

y/a=0.0, $z/\frac{c}{2}$=0.0

x/b	θ	SD(K)
.0254	.4647	2.9
.0525	.2503	3.8
.0797	.0886	1.5
.1610	.0240	0
.2424	.0296	0
.4322	.0274	0.4
.6220	.0347	4.1
.8119	.1651	12.0
.8661	.2257	16.4
.9203	.2949	12.3
.9475	.3505	14.5
.9746	.4495	14.7

a/b=1.0, α=0

Tbot=400.2 ±5.3 (C), Tbac=400.8 ±5.7 (C)

Ttop=335.4 ±4.5 (C), T_∞ =24.5 (C)

$\Delta T/T_\infty$ =1.19 , Gr=4.03 E7

Gr/Re**2=15.6 , N = 50

y/a=0.0, z/c=0.0

x/b	$\bar{\theta}$	SD(K)
.0254	.3607	2.4
.0525	.1394	2.8
.0797	.0308	0.5
.1610	.0212	0
.2424	.0271	0.3
.4322	.0240	0
.6220	.0225	1.3
.8119	.1476	12.4
.8661	.2021	12.7
.9203	.2916	9.2
.9475	.3754	16.0
.9746	.5089	13.0

a/b=1.0, α =0

Tbot=400.2± 5.5 (C), Tbac=402.2 ± 6.1 (C)

Ttop=335.1 ±4.5 (C), T_∞ =24.5 (C)

$\Delta T/T_\infty$ =1.19 , Gr=4.03 E7

Gr/Re**2=5.36 , N = 50

y/a=0.0, z/c=0.0

x/b	$\bar{\theta}$	SD(K)
.0254	.2309	7.0
.0525	.0485	3.5
.0797	.0186	0
.1610	.0192	0.5
.2424	.0254	0.5
.4322	.0211	0
.6220	.0423	4.1
.8119	.1474	7.5
.8661	.2075	15.5
.9203	.2943	11.3
.9475	.3705	14.0
.9746	.4925	11.9

a/b=1.0, α=0

Tbot=400.8 ± 5.6 (C), Tbac=404.4 ± 6.1 (C)

Ttop=336.5 ± 4.8 (C), T_∞ =24.5 (C)

$\Delta T/T_\infty$ =1.2 , Gr=4.06 E7

Gr/Re**2=2.28 , N = 50

y/a=0.0, z/$\frac{c}{2}$=0.0

x/b	θ	SD(K)
.0254	.1665	5.2
.0525	.0334	1.1
.0797	.0183	0
.1610	.0183	0
.2424	.0239	0
.4322	.0202	0.5
.6220	.0320	2.9
.8119	.1269	5.0
.8661	.1769	10.9
.9203	.2730	9.4
.9475	.3578	13.2
.9746	.4993	10.0

a/b=1.0, α=0

Tbot=400.2 ± 6.0 (C), Tbac=404.8 ± 5.8 (C)

Ttop=336.7 ± 5.0 (C), T_∞ =24.5 (C)

$\Delta T/T_\infty$ =1.2 , Gr=4.06 E7

Gr/Re**2=1.14 , N = 100

y/a=0.0, z/$\frac{c}{2}$=0.0

x/b	θ	SD(K)
.0254	.0239	0.6
.0525	.0183	0
.0797	.0157	0.2
.1610	.0183	0
.2424	.0211	0
.4322	.0183	0
.6220	.0213	2.2
.8119	.0949	14.2
.8661	.1356	25.9
.9203	.1620	28.8
.9475	.2092	37.0
.9746	.2786	30.2

a/b=1.0, α=0

Tbot=399.8 ± 6.0 (C), Tbac=404.4 ± 5.8 (C)

Ttop=335.5 ± 4.5 (C), T_∞ =25.0 (C)

$\Delta T/T_\infty$ =1.19 , Gr=4.03 E7

Gr/Re**2=0.55 , N = 100

y/a=0.0, $z/\frac{c}{2}$=0.0

x/b	θ	SD(K)
.0254	.0166	0.4
.0525	.0169	0
.0797	.0147	0.4
.1610	.0169	0
.2424	.0203	0.4
.4322	.0169	0
.6220	.0163	0.5
.8119	.0178	0.5
.8661	.0231	5.5
.9203	.0307	7.6
.9475	.0513	13.2
.9746	.1124	19.5

a/b=1.0, α=20 , Free Convection (Re=0)

Tbot=401.3 ± 5.5 (C), Tbac=416.6 ± 6.2 (C)

Ttop=348.5 ± 4.6 (C), T_∞ =20.0 (C)

$\Delta T/T_\infty$ =1.26 , Gr=4.27 E7 , N = 100

y/a=0.0, $z/\frac{c}{2}$=0.0

x/b	θ	SD(K)
.0254	.3704	8.4
.0525	.1245	7.5
.0797	.0450	3.1
.1610	.0304	0.6
.2424	.0274	0.8
.4322	.0263	0.7
.6220	.0369	3.2
.8119	.2034	11.9
.8661	.2871	14.6
.9203	.4187	11.2
.9475	.4317	20.4
.9746	.5548	12.7

a/b=1.0, α=20

Tbot=402.8 ± 5.2 (C), Tbac=418.1 ± 6.1 (C)

Ttop=351.3 ± 4.7 (C), T_∞ =20.0 (C)

$\Delta T/T_\infty$ =1.26 , Gr=4.27 E7 , Gr/Re**2=231.87

y/a=0.0, $z/\frac{c}{2}$=0.0 , N = 100

x/b	θ	SD(K)
.0254	.3566	0.6
.0525	.1082	0.3
.0797	.0405	0
.1610	.0329	0.4
.2424	.0297	0
.4322	.0283	0.5
.6220	.0340	0.5
.8119	.1756	15.2
.8661	.3127	19.2
.9203	.4599	21.9
.9475	.4524	19.9
.9746	.4958	8.7

a/b=1.0, α=20

Tbot=403.3 ± 5.5 (C), Tbac=418.4 ± 5.8 (C)

Ttop=353.4 ± 4.5 (C), T_∞ =20.5 (C)

$\Delta T/T_\infty$ =1.26 , Gr=4.27 E7, Gr/Re**2=16.64

y/a=0.0, z/c=0.0, N = 100

x/b	θ	SD(K)
.0254	.2974	12.3
.0525	.0283	2.4
.0797	.0175	0
.1610	.0272	0.7
.2424	.0256	1.7
.4322	.0372	2.7
.6220	.0563	2.1
.8119	.1716	14.8
.8661	.2872	19.9
.9203	.3852	19.9
.9475	.4604	23.7
.9746	.5339	13.8

a/b=1.0, α=20

Tbot=400.3 ± 4.9 (C), Tbac=424.2 ± 3.9 (C)

Ttop=346.4 ± 4.1 (C), T_∞ =21.0 (C)

$\Delta T/T_\infty$ =1.26 , Gr=4.27 E7, Gr/Re**2=5.75

y/a=0.0, z/c=0.0, N = 50

x/b	θ	SD(K)
.0254	.0322	4.5
.0525	.0176	0.5
.0797	.0162	0.7
.1610	.0181	2.0
.2424	.0320	2.8
.4322	.0639	2.3
.6220	.1078	5.9
.8119	.2610	12.3
.8661	.3084	21.2
.9203	.3740	11.6
.9475	.4517	11.3
.9746	.5188	9.7

a/b=1.0, α =20

Tbot=403.4 ±5.7 (C), Tbac=428.1 ± 3.8 (C)

Ttop=352.0 ±4.2 (C), T_∞ =21.0 (C)

$\Delta T/T_\infty$ =1.27 , Gr=4.31 E7, Gr/Re**2=2.47

y/a=0.0, $z/\frac{c}{2}$=0.0, N = 50

x/b	θ	SD(K)
.0254	.0177	0.5
.0525	.0182	0.4
.0797	.0150	0.5
.1610	.0134	0
.2424	.0187	0
.4322	.0313	4.9
.6220	.1218	6.9
.8119	.2509	6.2
.8661	.2908	9.7
.9203	.3515	5.6
.9475	.4110	6.3
.9746	.5296	7.9

a/b=1.0, α=20

Tbot=404.2 ±6.2 (C), Tbac=429.3 ± 3.8 (C)

Ttop=353.2 ±4.2 (C), T_∞ =21.0 (C)

$\Delta T/T_\infty$ =1.27 , Gr=4.31 E7, Gr/Re**2=1.24

y/a=0.0, $z/\frac{c}{2}$=0.0, N = 50

x/b	θ	SD(K)
.0254	.0160	0
.0525	.0160	0.2
.0797	.0136	0.3
.1610	.0112	0.4
.2424	.0187	0.9
.4322	.0200	3.7
.6220	.0203	3.9
.8119	.2005	6.9
.8661	.2968	6.2
.9203	.3540	2.5
.9475	.4311	4.3
.9746	.5382	3.6

a/b=1.0, α=20

Tbot=401.0 ± 5.8 (C), Tbac=413.3 ± 5.7 (C)

Ttop=347.9 ± 5.3 (C), T_∞ =20.5 (C)

$\Delta T/T_\infty$ =1.25 , Gr=4.24 E7, Gr/Re**2=0.58

y/a=0.0, z/c/2=0.0, N = 50

x/b	θ	SD(K)
.0254	.0177	1.2
.0525	.0166	2.1
.0797	.0136	0.7
.1610	.0213	1.9
.2424	.0202	2.3
.4322	.0218	3.3
.6220	.0338	6.0
.8119	.0286	3.5
.8661	.0398	6.2
.9203	.1096	8.6
.9475	.2300	8.0
.9746	.3745	6.1

a/b=1.0, α=45 , Free Convection (Re=0)

Tbot=401.0 ± 5 (C), Tbac=421.3 ± 5.7 (C)

Ttop=358.1 ± 4.3 (C), T_∞ =20.5 (C)

$\Delta T/T_\infty$ =1.27 , Gr=4.31 E7

y/a=0.0, z/$\frac{c}{2}$=0.0 , N = 50

x/b	θ	SD(K)
.0254	.3568	6.8
.0525	.1088	5.2
.0797	.0477	3.4
.1610	.0359	0.9
.2424	.0332	0.8
.4322	.0319	0.8
.6220	.0413	2.2
.8119	.2424	9.7
.8661	.3686	12.1
.9203	.4882	9.2
.9475	.5560	9.0
.9746	.6190	10.7

a/b=1.0, α=45

Tbot=399.2 ± 5.1 (C), Tbac=421.5 ± 5.8 (C)

Ttop=358.2 ± 4.4 (C), T_∞ =20.5 (C)

$\Delta T/T_\infty$ =1.27 , Gr=4.31 E7, Gr/Re**2=233.71

y/a=0.0, z/$\frac{c}{2}$=0.0, N = 50

x/b	θ	SD(K)
.0254	.3050	0.5
.0525	.0792	0.6
.0797	.0338	0.3
.1610	.0387	0.3
.2424	.0336	0
.4322	.0341	0.4
.6220	.0405	0.5
.8119	.2040	2.7
.8661	.3232	3.0
.9203	.4542	2.8
.9475	.5315	2.3
.9746	.6199	2.1

a/b=1.0, α=45

Tbot=399.2 ± 5.3 (C), Tbac=421.9 ± 5.8 (C)

Ttop=358.2 ± 4.4 (C), T_∞ =20.5 (C)

$\Delta T/T_\infty$ =1.27 , Gr=4.31 E7, Gr/Re**2=47.19

y/a=0.0, z/c=0.0, N = 50

x/b	θ	SD(K)
.0254	.1680	8.8
.0525	.0212	0.5
.0797	.0199	0.4
.1610	.0368	2.0
.2424	.0480	1.4
.4322	.0537	1.2
.6220	.0582	2.4
.8119	.3264	14.0
.8661	.3819	18.0
.9203	.4605	12.6
.9475	.5118	12.9
.9746	.5870	8.4

a/b=1.0, α=45

Tbot=398.0 ± 6.3 (C), Tbac=421.5 ± 5.8 (C)

Ttop=357.5 ± 4.6 (C), T_∞ =21.0 (C)

$\Delta T/T_\infty$ =1.26 , Gr=4.27 E7, Gr/Re**2=5.65

y/a=0.0, z/c=0.0, N = 50

x/b	θ	SD(K)
.0254	.0789	9.0
.0525	.0703	3.8
.0797	.0805	4.3
.1610	.1102	4.6
.2424	.1212	3.9
.4322	.1584	4.4
.6220	.2182	5.4
.8119	.3412	6.2
.8661	.3779	8.9
.9203	.4231	7.0
.9475	.4783	9.9
.9746	.5448	8.2

a/b=1.0, α=45

Tbot=397.7 ± 7.1 (C), Tbac=420.7± 5.4 (C)

Ttop=355.7 ± 4.6 (C), T_∞ =21.0 (C)

$\Delta T/T_\infty$ =1.26 , Gr=4.27 E7, Gr/Re**2=2.43

y/a=0.0, z/c=0.0, N = 50
2

x/b	θ	SD(K)
.0254	.0235	2.9
.0525	.0410	5.6
.0797	.0613	6.0
.1610	.1547	5.9
.2424	.2122	7.5
.4322	.2918	7.4
.6220	.3402	4.9
.8119	.3855	4.5
.8661	.4023	6.3
.9203	.4141	4.2
.9475	.4638	4.3
.9746	.5456	2.9

a/b=1.0, α=45

Tbot=397.2 ± 7.9 (C), Tbac=418.1± 5.3 (C)

Ttop=351.7 ± 5.1 (C), T_∞ =21.0 (C)

$\Delta T/T_\infty$ =1.25 , Gr=4.24 E7 , Gr/Re**2=1.19

y/a=0.0, z/c=0.0, N=50
2

x/b	θ	SD(K)
.0254	.0495	6.9
.0525	.0560	9.5
.0797	.0823	12.2
.1610	.1215	12.4
.2424	.1666	18.3
.4322	.1967	16.5
.6220	.2236	16.4
.8119	.2739	7.1
.8661	.2929	6.3
.9203	.3062	3.0
.9475	.3799	3.3
.9746	.4622	2.5

a/b=1.0, α=45

Tbot=392.8 ± 5.8 (C), Tbac=412.2 ± 5.4 (C)

Ttop=343.7 ± 5.7 (C), T_∞ =21.0 (C)

$\Delta T/T_\infty$ =1.23 , Gr=4.17 E7

Gr/Re**2=0.57 , N = 50

y/a=0.0, z/c=0.0

x/b	$\bar{\theta}$	SD(K)
.0254	.0671	6.6
.0525	.0600	5.1
.0797	.0630	6.3
.1610	.0788	7.3
.2424	.1031	7.4
.4322	.1307	10.1
.6220	.1473	10.3
.8119	.1553	6.2
.8661	.1782	6.4
.9203	.2329	4.5
.9475	.3053	4.0
.9746	.3802	4.4

a/b=1.46, α=0 , Free Convection (Re=0)

Tbot=398.9 ± 1.7 (C), Tbac=433.5 ± 5.1 (C)

Ttop=326.8 ± 5.0 (C), T_∞ =21.0 (C)

$\Delta T/T_\infty$ =1.24 , Gr=4.2 E7

y/a=0.0, z/c=0.0 , N = 50

x/b	$\overline{\theta}$	SD(K)
.0254	.5999	9.1
.0525	.2589	20.0
.0797	.1305	22.2
.1610	.0268	3.0
.2424	.0312	2.8
.4322	.0274	2.0
.6220	.0583	10.5
.8119	.1716	17.2
.8661	.2132	22.1
.9203	.2786	15.7
.9475	.3243	23.0
.9746	.4527	20.7

a/b=1.46, α=0

Tbot=399.1 ± 2.1 (C), Tbac=432.1 ± 5.0 (C)

Ttop=328.2 ± 5.2 (C), T_∞ =21.0 (C)

$\Delta T/T_\infty$ =1.24 , Gr=4.2 E7, Gr/Re**2=117.37

y/a=0.0, z/c=0.0, N = 50

x/b	$\overline{\theta}$	SD(K)
.0254	.5092	1.4
.0525	.1981	1.1
.0797	.0594	0.6
.1610	.0233	0.5
.2424	.0301	0
.4322	.0274	0
.6220	.0566	5.3
.8119	.2074	6.5
.8661	.2443	8.3
.9203	.3026	9.0
.9475	.3551	11.5
.9746	.4747	9.7

a/b=1.46, α=0

Tbot=399.0 ± 1.4 (C), Tbac=430.9 ± 4.8 (C)

Ttop=327.6 ±5.0 (C), T_∞ =21.0 (C)

$\Delta T/T_\infty$ =1.24 , Gr=4.2 E7, Gr/Re**2=5.66

y/a=0.0, z/$\frac{c}{2}$=0.0, N = 50

x/b	θ	SD(K)
.0254	.2941	4.3
.0525	.0359	1.0
.0797	.0184	0.5
.1610	.0164	0
.2424	.0238	0.5
.4322	.0244	2.3
.6220	.0847	6.0
.8119	.1757	6.3
.8661	.2259	10.1
.9203	.3018	9.5
.9475	.3583	10.9
.9746	.4740	12.5

a/b=1.46, α=0

Tbot=398.6 ±1.5 (C), Tbac=429.6 ± 5.2 (C)

Ttop=326.6 ±5.6 (C), T_∞ =21.0 (C)

$\Delta T/T_\infty$ =1.24 , Gr=4.2 E7, Gr/Re**2=2.43

y/a=0.0, z/$\frac{c}{2}$=0.0, N = 50

x/b	θ	SD(K)
.0254	.1805	7.5
.0525	.0225	0.5
.0797	.0190	0.3
.1610	.0165	0
.2424	.0247	0
.4322	.0283	4.3
.6220	.1044	10.7
.8119	.2113	10.2
.8661	.2376	13.8
.9203	.3077	11.9
.9475	.3453	13.5
.9746	.4407	18.6

a/b=1.46, α =0

Tbot=401.0 ±3.8 (C), Tbac=429.2 ± 5.3 (C)

Ttop=327.0 ±5.7 (C), T_∞ =21.0 (C)

$\Delta T/T_\infty$ =1.24 , Gr=4.2 E7, Gr/Re**2=1.22

y/a=0.0, z/$\frac{c}{2}$=0.0, N = 50

x/b	θ	SD(K)
.0254	.3641	23.5
.0525	.1009	11.8
.0797	.0282	3.6
.1610	.0167	0.3
.2424	.0247	0.2
.4322	.0219	0.8
.6220	.0387	8.0
.8119	.1645	16.6
.8661	.2207	22.3
.9203	.2726	13.5
.9475	.3271	14.7
.9746	.4132	13.2

a/b=1.46, α=0

Tbot=399.7 ± 4.3 (C), Tbac=428.8 ± 4.8 (C)

Ttop=326.7 ± 6.0 (C), T_∞ =21.0 (C)

$\Delta T/T_\infty$ =1.24 , Gr=4.2 E7, Gr/Re**2=0.57

y/a=0.0, z/$\frac{c}{2}$=0.0, N = 100

x/b	θ	SD(K)
.0254	.1879	17.9
.0525	.0596	8.1
.0797	.0261	3.3
.1610	.0165	0
.2424	.0225	0.4
.4322	.0217	0.2
.6220	.0190	0.3
.8119	.0305	3.9
.8661	.0629	16.0
.9203	.1508	13.9
.9475	.2208	18.7
.9746	.3603	13.8

a/b=1.46, α=20 , Free Convection (Re=0)

Tbot=397.5± 5.7 (C), Tbac=397.4 ±5.3 (C)

Ttop=317.7 ± 4.0 (C), T_∞ =21.0 (C)

$\Delta T/T_\infty$ =1.19 , Gr=4.03 E7

y/a=0.0, $z/\frac{c}{2}$=0.0, N = 50

x/b	θ	SD(K)
.0254	.3147	7.4
.0525	.1278	5.2
.0797	.0557	2.4
.1610	.0289	0.4
.2424	.0363	0.5
.4322	.0354	0.5
.6220	.0346	0.4
.8119	.2221	9.9
.8661	.3607	10.4
.9203	.4598	7.4
.9475	.4964	8.3
.9746	.5693	8.2

a/b=1.46, α=20

Tbot=410.9 ±5.3 (C), Tbac=401.5 ± 4.5 (C)

Ttop=321.9 ±4.1 (C), T_∞ =21.5 (C)

$\Delta T/T_\infty$ =1.21 , Gr=4.1 E7, Gr/Re**2=701.55

y/a=0.0, $z/\frac{c}{2}$=0.0 , N = 50

x/b	θ	SD(K)
.0254	.2720	0.6
.0525	.0996	0
.0797	.0409	0.3
.1610	.0266	0
.2424	.0351	0
.4322	.0322	0
.6220	.0294	0
.8119	.1854	4.2
.8661	.3102	5.9
.9203	.4593	4.7
.9475	.5059	5.6
.9746	.5709	5.5

a/b=1.46, α=20

Tbot=409.0 ± 5.9 (C), Tbac=401.8 ± 5.1 (C)

Ttop=323.9 ± 4.7 (C), T_∞ =21.5 (C)

$\Delta T/T_\infty$ =1.21 , Gr=4.1 E7, Gr/Re**2=5.62

y/a=0.0, z/$\frac{c}{2}$=0.0, N = 50

x/b	θ	SD(K)
.0254	.0230	1.8
.0525	.0193	0.5
.0797	.0179	0.2
.1610	.0185	1.8
.2424	.0378	0.7
.4322	.0872	3.3
.6220	.1391	6.6
.8119	.3050	14.3
.8661	.3361	18.8
.9203	.4197	14.2
.9475	.4432	14.7
.9746	.4999	13.0

a/b=1.46, α=20

Tbot=408.6 ± 6.7 (C), Tbac=402.2 ± 4.9 (C)

Ttop=324.7 ± 4.8 (C), T_∞ =21.5 (C)

$\Delta T/T_\infty$ =1.21 , Gr=4.1 E7, Gr/Re**2=2.39

y/a=0.0, z/$\frac{c}{2}$=0.0, N = 50

x/b	θ	SD(K)
.0254	.0182	0
.0525	.0193	0.5
.0797	.0179	0.3
.1610	.0154	0
.2424	.0218	0.6
.4322	.0294	4.6
.6220	.1308	11.2
.8119	.2599	8.0
.8661	.3132	14.1
.9203	.3664	6.9
.9475	.3964	10.1
.9746	.4599	9.3

a/b=1.46, α=20

Tbot=408.0 ± 7.3 (C), Tbac=400.7 ± 4.9 (C)

Ttop=323.2 ± 5.3 (C), T_∞ =21.5 (C)

$\Delta T/T_\infty$ =1.21 , Gr=4.1 E7, Gr/Re**2=1.18

y/a=0.0, z/c=0.0, N = 50

x/b	θ	SD(K)
.0254	.0183	0
.0525	.0185	0.3
.0797	.0171	0.5
.1610	.0155	0
.2424	.0202	0.5
.4322	.0157	0.3
.6220	.0340	4.0
.8119	.1996	10.3
.8661	.2780	8.9
.9203	.3420	4.4
.9475	.3651	4.8
.9746	.4536	4.3

a/b=1.46, α=20

Tbot=408.4 ± 7.8 (C), Tbac=399.0 ± 4.9 (C)

Ttop=317.3 ± 5.8 (C), T_∞ =22.0 (C)

$\Delta T/T_\infty$ =1.21 , Gr=4.1 E7, Gr/Re**2=0.58

y/a=0.0, z/c=0.0 , N = 50

x/b	θ	SD(K)
.0254	.0170	0
.0525	.0170	0
.0797	.0142	0
.1610	.0142	0
.2424	.0181	0.5
.4322	.0153	0.5
.6220	.0142	0
.8119	.0179	1.1
.8661	.0326	3.7
.9203	.1116	6.7
.9475	.1576	8.2
.9746	.2757	6.5

a/b=1.46, α=45 , Free Convection (Re=0)

Tbot=403.5 ± 5.7 (C), Tbac=400.2 ± 4.4 (C)

Ttop=327.9 ± 3.7 (C), T_∞ =22.0 (C)

$\Delta T/T_\infty$ =1.2 , Gr=4.06 E7

y/a=0.0, z/c=0.0 , N = 50
$\frac{}{2}$

x/b	θ	SD(K)
.0254	.3877	8.2
.0525	.1298	6.9
.0797	.0524	2.1
.1610	.0290	0.8
.2424	.0358	0.9
.4322	.0343	0.5
.6220	.0448	3.5
.8119	.2706	6.9
.8661	.3809	7.8
.9203	.5124	5.5
.9475	.5653	8.0
.9746	.6410	5.8

a/b=1.46, α=45

Tbot=403.5 ± 5.7 (C), Tbac=399.8 ± 4.3 (C)

Ttop=328.4 ± 3.7 (C), T_∞ =22.0 (C)

$\Delta T/T_\infty$ =1.2 , Gr=4.06 E7, Gr/Re**2=695.75

y/a=0.0, z/c=0.0, N = 50
$\frac{}{2}$

x/b	θ	SD(K)
.0254	.3685	0.4
.0525	.1154	0.2
.0797	.0431	0.4
.1610	.0282	0
.2424	.0366	0
.4322	.0363	0.3
.6220	.0343	0.4
.8119	.2314	2.8
.8661	.3702	2.9
.9203	.5155	2.0
.9475	.5839	1.8
.9746	.6441	1.3

a/b=1.46, α=45

Tbot=405.7 ± 5.7 (C), Tbac=400.7 ± 4.3 (C)

Ttop=329.2 ± 3.9 (C), T_∞ =22.0 (C)

$\Delta T/T_\infty$ =1.21 , Gr=4.1 E7, Gr/Re**2=47.33

y/a=0.0, z/c=0.0, N = 100

x/b	θ	SD(K)
.0254	.2098	5.9
.0525	.0255	0.4
.0797	.0208	0.5
.1610	.0281	1.5
.2424	.0477	2.0
.4322	.0547	1.2
.6220	.0819	7.1
.8119	.2738	12.8
.8661	.3436	15.1
.9203	.4415	10.7
.9475	.5153	12.3
.9746	.5896	9.3

a/b=1.46, α =45

Tbot=403.7 ± 6.6 (C), Tbac=401.1 ± 4.4 (C)

Ttop=327.6 ± 4.1 (C), T_∞ =22.0 (C)

$\Delta T/T_\infty$ =1.2 , Gr=4.06 E7, Gr/Re**2=5.6

y/a=0.0, z/c=0.0, N = 50

x/b	θ	SD(K)
.0254	.0847	10.2
.0525	.0759	3.3
.0797	.0827	3.6
.1610	.1021	3.9
.2424	.1246	3.8
.4322	.1603	5.0
.6220	.2231	6.2
.8119	.3266	6.0
.8661	.3775	7.3
.9203	.4304	6.0
.9475	.4788	8.2
.9746	.5333	9.9

a/b=1.46, α=45

Tbot=403.7 ±7.8 (C), Tbac=402.5 ±4.4 (C)

Ttop=326.3 ± 4.6 (C), T_∞ =22.0 (C)

$\Delta T/T_\infty$ =1.2 , Gr=4.06 E7, Gr/Re**2=2.39

y/a=0.0, z/c=0.0, N = 50

x/b	$\bar{\theta}$	SD(K)
.0254	.0166	0.4
.0525	.0172	0.3
.0797	.0208	0.7
.1610	.0813	3.6
.2424	.1719	3.4
.4322	.2653	1.6
.6220	.3159	2.0
.8119	.3226	1.7
.8661	.3941	4.1
.9203	.4290	2.4
.9475	.4706	2.5
.9746	.5266	2.0

a/b=1.46, α=45

Tbot=403.2 ±8.5 (C), Tbac=400.5 ±4.0 (C)

Ttop=322.8 ±5.1 (C), T_∞ =22.0 (C)

$\Delta T/T_\infty$ =1.2 , Gr=4.06 E7, Gr/Re**2=1.18

y/a=0.0, z/c=0.0 , N = 50

x/b	$\bar{\theta}$	SD(K)
.0254	.0314	2.9
.0525	.0320	3.0
.0797	.0365	3.6
.1610	.0484	4.0
.2424	.0733	2.9
.4322	.1188	3.4
.6220	.2198	3.9
.8119	.2040	3.3
.8661	.3397	3.4
.9203	.3694	1.9
.9475	.4218	1.7
.9746	.4812	1.2

a/b=1.46, α=45

Tbot=408.1 ± 9.5 (C), Tbac=400.9 ± 4.2 (C)

Ttop=319.2 ± 6.1 (C), T_∞ =22.5 (C)

$\Delta T/T_\infty$ =1.2 , Gr=4.06 E7

Gr/Re**2=0.58 , N = 50

y/a=0.0, z/c=0.0
2

x/b	θ	SD(K)
.0254	.0741	5.9
.0525	.0608	4.6
.0797	.0518	4.8
.1610	.0670	7.0
.2424	.0611	4.2
.4322	.0772	4.4
.6220	.0970	5.5
.8119	.1626	2.5
.8661	.2811	4.2
.9203	.3312	2.6
.9475	.3911	2.4
.9746	.4406	2.1

APPENDIX C

Flow Diagram and Listing of Computer Programs for Automatic Data Acquisition and Statistical Reduction

Brief Description

The main program is started by entering the system parameters through the console terminal such as: calibration factor (or fringe spacing), beam intersection angle, γ; index of refraction of fluid medium; the sampling size, N; the net frequency shift, f_s; the origin of the space coordinate, $\vec{X}_0$, the coordinate rotation angle, ϕ; and the permanent data file name, etc.

With reference to the flow diagram below:

1. The INTRAL subroutine requires the user to enter the parameters controlling the next sequence of stepping motor movements, which include the initial position, $\vec{X}_i$, the increment, $\Delta\vec{X}_i$, and the number of measuring positions, NMP.

2. The MOTMOV subroutine deals with the DR 11-M output interface board to direct the stepping motor movements.

3. The HANSHK subroutine deals with the DR 11-L input interface board to perform the data fetching and the storage of the data in a temporary array.

4. The CONVRS subroutine converts the data from binary form to decimal equivalent. The statistical reduction and storage of the data into a permanent file are subsequently accomplished.

5. The mean values and turbulent stresses are then displayed on the console terminal following the bell rings.

6. The LPRNTR subroutineprints the data on the line printer.

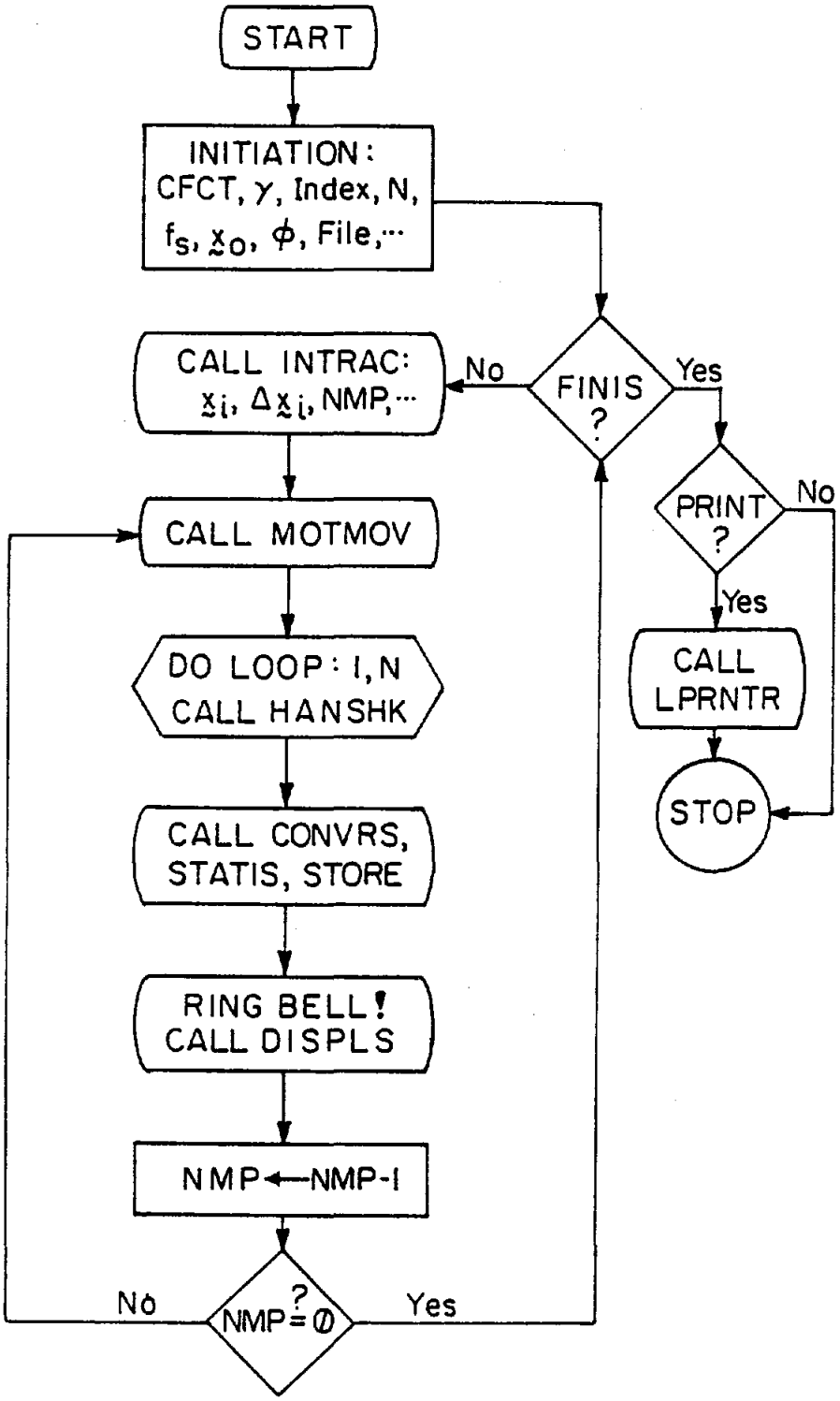
START
INITIATION:
CFCT, γ, Index, N,
f_s, $\underset{\sim}{x}_0$, φ, File,···
FINIS ?
No
Yes
CALL INTRAC:
$\underset{\sim}{x}_i$, $\Delta\underset{\sim}{x}_i$, NMP,···
PRINT ?
No
Yes
CALL MOTMOV
CALL LPRNTR
DO LOOP: I, N
CALL HANSHK
STOP
CALL CONVRS,
STATIS, STORE
RING BELL!
CALL DISPLS
NMP←NMP-1
NMP = 0 ?
No
Yes

```
      PROGRAM DAMLDV
C     ********************************************************************
C     DATA ACQUISITION PACKAGE FOR LDV 1- OR 2-COMPONENT MEASUREMENTS *
C     ************************* AUTHOR: A. MODAVI  ********************
C     ************************* REVISED: K-S CHEN  ********************
C                                                                       *
C     STORES POSITION [XYZ(3)], MEAN AND RMS VALUES, ETC., IN THE       *
C     FILE UNDER 'FILNAM'. DK: MUST BE ASSIGNED TO UNIT #2.             *
C                                                                       *
C     MAIN PROGRAM IS IN FILE UNDER (FILE DAPLDV.SUM) WHICH CONSISTS    *
C     OF FIVE SECTIONS GROUPED INTO TWO CHAPTERS AS FOLLOWING:          *
C                                                                       *
C                         DAMLDV.SE1 --*                                *
C                         DAMLDV.SE2   * DAMLDV.CH1 --*                 *
C                         DAMLDV.SE3 --*               * (DAMLDV.SUM)   *
C                                                      *                *
C                         DAMLDV.SE4 --* DAMLDV.CH2 --*                 *
C                         DAMLDV.SE5 --*                                *
C                                                                       *
C           SUBROUTINES: INTRAC (FILE UNDER INTRAC.FOR) -*              *
C                        INCREM (FILE UNDER INCREM.FOR)  * (ROUT.001)   *
C                        MOTMOV (FILE UNDER MOVMOT.FOR) -*              *
C                                                                       *
C                        HANSHK (FILE UNDER HANSHK.FOR) -*              *
C                        CONVRS (FILE UNDER CONVRS.FOR)  * (ROUM.002)   *
C                        DISPLS (FILE UNDER DISPLS.FOR) -*              *
C                                                                       *
C                        SDEROR (FILE UNDER SDEROR.FOR) -*              *
C                        STORE  (FILE UNDER STORE .FOR)  * (ROUT.003)   *
C                        LPRNTR (FILE UNDER LPRNTR.FOR) -*              *
C                                                                       *
C                        DSAFLT (FILE UNDER DSAFLT.MAC)                 *
C                                                                       *
C     ********************** DAMLDV.SE1 ENDS ***************************
```

```
C  ********************* DAMLDV.SE2 BEGINS  ************************
   LOGICAL*1 FILNAM(11),LIKE,INITI,FINISH,IDIR
   INTEGER CSRL0A,DBRL0A,CNTCSR,CSRL0B,DBRL0B,ADSCSR,ADSDBR
   INTEGER ABORT(5),IFD(2,1000),COUNTR,COIN
   REAL LP,XYZ(3),SHIFT(2),CFCT(2),INCX,INCY,INCZ,TSHIFT(2),TCFCT(2)
   COMMON /ADSREG/CSRL0A,DBRL0A,CSRL0B,DBRL0B,ADSCSR,ADSDBR
  &       /FILE/FILNAM/FCTRS/CFCT/COMP/NCHANL,COUNTR/RECOD/NRECOD
  &       /RINDEX/RICX,RICY,RICZ/FRQSFT/SHIFT/BFLOW/VBULK/SIZE/IRES
  &       /OLD/XFOLD,YFOLD,ZFOLD/POP/NPOP/SRVB1/IFD,NC/INTFCE/COIN
  &       /DATA/XI,YI,ZI,XF,YF,ZF,DX,DY,DZ,SIGNX,SIGNY,SIGNZ
  &       /ASK1/X0,Y0,Z0/ASK2/ICO/MOVE/LP,XYZ/SIGN/SIGNA,SIGNB
   COMMON /ARG/UMEAN,VMEAN,UMS,VMS,UVMS,U2V,V2U,UMEAN1,VMEAN1,UMS1,
  &VMS1,UVMS1,U2V1,V2U1/INCL/ANGLE/SWEEP/IDIR/TIL/THETA
   COMMON /ARGF/UMF,VMF,UMSF,VMSF,UVMSF,U2VF,V2UF,UMT,VMT,UMST,
  &VMST,UVMST,U2VT,V2UT/TWM/TSHIFT,TCFCT
   COMMON /SERORW/SU,SV,SUU,SVV,SUVU,SUVL,R/PLAY/NPRTR
   COMMON /SERORU/SU1,SV1,SUU1,SVV1,SUVU1,SUVL1,R1
   COMMON /SERORF/SUF,SVF,SUUF,SVVF,SUVUF,SUVLF,RF
   COMMON /SERORT/SUT,SVT,SUUT,SVVT,SUVUT,SUVLT,RT
C  INITIATION
   DATA FILNAM/6*'0',',',3*'0',' '/,XYZ/3*0.0/,NPRTR/0/
   DATA XI,YI,ZI,XF,YF,ZF,DX,DY,DZ/9*0.0/,ICO/'CA'/
   DATA X0,Y0,Z0/3*0.0/,FINISH/.FALSE./NRECOD/0/,NPOP/1/
   CSRL0A='164010
   DBRL0A='164012
   CSRL0B='164014
   DBRL0B='164016
   TYPE *,' ENTER CHANNEL NO. ('1':1-COMPONENT;'2':2-COMPONENT)'
   ACCEPT *,NCHANL
   IF(NCHANL .EQ. 2) GO TO 36
   TYPE *,' ENTER COUNTER NO. ('1':COUNTER-A;'2':COUNTER-B)'
   ACCEPT *, COUNTR
   ADSCSR=CSRL0A+4*(COUNTR-1)
   ADSDBR=DBRL0A+4*(COUNTR-1)
   GO TO 39
36 TYPE *,' COINCIDENCE IN TWO CHANNELS ? ENTER 'Y':YES; 'N':NO'
   ACCEPT 38, COIN
   TYPE *,' ENTER FREQ. SHIFT FOR 'TWM' IN ONE-CHANNEL MEASUREMENT'
   ACCEPT *,TSHIFT
   TYPE *,' ENTER CALI. FACTORS FOR 'TWM' IN ONE-CHANNEL MEASUREMENT'
   ACCEPT *, TCFCT
38 FORMAT(A1)
   ADSCSR=CSRL0B
   ADSDBR=DBRL0B
39 ABORT(1)=ADSCSR
   ABORT(2)=0
   ABORT(3)='164000
   ABORT(4)=0
   ABORT(5)=0
   TYPE *,' ENTER THE ANGLE FOR COORDINATE TRANSFORMATIO IN DEG.'
   ACCEPT *, THETA
   THETA=THETA/180.*3.1415926
C  ********************* DAMLDV.SE2 ENDS  ************************
```

```
C  ********************  DAMLDV.SE3 BEGINS ************************
   CALL DEVICE(ABORT)
C  COMPUTE INTERRUPT VECTOR & PRIORITY LEVEL
   CNTCSR= IPEEK(ADSCSR)
   IPRIL0=((CNTCSR .AND. '60)/'20)+4
   IVECL0= (CNTCSR .AND. '77000)/'100
C  FILE STORAGE SPECIFICATION
   TYPE *,' ENTER BEGINNING FOUR CHARACTERS IN THE FILE SPEC.'
   READ(5,10) (FILNAM(I),I=1,4)
10 FORMAT(4A1)
   WRITE(5,11) (FILNAM(I),I=1,4)
11 FORMAT(' BEGINNING FILE SPEC. CHOSEN IS ',/, 5X,4A1)
   TYPE *,' ENTER LAST THREE CHARACTERS IN THE FILE SPEC., E.G.,"001"
  &, OR "DAT"'
   READ(5,12) (FILNAM(I),I=8,10)
12 FORMAT(3A1)
   TYPE 14, FILNAM
14 FORMAT(' YOUR STORED FILE NAME IS  ', 11A1)
C  ENTER SIGN FOR BOTH COUNTERS
   TYPE *,' ENTER SIGNS IN TWO CHANNELS'
   TYPE *,' IF (FLO > FO), ENTER "-1"; OTHERWISE ENTER "1"'
   ACCEPT *, SIGNA, SIGNB
C  ENTER NC (NUMBER OF COUNTS TO BE TAKEN)
   TYPE *,' ENTER NO. OF COUNTS/POPULATION (EVEN INTEGER, MAX.:1000)'
   ACCEPT *,NC
C  ENTER CALIBRATION FACTOR (SEE DISA MANUAL)
   TYPE *,' ENTER CALIBRATION FACTOR IN BOTH CHANNELS (M/S/MHZ)'
   ACCEPT *, CFCT
C  ENTER FREQUENCY SHIFT.
   TYPE *,' ENTER FREQUENCY SHIFTS IN BOTH CHANNELS (MHZ)'
   ACCEPT *, SHIFT
   SHIFT(1)=ABS(SHIFT(1))
   SHIFT(2)=ABS(SHIFT(2))
   TYPE *,' ENTER THE COORDINATES "XYZ" OF STARTING POINT'
   ACCEPT *, XYZ
   TYPE *,' ENTER SWEEPING DIR. FOR TR-TABLE, "Y":Y-DIR.,"Z":Z-DIR'
   ACCEPT 17, IDIR
17 FORMAT(A1)
   TYPE *,' ENTER THE BEAM INCLINATION ANGLE IN (DEG.)'
   ACCEPT *, ANGLE
   ANGLE=3.1415926*ANGLE/180.
C  ENTER BULK VELOCITY (OR REFERENCE VELOCITY)
   TYPE *,' ENTER BULK VELOCITY (M/S)'
   ACCEPT *,VBULK
C  ENTER CORRECTIONS FOR CHANGE IN INDEX OF REFRACTION
   TYPE *,' ENTER REFRACTIVE INDEX CORRECTION FACTORS:RICX,RICY,RICZ'
   ACCEPT *,RICX,RICY,RICZ
C  ************************ DAMLDV.SE3 ENDS ************************
```

```
C  ************************  DAMLDV.SE4 BEGINS  ********************
C  SET DAE
   CALL IPOKE(CSRL0A,'400)
   CALL IPOKE(CSRL0B,'400)
   TYPE *,' '
   TYPE *,'  COUNTER ON FREE RUN & INTERRUPT DISABLE'
   TYPE *,'  '
   TYPE *,' DISABLE XYZ TABLE JOYSTICK (SWITCH TO COMP. CONTROL)'
   PAUSE
   TYPE *,' NOW POSITION XYZ TABLE BY JOYSTICK IF YOU WISH'
   TYPE *,' WHEN IN POSITION SWITCH TO COMP. CONTROL & RETURN'
   PAUSE
   TYPE *,' ******* READY FOR DATA ACQUISITION *******'
   PAUSE
C  ENABLE THE COUNTER
   CALL IPOKE(CSRL0A,1)
   CALL IPOKE(CSRL0B,1)
C  INITIALIZE THE ARMING OF THE COUNTERS
   IDM=IPEEK(DBRL0A)
   IDM=IPEEK(DBRL0B)
C
C  OPEN THE FILE ON THE UNIT 2 FOR THE STORAGE OF DATA
   IRES=3*2+4*2
   IF(NCHANL .EQ. 2) IRES=3*2+14*4
   OPEN(UNIT=2,NAME=FILNAM,TYPE='NEW',FORM='UNFORMATTED',
  & ACCESS='DIRECT',RECORDSIZE=IRES)
C  ************************  DAMLDV.SE4 ENDS  ************************
```

```
C    ********************  DAMLDV.SE5 BEGINS  ********************
     NMPSUM=0
295  XFOLD=XYZ(1)
     YFOLD=XYZ(2)
     ZFOLD=XYZ(3)
     CALL INTRAC(FINISH,NMP)
     NMPSUM=NMPSUM+NMP
     IF(FINISH) GO TO 355
C    MOVING STEPPING MOTOR IS DONE BY CALLING SUBROUTINES 'INCREM' &
C    'MOTMOV'.
     CALL INCREM(INCX,INCY,INCZ)
     GO TO 305
301  CALL MOTMOV(INCX,INCY,INCZ,130,150)
305  WRITE(5,308) XYZ
308  FORMAT(/,' TR MOVES TO',' X=',F7.3,' Y=',F7.3,' Z=',F7.3,/)
     CALL HANSHK
     CALL CONVRS
     CALL DISPLS
C    BELL RINGS TO NOTIFY THAT THE MEASUREMENTS AT A POINT HAS BEEN
C    COMPLETED.
     DO 335 I=1,5
     TYPE *'!BEL'
     IDLE=ISLEEP(0,0,0,30)
335  CONTINUE
     NMP=NMP-1
     CALL SDEROR(NC,UMS,VMS,UVMS,SU,SV,SUU,SVV,SUVU,SUVL,R)
     CALL SDEROR(NC,UMS1,VMS1,UVMS1,SU1,SV1,SUU1,SVV1,SUVU1,SUVL1,R1)
     CALL SDEROR(NC,UMSF,VMSF,UVMSF,SUF,SVF,SUUF,SVVF,SUVUF,SUVLF,RF)
     CALL SDEROR(NC,UMST,VMST,UVMST,SUT,SVT,SUUT,SVVT,SUVUT,SUVLT,RT)
     CALL STORE
     IF(NMP .EQ. 0) GO TO 295
     GO TO 301
     TYPE *,'  '
353  TYPE *,' DO YOU WANT TO PRINT THE DATA ? ENTER 'Y':YES;'N':NO'
     ACCEPT 365, IPRINT
365  FORMAT(A1)
     IF(IPRINT .NE. 'Y') GO TO 370
     CALL LPRNTR(NMPSUM)
     CLOSE(UNIT=2,DISPOSE='SAVE')
     STOP
370  TYPE 375, FILNAM,NMPSUM
375  FORMAT(//,2X,' THE DATA ARE STORED IN THE FILE  ',11A1,
    &'  WITH TOTAL DATA POINTS ',I5)
     CLOSE(UNIT=2,DISPOSE='SAVE')
     STOP
     END
C    ************************  DAMLDV.SE5 ENDS  ********************
```

```
      SUBROUTINE INTRAC(FINISH,NMP)
C     ********************  AUTHOR: A. MODAVI  ********************
C     ********************  MOD.: K-S CHEN  ***********************
C                                                                   *
C     INTERACTIVE SUBROUTINE                                        *
C                                                                   *
C     *******************************************************************
      REAL XYZ(3),LP,CFCT(2),SHIFT(2)
      LOGICAL*1 FINISH
      COMMON /DATA/XI,YI,ZI,XF,YF,ZF,DX,DY,DZ,SIGNX,SIGNY,SIGNZ
      COMMON /MOVE/LP,XYZ/FCTRS/CFCT/FRQSFT/SHIFT/SIGN/SIGNA,SIGNB
      COMMON /INCL/ANGLE
C
      TYPE 50, XYZ
50    FORMAT(/,'  THE LASER IS PROBING AT ','X=',F7.3,' Y=',F7.3,' Z
     &=', F7.3,/)
      TYPE *,' ARE MEASUREMENTS ALL DONE ? ENTER ("T":YES;"F":NO)'
      ACCEPT 40, FINISH
40    FORMAT(L1)
      IF(FINISH) RETURN
C     ENTER INITIAL POSITION OF NEXT MEASUREMENT
      TYPE *,' ENTER XI,YI,ZI,THE INITIAL POSITION OF NEXT MEASUREME
     &NTS'
      ACCEPT *, XI,YI,ZI
C     ENTER THE INCREMENTS IN THIS MOVING SEQUENCE
      TYPE *,' ENTER DX,DY,DZ,THE INCREMENTS OF THIS SEQUENCE'
      ACCEPT *, DX,DY,DZ
C     ENTER THE NO. OF MEASURING POINTS IN THIS SEQUENCE
      TYPE *,' ENTER THE NO. OF MEASURING POINTS IN THIS SEQUENCE'
      ACCEPT *, NMP
C
      TYPE 90, XI,YI,ZI
90    FORMAT(' THE NEXT INITIAL POINT TO BE MEASURED IS ','XI=',F7.3,
     &' YI=',F7.3,' ZI=',F7.3)
      TYPE 95, NMP
95    FORMAT(' THE NO. OF MEASURING POINTS IN THIS SEQUENCE IS', I4,/)
      TYPE *,' ALL SETTINGS REMAIN THE SAME ? ENTER "Y": YES;"N":NO'
      ACCEPT 100, ISET
100   FORMAT(A1)
      IF(ISET .EQ. 'Y') RETURN
      TYPE *,' ENTER THE CALIBRATION FACTORS IN 2 CHANNELS
      ACCEPT *, CFCT
      TYPE *,' ENTER THE FREQ. SHIFT IN 2 CHANNELS'
      ACCEPT *, SHIFT
      TYPE *,' ENTR THE SIGNS IN 2 CHANNELS'
      ACCEPT *, SIGNA,SIGNB
      TYPE *,' ENTER THE BEAM INCLINATION ANGLE IN (DEG.)'
      ACCEPT *, ANGLE
      ANGLE=3.1415926*ANGLE/180.
      RETURN
      END
C     **********************  INTRAC.FOR ENDS ************************
```

```
      SUBROUTINE INCREM(INCX,INCY,INCZ)
C     ******************** AUTHOR: JIMMY WONG *** MOD.: A. MODAVI  *****
C     ********************* FURTHER MOD.: P. TURI, M. ARNAL  ***********
C     ********************* MOD.: K-S CHEN  ****************************
C                                                                       *
C     THE "INCREM" FIRST MOVES THE TRAVERSING TABLE TO THE INITIAL      *
C     MEASURING POSITION, THEN DETERMINE THE MOVING INCREMENTS IN THE   *
C     SUBSEQUENT MEASUREMENTS.                                          *
C                                                                       *
C     ***********************************************************************
      REAL XYZ(3),LP
      REAL INCX,INCY,INCZ
      COMMON /DATA/XI,YI,ZI,XF,YF,ZF,DX,DY,DZ,SIGNX,SIGNY,SIGNZ
     &       /ASK2/ICO/MOVE/LP,XYZ/ASK1/XO,YO,ZO
     &       /POF/NPOF/OLD/XFOLD,YFOLD,ZFOLD
     &       /RINDEX/RICX,RICY,RICZ
C     SET THE VALUE OF "LP", THE SMALLEST MOTOR INCREMENTATION.
      DATA LP/0.005/,SIGNX,SIGNY,SIGNZ/3*1.0/
C     MOVE THE MOTOR TO THE INITIAL POSITION OF SUBSEQUENT MEASURMENTS.
      INCX=(XI-XFOLD)/LP
      INCY=(YI-YFOLD)/LP
      INCZ=(ZI-ZFOLD)/LP
C     CHECK FOR COORDINATE SYSTEM TYPE.
      IF(ICO .EQ. 'CA') GO TO 117
C     IF YOU WANT, SUPPLY YOUR OWN FORMULA
117   INCX=INCX/RICX
      INCY=INCY/RICY
      INCZ=INCZ/RICZ
127   CALL MOTMOV(INCX,INCY,INCZ,130,150)
C     THE MOTOR HAS MOVED TO THE NEXT INITIAL POSITION.
C
C     DETERMINE THE STEPPS OF THE MOVEMENT FOR SUBSEQUENT MEASUREMENTS.
C
      IF(ICO .EQ. 'CA') GO TO 157
C     IF YOU WANT, SUPPLY YOUR OWN FORMULAS
      GO TO 177
157   INCX=SIGNX*DX/LP
      INCY=SIGNY*DY/LP
      INCZ=SIGNZ*DZ/LP
177   INCX=INCX/RICX
      INCY=INCY/RICY
      INCZ=INCZ/RICZ
      RETURN
      END
C     ************************ INCREM.FOR ENDS ************************
```

```
      SUBROUTINE MOTMOV(INCX,INCY,INCZ,LOOP1,LOOP2)
C     ***************************************************************************
C     ************************** AUTHOR: A. MODAVI                                *
C     ************************** MOD.: P. TURI, M. ARNAL                          *
C     ************************** MOD.: K.S. CHEN                                  *
C                                                                                 *
C     "MOTMOV" CONVERTS SPECIFIED MOVEMENT VALUES TO A FORM ACCEPTABLE           *
C     TO THE MOTOR CONTROL INTERFACE AND THEN DEPOSITS THESE VALUES IN           *
C     THE PROPER ADDRESS TO EFFECT MOTOR MOVEMENT.                               *
C                                                                                 *
C     ************************ MOVMOT.SE1 BEGINNS ***********************
      REAL INCX,INCY,INCZ
      REAL LP,XYZ(3)
C     THETA & TILT ARE THE COORDINATE ROTATION ANGLES
      COMMON /MOVE/LP,XYZ/INCL/ANGLE/TIL/THETA
      COMMON /RINDEX/RICX,RICY,RICZ
C     INCREMENTS ARE CONVERTED TO INTEGER VALUES.
      RINCX=INCX*COS(THETA)+INCZ*SIN(THETA)
      RINCY=-INCX*SIN(THETA)+INCZ*COS(THETA)
      RINCZ=INCZ
      IF(RINCX .GE. 0.) RINCX=RINCX+0.5
      IF(RINCX .LT. 0.) RINCX=RINCX-0.5
      IF(RINCY .GE. 0.) RINCY=RINCY+0.5
      IF(RINCY .LT. 0.) RINCY=RINCY-0.5
      IF(RINCZ .GE. 0.) RINCZ=RINCZ+0.5
      IF(RINCZ .LT. 0.) RINCZ=RINCZ-0.5
      INTX=INT(RINCX)
      INTY=INT(RINCY)
      INTZ=INT(RINCZ)
C
      XYZ(1)=XYZ(1)+(INTX*COS(THETA)-INTZ*SIN(THETA))*LP
      XYZ(3)=XYZ(3)+INTY*LP
      XYZ(2)=XYZ(2)+(INTX*SIN(THETA)+INTZ*COS(THETA))*LP
C     ************************ MOVMOT.SE1 ENDS ***************************
```

```
C  ********************** MOVMOT.SE2 BEGINS **********************
C  THE FOLLOWING IS AN EXPLANATION OF THE MOTOR MOVEMENT INTERFACE
C  CONTROL.  THE ADDRESS OF THE MOTOR MOVEMENT REGISTER IS "164002.
C  THIS REGISTER A SIX BIT BINARY NUMBER WHICH INDICATES POSITIVE,
C  NEGATIVE, OR ZERO MOVEMENT IN THE X,Y, AND Z DIRECTIONS. THIS
C  NUMBER HAS THE FOLLOWING FORM:
C
C    DIRECTION:          (Z)      (Y)      (X)
C    SIGN:              +   -    +   -    +   -
C    BIT NUMBER:        6   5    4   3    2   1
C                      --- ---  --- ---  --- ---
C
C
C  IF A POSITIVE MOVEMENT IN THE X,Y, OR Z DIRECTIONS IS DESIRED, THEN
C  A "1" APPEARS IN THE 2,4, OR 6 BIT LOCATIONS, RESPECTIVELY. FOR A
C  NEGATIVE MOVEMENT IN THE X,Y, OR Z DIRECTIONS, A "1" APPEARS IN
C  THE 1,3, OR 5 BIT LOCATIONS,RESPECTIVELY.  FOR ZERO MOVEMENT IN ANY
C  PARTICULAR DIRECTION,A "1" APPEARS IN BOTH BIT LOCATIONS ASSOCIATED
C
C  EXAMPLE : POSITIVE MOVEMENT IN THE X DIRECTION, ZERO MOVEMENT IN
C  THE Y DIRECTION, AND NEGATIVE MOVEMENT IN THE Z DIRECTION--
C
C    DIRECTION:          (Z)      (Y)      (X)
C    BIT NUMBER:        6   5    4   3    2   1
C    BINARY VALUE:      0   1    1   1    1   0
C                      --- ---  --- ---  --- ---
C
C  THE MOVEMENT OCCURS IN INCREMENTS OF 0.005 MM (THIS VALUE IS A
C  CHARACTERISTIC OF THE STEPPING MOTORS USED). TO MOVE DISTANCES
C  GREATER THAN ONE INCREMENT A "DO-LOOP" IS USED.
C
C  ********************** MOVMOT.SE2 ENDS **********************
```

```
C   ********************* MOVMOT.SE3 BEGINS ***********************
500 CONTINUE
C   MOVEMENT IN X DIRECTION
    IF(INTX) 10,11,12
10  I1=1
    INTX=INTX+1
    GO TO 200
11  I1=3
    INTX=INTX+0
    GO TO 200
12  I1=2
    INTX=INTX-1
    GO TO 200
C   MOVEMENT IN THE Y DIRECTION
200 IF(INTY) 20,21,22
20  I2=4
    INTY=INTY+1
    GO TO 300
21  I2=12
    INTY=INTY+0
    GO TO 300
22  I2=8
    INTY=INTY-1
    GO TO 300
C   MOVEMENT IN THE Z DIRECTION
300 IF(INTZ) 30,31,32
30  I3=16
    INTZ=INTZ+1
    GO TO 400
31  I3=48
    INTZ=INTZ+0
    GO TO 400
32  I3=32
    INTZ=INTZ-1
    GO TO 400
C   CALCULATE MOTOR INCRMENT VALUE AND INSERT INTO REGISTER.
400 ISTEP=I1+I2+I3
    CALL IPOKE(*164002,ISTEP)
C   THE SECONDARY TIME DELAY IS TO ALLOW FOR MOTOR MOVEMENT.
    DO 55 I=1,LOOP2
55  CONTINUE
    CALL IPOKE(*164002,63)
C   PRIMARY TIME DELAY LOOP
    DO 50 I=1,LOOP1
50  CONTINUE
C   CHECK IF FURTHER MOVEMENT IS REQUIRED.
    IF(INTX.NE.0 .OR. INTY.NE.0 .OR. INTZ.NE.0) GO TO 500
    RETURN
    END
C   ********************* MOVMOT.SE3 ENDS ************************
```

```
      SUBROUTINE HANSHK
C     HANDSHAKE MONITORNIG OF RQ(BIT 7 OF ADSCSR)
C     ************************  AUTHOR: A.  MODAVI  ****************
C     ************************  REVISED: K-S CHEN   ****************
C
      INTEGER CSRLOA,DBRLOA,CSRLOB,DBRLOB,ADSCSR,ADSDBR,CNTCSR
      INTEGER IFD(2,1000),COUNTR,COIN
      COMMON /ADSREG/CSRLOA,DBRLOA,CSRLOB,DBRLOB,ADSCSR,ADSDBR
      COMMON /COMP/NCHANL,COUNTR/SRVB1/IFD,NC/INTFCE/COIN
      IF(NCHANL .EQ. 2) GO TO 590
      IDM=IPEEK(ADSDBR)
      DO 500 I=1,NC
450   IDM=IPEEK(ADSDBR)
      IF((IPEEK(ADSCSR) .AND. '200) .NE. '200) GO TO 450
      IFD(1,I)=IPEEK(ADSDBR)
500   CONTINUE
      RETURN
C
590   IF(COIN .EQ. 'Y') GO TO 900
600   IDM=IPEEK(DBRLOA)
      IDM=IPEEK(DBRLOB)
      DO 800 I=1,NC
650   IDM=IPEEK(DBRLOA)
      IF((IPEEK(CSRLOA) .AND. '200) .NE. '200) GO TO 650
      IFD(1,I)=IPEEK(DBRLOA)
750   IDM=IPEEK(DBRLOB)
      IF((IPEEK(CSRLOB) .AND. '200) .NE. '200) GO TO 750
      IFD(2,I)=IPEEK(DBRLOB)
800   CONTINUE
      RETURN
C
900   IDM=IPEEK(DBRLOB)
      DO 950 I=1,NC
925   IDM=IPEEK(DBRLOB)
      IF((IPEEK(CSRLOB) .AND. '200) .NE. '200) GO TO 925
      IFD(1,I)=IPEEK(DBRLOA)
      IFD(2,I)=IPEEK(DBRLOB)
950   CONTINUE
      RETURN
      END
C     ************************  HANSHK.FOR ENDS  ********************
```

```
      SUBROUTINE CONVRS
C     ********************** AUTHOR: A. MODAVI **********************
C     ************************** MOD.: J. FLORES, P. TURI *************
C     ************************** MOD.: K-S CHEN    ********************
C     ************************** CONVRS.SE1 BEGINNS  ******************
      REAL CFCT(2),SHIFT(2)
      INTEGER IFD(2,1000),COUNTR
      COMMON /SRVB1/IFD,NC/COMP/NCHANL,COUNTR/FRQSFT/SHIFT
     &       /FCTRS/CFCT/BFLOW/VBULK/SIGN/SIGNA,SIGNB/INCL/ANGLE
      COMMON /ARG/UMEAN,VMEAN,UMS,VMS,UVMS,U2V,V2U,UMEAN1,VMEAN1,UMS1,
     &VMS1,UVMS1,U2V1,V2U1/TWM/TSHIFT(2),TCFCT(2)
      COMMON /ARGF/UMF,VMF,UMSF,VMSF,UVMSF,U2VF,V2UF,UMT,VMT,UMST,
     &VMST,UVMST,U2VT,V2UT
C     FOR THE UNWEIGHTED MEANS
      USUM=0.
      VSUM=0.
      UVSUM=0.
      USUMSQ=0.
      VSUMSQ=0.
      U2VS=0.
      V2US=0.
C     FOR THE WEIGHTED MEANS
      UDEN=0.
      VDEN=0.
      UVDEN=0.
      USQDEN=0.
      VSQDEN=0.
      VELSUM=0.
      U2VDEN=0.
      V2UDEN=0.
C     FOR THE FINITE-WEIGHTED MEANS AS [V] --> 0.
      UDENF=0.
      VDENF=0.
      UVDENF=0.
      USQDNF=0.
      VSQDNF=0.
      VELSMF=0.
      U2VDNF=0.
      V2UDNF=0.
C     FOR THE TIME-WEIGHTED MEANS BASED ON 8 COUNTS OF ZERO-CROSSING
      UDENT=0.
      VDENT=0.
      UDENTP=0.
      VDENTP=0.
      UVDENT=0.
      USQDNT=0.
      VSQDNT=0.
      USQDTP=0.
      VSQDTP=0.
      VELSTU=0.
C     **********************  CONVRS.SE1 ENDS  ************************
```

```
C  ********************  CONVRS.SE2 BEGINNS  **********************
   VELSTV=0.
   VELSUV=0.
   U2VDNT=0.
   V2UDNT=0.
   IF(NCHANL .EQ. 1) V=0.0
   DO 100 I=1,NC
   IDUMY1=IFD(1,I)
   U=SIGNA*(14.96*DSAFLT(IDUMY1)/1000000.-SHIFT(1))*CFCT(1)
   U=U/COS(ANGLE)
   IF(NCHANL .EQ. 2) GO TO 80
   GO TO 90
80 IDUMY2=IFD(2,I)
   V=SIGNB*(14.96*DSAFLT(IDUMY2)/1000000.-SHIFT(2))*CFCT(2)
   UB=TSHIFT(1)*TCFCT(1)
   UG=TSHIFT(2)*TCFCT(2)
   DTU=(8.*CFCT(1))/(UB+U)
   DTV=(8.*CFCT(2))/(UG+V)
   DTF=(DTU+DTV)
90 USUM=USUM+U
   VSUM=VSUM+V
   UU=U*U
   VV=V*V
   UV=U*V
   UVSUM=UVSUM+UV
   USUMSQ=USUMSQ+UU
   VSUMSQ=VSUMSQ+VV
   U2VS=U2VS+UU*V
   V2US=V2US+VV*U
C  FOR WEIGHTED MEANS
   VEL=SQRT(UU+VV)
   VELF=VEL
   IF(VEL .EQ. 0.) VEL=1.0E-28
   IF(VELF .LE. 0.05) VELF=0.05
   VELSUM=VELSUM+1.0/VEL
   UDEN=UDEN+U/VEL
   VDEN=VDEN+V/VEL
   UVDEN=UVDEN+UV/VEL
   USQDEN=USQDEN+UU/VEL
   VSQDEN=VSQDEN+VV/VEL
   U2VDEN=U2VDEN+UU*V/VEL
   V2UDEN=V2UDEN+VV*U/VEL
C  **********************  CONVRS.SE2 ENDS  **********************
```

```
C    ********************  CONVRG.SE3 BEGINNS  ********************
C    FOR FINITE-WEIGHTED MEANS
     VELSMF=VELSMF+1.0/VELF
     UDENF=UDENF+U/VELF
     VDENF=VDENF+V/VELF
     UVDENF=UVDENF+UV/VELF
     USQDNF=USQDNF+UU/VELF
     VSQDNF=VSQDNF+VV/VELF
     U2VDNF=U2VDNF+UU*V/VELF
     V2UDNF=V2UDNF+VV*U/VELF
C    FOR THE TIME-WEIGHTED MEANS
     VELSTU=VELSTU+DTU
     VELSTV=VELSTV+DTV
     VELSUV=VELSUV+DTP
     UDENT=UDENT+U*DTU
     VDENT=VDENT+V*DTV
     USQDNT=USQDNT+UU*DTU
     USQDTP=USQDTP+UU*DTP
     VSQDNT=VSQDNT+VV*DTV
     VSQDTP=VSQDTP+VV*DTP
     UDENTP=UDENTP+U*DTP
     VDENTP=VDENTP+V*DTP
     UVDENT=UVDENT+UV*DTP
     U2VDNT=U2VDNT+UU*V*DTP
     V2UDNT=V2UDTP+VV*U*DTP
100  CONTINUE
     UMEAN1=USUM/NC
     VMEAN1=VSUM/NC
     UMS1=(USUMSQ/NC)-UMEAN1*UMEAN1
     VMS1=(VSUMSQ/NC)-VMEAN1*VMEAN1
     UVMS1=(UVSUM/NC)-UMEAN1*VMEAN1
     U2V1=U2VS/NC-VMEAN1*UMS1-2.*UMEAN1*(UVSUM/NC)-UMEAN1*UMEAN1*
    &VMEAN1
     V2U1=V2US/NC-UMEAN1*VMS1-2.*VMEAN1*(UVSUM/NC)-VMEMN1*VMEAN1*
    &UMEAN1
     URMS=SQRT(ABS(UMS1))
     UTI1=(URMS/VBULK)*100.
C    ********************  CONVRG.SE3 ENDS  ********************
```

```
C  ********************  CONVRS.SE4 BEGINNS  ********************
C  CALCULATE MEAN VALUES USING THE WEIGHTED FORMULA
   UMEAN=UDEN/VELSUM
   VMEAN=VDEN/VELSUM
   UMS=USQDEN/VELSUM-UMEAN*UMEAN
   VMS=VSQDEN/VELSUM-VMEAN*VMEAN
   UVMS=UVDEN/VELSUM-UMEAN*VMEAN
   U2V=U2VDEN/VELSUM-2.*UMEAN*(UVDEN/VELSUM)+2.*(UMEAN*UMEAN)*VMEAN
  &-(USQDEN/VELSUM)*VMEAN
   V2U=V2UDEN/VELSUM-2.*VMEAN*(UVDEN/VELSUM)+2.*(VMEAN*VMEAN)*UMEAN
  &-(VSQDEN/VELSUM)*UMEAN
   URMS=SQRT(ABS(UMS))
   UTI=(URMS/VBULK)*100.
C  CALCULATE MEANS USING FINITE-WEIGHTING
   UMF=UDENF/VELSMF
   VMF=VDENF/VELSMF
   UMSF=USQDNF/VELSMF-UMF*UMF
   VMSF=VSQDNF/VELSMF-VMF*VMF
   UVMSF=UVDENF/VELSMF-UMF*VMF
   U2VF=U2VDNF/VELSMF-2.*UMF*(UVDENF/VELSMF)+2.*(UMF*UMF)*VMF
  &-(USQDNF/VELSMF)*VMF
   V2UF=V2UDNF/VELSMF-2.*VMF*(UVDENF/VELSMF)+2.*(VMF*VMF)*UMF
  &-(VSQDNF/VELSMF)*UMF
C  CALCULATE MEANS USING TIME-WEIGHTING
   IF(VELSTU .LE. 1.0E-8) VELSTU=1.0E-8
   IF(VELSTV .LE. 1.0E-8) VELSTV=1.0E-8
   IF(VELSUV .LE. 1.0E-8) VELSUV=1.0E-8
   UMT=UDENT/VELSTU
   VMT=VDENT/VELSTV
   UMST=USQDNT/VELSTU-UMT*UMT
   VMST=VSQDNT/VELSTV-VMT*VMT
   UVMST=(UVDENT-VMT*UDENTP-UMT*VDENTP)/VELSUV+UMT*VMT
   U2VDNT=(U2VDNT-VMT*USQDTP-UMT*UVDENT-UMT*VMT*UDENTP+UMT*VMT*
  &UDENTP)/VELSUV-(UMT*UMT*VMT)
   V2UDNT=(V2UDNT-UMT*VSQDTP-VMT*UVDENT-VMT*UMT*VDENTP+VMT*UMT*
  &VDENTP)/VELSUV-(VMT*VMT*UMT)
   RETURN
   END
C  ********************** CONVRS.SE4 ENDS **********************
```

```
      SUBROUTINE SDEROR(N,VX,VY,CVXY,SX,SY,SVX,SVY,SVXYU,SVXYL,CXY)
C     ****************************  AUTHOR: K-S CHEN  ****************
C                                                                      *
C     THIS ROUTINE COMPUTES ALL THE STANDARD ERRORS FOR THE STATISTICAL*
C     QUANTITES BETWEEN TWO RANDOM VARIABLES WITH CONFIDENCE INTERVAL  *
C     95%, NAMELY, ZC=1.96.  N IS SAMPLING SIZE.                       *
C                                                                      *
C     ********************  SDEROR.FOR BEGINNS  ************************
      DATA ZC/1.96/
      SIGMX=SQRT(ABS(VX))
      SIGMY=SQRT(ABS(VY))
      RN=FLOAT(N)
      SX=ZC*SIGMX/SQRT(RN)
      SY=ZC*SIGMY/SQRT(RN)
      SVX=ZC*VX*(SQRT(2./RN))
      SVY=ZC*VY*(SQRT(2./RN))
C
      IF((SIGMX .EQ. 0.) .OR. (SIGMY .EQ. 0.)) GO TO 10
      CXY=CVXY/(SIGMX*SIGMY)
      IF(CXY .EQ. 1.) GO TO 10
      ARG=(1.+CXY)/(1.-CXY)
      IF(ARG .LE. 0.) GO TO 10
      Z=0.5*ALOG(ARG)
      IF(RN .LE. 3) GO TO 10
      ZU=Z+ZC*(1./SQRT(RN-3.))
      ZL=Z-ZC*(1./SQRT(RN-3.))
      CXYU=(EXP(2.*ZU)-1.)/(EXP(2.*ZU)+1.)
      CXYL=(EXP(2.*ZL)-1.)/(EXP(2.*ZL)+1.)
      SVXYU=CXYU*(SIGMX*SIGMY)
      SVXYL=CXYL*(SIGMX*SIGMY)
      RETURN
   10 SVXYU=1.0
      SVXYL=1.0
      CXY=1.0
      RETURN
      END
C     ****************************  SDEROR.FOR ENDS  ******************
```

```
      SUBROUTINE STORE
C     ****************************  AUTHOR: K-S CHEN  ************************
C                                                                             *
C     THIS SUBROUTINE STORES THE SAMPLE MEANS & STANDARD DEVIATIONS           *
C     INTO THE FILE 'FILNAM'.                                                 *
C                                                                             *
C     ***************************************************************************
      REAL LP,XYZ(3)
      INTEGER COUNTR
      COMMON /MOVE/LP,XYZ/COMP/NCHANL,COUNTR/RECOD/N
      COMMON /ARG/UARG,VARG,UMSARG,VMSARG,UVMSAG,U2V,V2U,UARG1,
     &            VARG1,UMSAG1,VMSAG1,UVMSA1,U2V1,V2U1
      COMMON /ARGF/UMF,VMF,UMSF,VMSF,UVMSF,U2VF,V2UF,UMT,
     &            VMT,UMST,VMST,UVMST,U2VT,V2UT
      COMMON /SERORW/SU,SV,SUU,SVV,SUVU,SUVL,R
      COMMON /SERORU/SU1,SV1,SUU1,SVV1,SUVU1,SUVL1,R1
      COMMON /SERORF/SUF,SVF,SUUF,SVVF,SUVUF,SUVLF,RF
      COMMON /SERORT/SUT,SVT,SUUT,SVVT,SUVUT,SUVLT,RT
C
      IF(NCHANL .EQ. 2) GO TO 150
      N=N+1
      WRITE(2'N) (XYZ(I),I=1,3), UARG,UMSARG,SIGMAU,SIGUMS,
     &                           UARG1,UMSAG1,SIGMU1,SIUMS1
      RETURN
C
150   N=N+1
      WRITE(2'N) (XYZ(I),I=1,3), UARG,VARG,UMSARG,VMSARG,UVMSAG,
     &           U2V,V2U,SU,SV,SUU,SVV,SUVU,SUVL,R
      N=N+1
      WRITE(2'N) (XYZ(I),I=1,3), UARG1,VARG1,UMSAG1,VMSAG1,UVMSA1,
     &           U2V1,V2U1,SU1,SV1,SUU1,SVV1,SUVU1,SUVL1,R1
      N=N+1
      WRITE(2'N) UMF,VMF,UMSF,VMSF,UVMSF,U2VF,V2UF,SUF,SVF,SUUF,SVVF,
     &          SUVUF,SUVLF,RF
      N=N+1
      WRITE(2'N) UMT,VMT,UMST,VMST,UVMST,U2VT,V2UT,SUT,SVT,SUUT,SVVT,
     &          SUVUT,SUVLT,RT
      RETURN
      END
C     ************************** STORE.FOR ENDS  ***************************
```

```
      SUBROUTINE DISPLS
C     ************************  AUTHOR: K-S CHEN  ********************
C
      INTEGER COUNTR
      COMMON /COMP/NCHANL,COUNTR/PLAY/N
      COMMON /ARG/UMEAN,VMEAN,UMS,VMS,UVMS,U2V,V2U,UMEAN1,VMEAN1,UMS1,
     &VMS1,UVMS1,U2V1,V2U1
      COMMON /ARGF/UMF,VMF,UMSF,VMSF,UVMSF,U2VF,V2UF,UMT,VMT,UMST,
     &VMST,UVMST,U2VT,V2UT
C
      N=N+1
      IF(NCHANL .EQ. 2) GO TO 130
      TYPE 100, UMEAN,UMS
100   FORMAT(1X,' WM : ',2(E10.3,2X))
      TYPE 120, UMEAN1,UMS1
120   FORMAT(1X,' UM : ',2(E10.3,2X))
      RETURN
C
130   TYPE 140, N,UMEAN1,VMEAN1,UMS1,VMS1,UVMS1
140   FORMAT(1X,I2,' UW : ',5(E10.3,X))
      TYPE 160, N,UMT,VMT,UMST,VMST,UVMST
160   FORMAT(1X,I2,' TW : ',5(E10.3,X))
      TYPE 220, N,UMEAN,VMEAN,UMS,VMS,UVMS
220   FORMAT(1X,I2,' WM : ',5(E10.3,X))
      TYPE 240, N,UMF,VMF,UMSF,VMSF,UVMSF
240   FORMAT(1X,I2,' FW : ',5(E10.3,X))
      RETURN
      END
C     ************************  DISPLS.FOR ENDS  ********************
```

```
      SUBROUTINE LPRNTR(NDATA)
C     ***************************  AUTHOR: K-S CHEN  ****************
C                                                                     *
C     THIS PROGRAM FETCHES THE DATA STORED IN THE UNIT #2 UNDER       *
C     FILE 'FILNAM'.                                                  *
C                                                                     *
C     ***************************  LPRNTR.SE1 BEGINNS  **************
      INTEGER IFD(2,1000)
      REAL X(20),Y(20),Z(20),UARG(20),VARG(20),UMSARG(20)
      REAL VMSARG(20),UVMSAG(20),SU(20),SV(20),SUU(20),SVV(20),SUVU(20)
      REAL SUVL(20),UARG1(20),VARG1(20),UMSAG1(20),VMSAG1(20),V2U1(20)
      REAL UVMSA1(20),SU1(20),SV1(20),SUU1(20),SVV1(20),SUVU1(20)
      REAL SUVL1(20),R(20),R1(20),XYZ(3),LP,U2V(20),V2U(20),U2V1(20)
      REAL UMF(20),VMF(20),UMSF(20),VMSF(20),UVMSF(20),SUF(20),SVF(20)
      REAL SUUF(20),SVVF(20),SUVUF(20),SUVLF(20),RF(20),UMT(20),VMT(20)
      REAL UMST(20),VMST(20),UVMST(20),SUT(20),SVT(20),SUUT(20)
      REAL SVVT(20),SUVUT(20),SUVLT(20),RT(20),U2VF(20),V2UF(20)
      REAL U2VT(20),V2UT(20)
      COMMON /COMP/NCHANL,COUNTR/SIZE/IRES/FILE/FILNAM/SWEEP/IDIR
      COMMON /MOVE/LP,XYZ/SRVB1/IFD,NC
      INTEGER COUNTR
      LOGICAL*1 FILNAM(11),IDIR
      DATA N/0/
C     OPEN(UNIT=2,NAME=FILNAM,TYPE='OLD',FORM='UNFORMATTED',
C    &ACCESS='DIRECT',RECORDSIZE=IRES)
C
      PRINT 111, FILNAM
  111 FORMAT(//,' DATA ARE STORED IN UNIT 2 UNDER FILE ',11A1)
      PRINT 122, NDATA
  122 FORMAT(/,' NO. OF DATA POINTS IN THE FILE ARE :',I4)
      PRINT 124, NC
  124 FORMAT(' THE SAMPLING SIZE IS :',I5,/)
      IF(NCHANL .EQ. 2) GO TO 450
      DO 145 J=1,NDATA
      N=N+1
      READ(2'N) X(J),Y(J),Z(J), UARG(J),UMSARG(J),SU(J),SUU(J),
     &                          UARG1(J),UMSAG1(J),SU1(J),SUU1(J)
  145 CONTINUE
      PRINT 150
  150 FORMAT(4X,'  X  ',7X,'  Y  ',7X,'  Z  ',5X,'  UMEAN  ',3X,
     &'  UMS  ',4X,' SIGMAU ',2X,'  SIGUMS  ',/)
      DO 180 I=1,NDATA
      PRINT 160, X(I),Y(I),Z(I),UARG(I),UMSARG(I),SU(I),SUU(I)
  160 FORMAT(X,'W:',3(E11.4,X),4(E10.3,X))
      PRINT 165, X(I),Y(I),Z(I),UARG1(I),UMSAG1(I),SU1(I),SUU1(I)
  165 FORMAT(X,'U:'3(E11.4,X),4(E10.3,X),/)
  180 CONTINUE
      RETURN
C     *************************  LPRNTR.SE1 ENDS  ******************
```

```
C   ************************  LPRNTR.SE2 BEGINNS  ********************
450 CONTINUE
C** IF(IDIR .EQ. 'X') PRINT 456
    IF(IDIR .EQ. 'Z') PRINT 457
    IF(IDIR .EQ. 'Y') PRINT 458
457 FORMAT(//,3X,'    Z     ',2X,'   U     ',2X,'   V     ',3X,
   &'  U''**2  ',2X,'  V''**2  ',2X,'  U''V''  ',2X,'   SU    ',3X,
   &'   SV    ',X,'   SU''**2  ','   SV''**2  ',3X,' SU''V''U ',3X,
   &' SU''V''L ')
458 FORMAT(//,3X,'    Y     ',2X,'   U     ',2X,'   V     ',3X,
   &'  U''**2  ',2X,'  V''**2  ',2X,'  U''V''  ',2X,'   SU    ',3X,
   &'   SV    ',X,'   SU''**2  ','   SV''**2  ',3X,' SU''V''U ',3X,
   &' SU''V''L ')
    PRINT 460
460 FORMAT(5X,'-----',3X,'---------',2X,'---------',2X,'---------',
   &2X,'---------',2X,'---------',X,' ---------',X,' ---------',2X,
   &'---------',2X,'---------',2X,'---------',2X,'---------')
    DO 470 I=1,NDATA
    N=N+1
    READ(2'N) X(I),Y(I),Z(I), UARG(I),VARG(I),UMSARG(I),VMSARG(I),
   &UVMSAG(I),U2V(I),V2U(I),SU(I),SV(I),SUU(I),SVV(I),SUVU(I),SUVL(I)
   &,R(I)
    N=N+1
    READ(2'N) X(I),Y(I),Z(I), UARG1(I),VARG1(I),UMSAG1(I),VMSAG1(I),
   &UVMSA1(I),U2V1(I),V2U1(I),SU1(I),SV1(I),SUU1(I),SVV1(I),SUVU1(I),
   &SUVL1(I),R1(I)
    N=N+1
    READ(2'N) UMF(I),VMF(I),UMSF(I),VMSF(I),UVMSF(I),U2VF(I),V2UF(I),
   &SUF(I),SVF(I),SUUF(I),SVVF(I),SUVUF(I),SUVLF(I),RF(I)
    N=N+1
    READ(2'N) UMT(I),VMT(I),UMST(I),VMST(I),UVMST(I),U2VT(I),V2UT(I),
   &SUT(I),SVT(I),SUUT(I),SVVT(I),SUVUT(I),SUVLT(I),RT(I)
470 CONTINUE
C
    DO 570 J=1,NDATA
    PRINT 489,X(J),Y(J),Z(J)
489 FORMAT(5X,' X= ',F7.3,' Y= ',F7.3,' Z= ',F7.3)
    PRINT 520,CC,UARG1(J),VARG1(J),UMSAG1(J),VMSAG1(J),UVMSA1(J),
   &SU1(J),SV1(J),SUU1(J),SVV1(J),SUVU1(J),SUVL1(J)
    PRINT 530,CC,UMT(J),VMT(J),UMST(J),VMST(J),UVMST(J),SUT(J),
   &SVT(J),SUUT(J),SVVT(J),SUVUT(J),SUVLT(J)
    PRINT 500,CC,UARG(J),VARG(J),UMSARG(J),VMSARG(J),UVMSAG(J),
   &SU(J),SV(J),SUU(J),SVV(J),SUVU(J),SUVL(J)
    PRINT 540,CC,UMF(J),VMF(J),UMSF(J),VMSF(J),UVMSF(J),SUF(J),
   &SVF(J),SUUF(J),SVVF(J),SUVUF(J),SUVLF(J)
500 FORMAT(X,'W:',F7.3,X,11(E11.3))
520 FORMAT(X,'U:',F7.3,X,11(E11.3))
530 FORMAT(X,'T:',F7.3,X,11(E11.3))
540 FORMAT(X,'F:',F7.3,X,11(E11.3))
570 CONTINUE
C   ************************  LPRNTR.SE2 ****************************
```

```
C  ******************  LPRNTR.SE3 BEGINNS  ************************
   PRINT *,' THE TRIPLE-CORRELATION FOR UW-,TW-,W- & FW- ARE :'
   PRINT *,' '
   PRINT *,(U2V1(J),J=1,NDATA)
   PRINT *,' '
   PRINT *,(V2U1(J),J=1,NDATA)
   PRINT *,' '
   PRINT *,(U2VT(J),J=1,NDATA)
   PRINT *,' '
   PRINT *,(V2UT(J),J=1,NDATA)
   PRINT *,' '
   PRINT *,(U2V(J),J=1,NDATA)
   PRINT *,' '
   PRINT *,(V2U(J),J=1,NDATA)
   PRINT *,' '
   PRINT *,(U2VF(J),J=1,NDATA)
   PRINT *,' '
   PRINT *,(V2UF(J),J=1,NDATA)
   PRINT *,' '
   PRINT *,' THE CORRELATION COEFICIENT ARE:'
   PRINT *,(R1(J),J=1,NDATA)
   PRINT *,' '
   PRINT *,(RT(J),J=1,NDATA)
   PRINT *,' '
   PRINT *,(R(J),J=1,NDATA)
   PRINT *,' '
   PRINT *,(RF(J),J=1,NDATA)
   RETURN
   END
C  ****************** LPRNTR.SE3 ENDS  ****************************
```

```
  .TITLE DSAFLT
  .IDENT /28JAN80/
; FORTRAN-CALLABLE SUBROUTINE TO CONVERT DISA FLOATING
; POINT TO PDP-11 FORMAT
;
DSAFLT::  MOV   (R5)+, R0          ; FETCH # OF ARGUMENTS
          MOV   @(R5)+, R0         ; FETCH ARGUMENT
          MOV   R0, R1             ; POSITION EXPONENT
          SWAB  R0                 ; POSITION MANTISSA
          BIC   #177400, R0        ; DELETE EXPONENT FROM R0
          BIC   #177760, R1        ; DELETE MANTISSA FROM R1
          TSTB  R0                 ; CHECK FOR NORM OR ZERO
          BMI   NORMAL             ; BRANCH IF NORMALIZED
          BEQ   ZERO               ; BRANCH IF ZERO
NORM:     ASL   R0                 ; NORMALIZE
          DEC   R1                 ; IF NEEDED
          TSTB  R0                 ; SEE IF NORM NOW
          BPL   NORM               ; LOOP IF NOT
NORMAL:   ADD   #210, R1           ; BIAS AND SHIFT BINARY POINT
          SWAB  R1                 ; MOVE EXPONENT TO HIGH BIT
          ROR   R1                 ; POSITION AT BIT 7
          BIC   #200, R0           ; HIDE BIT
          BIS   R1, R0             ; PACK EXPONENT
          BR    CLRLOW             ; PACKING DONE
ZERO:     CLR   R0                 ; SPECIAL ZERO STORAGE
CLRLOW:   CLR   R1                 ; CLEAR LOW ORDER WORD
          RTS   PC                 ; DONE
          .END
```

APPENDIX D

Internal Wave Analysis

The following is a highly simplified analysis of internal wave propagation on the stably-stratified layer in the top of the cavity. It neglects viscosity and velocity shear and employs the Boussinesq approximation to the effects of variable density. Thus it starts with the identification of a small vertical perturbation velocity, $\tilde{w}$, which is supposed to behave sinusoidally in x - ct. Specifically

$$\tilde{w}(x,z,t) = \mathrm{Re}\{\bar{w}(z)e^{ik(x-ct)}\} \quad . \tag{D-1}$$

In this appendix, we employ the coordinate system x (horizontal), z (vertically upward), which is usually adopted in the literature on internal waves.

The differential equation governing the complex amplitude $\bar{w}(z)$ is taken from Phillips [1966], (Chapt. 5, Eq. 5.2.9),

$$\bar{w}'' + k^2\left(\frac{N^2}{n^2} - 1\right)\bar{w} = 0 \tag{D-2}$$

where $k = 2\pi/\lambda$ is the horizontal wave number for a wave of length λ; $n \equiv kc$ where c is the horizontal phase speed; and

$$N^2 = -\frac{g}{\rho_m}\frac{d\rho_o}{dz} \tag{D-3}$$

is the square of the Brunt-Väisälä frequency, which characterizes the stable density stratification. $\rho_o(z)$ is the density profile of the unperturbed fluid; ρ_m is a constant mean value of ρ_o.

We shall imagine a density profile

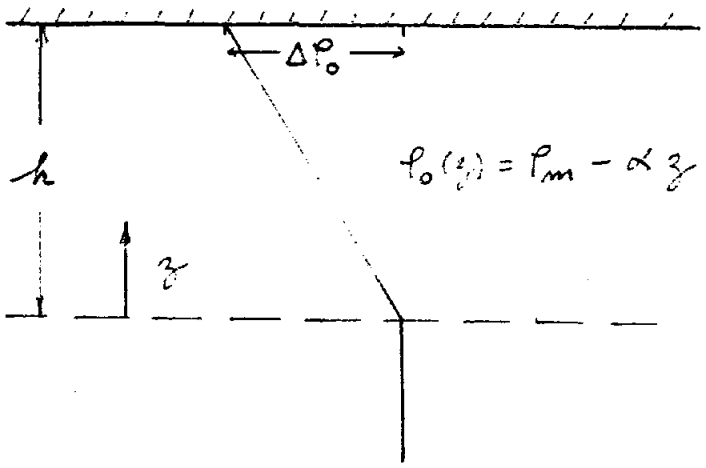

for which $N^2 = \alpha g/\rho_m = \frac{\Delta\rho_o}{\rho_m}\frac{g}{h}$ in $0 < z < h$ and $N^2 = 0$ in $z < 0$.

For the cavity flow, we estimate $h \approx 0.3\ b \approx 0.03$ m; $\Delta\rho_o/\rho_m \approx \Delta T/T_\infty \approx 1.2$. This gives

$$N \approx 20 \text{ rad/sec} \quad \text{and} \quad f = \frac{N}{2\pi} \approx 3 \text{ Hz} \quad .$$

Internal waves correspond to oscillatory solutions of (D-2) and hence will have circular frequencies $n < N$.

The boundary conditions on $\bar{w}$ are those appropriate to a free oscillation:

$$\bar{w} = 0 \quad \text{at} \quad z = h \ ; \quad \bar{w} \to 0 \quad \text{as} \quad z \to -\infty \quad .$$

The solution that satisifes the boundary condition will have the form

$$\bar{w} = A \sin \alpha\ (z - h) \quad \text{in} \quad 0 < z < h$$

and

$$\bar{w} = B\ e^{kz} \qquad \text{in} \quad z < 0 \quad .$$

Here $\alpha = k\left(\frac{N^2}{n^2} - 1\right)^{1/2}$.

We impose continuity of w, and of u, at z = 0. This translates into continuity of $\bar{\omega}$ and $\bar{\omega}'$. So

$$- A \sin \alpha h = B ,$$

and

$$A \alpha \cos \alpha h = kB .$$

Together these determine the dispersion relationship

$$\tan \alpha h = - \left(\frac{N^2}{n^2} - 1 \right)^{1/2} \tag{D-4}$$

Since we have implied that $\alpha > 0$, we evaluate the root

$$\alpha h = \pi - \tan^{-1} \left(\frac{N^2}{n^2} - 1 \right)^{1/2}$$

or

$$k h = \left(\frac{N^2}{n^2} - 1 \right)^{-1/2} \left(\pi - \tan^{-1} \left(\frac{N^2}{n^2} - 1 \right)^{1/2} \right) \tag{D-5}$$

We want to use (D-5) to find the frequencies, n_i, for those modes that have antinodes at x = 0 and x = a (our cavity depth). These have

$$k_i = \pi i / a \quad \text{or} \quad k_i h = \pi i \, \frac{h}{a} \quad . \tag{D-6}$$

For the shallow cavity a/b = 0.5, we have $h/a \approx 0.6$, so

$$k_i h \approx 1.88, 3.76, \text{ etc.}$$

The corresponding frequencies are

$$n/N = 0.639, 0.828, 0.902, \text{ etc.}$$

For $N/2\pi \approx 3$ Hz, we find that $n/2\pi$ lies between 1.9 and 3 Hz. Thus, these crude estimates lie close to the observed frequencies.

The horizontal propagation speeds that correspond to these values of k and n are

$$c = n/k = 0.20,\ 0.13,\ \text{etc. (m/s)}.$$

The fact that these values lie within the range of our observed values of V implies that we should not have neglected velocity shear in the above analysis, and that a better analysis would have to account for the existence of a critical layer, where V = c, for the outward running waves. Shear would be relatively unimportant for the inward-running waves.

Even a linearized analysis of the effect of shear is too complicated (see Booker and Bretherton [1967]) to justify its presentation here.

UNLIMITED RELEASE
INITIAL DISTRIBUTION

U. S. Department of Energy (5)
Forrestal Building
1000 Independence Avenue, S.W.
Washington, D.C. 20585
Attn: H. Coleman
C. Carwile
C. Mangold
F. Morse
M. Scheve

U. S. Department of Energy (2)
1333 Broadway
Oakland, CA 94612
Attn: R. W. Hughey
T. Veath

U. S. Department of Energy (2)
Albuquerque Operations Office
P. O. Box 5800
Albuquerque, NM 87115
Attn: J. Weisiger
D. Graves

Purdue University
Department of Mechanical Engineering
Lafayette, IN 47907
Attn: R. Viskanta

Stanford University
Department of Mechanical Engineering
Stanford, CA 94305
Attn: J. Ferziger

University of California (13)
Mechanical Engineering Dept.
Berkeley, CA 94720
Attn: J.A.C. Humphrey (10)
R. Greif
F. S. Sherman
K. S. Chen

University of California - Irvine
Department of Mechanical Engineering
Irvine, CA 92717
Attn: M. Young

University of Houston
Solar Energy Laboratory
3801 Cullen Blvd.
Houston, TX 77004
Attn: A. F. Hildebrandt

University of Illinois
1206 W. Green Street
Urbana, IL 61820
Attn: A. M. Clausing

University of Notre Dame
Department of Mechanical Engineering
Notre Dame, IN 46556
Attn: K. T. Yang

Washington State University
Dept. of Mechanical Engineering
Pullman, WA 99164-2920
Attn: C. Crowe

Arco Power Systems
7061 S. University, Suite 300
Littleton, CO 80122
Attn: F. A. Blake

Arco Power Systems
302 Nichols Drive
Hutchins, TX 75141
Attn: R. L. Henry

Arizona Public Service Company
P. O. Box 21666
Phoenix, AZ 85036
Attn: E. Weber

Babcock and Wilcox
91 Stirling Avenue
Barberton, OH 44203
Attn: G. Grant

Battelle Pacific Northwest Laboratories
P. O. Box 999
Richland, WA 99352
Attn: T. A. Williams

Bechtel Group, Inc.
P. O. Box 3965
San Francisco, CA 94119
Attn: P. DeLaquil

Black and Veatch Consulting Engineers
P. O. Box 8405
Kansas City, Mo 64114
Attn: J. C. Grosskreutz

Boeing Aerospace Company
Energy Systems
P. O. Box 3999, MS87-63
Seattle, WA 98124
Attn: W. D. Beverly

Centre National De La Recherche Scientifique
Laboratorie d'Energetique Solaire
Odiello, B. P. 5, 66120 Font-Remeu
France
Attn: C. Royere

El Paso Electric Company
P. O. Box 982
El Paso, TX 79946
Attn: J. E. Brown

Electric Power Research Institute
P. O. Box 10412
Palo Alto, CA 94303
Attn: E. DeMeo

Foster Wheeler Development Corporation
12 Peach Tree Hill Road
Livingston, NJ 07039
Attn: R. J. Zoschak

Garrett-AiResearch Mfg. Co.
2525 W. 190th St.
Torrance, CA 90509
Attn: M. Combs

G. A. Technologies
P. O. Box 85608
San Diego, CA 92138
Attn: G. Besenbruch

Georgia Institute of Technology
Atlanta, GA 30332
Attn: R. A. Cassanova

Gibbs and Hill, Inc.
393 Seventh Avenue
New York, NY 10001
Attn: R. Prieto

Laboratorie D'Energetique Solaire
40 Avenue de Recteur Pineau
86022 Poitiers
France
Attn: P. LeQuere

Lawrence Berkeley Laboratories
University of California
Berkeley, CA 94720
Attn: A. J. Hunt

Los Angeles Department of Water and Power
111 North Hope St.
Los Angeles, CA 90051
Attn: D. Chu

McDonnell Douglas Astronatics Company (2)
5301 Bolsa Avenue
Huntington Beach, CA 92647
Attn: R. L. Gervais
J. Mavickas

Olin Chemical Company
120 Long Ridge Road
Stamford, CT 06904
Attn: L. C. Fioruccio

Pacific Gas and Electric Company
3400 Crow Canyon Road
San Ramon, CA 94526
Attn: G. Braun

The Ralph M. Parsons Company
100 West St.
Pasadena, CA 91124
Attn: N. W. Snyder

PFR Energy Systems, Inc.
P. O. Box 91890
Los Angeles, CA 90045
Attn: T. Rosenman

Polydyne, Inc.
1900 S. Norfolk St., Suite 209
San Mateo, CA 94403
Attn: P. B. Bos

Rockwell International
Energy Systems Group
8900 De Soto Avenue
Canoga Park, CA 91304
Attn: T. Springer

Rockwell International
Rocketdyne Division
6633 Canoga Avenue
Canoga Park, CA 91304
Attn: J. M. Friefeld

San Diego Gas and Electric Company
Mechanical Engineering
P. O. Box 1831
San Diego, CA 92112
Attn: R. E. Potthoff

Solar Energy Industries Association
1140 19th St., N.W.
Suite 600
Washington, D.C. 20036
Attn: C. LaPorta

Solar Energy Research Institute (4)
1617 Cole Boulevard
Golden, CO 80401
Attn: B. Gupta
D. Johnson
F. Kreith
J. Thornton

Solar Power Engineering Co.
P. O. Box 91
Morrison, CO 80465
Attn: H. C. Wroton

Southern California Edison
P. O. Box 800
Rosemead, CA 82807
Attn: J. N. Reeves

Spectra Technology, Inc.
2755 Northrup Way
Bellevue, WA 98004
Attn: R. R. Taussig

Stearns Catalytic Corp.
P. O. Box 5888
Denver, CO 80217
Attn: W. R. Lang

J. W. Nunziato, 1510
E. H. Beckner, 6000; Attn: V. Dugan, 6200
D. G. Schueler, 6220; Attn: L. Otts, 6226
R. S. Claassen, 8000; Attn: D. M. Olson, 8100
A. N. Blackwell, 8200
D. L. Hartley, 8300
C. S. Selvage, 8000A
J. S. Kraabel, 8132
R. J. Gallagher, 8201
C. W. Robinson, 8240; Attn: G. A. Benedetti, 8241
M. L. Callabresi, 8242
M. R. Birnbaum, 8243
C. M. Hartwig, 8244
R. J. Kee, 8245
R. T. Boehm, 8244
D. L. Siebers, 8362
R. C. Wayne, 8400; Attn: L. D. Bertholf, 8430
H. Hanser, 8440
M. Abrams, 8431
R. L. Rinne, 8470
A. C. Skinrood, 8471

P. K. Falcone, 8471
J. C. Swearengen, 8473
Publications Division 8265, for TIC (30)
Publications Division 8265/Technical Library Processes Division, 3141
Technical Library Processes Division, 3141 (3)
M. A. Pound, 8024, for Central Technical Files (3)

GPO 589-942/38241